AD-A128 368 PROPERTIES OF TUFFS GROUT AND OTHER MATERIALS(U) TERRA TEK INC SALT LAKE CITY UT C H COOLEY ET AL. 01 JAN 82 TTI-TR-82-05 DNA-5986F DNA001-78-C-0395 1/3

UNCLASSIFIED F/G 8/7 NL

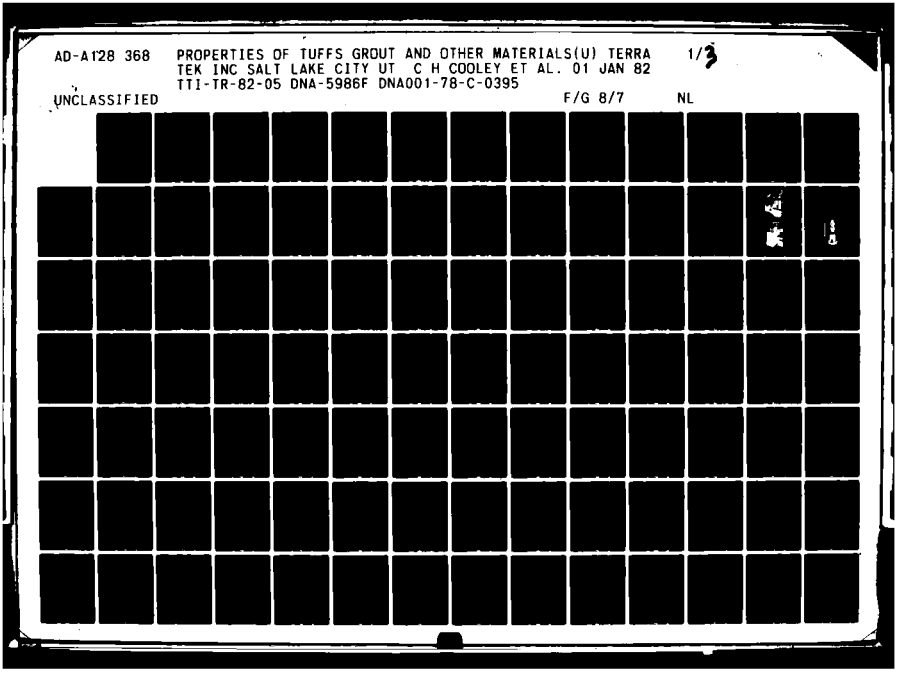

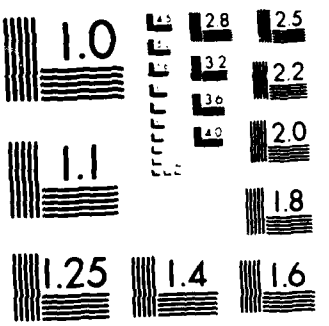

(12) AD-E301112

AD A123368

DNA 5986F

PROPERTIES OF TUFFS, GROUT AND OTHER MATERIALS

Terra Tek, Incorporated
420 Wakara Way
Salt Lake City, Utah 84108

1 January 1982

Final Report for Period 1 September 1979—31 November 1981

CONTRACT No. DNA 001-78-C-0395

APPROVED FOR PUBLIC RELEASE;
DISTRIBUTION UNLIMITED.

THIS WORK WAS SPONSORED BY THE DEFENSE NUCLEAR AGENCY
UNDER RDT&E RMSS CODE K400078462 J45GAXYX97310 H2590D.

Prepared for
Director
DEFENSE NUCLEAR AGENCY
Washington, DC 20305

Destroy this report when it is no longer needed. Do not return to sender.

PLEASE NOTIFY THE DEFENSE NUCLEAR AGENCY, ATTN: STTI, WASHINGTON, D.C. 20305, IF YOUR ADDRESS IS INCORRECT, IF YOU WISH TO BE DELETED FROM THE DISTRIBUTION LIST, OR IF THE ADDRESSEE IS NO LONGER EMPLOYED BY YOUR ORGANIZATION.

UNCLASSIFIED

SECURITY CLASSIFICATION OF THIS PAGE (When Data Entered)

REPORT DOCUMENTATION PAGE	READ INSTRUCTIONS BEFORE COMPLETING FORM
1. REPORT NUMBER: DNA 5986F	2. GOVT ACCESSION NO.: AD-A128 368
	3. RECIPIENT'S CATALOG NUMBER:
4. TITLE (and Subtitle): PROPERTIES OF TUFFS, GROUT AND OTHER MATERIALS	5. TYPE OF REPORT & PERIOD COVERED: Final Report for Period 1 Sep 79—31 Nov 81
	6. PERFORMING ORG. REPORT NUMBER: TR 82-05
7. AUTHOR(s): C. H. Cooley, R. H. Smith, J. F. Schatz	8. CONTRACT OR GRANT NUMBER(s): DNA 001-78-C-0395
9. PERFORMING ORGANIZATION NAME AND ADDRESS: Terra Tek, Incorporated, 420 Wakara Way, Salt Lake City, Utah 84108	10. PROGRAM ELEMENT, PROJECT, TASK AREA & WORK UNIT NUMBERS: Subtask J45GAXYX973-10
11. CONTROLLING OFFICE NAME AND ADDRESS: Director, Defense Nuclear Agency, Washington, D.C. 20305	12. REPORT DATE: 1 January 1982
	13. NUMBER OF PAGES: 214
14. MONITORING AGENCY NAME & ADDRESS(if different from Controlling Office)	15. SECURITY CLASS (of this report): UNCLASSIFIED
	15a. DECLASSIFICATION/DOWNGRADING SCHEDULE

16. DISTRIBUTION STATEMENT (of this Report)

Approved for public release, distribution unlimited.

17. DISTRIBUTION STATEMENT (of the abstract entered in Block 20, if different from Report)

18. SUPPLEMENTARY NOTES

This work was sponsored by the Defense Nuclear Agency under RDT&E RMSS Code K400078462 J45GAXYX97310 H2590D.

19. KEY WORDS (Continue on reverse side if necessary and identify by block number)

Nuclear Test	Tuff	Coal Tar Epoxy
Hydrostatic	Grout	Temperature
Uniaxial Strain	Pressure	Creep
Triaxial Compression	Load	Permeability

20. ABSTRACT (Continue on reverse side if necessary and identify by block number)

The mechanical and physical properties of various natural geologic and man-made materials have been determined for the Test Directorate, Field Command, DNA. The testing was performed in support of the Nevada Test Site nuclear test program and covered the period from 1 September 1979 to 31 November 1981. The contract number was DNA 001-78-C-0395 and Mr. J. W. LaComb was the Contracting Officer Representative.

The mechanical and physical properties of tuffs and grouts from the Nevada Test Site were determined. The tests performed included unconfined

DD FORM 1 JAN 73 1473 EDITION OF 1 NOV 65 IS OBSOLETE

UNCLASSIFIED

SECURITY CLASSIFICATION OF THIS PAGE (When Data Entered)

20. ABSTRACT (Continued)

compression, triaxial compression, and uniaxial strain. More specialized tests were also performed. These included drained hydrostatic compression tests on grout to study characteristic drainage times, triaxial compression tests on stress-cycled grout, permeability experiments on stress-cycled and pristine grout, and elevated and room temperature unconfined compression and creep tests on coal tar epoxy - pea gravel mixtures.

PREFACE

The authors express their thanks for the continued guidance and support of Mr. J. W. LaComb (DNA, Mercury, Nevada).

We also thank Mark Pickett and Robert Spencer for their assistance in conducting the laboratory tests and Mr. Lee Beard, Ms. Anne MacLeod and Mr. John Goodell for their efforts in the preparation of this report.

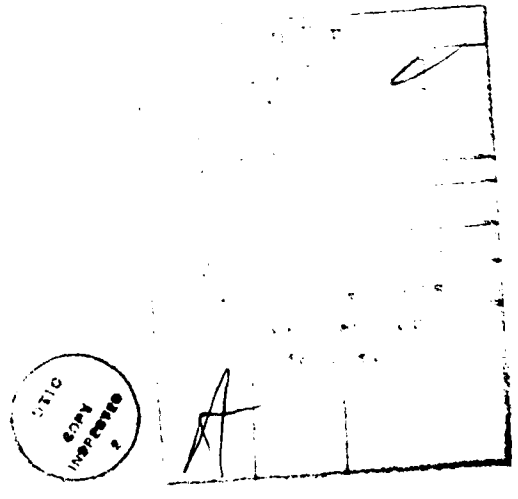

TABLE OF CONTENTS

LIST OF FIGURES

LIST OF TABLES

I. INTRODUCTION

The Defense Nuclear Agency (DNA) requires a knowledge of the mechanical and physical properties of materials (both natural and man made) which are used in conjunction with its underground testing program at the Nevada Test Site. This report describes the material testing program conducted by Terra Tek, Inc., Research and Development Division, from June 1980 to November 1981 for the Test Directorate, Field Command, DNA. Work completed between September 1979 and May 1980 has been included in a previous final report[1].

This report is divided into three sections. The first section contains the results of testing of several tuffs from the Nevada Test Site that are associated with nuclear events. These tests consisted, generally, of physical property measurements of bulk density, grain density, saturation, and air void content, followed by uniaxial strain experiments and ultrasonic velocity measurements.

The second section is the final version of a report on the mechanical and physical properties of 2C4 grout to be used in conjunction with small-scale explosive tests for effects evaluation. A preliminary version of this report has been distributed to the DNA Test Directorate as well as other interested government agencies and contractors. Tests conducted were uniaxial strain, triaxial compression, hydrostatic compression, strain rate, permeability and the measurement of physical properties on samples cured to a consistent age.

The third section consists of results of measurements of the properties of certain Coal Tar Epoxy (CTE) mixtures for stemming and containment evaluation. Included are room temperature triaxial compression and uniaxial strain results.

[1]Butters, S.W., J.M. Gronseth and J.F. Patterson, May 1980, "Material Properties of Nevada Test Site Tuff and Grout -- Final Report for Period September 1978 to August 1979.

II. NEVADA TEST SITE TUFFS

Introduction

A series of measurements of physical properties, ultrasonic velocities, and mechanical properties were made on tuffaceous material from the Nevada Test Site. The results of these tests are presented in this section where they are listed by bore hole identification numbers. Each bore hole is treated independently, with the graphical results of the mechanical tests forming an appendix. In such cases where a uniaxial strain test was not performed or was unsuccessful, only the physical properties and ultrasonic velocity data are given. This practice is consistently followed throughout this report. Also included is a section that explains the procedures used for determining physical properties, performing uniaxial strain tests, and measuring ultrasonic velocities.

UE12N#12

Physical properties, ultrasonic wave velocities and uniaxial strain tests were conducted on cored material from hole UE12N#12. This material was received from the DNA in September, 1980.

Table 1 lists physical properties, ultrasonic velocities and permanent compaction, resulting from uniaxial strain tests to 4 kbars confining pressure, as functions of drill hole depth. Summary plots of density, porosity, air void percentage, longitudinal velocity, and permanent compaction as functions of depth are shown in Figure 1.

The permanent compactions sustained in the uniaxial strain tests ranged from 0.1% to 7.5% and the maximum stress difference ranged from 0.06 kb to 1.3 kb. There is a general correlation between this compaction and the calculated air void volume for the majority of the tests. The reduced data from these tests are presented as plots of volume strain as functions of mean normal stress and confining pressure as functions of stress difference in Appendix A, Figures A1a-A14b.

One sample (drill hole depth of 1291 ft) was subjected to two consecutive uniaxial strain tests. These two tests are plotted together in Figures A6a and A6b.

Table 1

Physical Properties, Measured Permanent Compaction, and Ultrasonic Velocities on Samples from UE12n#12

Drill Hole Footage (m/ft)	Density (gm/cc)			Water by Wet Weight (%)	Porosity (%)	Saturation (%)	Calc. Air Voids (%)	Meas. Permanent Comp. (%)	Velocity (km/sec)	
	As-Received	Dry	Grain						Long	Shear
350.8/1151	1.97	1.69	2.41	14.1	29.9	92.9	2.1	3.8	3.8	2.0
353.6/1160	1.96	1.65	2.43	15.6	32.1	95.2	1.6	3.3	3.2	1.6
355.7/1167	1.77	1.38	2.43	22.2	43.3	91.0	3.9	2.3	2.8	1.2
359.4/1179	1.87	1.51	2.36	19.2	36.0	99.8	0.1	1.8	3.0	1.5
362.1/1188	1.80	1.43	2.36	20.3	39.3	93.1	2.7	2.2	2.7	1.3
366.1/1201	2.02	1.74	2.44	14.0	28.7	98.9	0.3	0.6	3.2	1.6
368.5/1209	1.87	1.57	2.39	16.4	34.4	89.2	3.7	0.1	3.5	1.9
371.9/1220	1.83	1.46	2.48	20.4	41.3	90.1	4.1	2.0	2.9	1.2
374.3/1228	1.87	1.51	2.54	19.6	40.7	90.0	4.1	1.8	2.6	1.0
377.3/1238	1.71	1.28	2.38	25.1	46.3	92.3	3.6	6.5	2.0	0.8
381.3/1251	1.80	1.40	2.38	22.4	41.2	97.8	0.9	1.7	2.9	1.4
384.0/1260	1.85	1.52	2.37	18.2	36.1	93.3	2.4	1.9	3.2	1.6
387.7/1272	1.67	1.24	2.39	25.7	48.2	88.9	5.3	1.0	1.8	0.8
389.5/1278	1.80	1.43	2.34	20.7	38.9	96.1	1.5	---	2.8	1.3
393.5/1291	1.77	1.39	2.38	21.5	41.6	91.6	3.5	0.3	2.6	1.1
397.2/1303	1.88	1.55	2.41	17.4	35.7	91.7	3.0	2.3	3.1	1.5
400.8/1315	1.88	1.57	2.38	16.8	34.1	92.8	2.4	---	3.2	1.7
404.2/1326	1.96	1.64	2.47	16.3	33.6	99.1	1.6	1.1	3.0	1.4
406.6/1334	1.97	1.67	2.51	15.2	33.3	89.8	3.4	1.8	3.0	1.5
410.3/1346	2.21	2.01	2.60	8.8	22.6	85.8	3.2	0.3	3.2	1.4
413.0/1355	1.85	1.46	2.47	20.8	40.8	94.0	2.5	2.0	2.6	1.1
416.1/1365	1.77	1.37	2.45	22.9	44.2	92.0	3.5	1.2	2.8	1.3
418.8/1374	1.89	1.55	2.45	18.4	36.9	94.3	2.1	1.1	2.8	1.2
422.5/1386	2.05	1.80	2.53	12.3	30.0	86.7	3.9	1.8	3.2	1.7
425.2/1395	2.07	1.90	2.40	8.4	20.9	83.7	3.4	---	4.0	2.4
430.7/1413	2.00	1.72	2.40	14.0	28.4	99.0	0.3	0.4	3.1	1.4
434.3/1425	1.92	1.62	2.41	15.9	32.8	93.4	2.2	2.5	3.2	1.6
437.4/1435	1.85	1.45	2.51	21.3	42.1	93.6	2.7	0.3	2.5	0.8
440.4/1445	1.85	1.49	2.36	19.4	36.8	97.7	0.8	1.8	2.9	1.4
444.1/1457	1.92	1.70	2.31	11.2	26.4	81.5	4.9	---	3.2	1.7
446.2/1464	1.79	1.39	2.40	22.5	42.3	95.2	2.0	2.4	2.6	1.1
448.4/1471	1.81	1.44	2.40	20.7	40.1	93.6	2.6	2.2	2.6	1.1
451.1/1480	1.85	1.47	2.49	20.5	41.1	92.1	3.3	1.4	2.5	1.0
453.2/1487	1.87	1.54	2.39	18.0	35.8	94.3	2.0	7.5	3.0	1.5
456.9/1499	1.83	1.50	2.38	18.0	36.8	89.7	3.8	4.2	2.5	1.1
459.9/1509	1.84	1.47	2.32	19.8	36.5	99.4	0.2	1.5	2.5	1.2
463.0/1519	1.87	1.54	2.35	17.4	34.3	94.4	1.9	1.4	2.9	1.3
465.1/1526	1.91	1.60	2.38	16.6	32.9	96.5	1.2	1.5	3.0	1.5
467.9/1535	1.85	1.47	2.39	20.7	38.7	98.9	0.4	---	2.7	---
471.8/1548	1.87	1.53	2.46	18.1	37.7	90.0	3.8	1.3	2.7	1.3
517.2/1697	2.14	1.88	2.64	12.2	29.0	89.8	3.0	0.5	3.0	1.4
518.8/1702	2.25	2.03	2.61	9.8	22.4	98.9	0.2	1.2	3.4	1.7
522.4/1714	2.17	1.88	2.63	12.7	28.4	96.4	1.0	---	1.7	0.7
524.9/1722	2.17	1.87	2.70	14.1	30.9	98.3	0.5	0.5	2.4	0.8

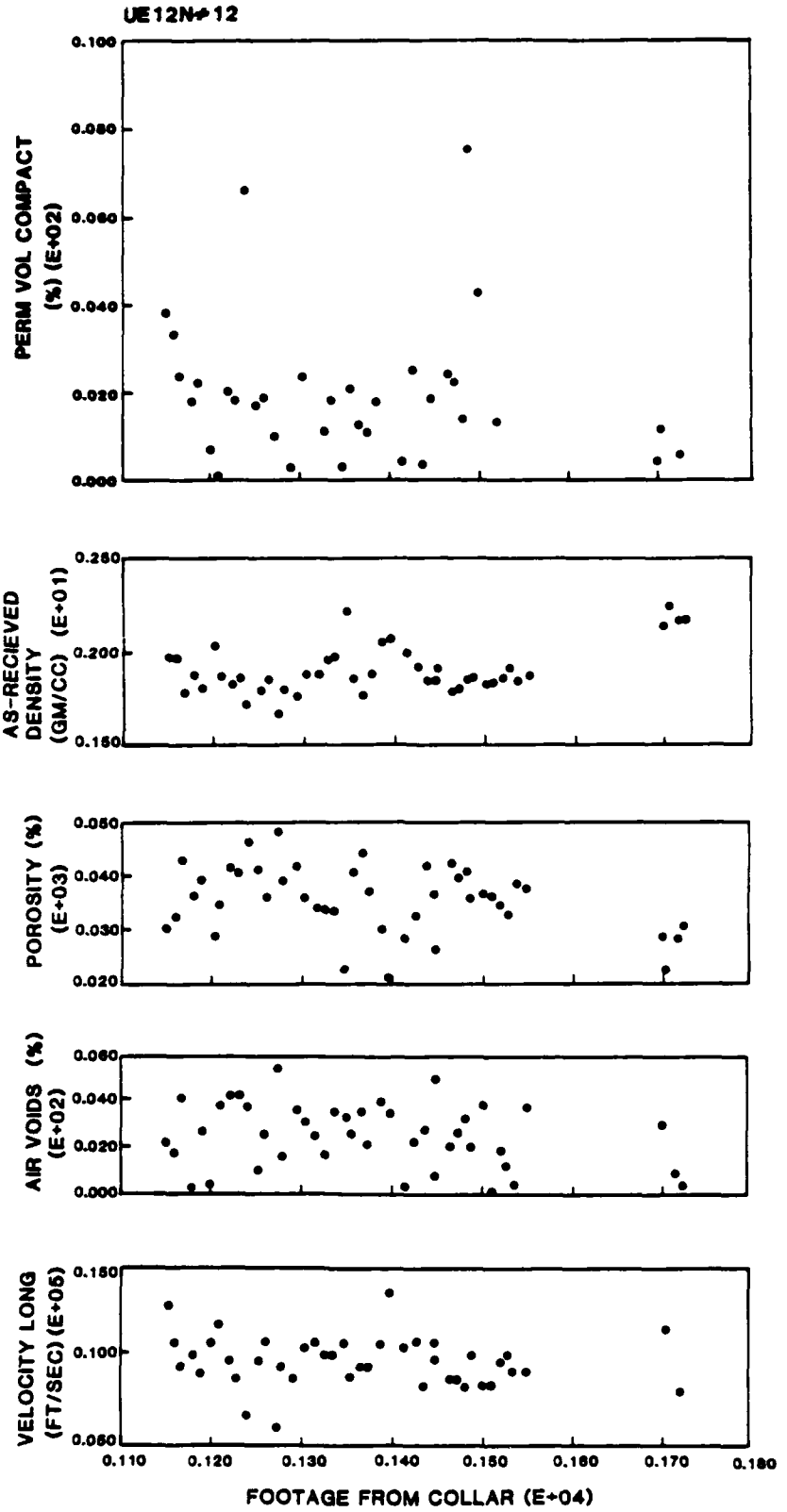

Figure 1.
UE12N #12. Selected Properties as a Function of Drill Hole Footage.

U12N.14-UG-1

Cored samples were received from hole number U12N.14-UG-1 on January 8, 1981. They were subjected to physical properties and ultrasonic wave velocity analysis, and tested in uniaxial strain.

Table 2 presents the physical properties, ultrasonic data, and the permanent volume compaction resulting from the uniaxial strain tests. Graphical representations of the density, porosity, air void percentage, longitudinal velocity and permanent compaction as functions of sample depth are shown in Figure 2.

The permanent compaction of these samples varied between 0.2% and 9.2%. The range of peak stress differences was from 0.2 to 1.0 kbars.

Plots for each successful uniaxial compression test showing volume strain versus the mean normal stress, and the stress difference versus the confining pressure are shown in Appendix B, Figures B1a-B15b.

Table 2

Physical Properties, Measured Permanent Compaction, and Ultrasonic Velocities on Samples from U12n.14 Ug-1

Drill Hole Footage (m/ft)	Density (gm/cc) As-Received	Dry	Grain	Water by Wet Weight (%)	Porosity (%)	Saturation (%)	Calc. Air Voids (%)	Meas. Permanent Comp. (%)	Velocity (km/sec) Long	Shear
214.6/704	1.84	1.44	2.56	21.6	43.7	90.9	4.0	2.3	3.00	1.50
222.8/731	2.05	1.75	2.65	14.6	33.8	88.5	3.9	0.7	3.10	1.30
230.1/755	2.06	1.77	2.62	14.1	32.4	89.7	3.4	1.9	2.00	1.00
238.0/781	2.17	1.94	2.66	10.6	27.2	85.0	4.1	0.7	3.50	1.70
244.4/802	2.06	1.77	2.73	14.4	35.3	84.2	5.6	1.2	2.10	0.90
252.4/828	2.09	1.81	2.66	13.6	32.0	88.7	3.6	1.5	--	--
259.1/850	2.03	1.69	2.69	16.6	37.2	90.7	3.4	---	2.80	1.40
267.6/878	2.05	1.79	2.61	12.7	31.4	82.9	5.4	0.2	2.50	1.30
276.1/906	2.02	1.70	2.63	16.0	35.3	91.4	3.0	0.8	2.70	1.10
282.9/928	2.16	1.92	2.70	11.3	29.0	84.5	4.5	0.8	2.80	1.20
291.4/956	2.09	1.82	2.69	12.9	32.2	84.2	5.1	0.8	2.80	1.10
297.2/975	2.12	1.86	2.61	12.3	28.8	90.6	2.7	2.7	2.70	1.10
304.5/999	2.17	1.88	2.66	13.3	29.4	98.4	0.5	0.7	2.70	1.10
312.7/1026	1.91	1.56	2.47	18.0	36.7	93.3	2.5	0.4	2.40	1.10
319.7/1049	1.90	1.57	2.56	17.5	38.7	86.4	5.3	0.7	2.90	1.40
326.1/1070	1.88	1.53	2.47	18.7	38.2	91.9	3.1	---	3.00	1.40
334.7/1098	1.90	1.54	2.44	18.9	37.5	93.0	2.67	1.6	2.81	1.28
343.2/1126	1.84	1.51	2.44	17.5	37.9	84.6	5.8	0.6	2.81	1.34
350.2/1149	1.94	1.61	2.47	16.8	34.7	93.5	2.2	1.0	2.85	1.35
358.4/1176	1.91	1.58	2.48	17.0	36.0	89.9	3.7	0.3	2.85	1.36
366.7/1203	1.95	1.63	2.47	16.2	33.8	93.2	2.3	1.5	3.06	1.44
372.8/1223	1.95	1.64	2.45	15.9	33.0	94.3	1.9	1.1	2.87	1.34
381.6/1252*	1.94	1.61	2.46	16.7	34.3	92.4	2.0	9.4	2.90	1.45
388.6/1275	1.95	1.62	2.49	16.9	34.8	94.5	1.9	1.6	2.92	1.30
395.9/1299	1.95	1.66	2.53	14.8	34.3	84.2	5.4	0.4	2.71	1.29
402.9/1322	1.97	1.67	2.48	15.0	32.4	90.9	3.0	1.3	2.92	1.51
411.8/1351	1.89	1.56	2.46	17.1	36.6	88.2	4.3	1.1	2.80	1.31
419.1/1375	1.78	1.35	2.43	23.9	44.4	95.5	2.0	0.7	2.91	1.41
426.4/1399	1.86	1.50	2.43	19.3	38.4	93.4	2.53	0.9	2.68	1.27
434.6/1426	1.80	1.40	2.42	22.0	42.1	93.8	2.6	1.8	2.83	1.35
442.0/1450	1.91	1.60	2.43	16.3	34.2	91.0	3.1	1.7	3.03	1.45
449.6/1475	1.89	1.56	2.45	17.8	36.6	91.9	3.0	3.8	2.75	1.34
457.5/1501	1.88	1.55	2.44	17.7	36.6	91.0	3.3	2.8	2.72	1.34
464.2/1523*	1.71	1.53	2.46	10.6	37.9	47.9	19.7	6.2	2.55	1.52
472.4/1550	1.81	1.48	2.48	18.3	40.4	82.0	7.3	3.2	2.95	1.36
479.5/1573*	1.82	1.58	2.50	13.3	36.9	65.6	12.7	---	2.55	1.46
488.6/1603	1.89	1.54	2.46	18.8	37.6	93.3	2.4	---	2.85	1.38
494.4/1622	1.89	1.56	2.42	17.6	35.7	93.3	2.4	4.7	3.20	1.52
502.9/1650	1.86	1.51	2.49	18.9	39.4	89.2	4.3	2.6	2.88	1.43
510.5/1675	1.76	1.35	2.42	23.3	44.2	92.7	3.2	2.3	3.33	1.37
516.0/1693	1.75	1.36	2.40	22.5	43.5	90.5	4.1	3.7	2.71	1.25
525.5/1724	1.77	1.35	2.45	24.0	45.1	94.2	2.6	3.5	2.66	1.24
533.7/1751	1.72	1.28	2.42	25.7	47.2	93.7	3.0	---	2.74	1.24
541.3/1776	1.76	1.33	2.40	24.3	44.5	96.1	1.7	5.2	2.46	1.11
548.3/1799	1.75	1.33	2.40	24.2	44.7	94.7	2.4	2.8	2.57	1.19
556.6/1826	1.78	1.40	2.43	21.5	42.5	90.1	4.2	5.5	2.99	1.41
565.1/1854	1.79	1.39	2.40	22.2	42.0	94.7	2.2	2.3	2.64	1.22
570.6/1872	1.81	1.42	2.44	21.3	41.6	92.6	3.1	3.5	2.72	1.29
578.8/1899	1.82	1.44	2.46	21.1	4.6	92.3	3.2	5.0	2.07	1.53
586.1/1923*	1.83	1.57	2.40	14.2	34.6	75.2	8.6	1.8	3.43	1.76
593.4/1947	1.91	1.61	2.40	15.7	32.9	91.1	2.9	---	4.34	2.23
601.4/1973	1.81	1.41	2.43	22.3	42.1	95.8	1.8	4.7	3.43	1.68
609.0/1998	1.71	1.26	2.46	26.4	48.8	92.4	3.7	9.2	--	--
616.6/2023	1.69	1.20	2.40	28.8	49.9	97.6	1.2	2.4	2.63	1.15
625.8/2053	1.94	1.61	2.43	17.2	33.9	98.4	0.5	2.7	3.36	1.82
631.5/2072	1.99	1.74	2.42	12.7	28.2	89.6	2.9	---	3.72	2.05
637.0/2090	1.99	1.75	2.44	12.0	28.2	84.6	4.4	---	3.92	2.23

*Sample not sealed well.

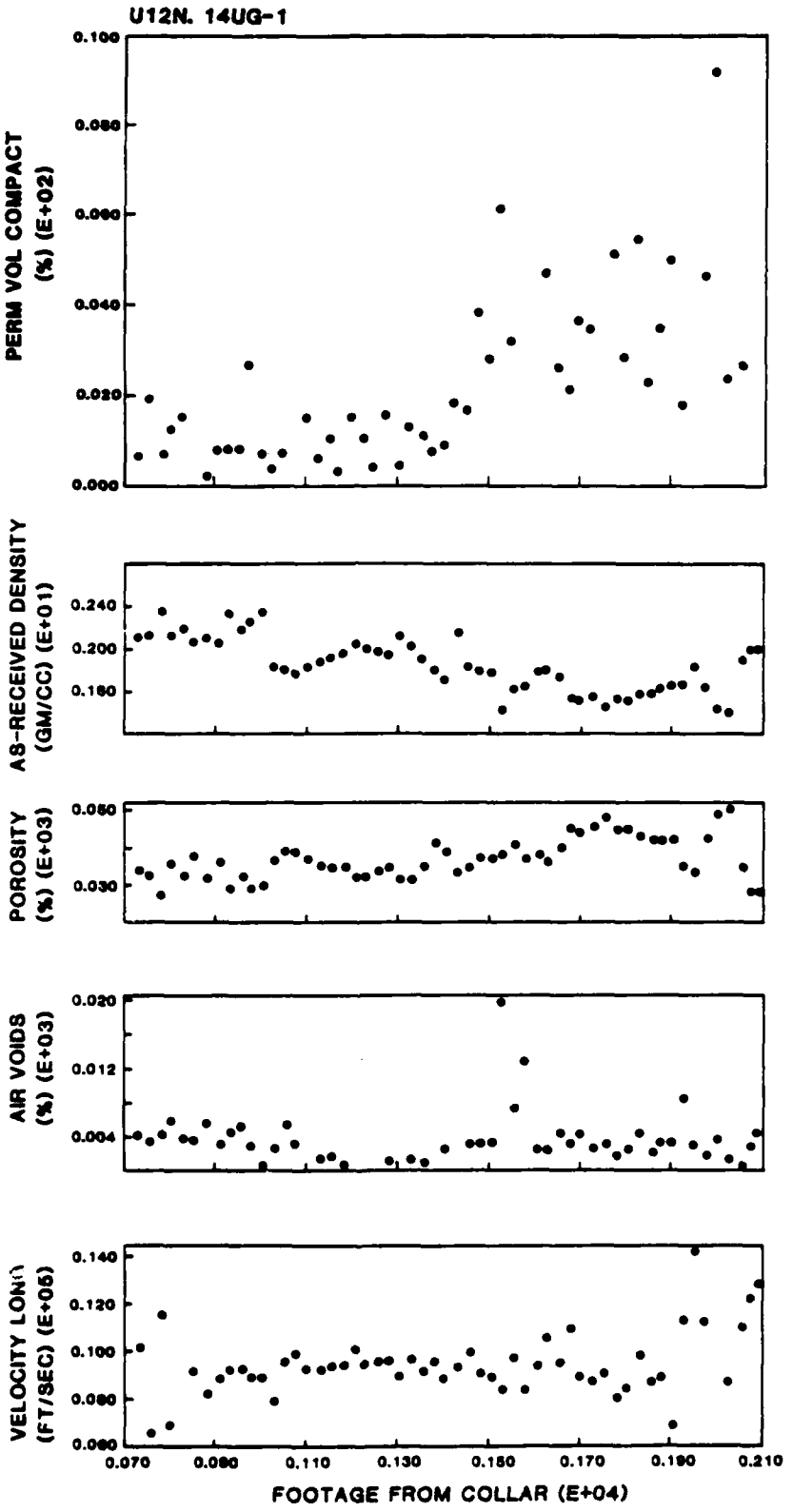

Figure 2.
U12N.14-UG-1. Selected Properties as a Function of Drill Hole Footage.

U12N.15UG-1, 2 and 3

Samples from drill holes U12N.15UG-1, 2 and 3 were received in June, 1981. These cores were subjected to uniaxial strain tests to 4 kbars confining pressure, and physical properties and ultrasonic wave velocity tests.

Tables 3-5 list the ultrasonic, physical properties and permanent compaction data for each footage from drill holes UG-1, UG-2 and UG-3, respectively. Summary plots for selected properties from these holes as functions of sample footage are shown in Figures 3-5.

Plots showing volume strain as functions of mean normal stress and the stress difference as functions of confining pressure are presented in Appendix C, Figures C1a-C10b.

Permanent compactions of the samples ranged between 0.4% and 3.1%. Peak stress differences ranged from 0.2 to 0.9 kbars.

Table 3

Physical Properties, Measured Permanent Compaction, and Ultrasonic Velocities on Samples from U12n.15 Ug-1

Drill Hole Footage (m/ft)	Density (gm/cc)			Water by Wet Weight (%)	Porosity (%)	Saturation (%)	Calc. Air Voids (%)	Meas. Permanent Comp. (%)	Velocity (km/sec)	
	As-Received	Dry	Grain						Long	Shear
2.8/9.2	2.06	1.76	2.56	14.5	31.2	95.7	1.3	0.4	2.74	1.16
10.7/35.2	1.82	1.46	2.34	19.8	37.6	95.8	1.6	2.0	2.75	1.23
18.8/61.7	1.85	1.50	2.33	18.7	35.5	97.6	0.9	1.4	2.71	1.15
25.5/83.5	1.86	1.51	2.39	18.8	36.8	95.0	1.8	1.7	3.12	1.48
33.8/111.0	1.85	1.50	2.40	18.9	37.5	93.3	2.5	1.8	2.62	1.09
41.8/137.2	1.85	1.52	2.32	18.0	34.6	96.2	1.3	1.9	3.58	1.79
49.3/161.7	1.87	1.54	2.32	17.6	33.6	98.0	0.7	1.5	2.67	1.12
56.4/184.9	1.95	1.67	2.35	14.5	29.1	97.3	0.8	2.3	3.32	1.70
63.2/207.4	1.96	1.64	2.42	16.2	32.1	98.8	0.4	1.2	2.92	1.33
70.1/230.0	2.17	1.92	2.58	11.6	25.7	98.1	0.5	2.4	2.82	1.17
77.2/253.5	2.09	1.85	2.46	11.5	24.8	96.9	0.8	0.6	3.31	1.59
86.6/284.0	2.50	2.49	2.55	0.2	2.16	23.2	1.7	---	5.84	3.62

Table 4

Physical Properties, Measured Permanent Compaction, and Ultrasonic Velocities on Samples from U12n.15 Ug-2

Drill Hole Footage (m/ft)	Density (gm/cc)			Water by Wet Weight (%)	Porosity (%)	Saturation (%)	Calc. Air Voids (%)	Meas. Permanent Comp. (%)	Velocity (km/sec)	
	As-Received	Dry	Grain						Long	Shear
1.8/5.9	2.12	1.84	2.61	13.4	29.7	95.8	1.3	1.5	3.03	1.47
9.3/30.5	1.86	1.60	2.18	13.8	26.5	97.0	0.8	1.0	3.25	1.57
16.4/53.7	1.89	1.57	2.38	17.0	34.1	94.3	1.9	0.8	2.64	1.16
25.4/83.2	1.92	1.59	2.42	17.3	34.4	96.6	1.2	2.9	2.93	1.26
30.8/101.2	1.84	1.51	2.29	17.7	33.9	96.2	1.3	1.7	3.86	2.27
38.3/125.5	1.80	1.42	2.32	29.9	38.6	97.4	1.0	3.0	2.63	1.06
44.3/145.5	1.85	1.48	2.38	20.0	37.6	97.8	0.8	1.0	2.68	1.13

Table 5

Physical Properties, Measured Permanent Compaction, and Ultrasonic Velocities on Samples from U12n.15 Ug-3

Drill Hole Footage (m/ft)	Density (gm/cc)			Water by Wet Weight (%)	Porosity (%)	Saturation (%)	Calc. Air Voids (%)	Meas. Permanent Comp. (%)	Velocity (km/sec)	
	As-Received	Dry	Grain						Long	Shear
1.9/6.2	1.96	1.66	2.37	15.1	29.8	99.4	0.2	1.2	2.98	1.39
7.6/25.0	1.94	1.66	2.34	14.6	29.2	97.0	0.9	0.9	2.83	1.36
14.8/48.6	1.93	1.66	2.33	14.2	28.9	94.7	1.5	2.5	3.01	1.51
23.2/76.0	1.95	1.64	2.38	15.8	31.0	99.4	0.2	1.4	2.87	1.39
37.5/123.1	1.93	1.60	2.40	16.9	33.2	98.3	0.6	3.1	3.19	1.64
45.0/147.7	1.93	1.63	2.36	15.4	30.8	96.5	1.1	1.7	2.46	1.02

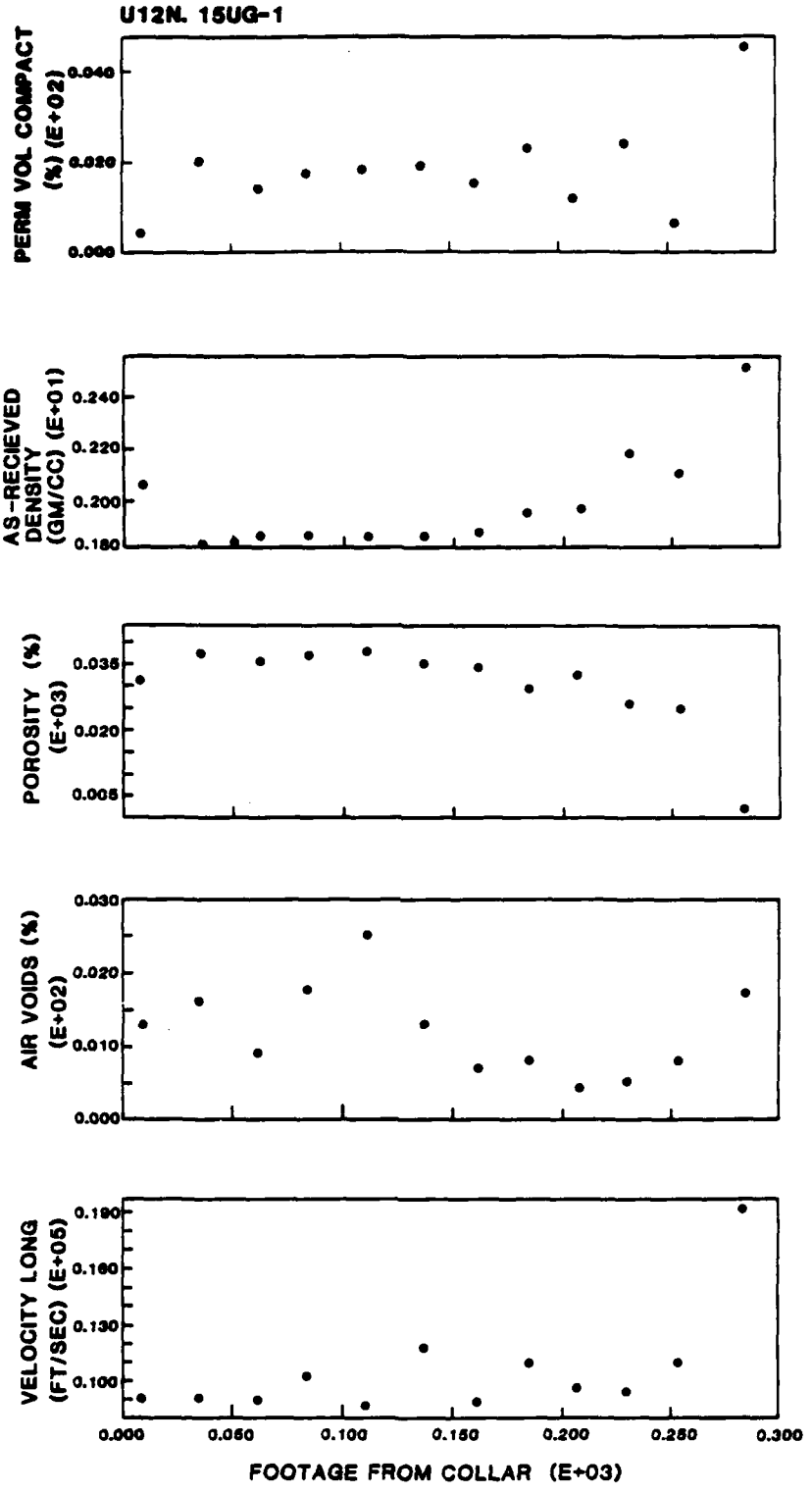

Figure 3.
U12N.15-UG-1. Selected Properties as a Function of Drill Hole Footage.

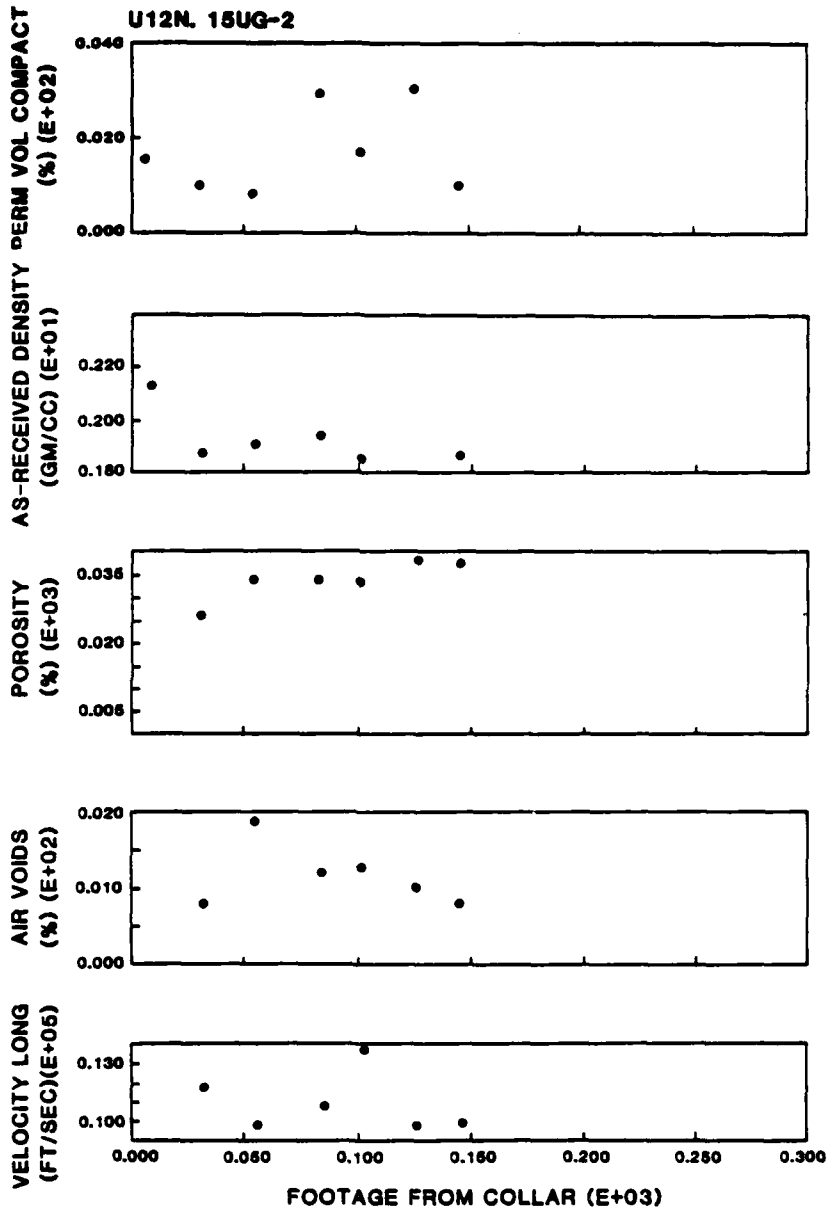

Figure 4.
U12N.15-UG-2. Selected Properties as a Function of Drill Hole Footage.

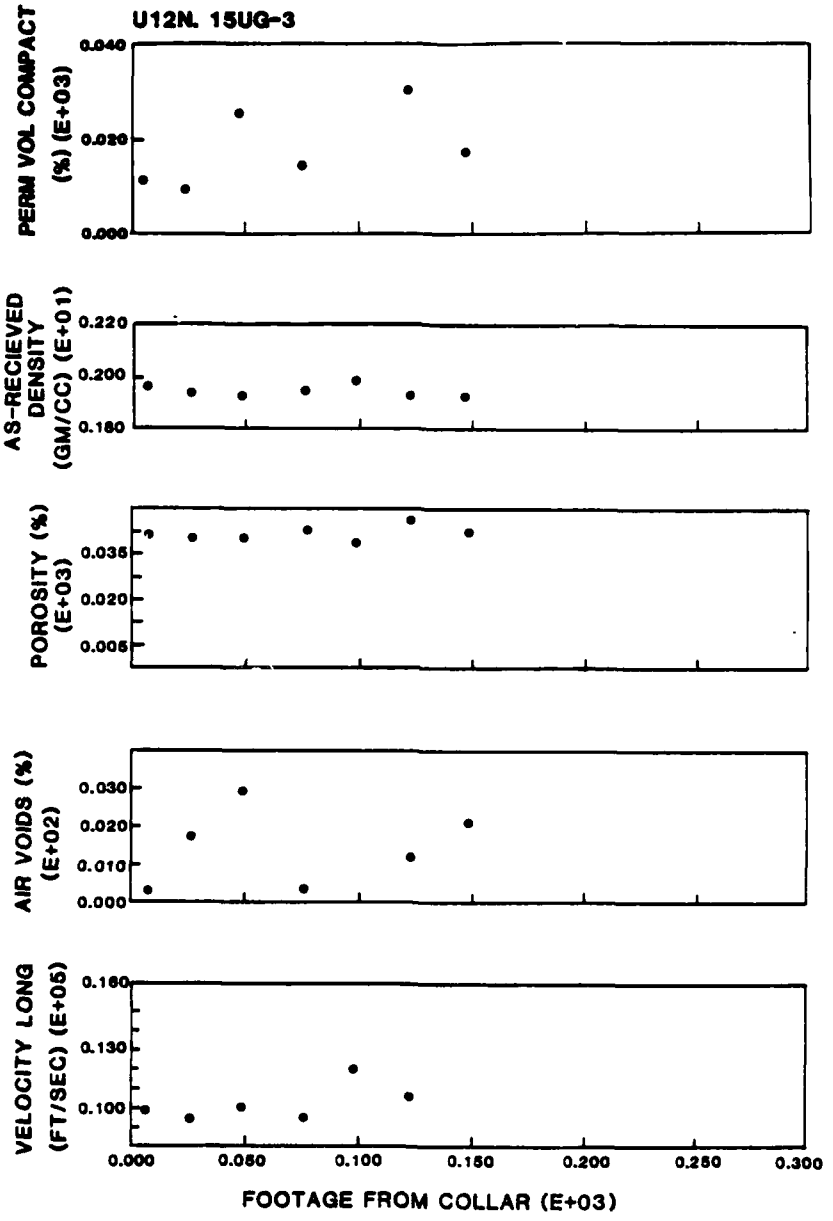

Figure 5.
U12N.15-UG-3. Selected Properties as a Function of Drill Hole Footage.

Testing Procedures

Sample Handling and Preparation Techniques - Samples of tuff as-received have been wrapped in foil and sealed in beeswax in the field. Density and moisture content were determined from small pieces (i.e. ~50 cm^3) chipped from the core. Mechanical test specimens were cut to 2.5 inch (6.4 cm) length using a diamond cut-off saw and water coolant. The ends were subsequently ground to be parallel to within 0.001 inches (0.0025 cm). After cutting and grinding, specimens were wrapped in a urethane jacket and mounted to steel endcaps. The jacket was then sealed to the endcaps with rubber tape and wire.

Physical Properties Determination - The "as-received" density was determined by weighing the chipped-off test specimen, coating it with wax, and measuring its volume using mercury displacement. The same specimen was then stripped of wax, weighed, and dried in an oven at 105°C for 24 hours. From the dried sample weight, the percentage water by wet weight (% H_2O) was determined. The piece was then crushed and pulverized (100 mesh) to determine grain density. Grain volume was measured by water immersion and gas evacuation. All weights were determined to ±0.05 percent accuracy; volumes are accurate to ±1.0 percent.

Nomenclature and equations used for the measured and calculated physical properties are as follows:

Nomenclature

$*\rho_w$ = in-situ bulk density (wet or "as-received" density)(gm/cm^3)

$*\rho_g$ = grain density (density of solids)(gm/cm^3)

ρ_{H_2O} = density of water (gm/cm^3)

$*w$ = moisture content (percent by wet weight)

*Measured parameters.

ρ_d = dry bulk density after oven drying (gm/cm^3)

η_t = total porosity (percent of total rock volume)

S_r = degree of saturation (percent of void volume)

V_{av} = air void content (percent of total rock volume)

Equations

$$\rho_d = \rho_w \left(1 - \frac{w}{100}\right)$$

$$\eta_t = 100 \times \left(1 - \frac{\rho_d}{\rho_g}\right)$$

$$S_r = 100 \times \frac{(w \times \rho_w)}{(\eta_t \times \rho_{H_2O})}$$

$$V_{av} = 100 \times [1 + \rho_d (1 - 1/\rho_g) - \rho_w]$$

Mechanical Tests - All mechanical tests were conducted using a servo-controlled hydraulic press in combination with a servo-controlled intensifier as shown in Figures 6 and 7, respectively. A variety of different tests are possible with this machine, including hydrostatic and triaxial compression and uniaxial strain. The upper loading actuator has a 130,000 pound capacity and the pressure vessel is capable of 60,000 pounds per square inch, or about 4 kilobars (400 MPa).

Data are recorded using X-Y recorders. Signal conditioning equipment and calibration methods provide an accuracy of ±2% on pressure and stress measurements.

Strain Measurements - Strains are measured using cantilever arms inside the pressure vessel. A schematic diagram of a mechanical test specimen with axial and transverse strain cantilevers is shown in Figure 8. A photograph of a test specimen is shown in Figure 9.

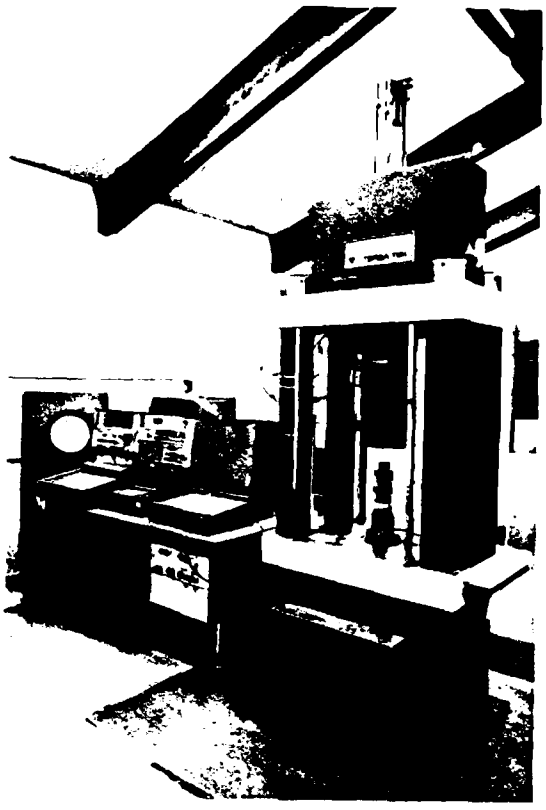

Figure 6. 4 Kbar Test Machine with Associated Electronic Equipment.

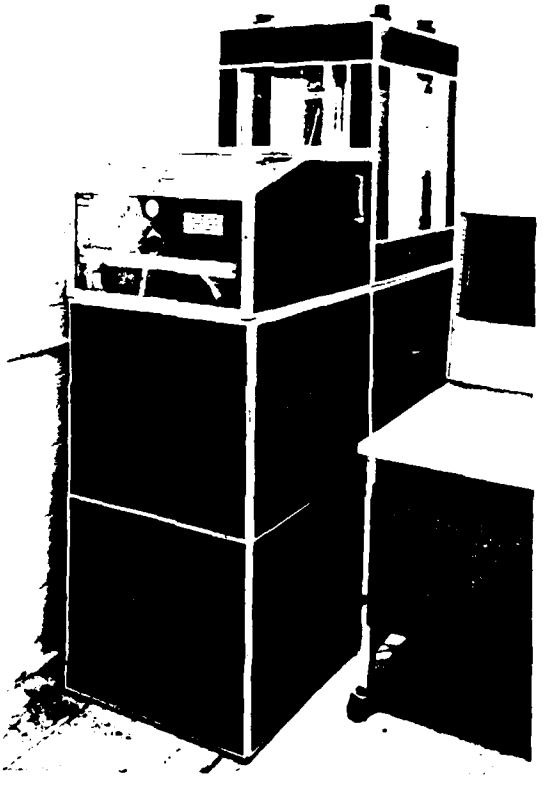

Figure 7. 4 Kbar Pressure Intensifier.

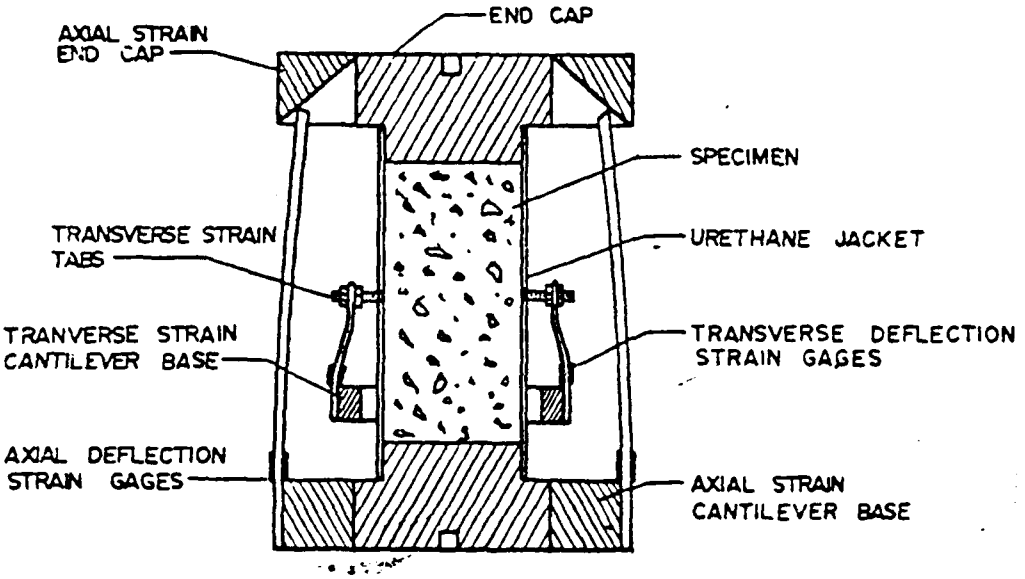

Figure 8. Schematic Drawing of a Specimen with the Axial and Transverse Strain Transducers.

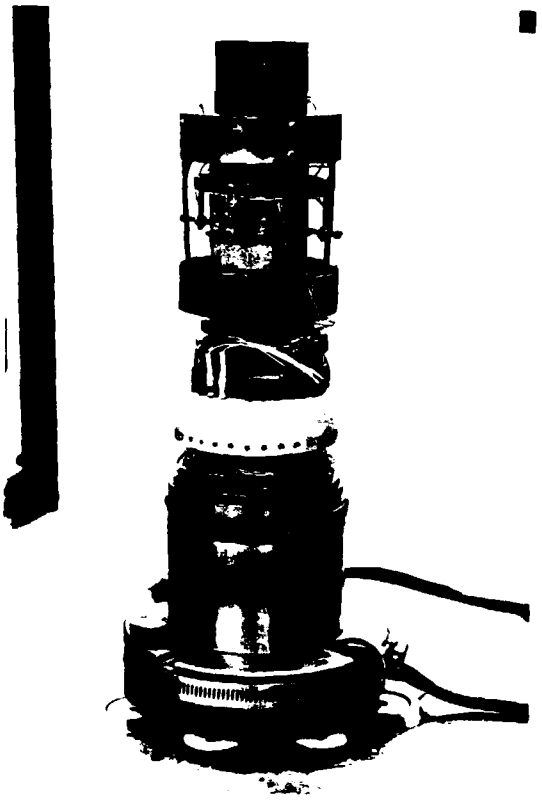

Figure 9. Test Sample with Axial and Transverse Strain-measurement Cantilevers.

Data Presentation - Data are plotted as either hydrostatic pressure or mean normal stress versus volume change, stress difference versus individual strains, or stress difference versus confining pressure where compressive stresses and shortening strains are positive. Here σ_1, σ_2, σ_3 and ε_1, ε_2, ε_3 refer to principal stresses and strains, respectively. For all tests, σ_1 and ε_1 refer to axial direction, and $\sigma_2 = \sigma_3$ are the lateral stresses applied by the liquid pressure. The term ε_2, which for an isotropic material is assumed equal to ε_3, refers to transverse strain. Other terms frequently used in the text are defined as follows:

Mean normal stress $= \dfrac{(\sigma_1 + \sigma_2 + \sigma_3)}{3}$

Volume strain $= \varepsilon_1 + \varepsilon_2 + \varepsilon_3$

$= \varepsilon_1$ (for uniaxial strain loading)

Stress difference $= \sigma_1 - \sigma_3$

Confining pressure $= \sigma_3$

Ultrasonic Velocities - The through-transmission technique is employed to obtain ultrasonic velocity data; the system used to obtain the data is shown schematically in Figure 10. The main advantage of this technique is the high accuracy with which wave transit time can be measured. The received signal is viewed (on the oscilloscope) alternately with the signal from the variable frequency synthesizer after it has passed through a shaper. The shape of the latter is adjusted for an exact match of the initial wave arriving through the specimen. The pulse that excites the transmitting transducer is next viewed and its shape matched to that of the comparison wave. Once this is done, the frequency of the synthesizer is adjusted for an exact number of cycles between the transmitted and received waves. The number of cycles divided by the frequency is the transit time through the specimen.

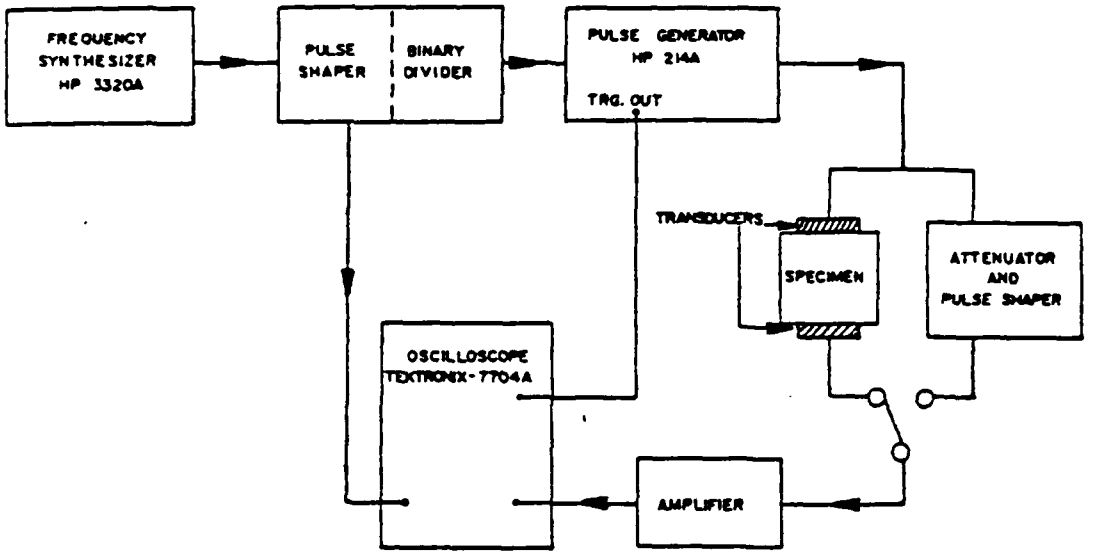

THROUGH TRANSMISSION SYSTEM

Figure 10. Schematic of Ultrasonic Velocity Measuring Equipment.

The ultrasonic longitudinal and shear wave transit times are measured and, along with the specimen length and density, can be used to calculate the apparent Poisson's ratio, ν, and Young's modulus, E, as follows:

$$\nu = \frac{(V^2_l) - 2\,(V^2_s)}{2\,(V^2_l - V^2_s)}$$

V_l = longitudinal velocity

V_s = shear velocity

$$E = 3\rho V^2_s\,(V^2_l - \tfrac{4}{3}\,V^2_s)/(V^2_l - V^2_s)$$

where ρ is the specimen density.

APPENDIX A - UE12N#12

UNIAXIAL COMPRESSION DATA (36 TESTS)

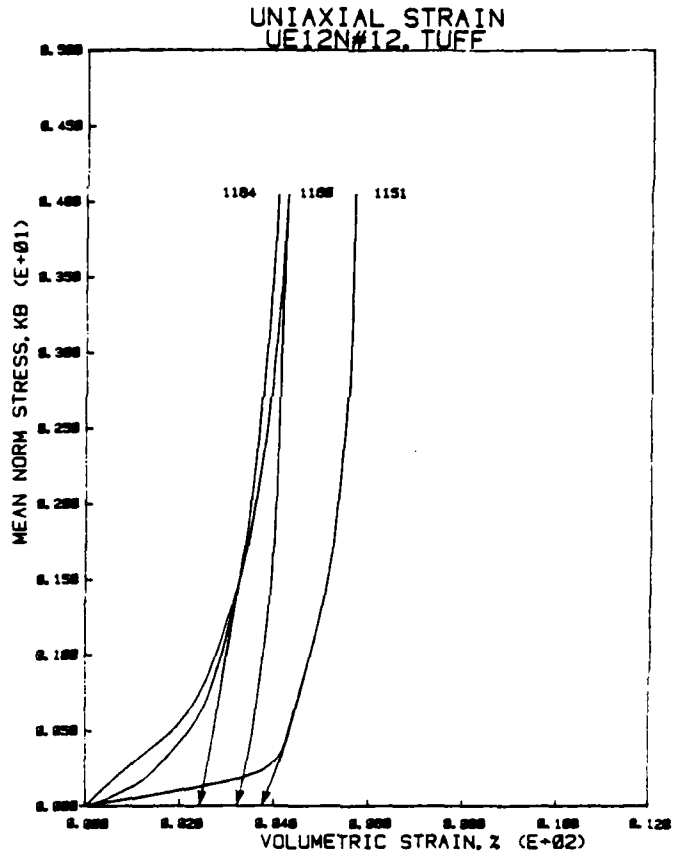

Figure A1a

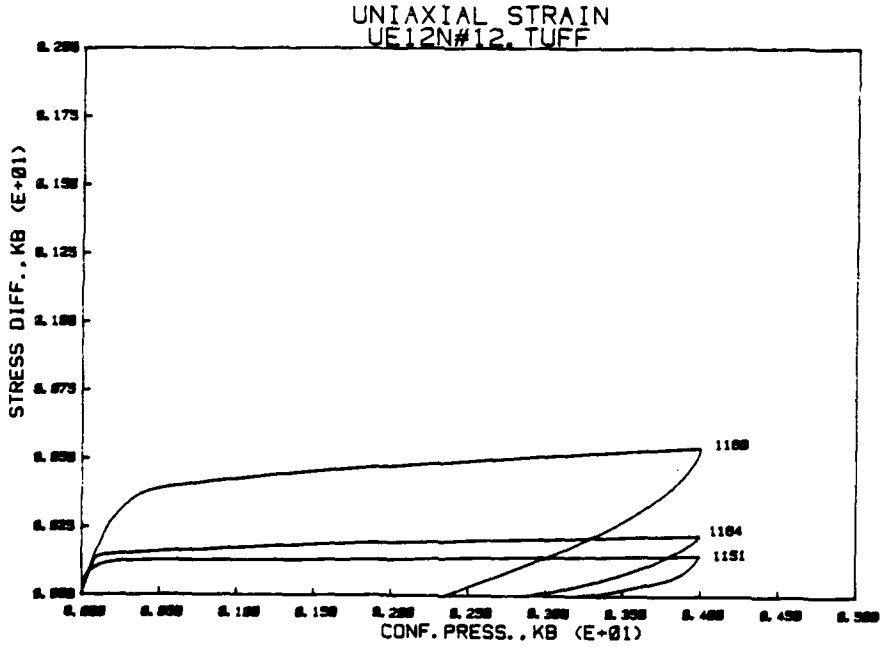

Figure A1b

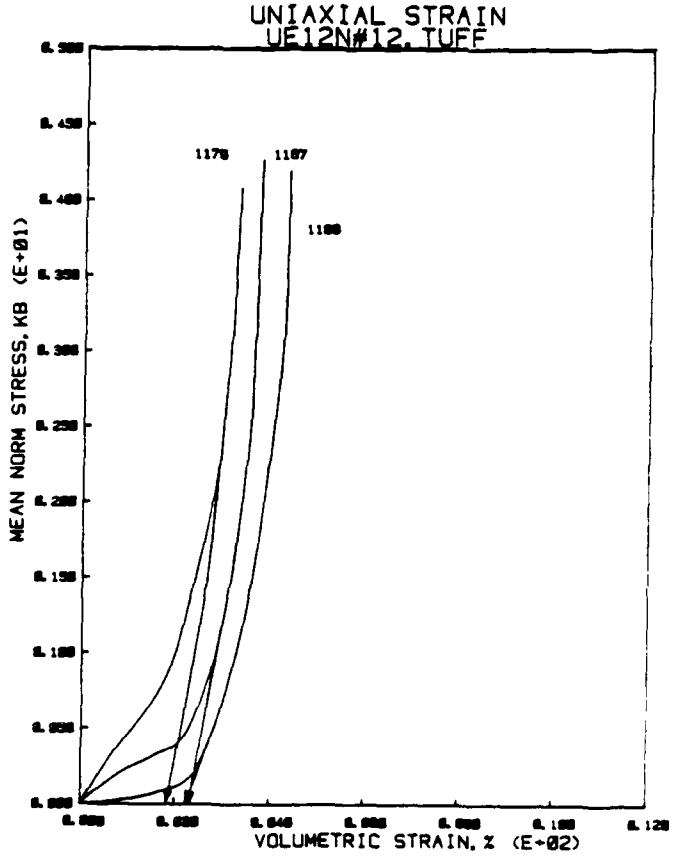

Figure A2a

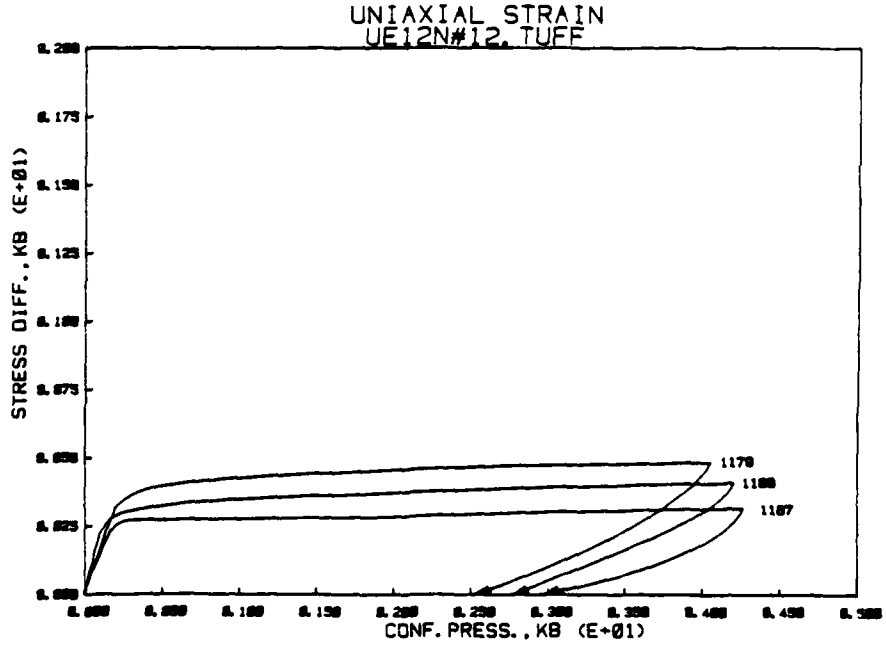

Figure A2b

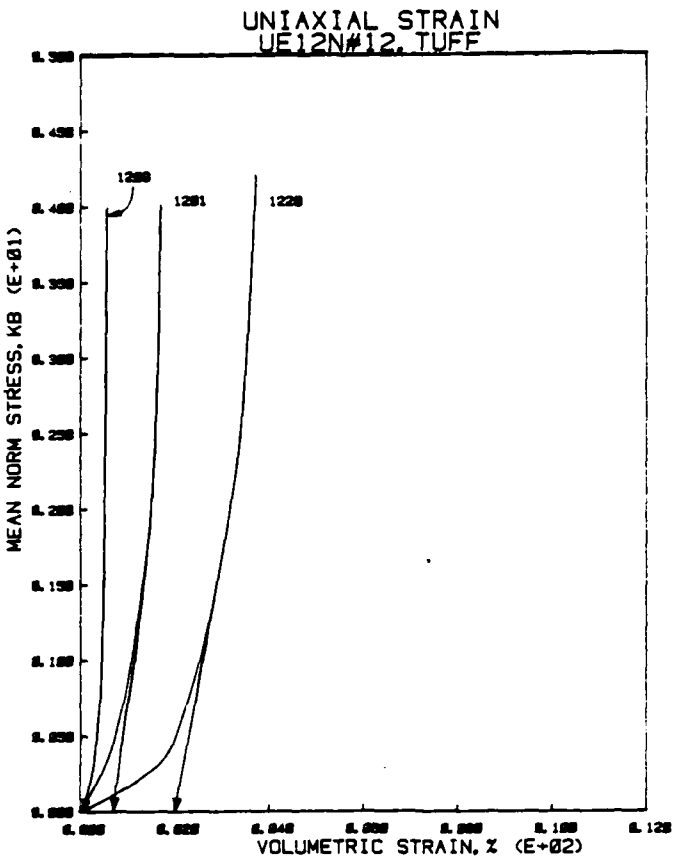

Figure A3a

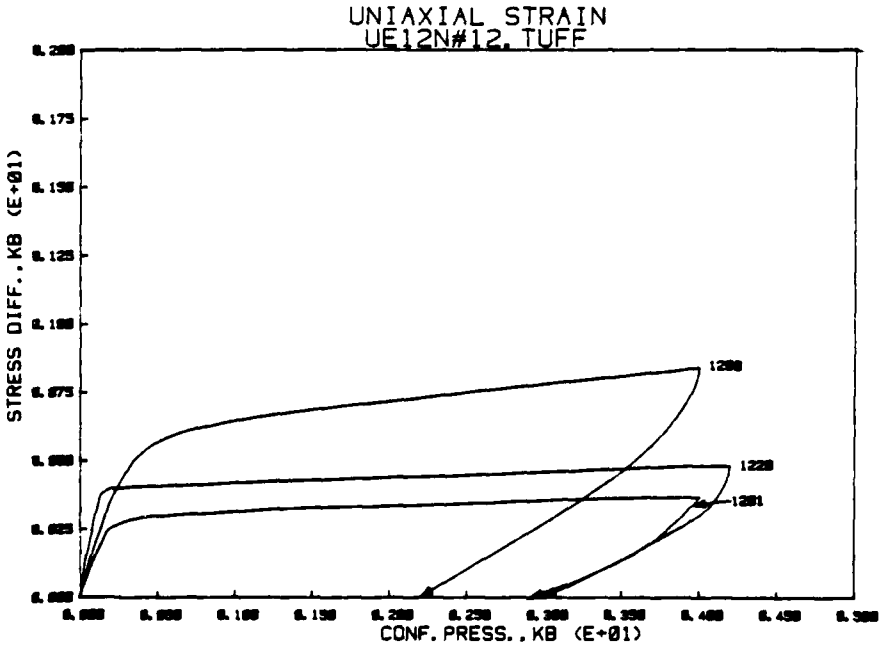

Figure A3b

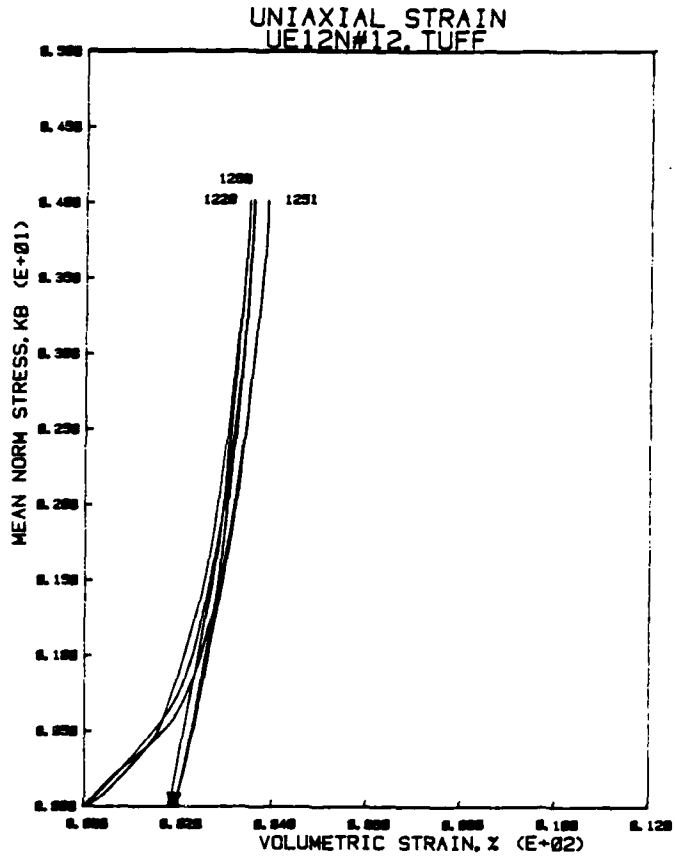

Figure A4a

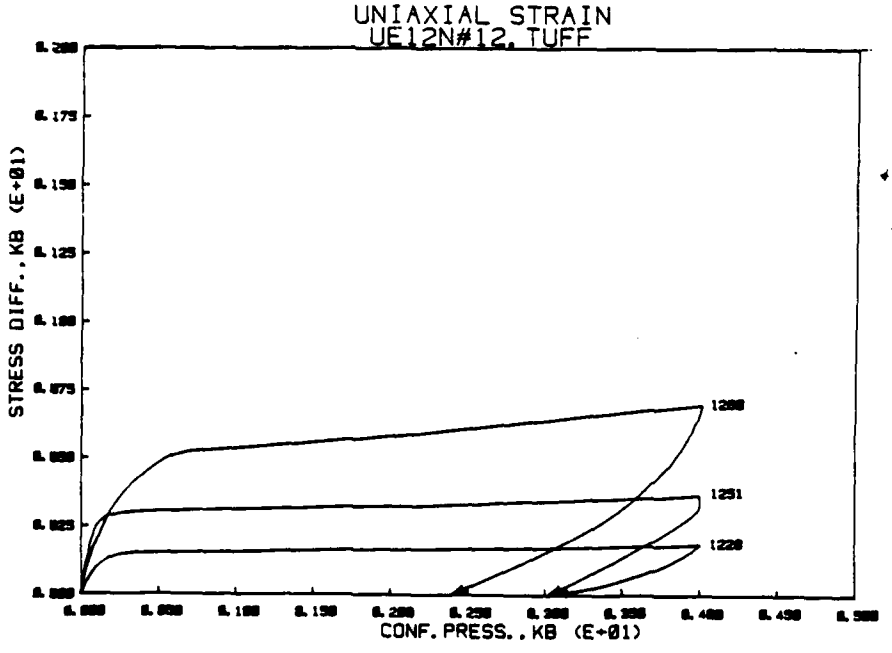

Figure A4b

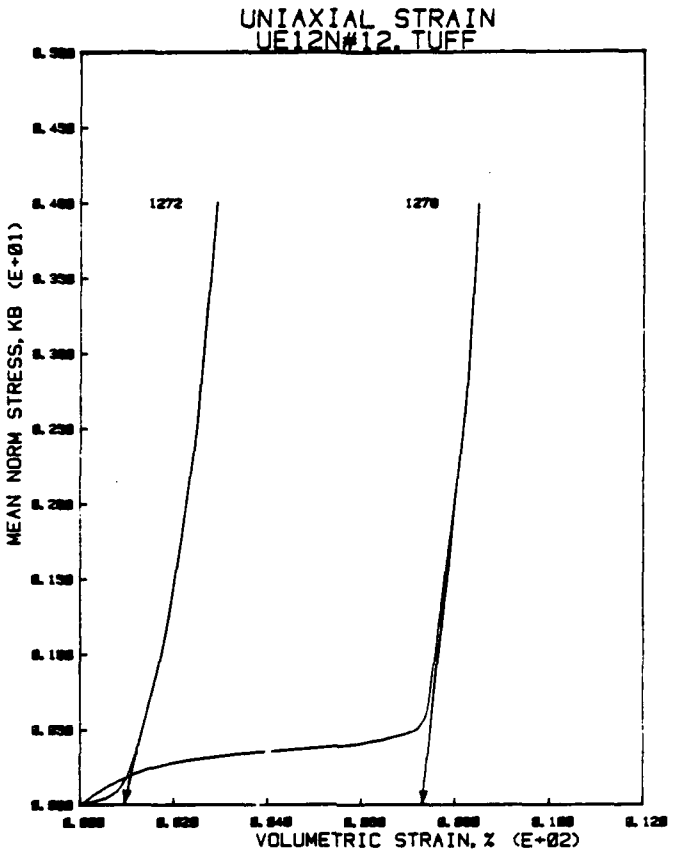

Figure A5a

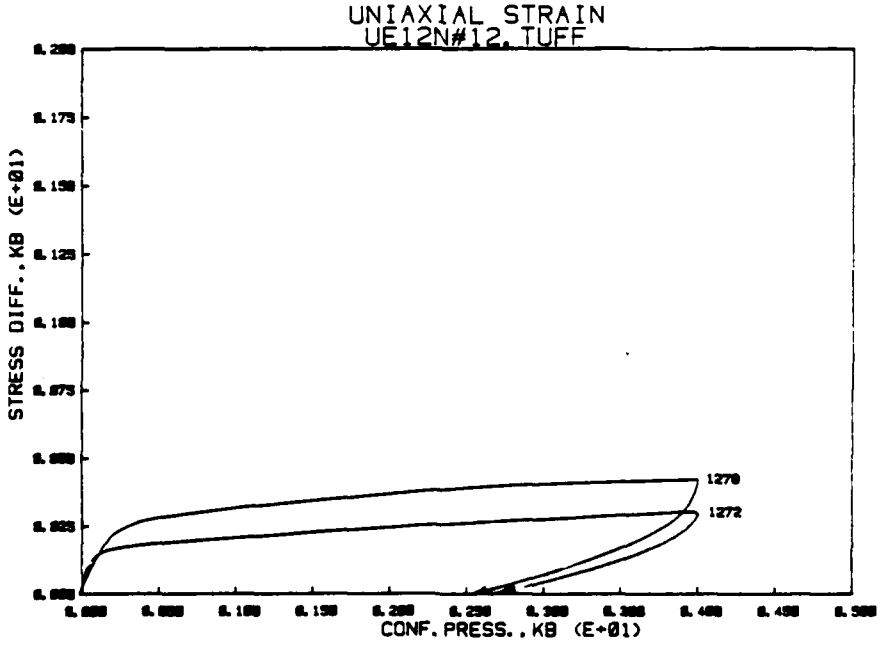

Figure A5b

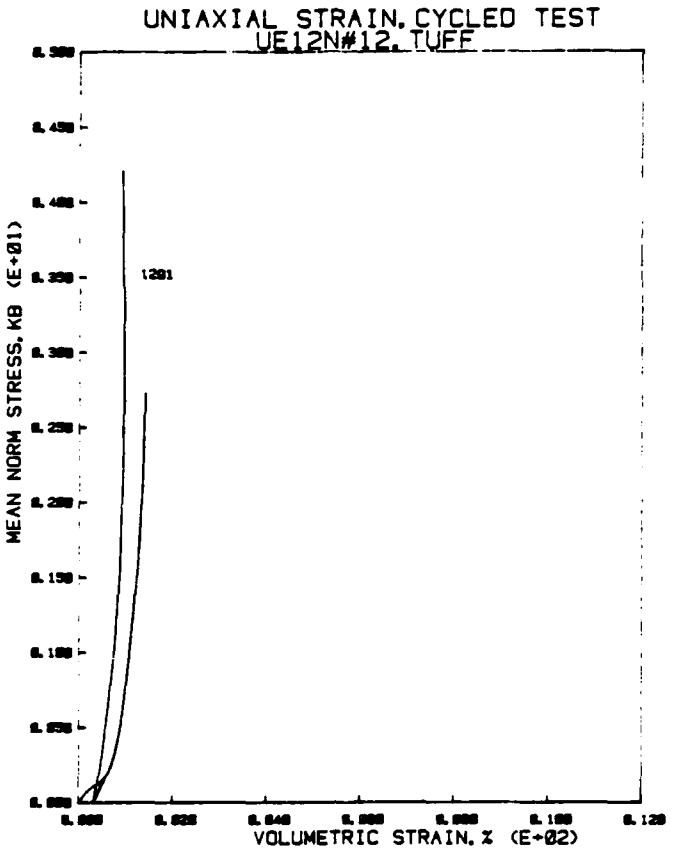

Figure A6a

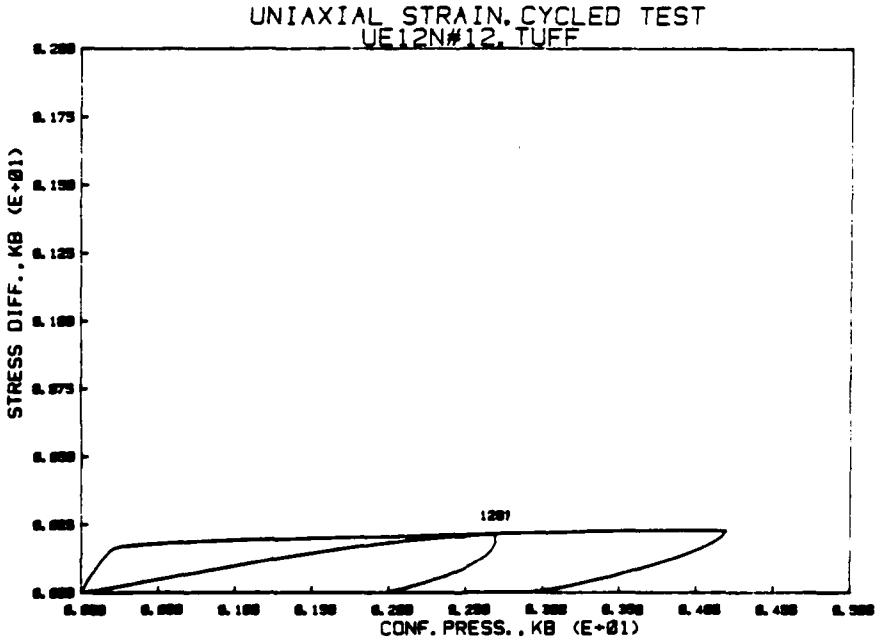

Figure A6b

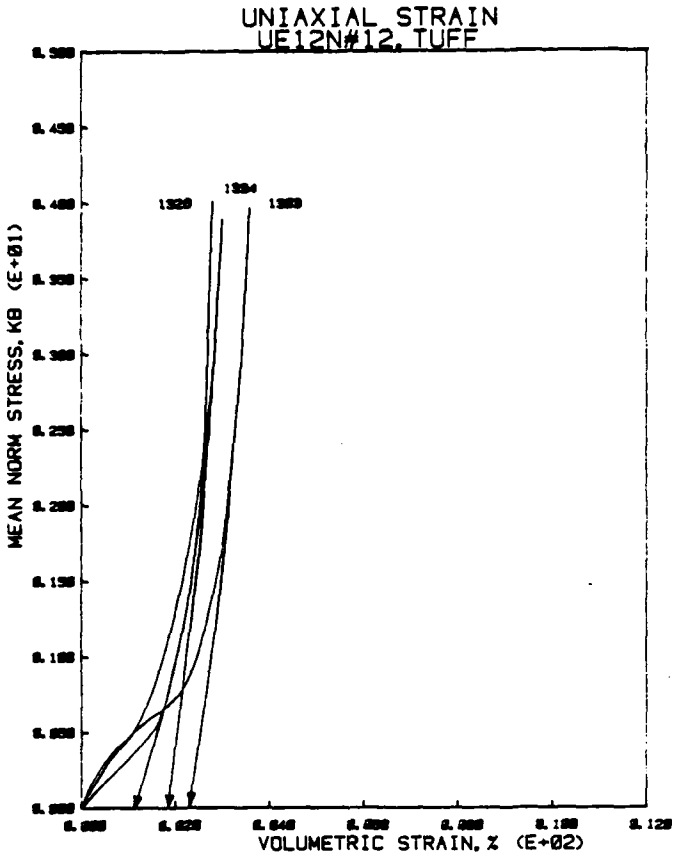

Figure A7a

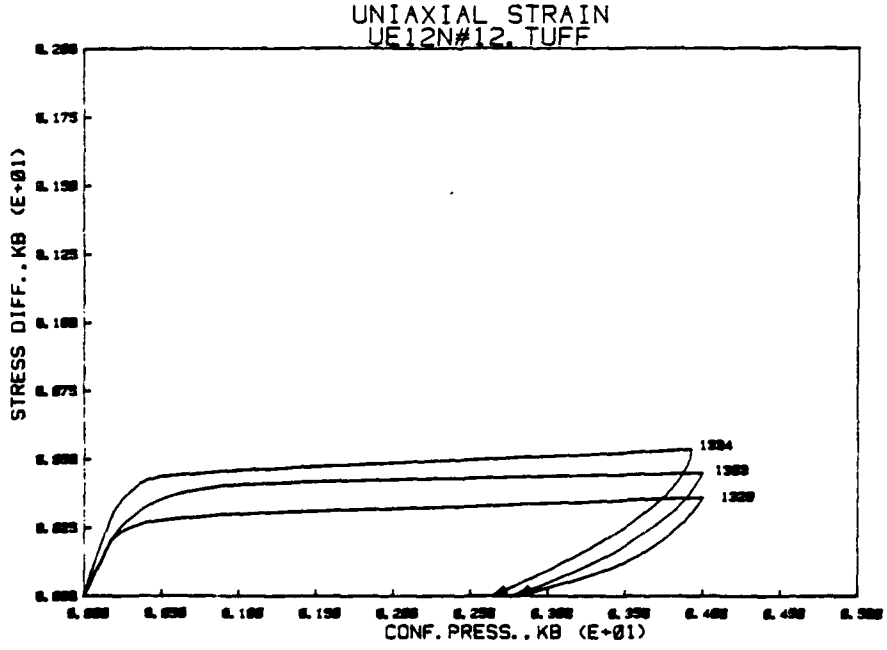

Figure A7b

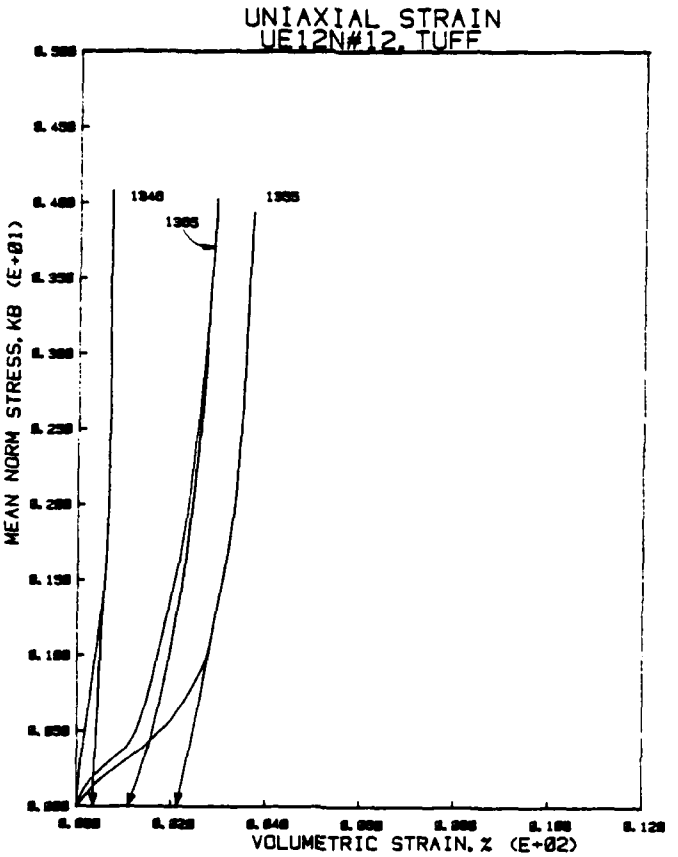

Figure A8a

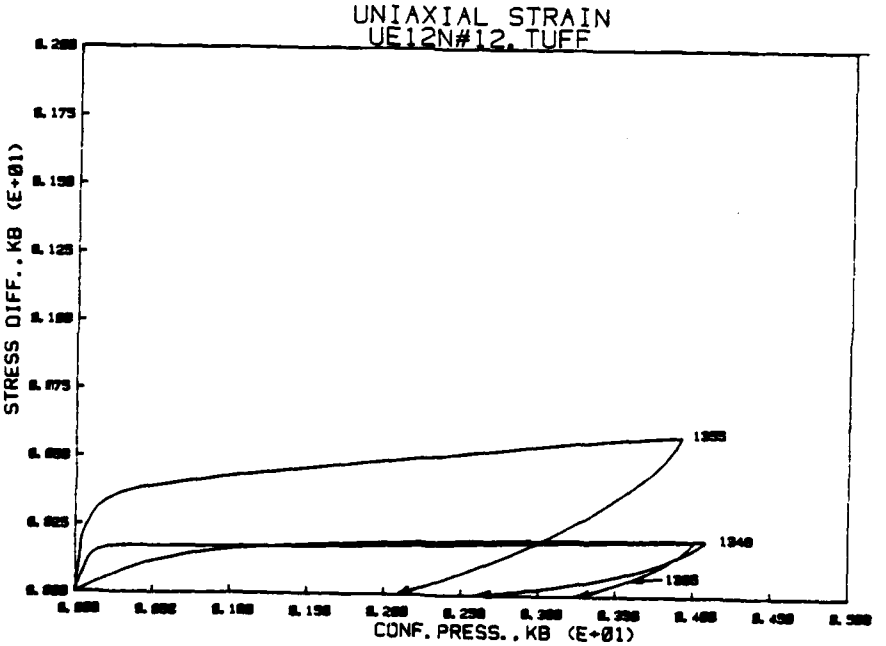

Figure A8b

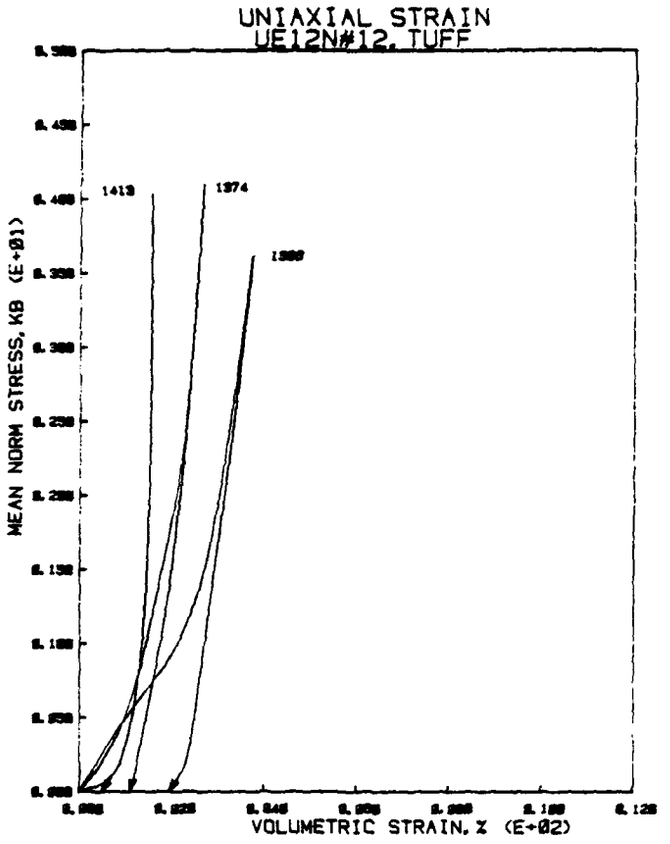

Figure A9a

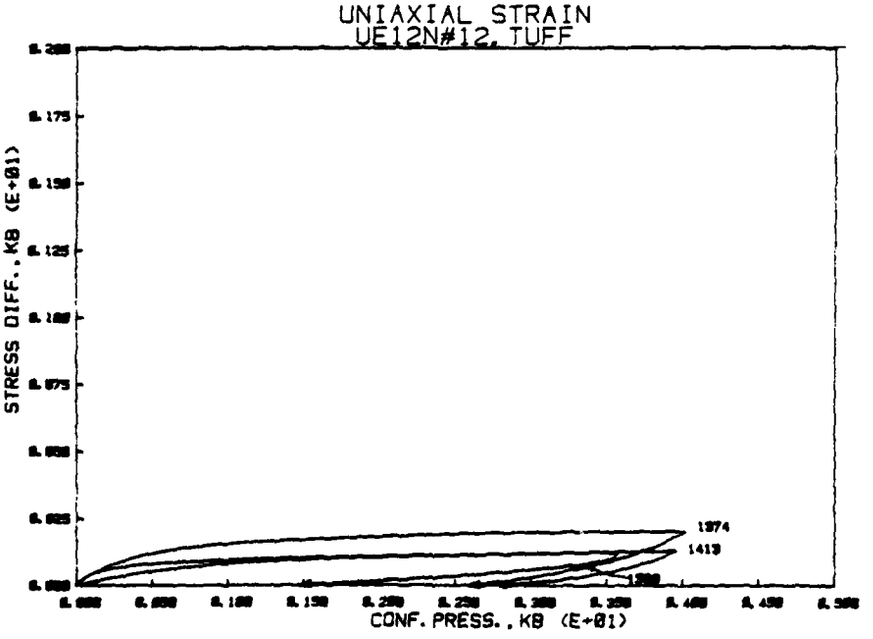

Figure A9b

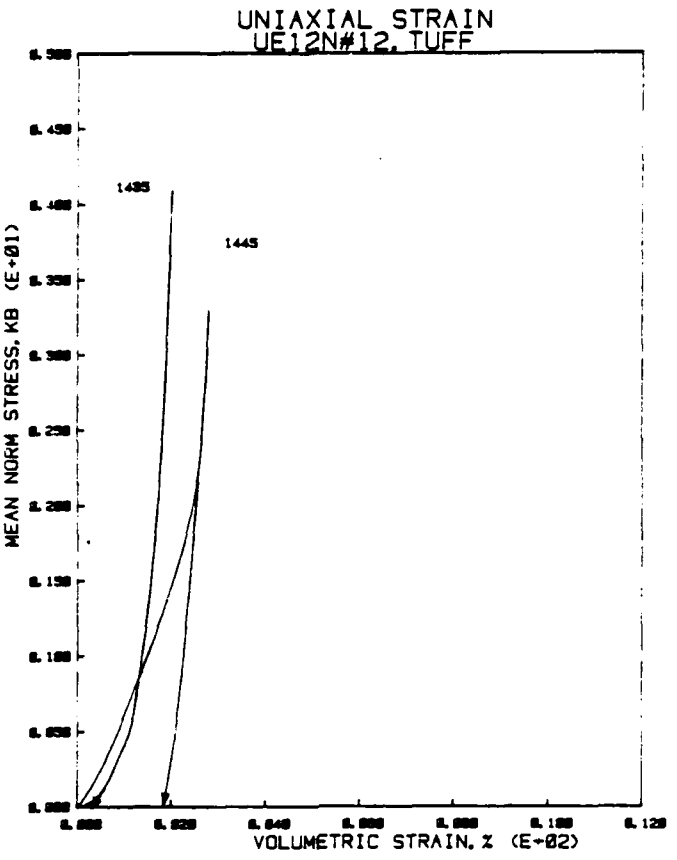

Figure A10a

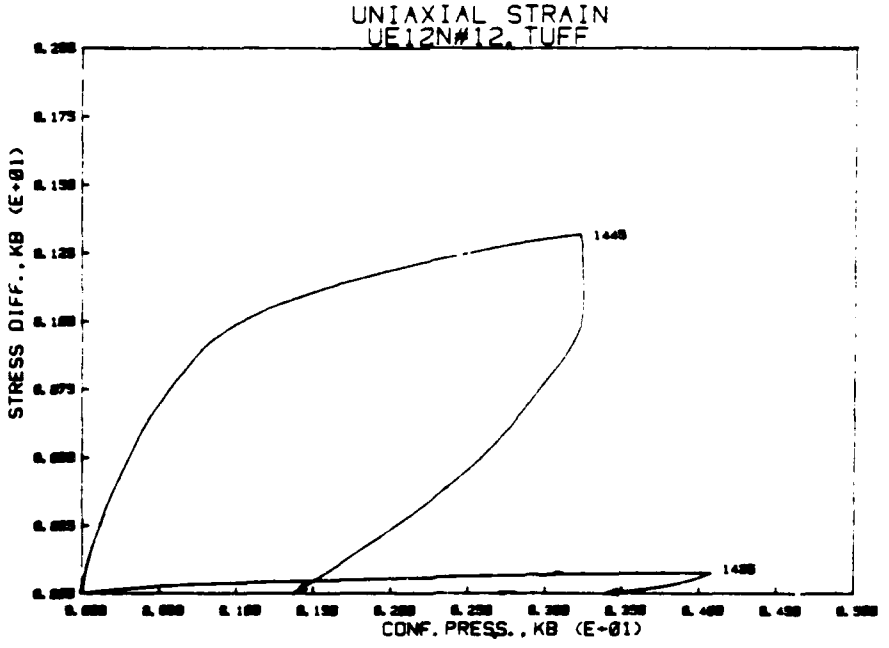

Figure A10b

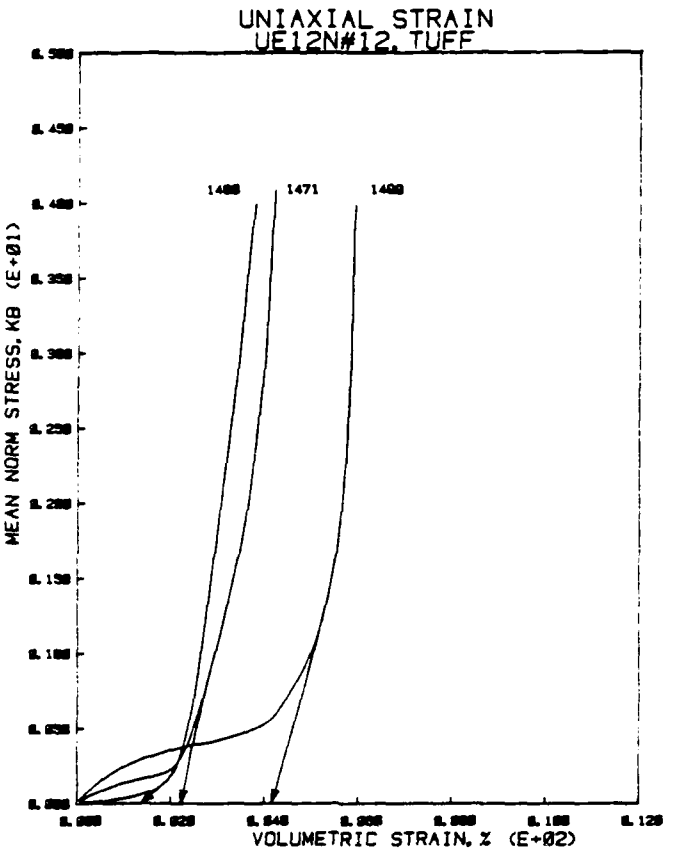

Figure A11a

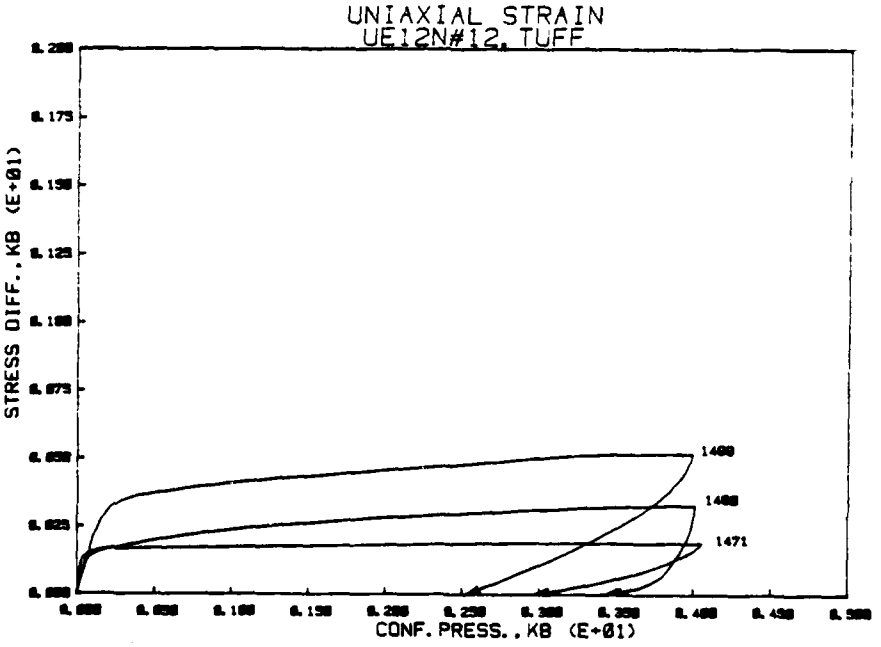

Figure A11b

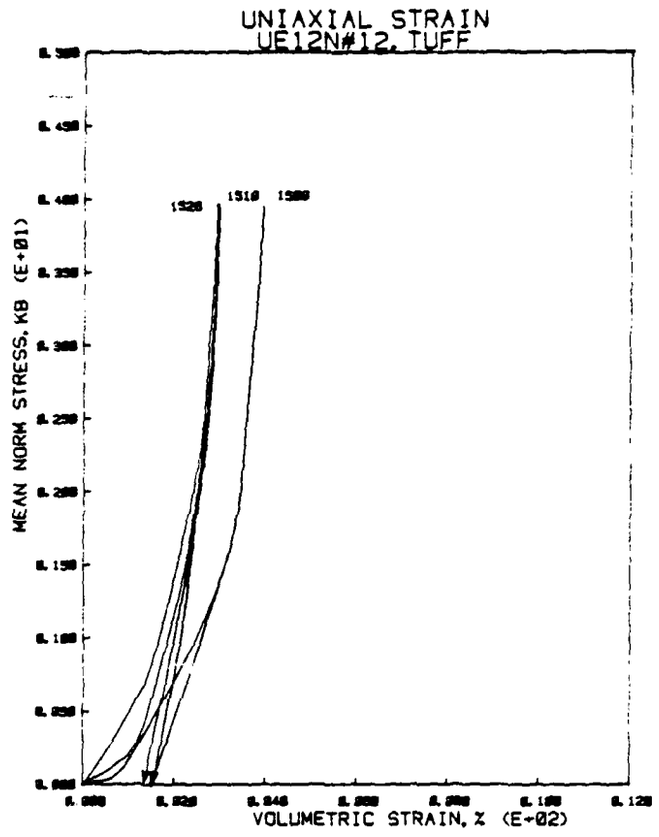

Figure A12a

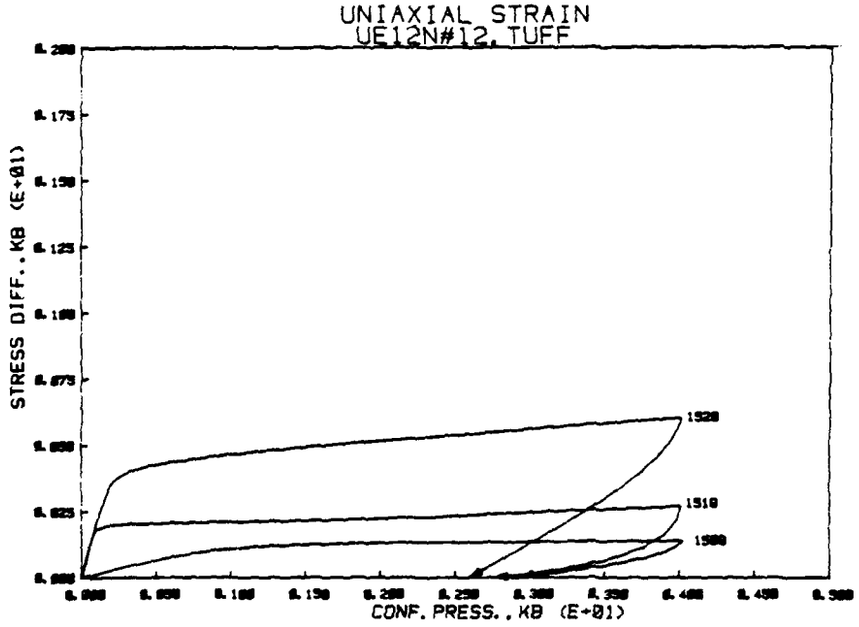

Figure A12b

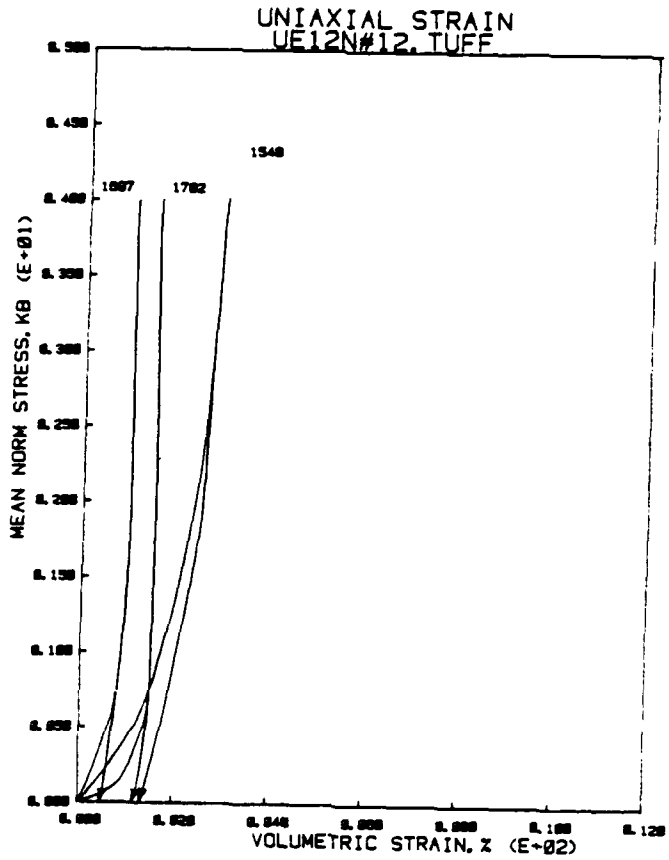

Figure A13a

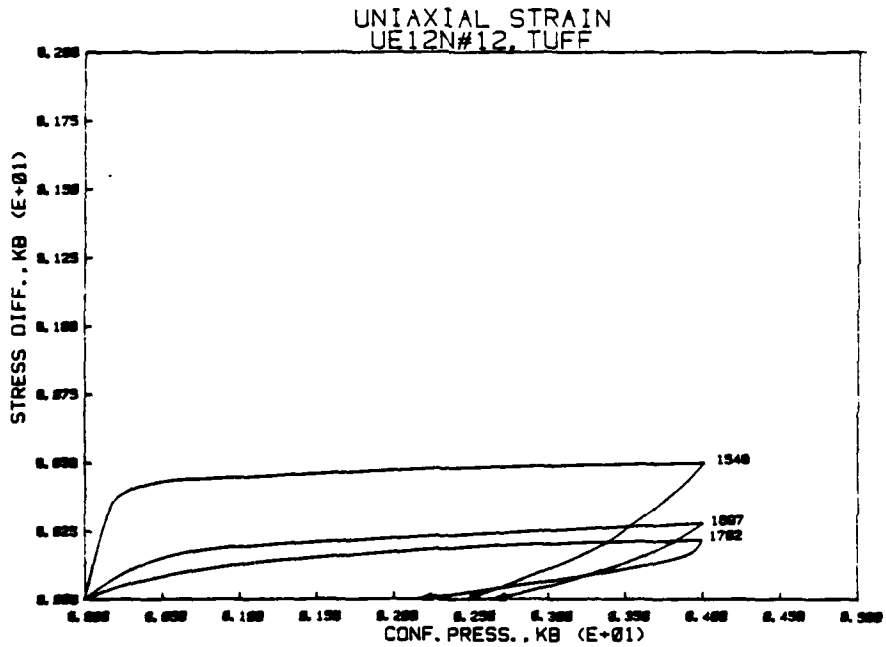

Figure A13b

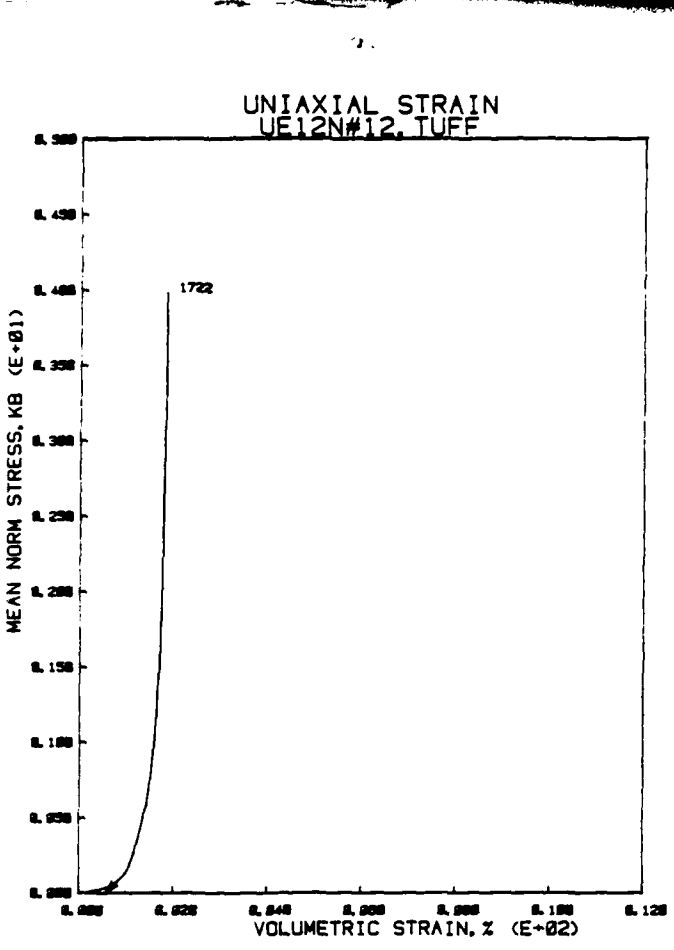

Figure A14a

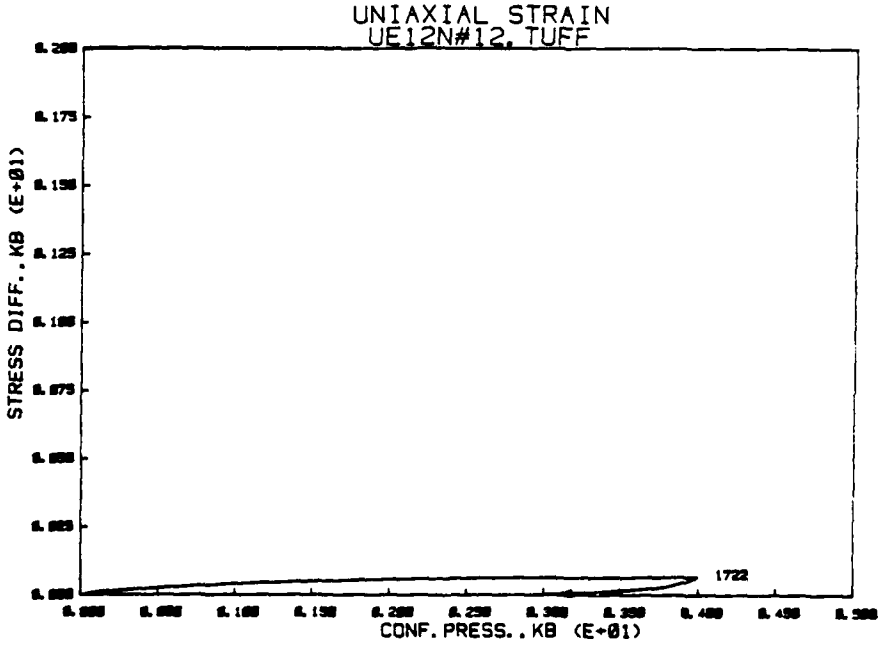

Figure A14b

APPENDIX B - U12N.14-UG-1

UNIAXIAL COMPRESSION DATA (45 TESTS)

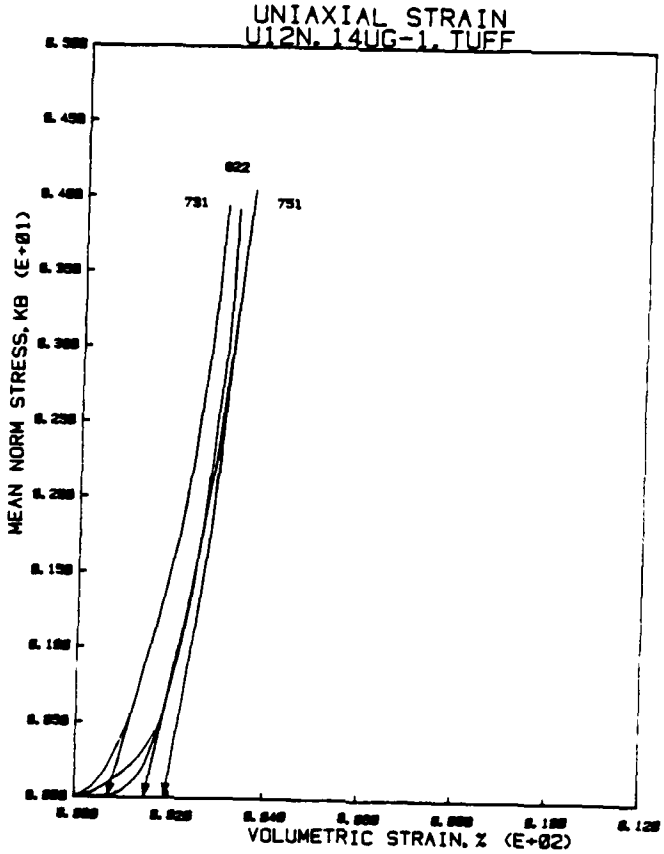

Figure B1a

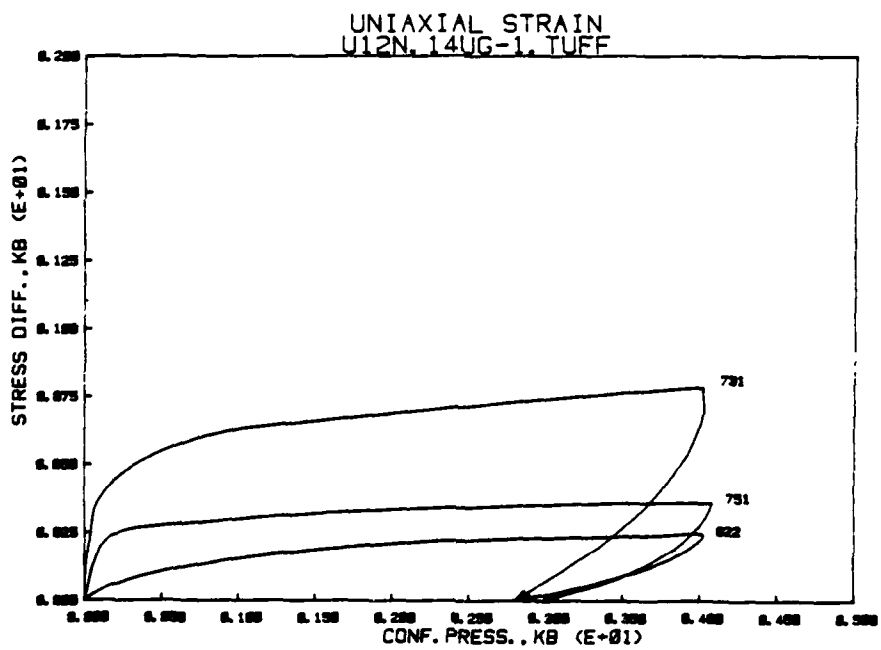

Figure B1b

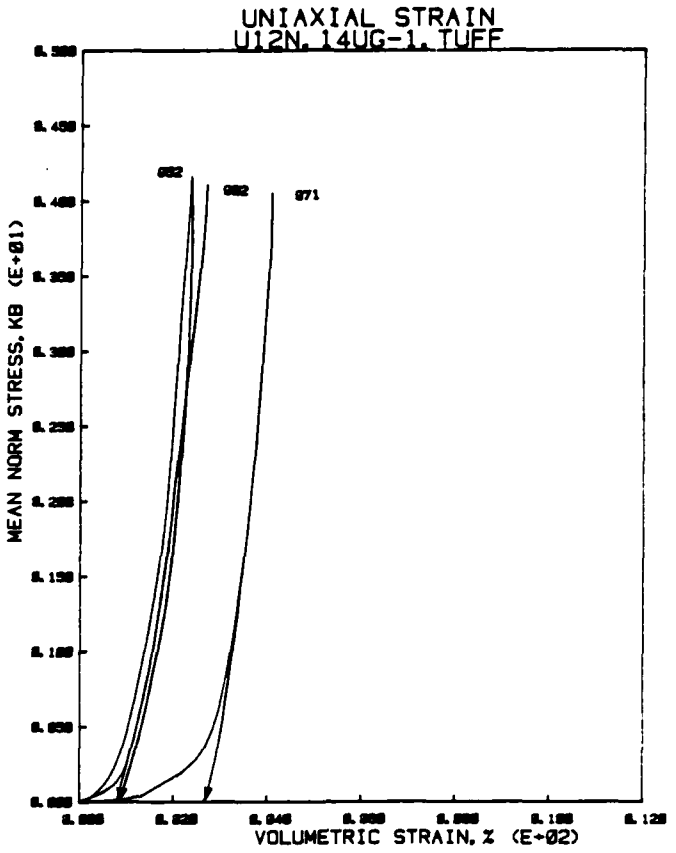

Figure B2a

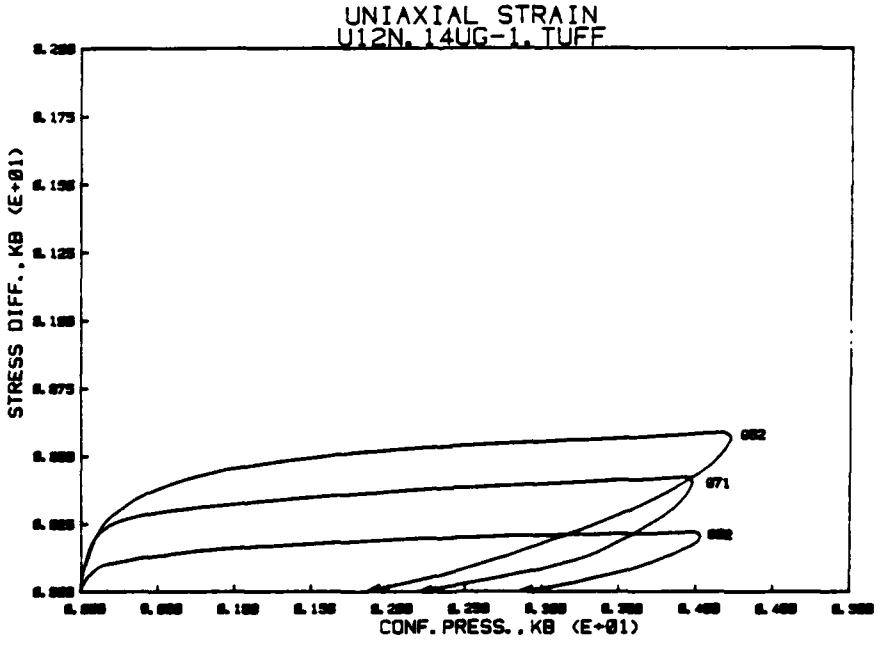

Figure B2b

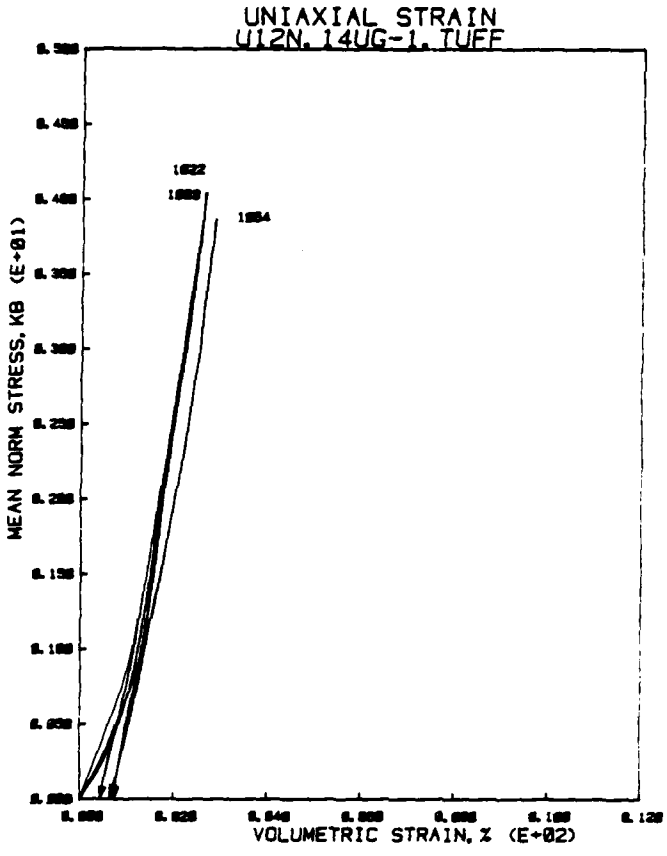

Figure B3a

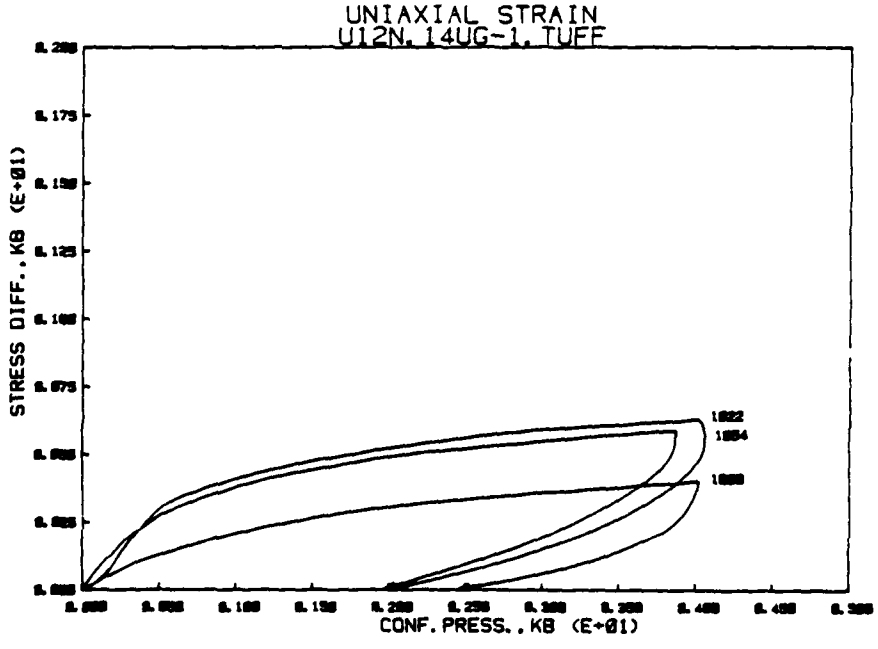

Figure B3b

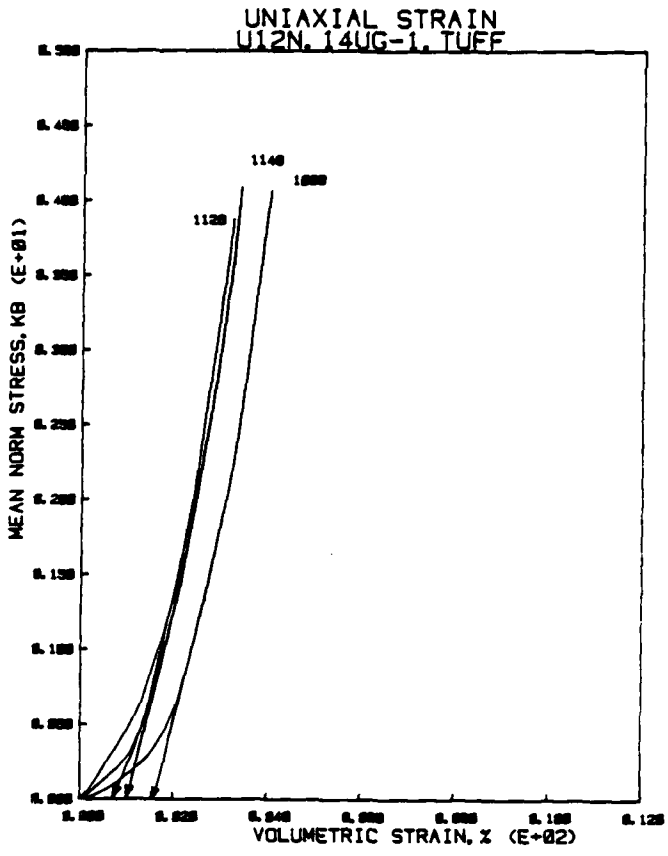

Figure B4a

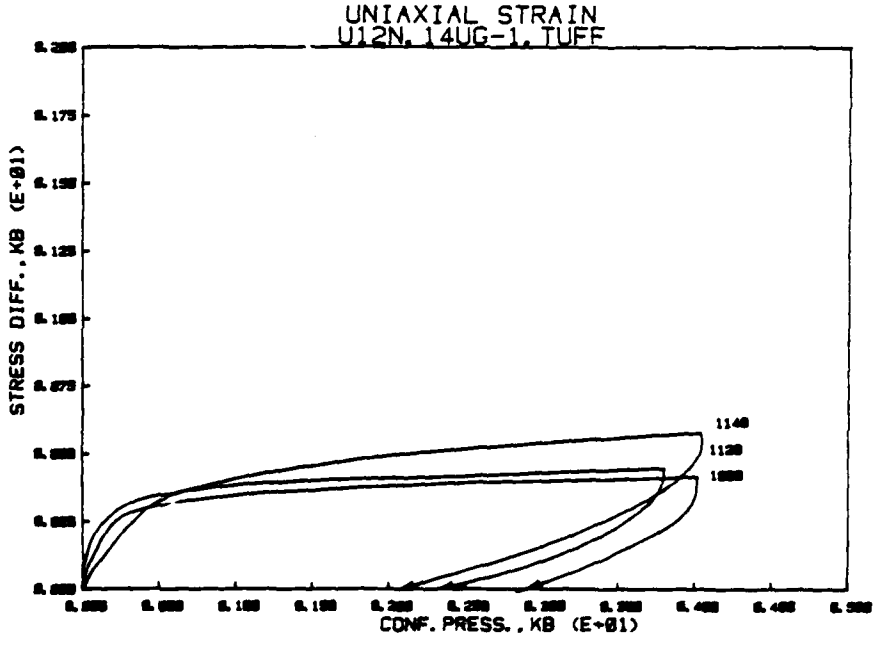

Figure B4b

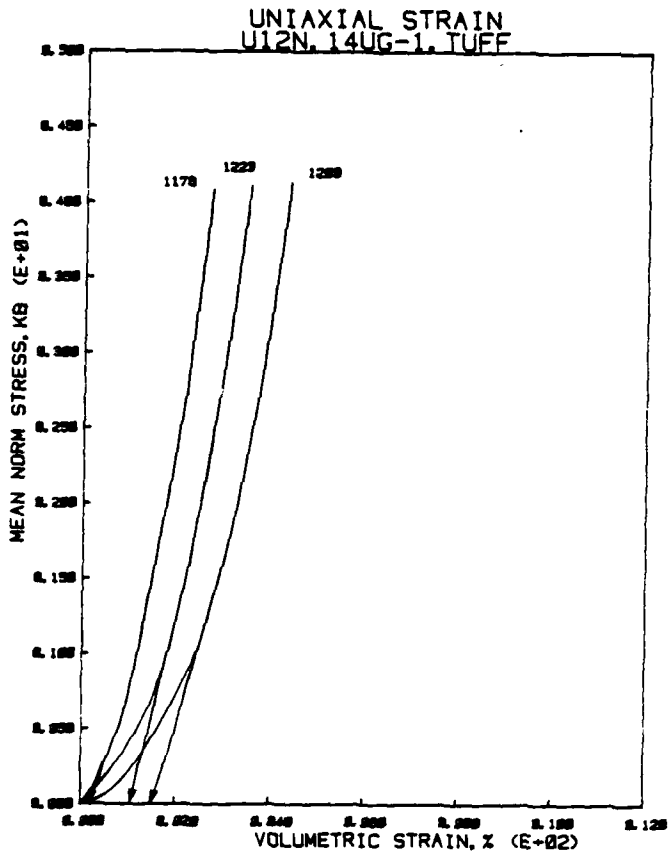

Figure B5a

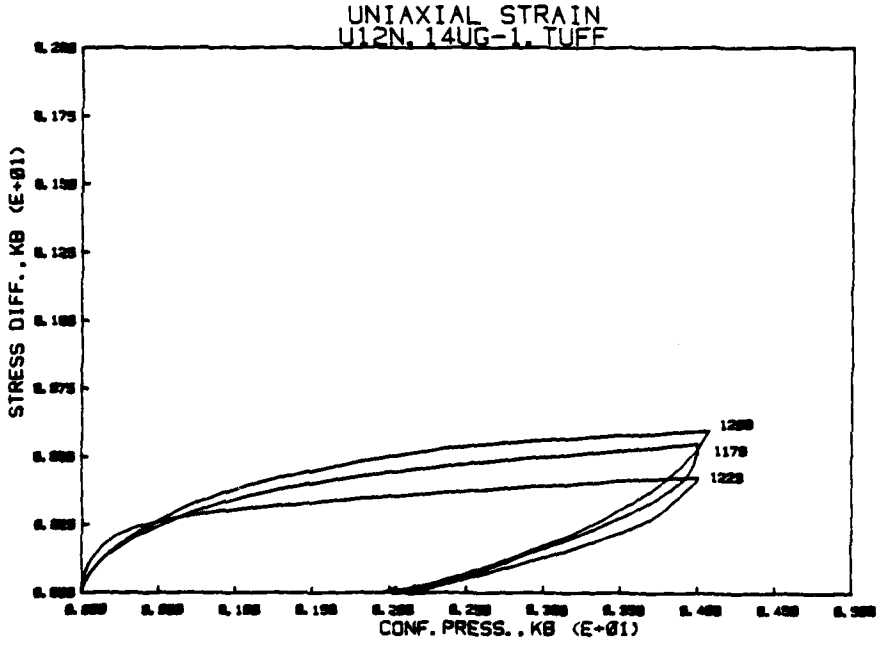

Figure B5b

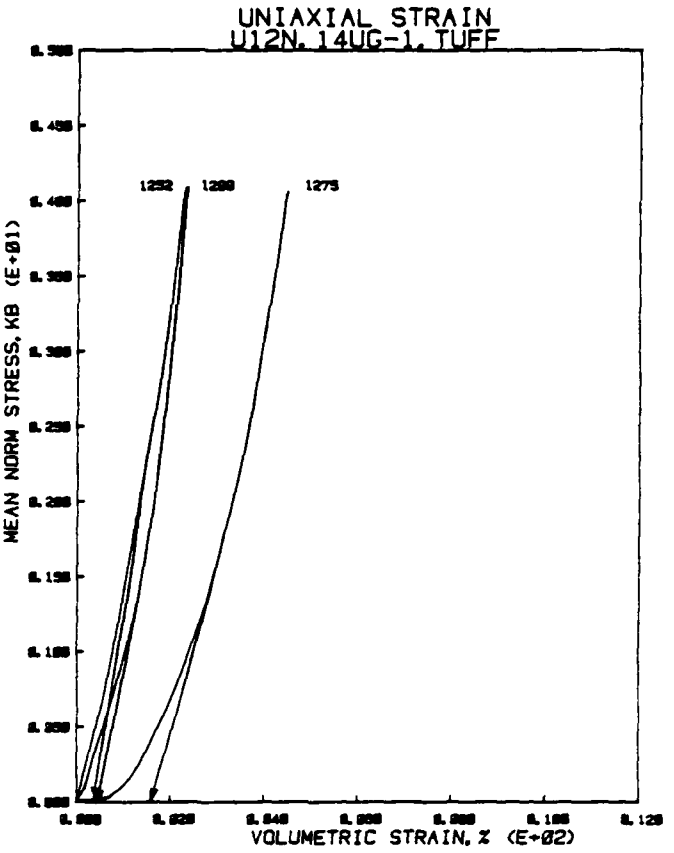

Figure B6a

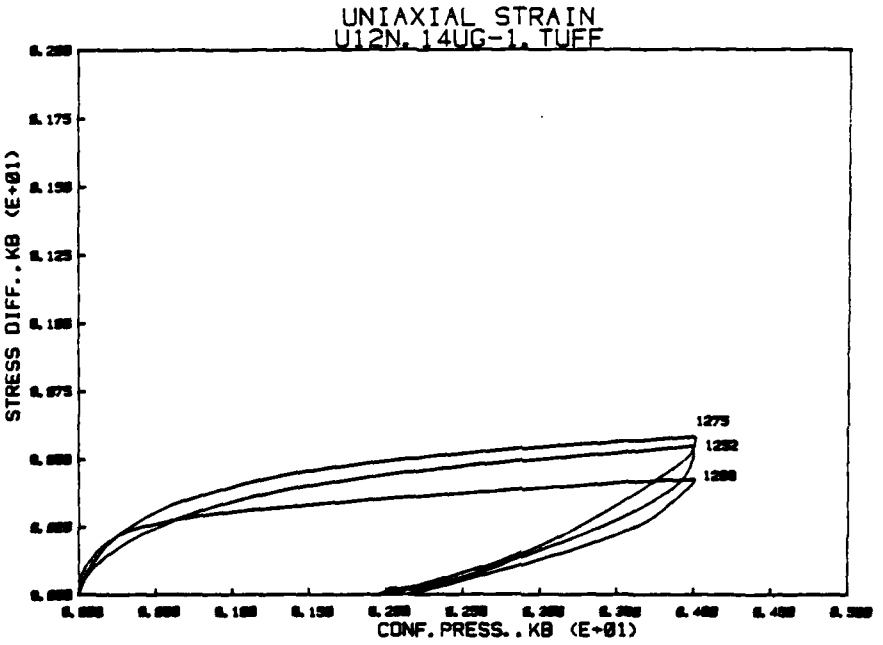

Figure B6b

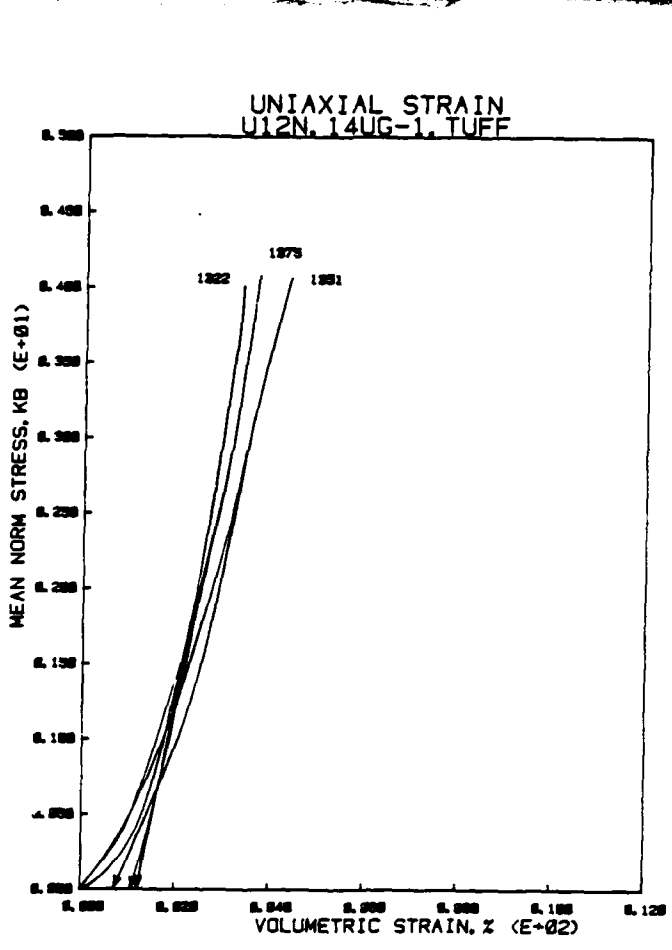

Figure B7a

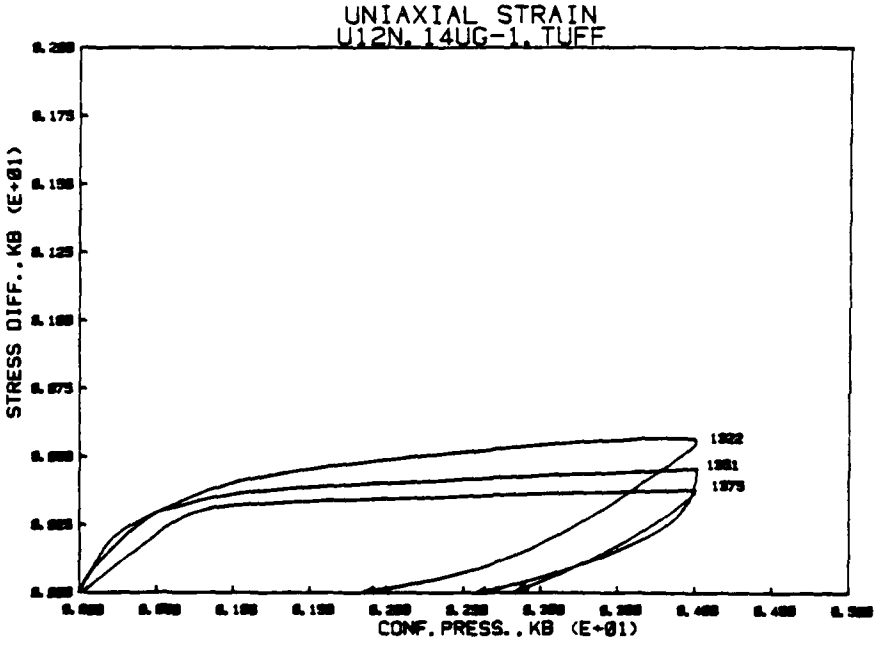

Figure B7b

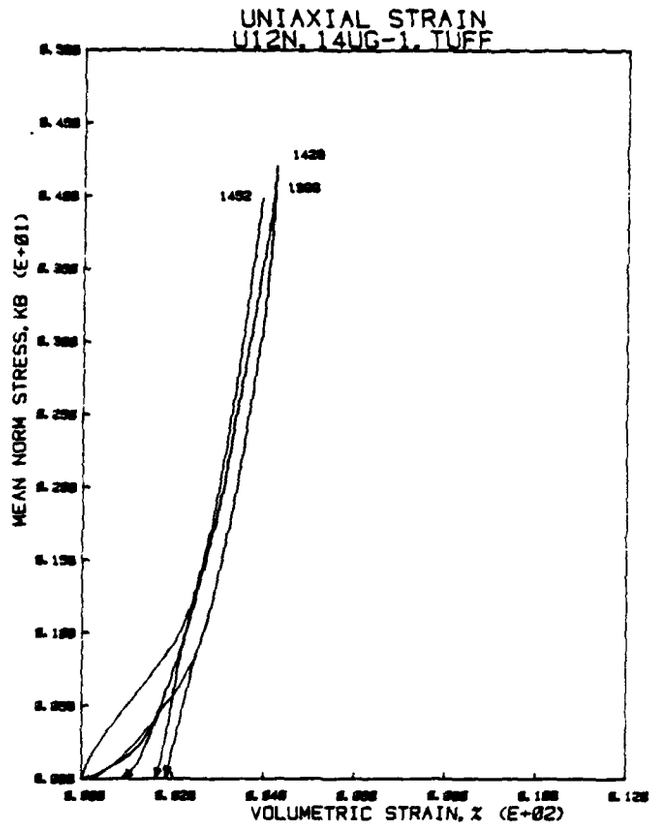

Figure B8a

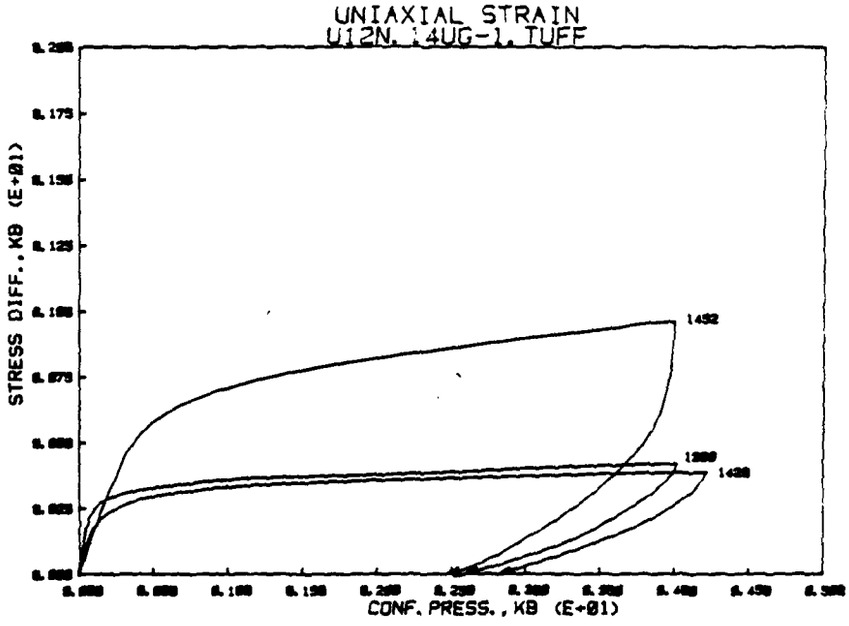

Figure B8b

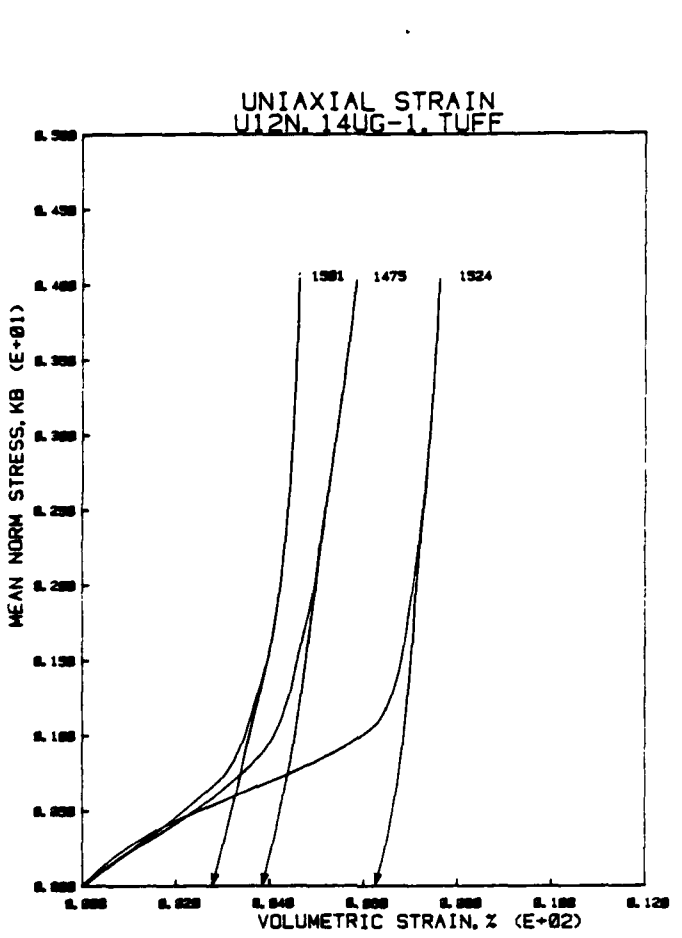

Figure B9a

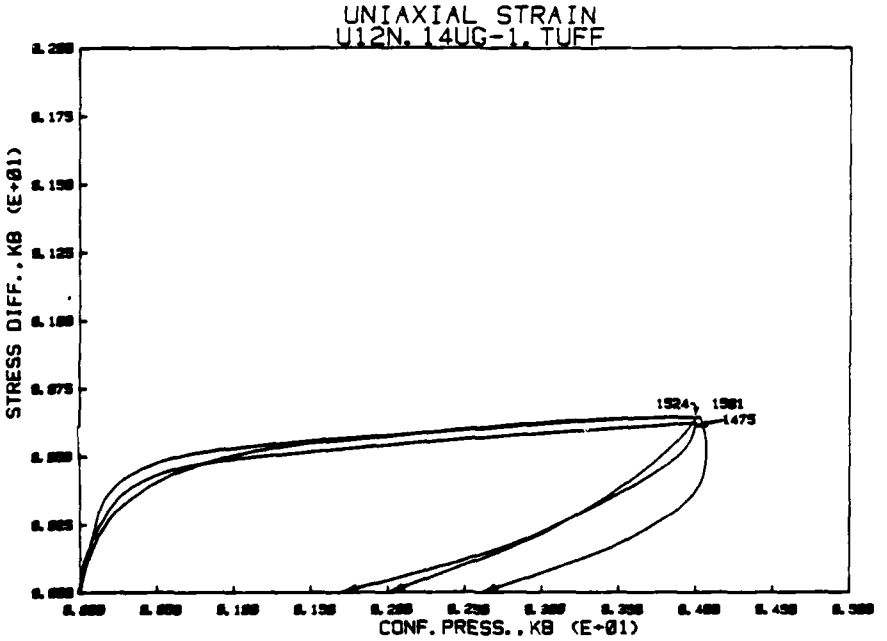

Figure B9b

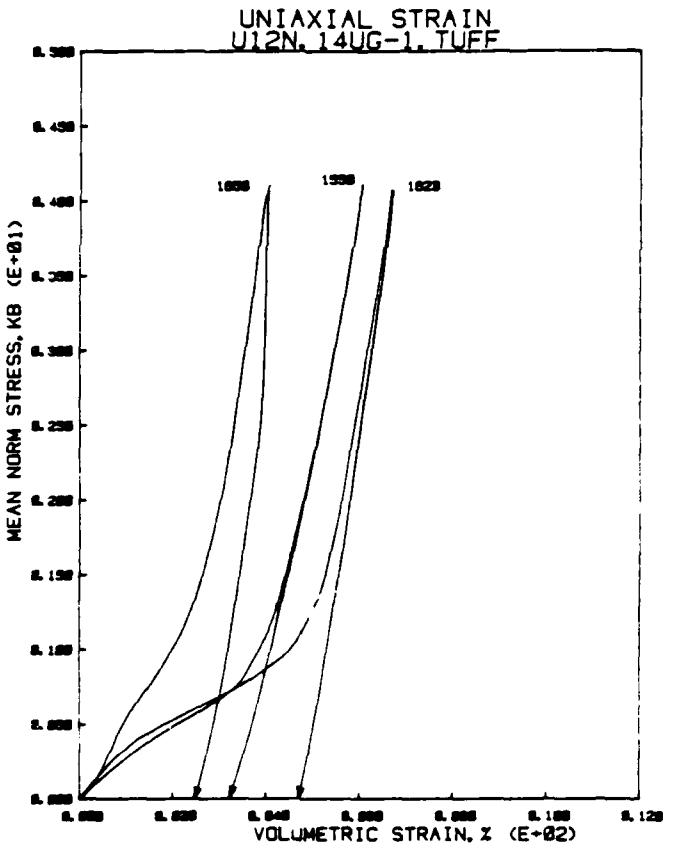

Figure B10a

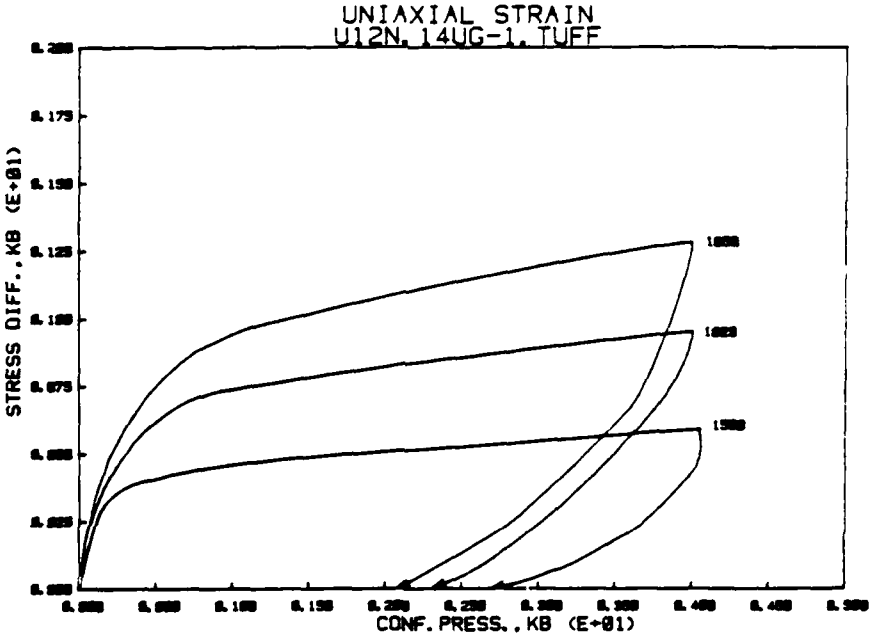

Figure B10b

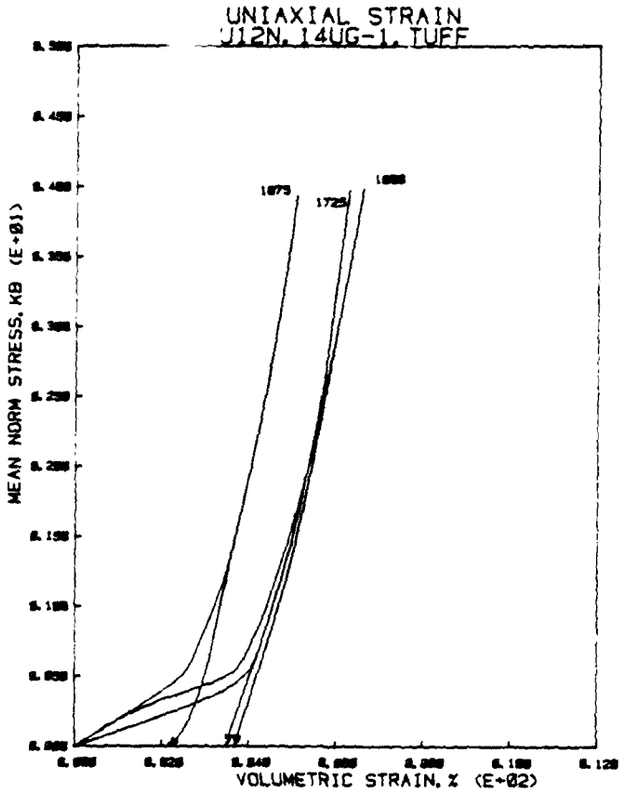

Figure B11a

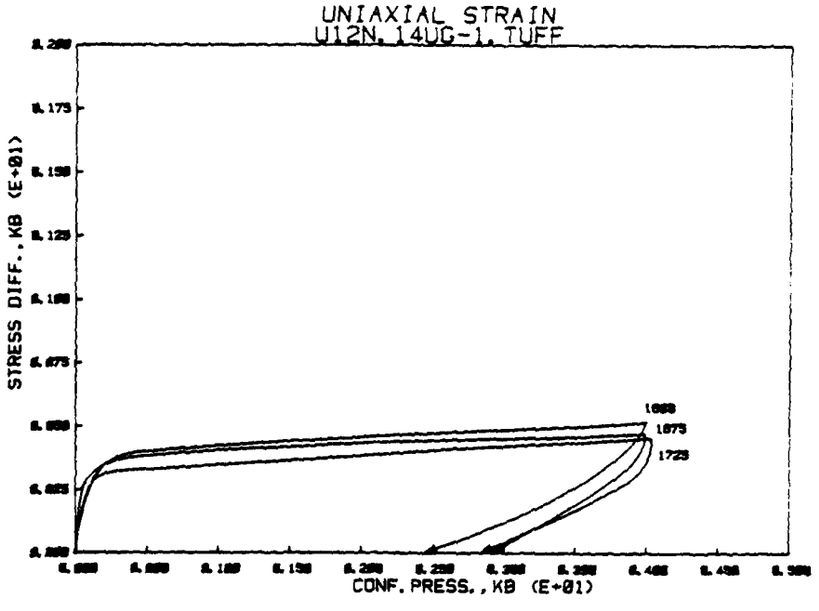

Figure B11b

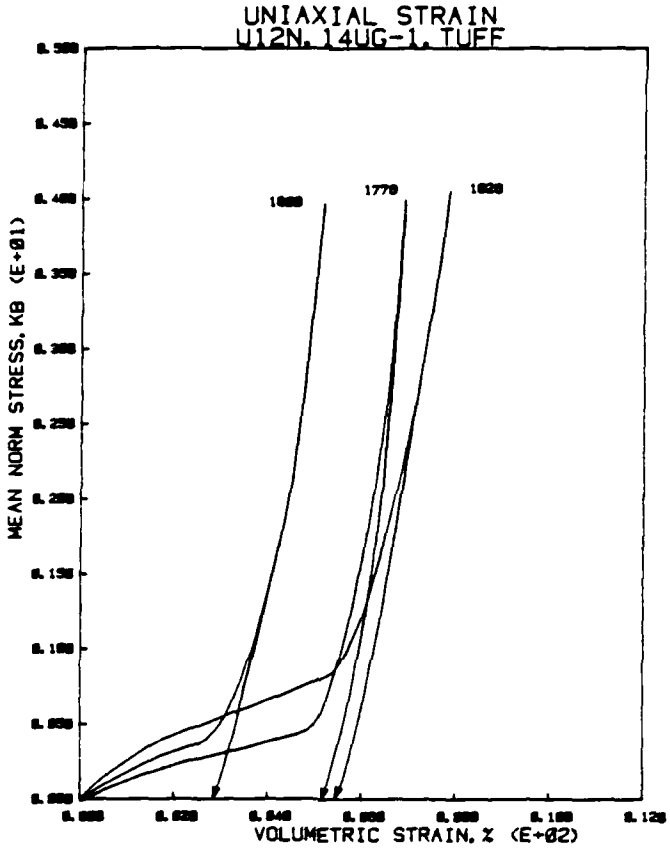

Figure B12a

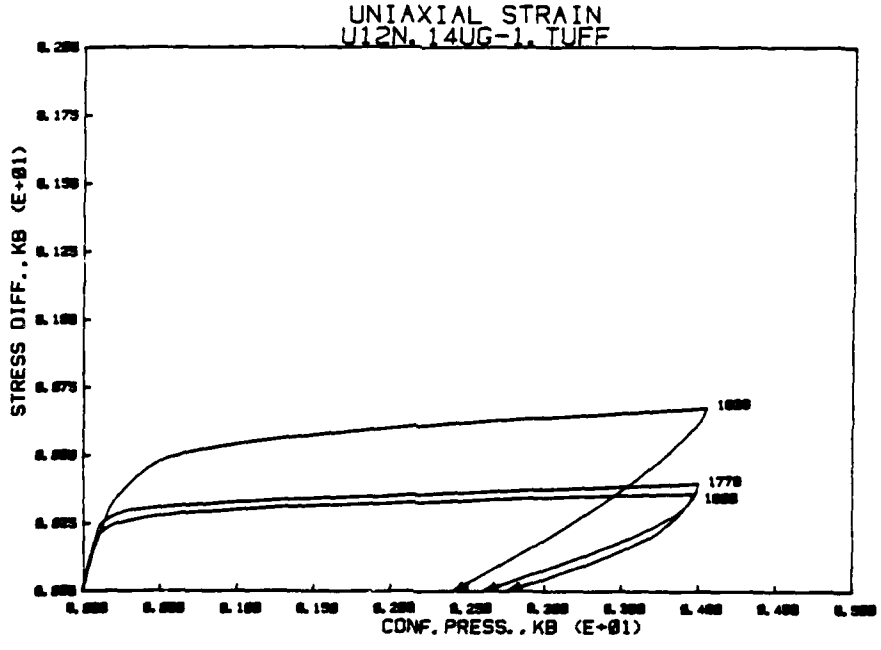

Figure B12b

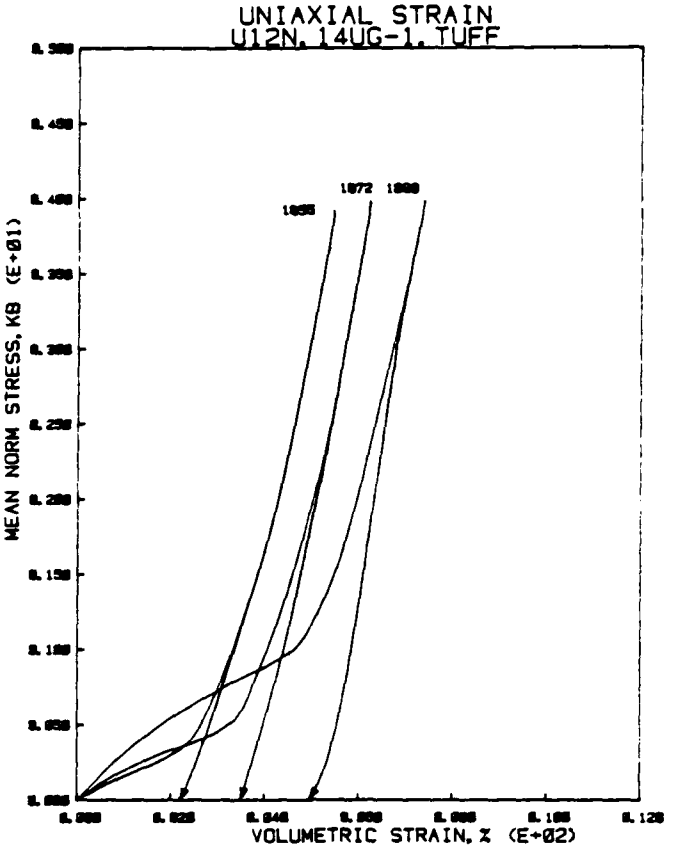

Figure B13a

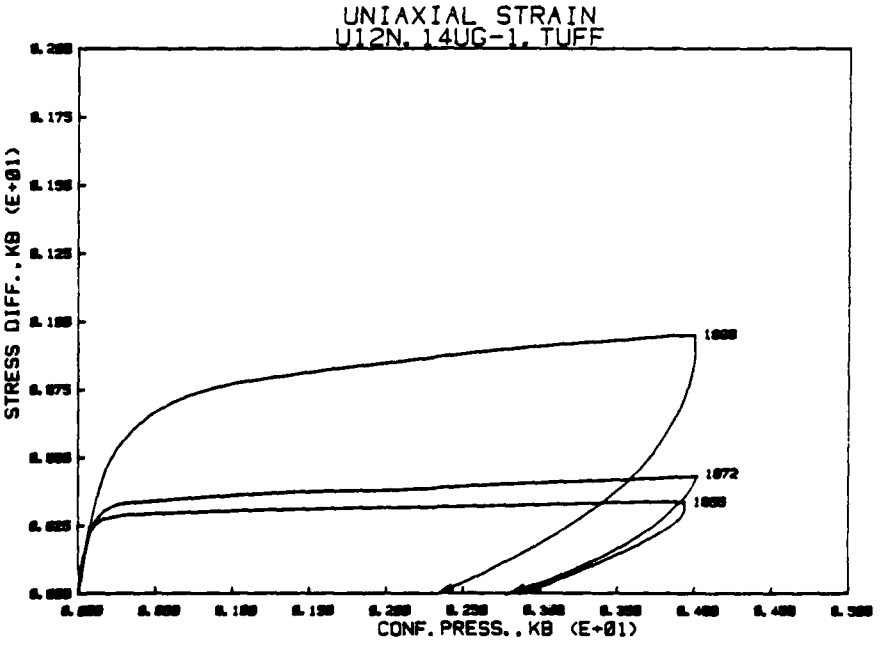

Figure B13b

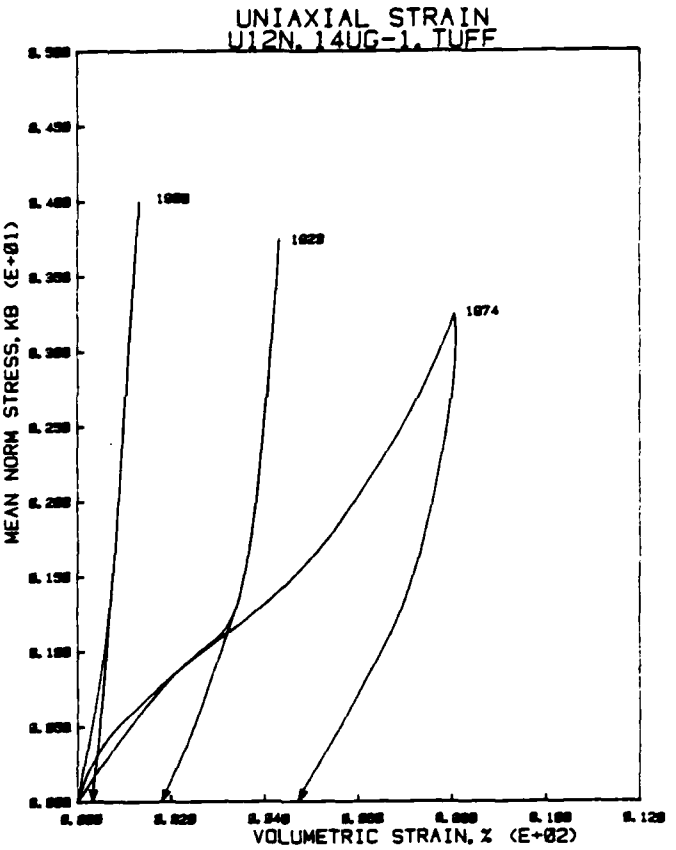

Figure B14a

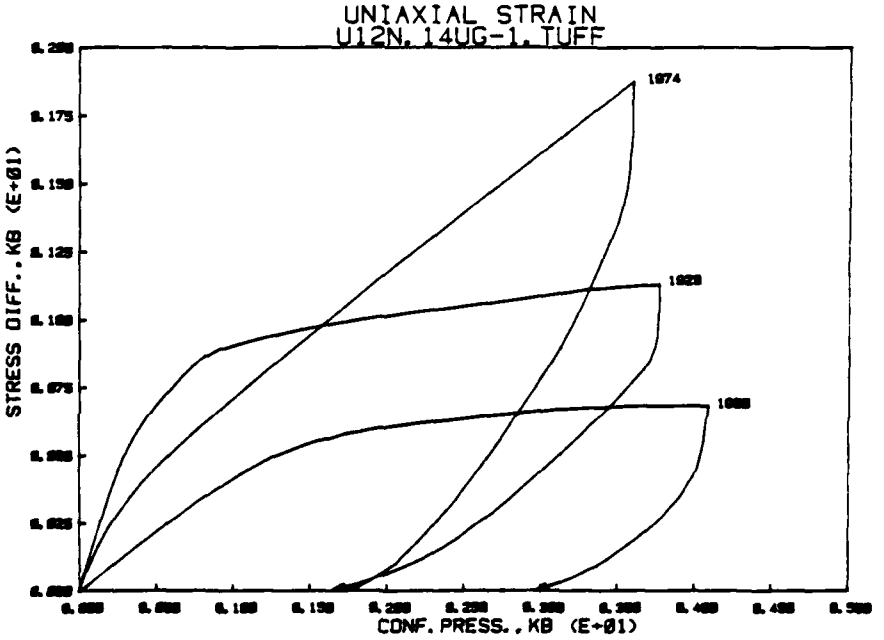

Figure B14b

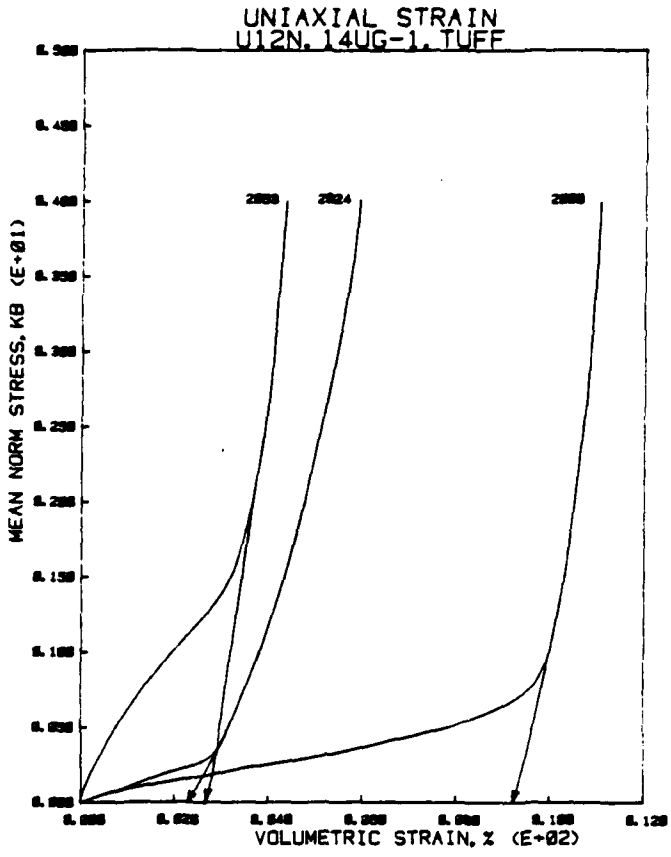

Figure B15a

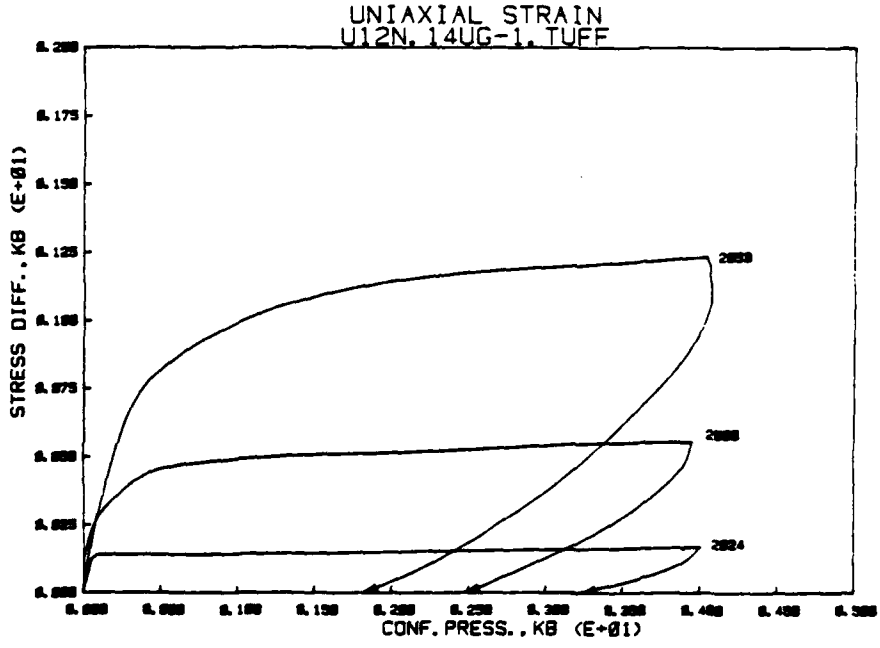

Figure B15b

APPENDIX C - U12N.15-UG-1,2,3

UNIAXIAL COMPRESSION DATA (25 TESTS)

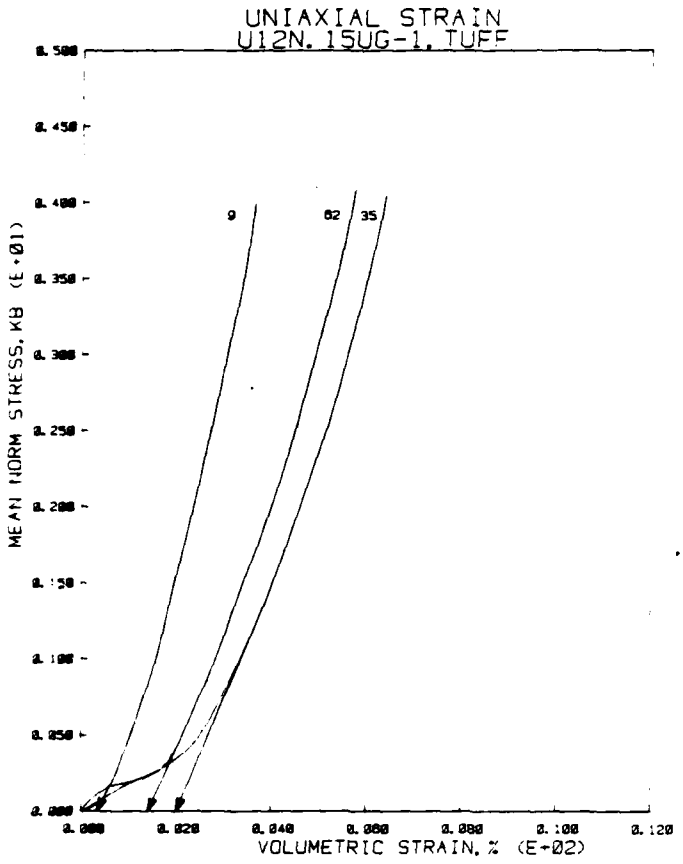

Figure C1a

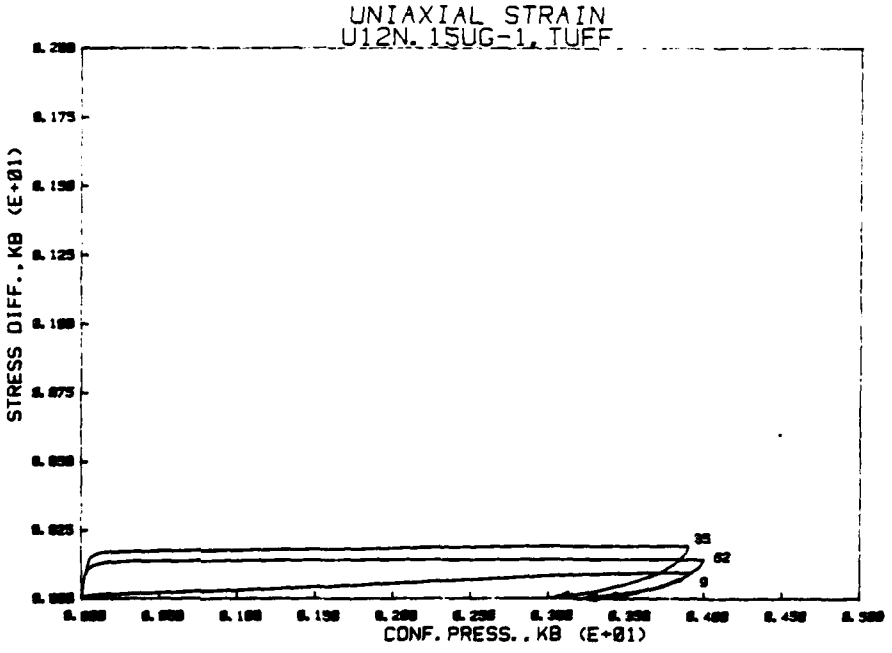

Figure C1b

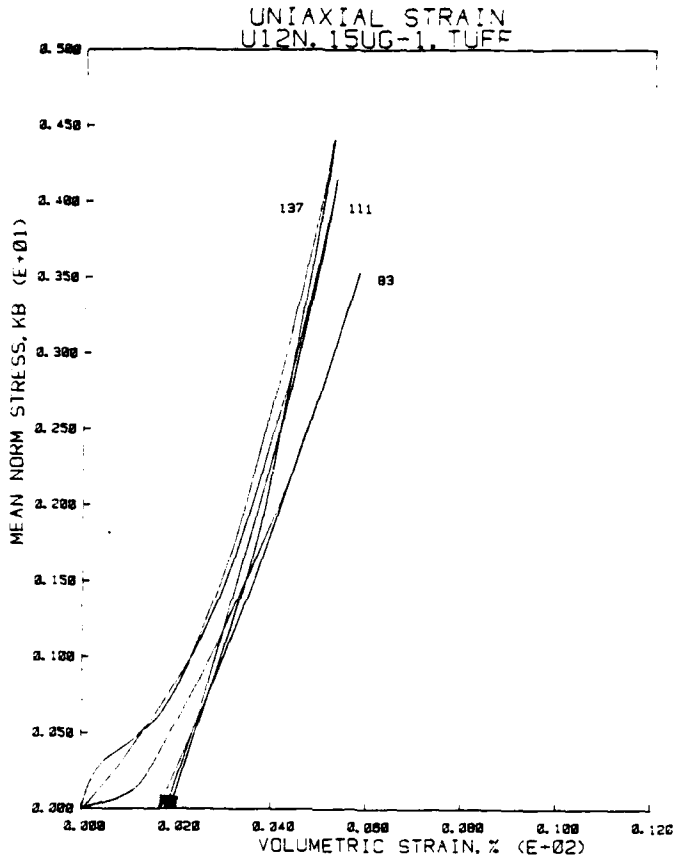

Figure C2a

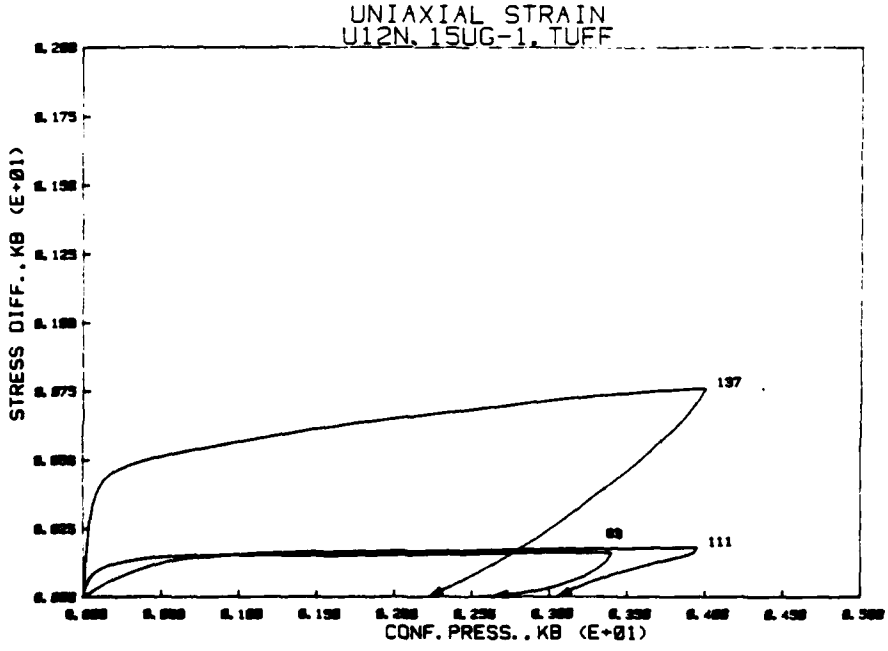

Figure C2b

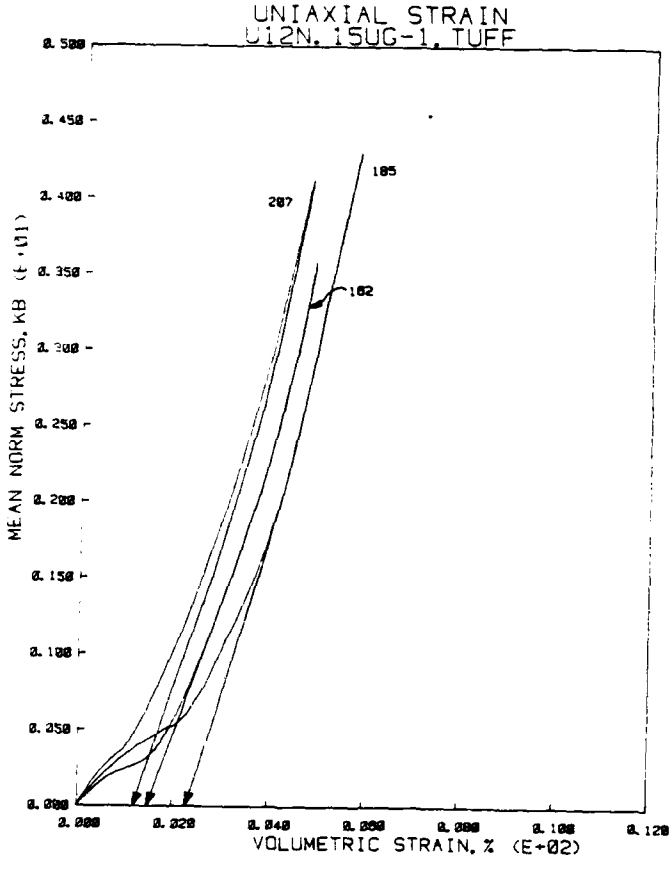

Figure C3a

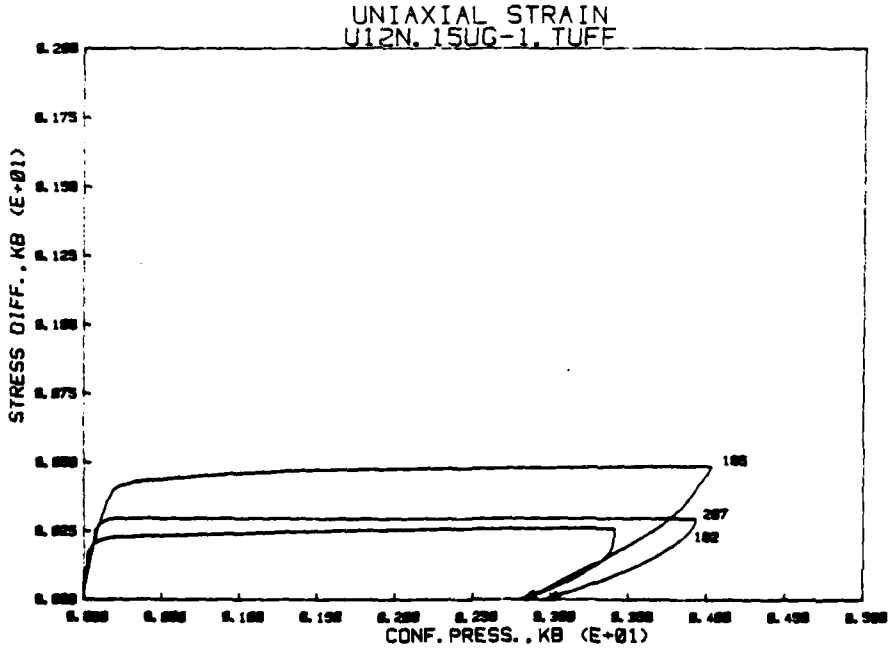

Figure C3b

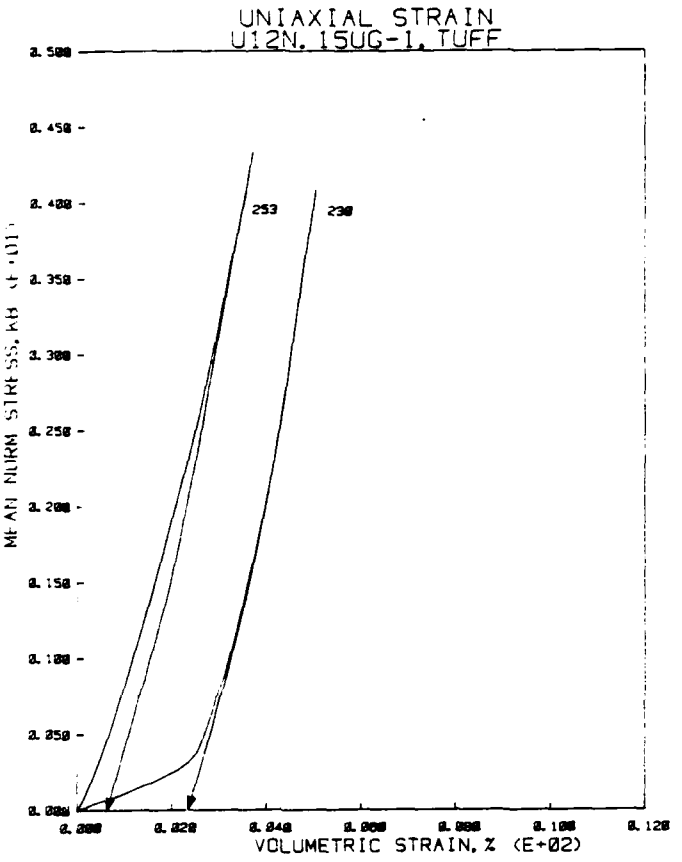

Figure C4a

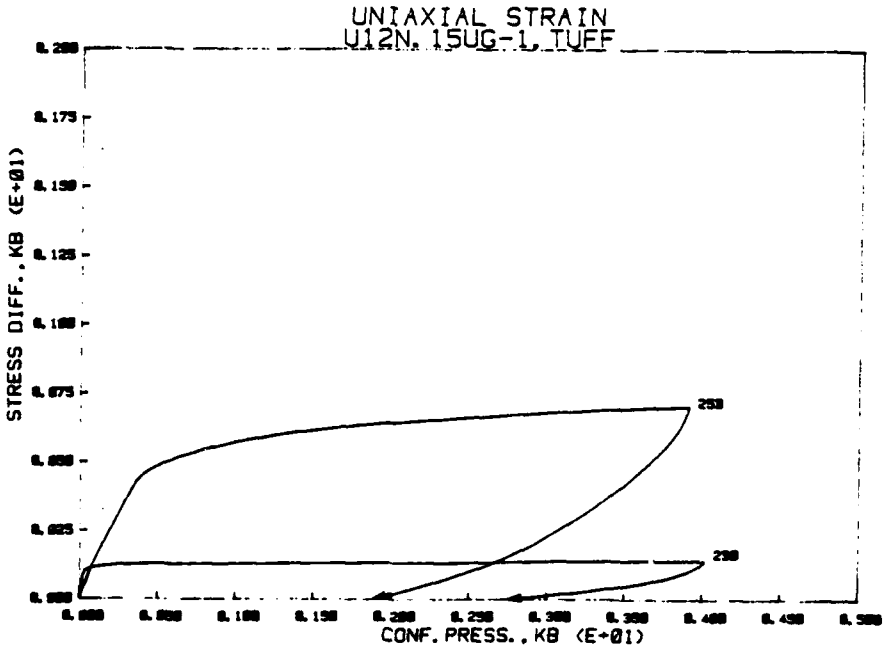

Figure C4b

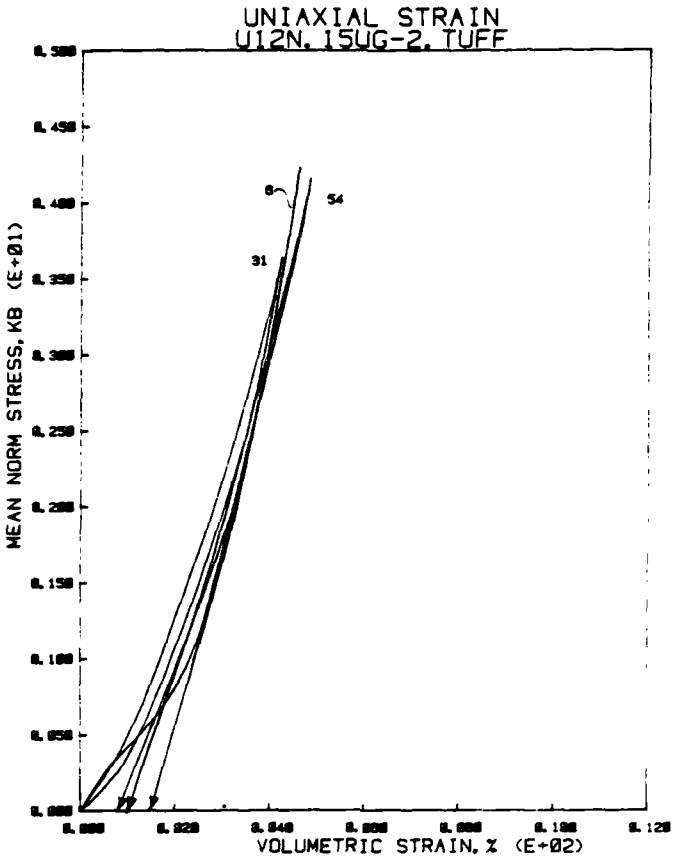

Figure C5a

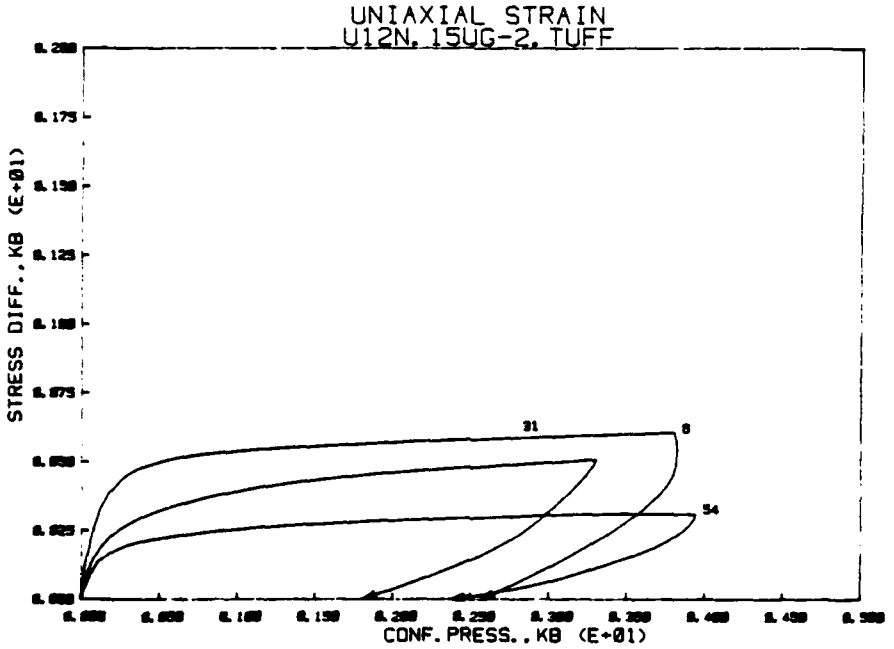

Figure C5b

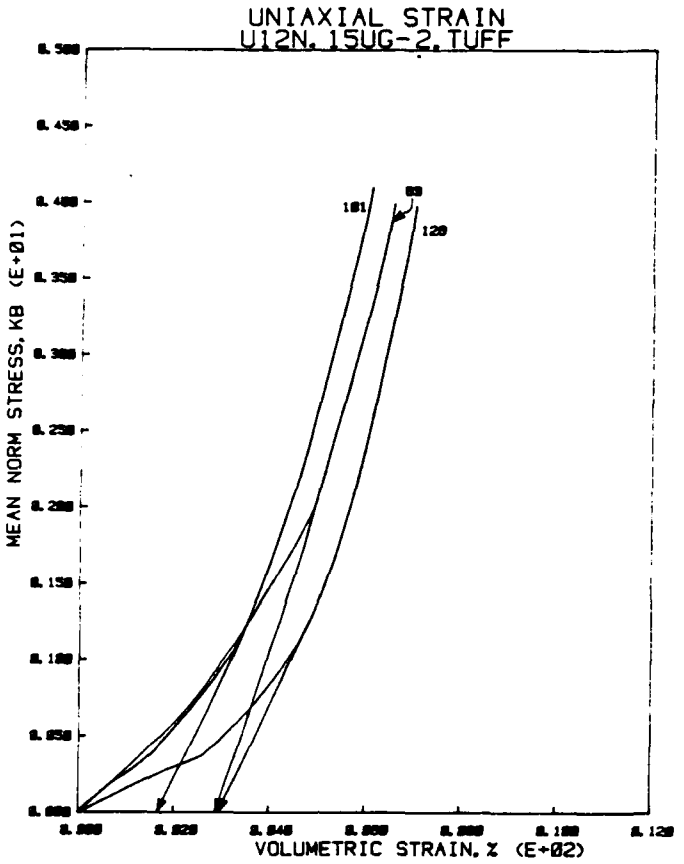

Figure C6a

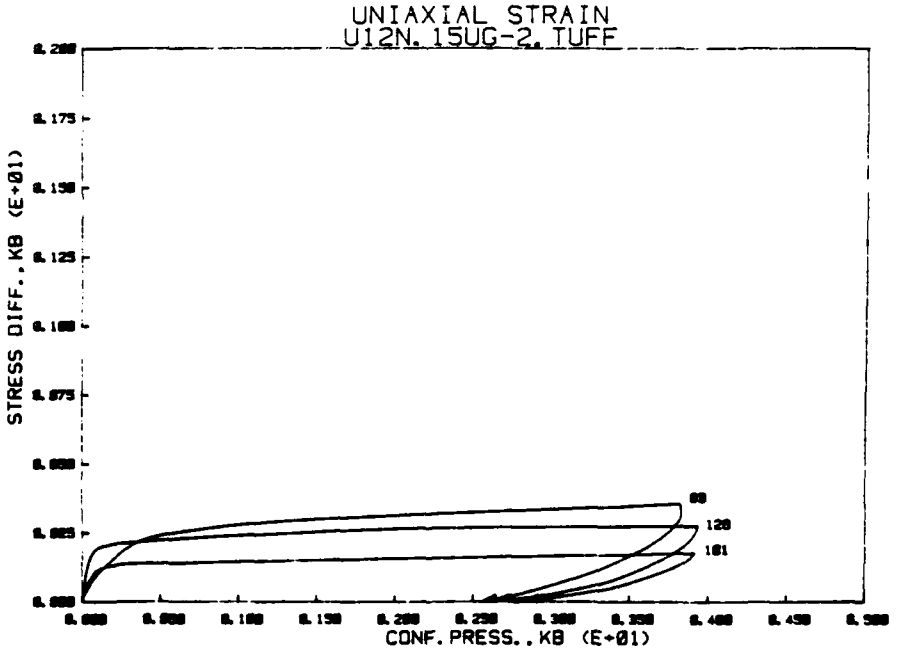

Figure CCb

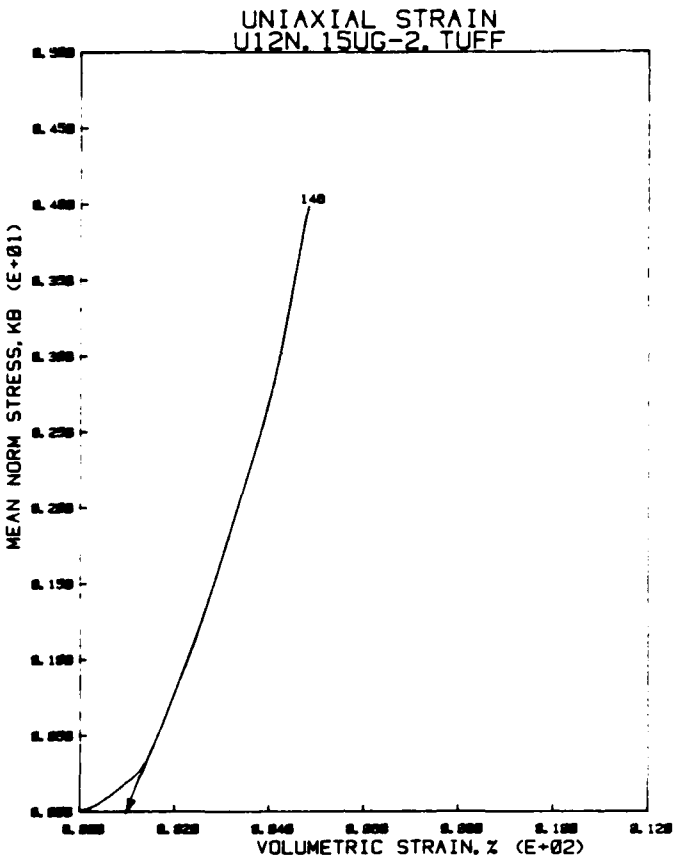

Figure C7a

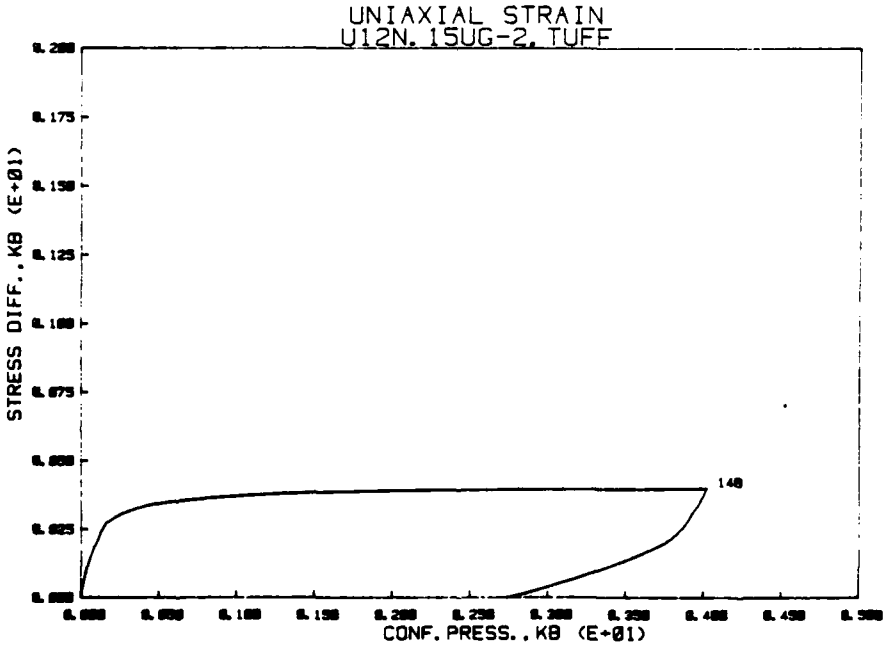

Figure C7b

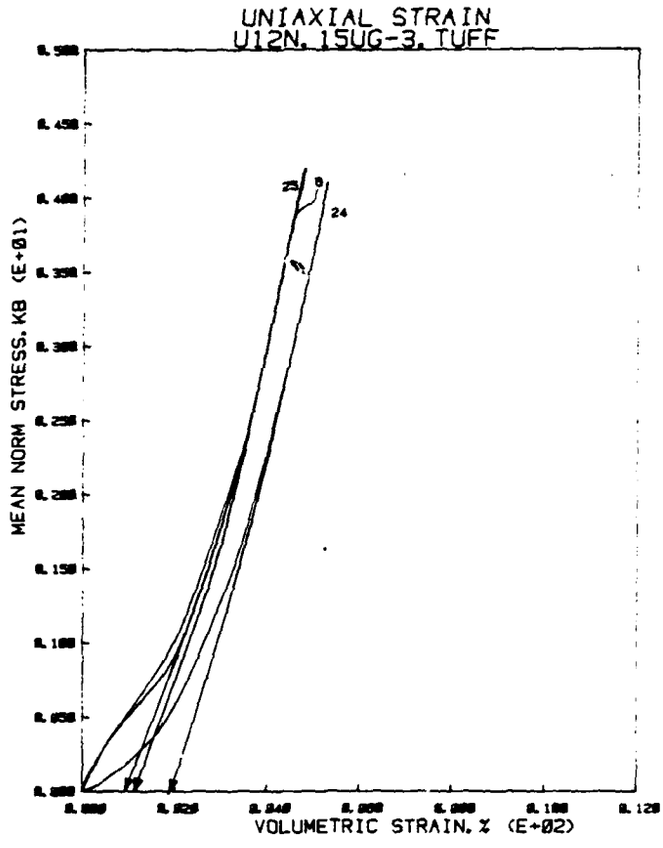

Figure C3a

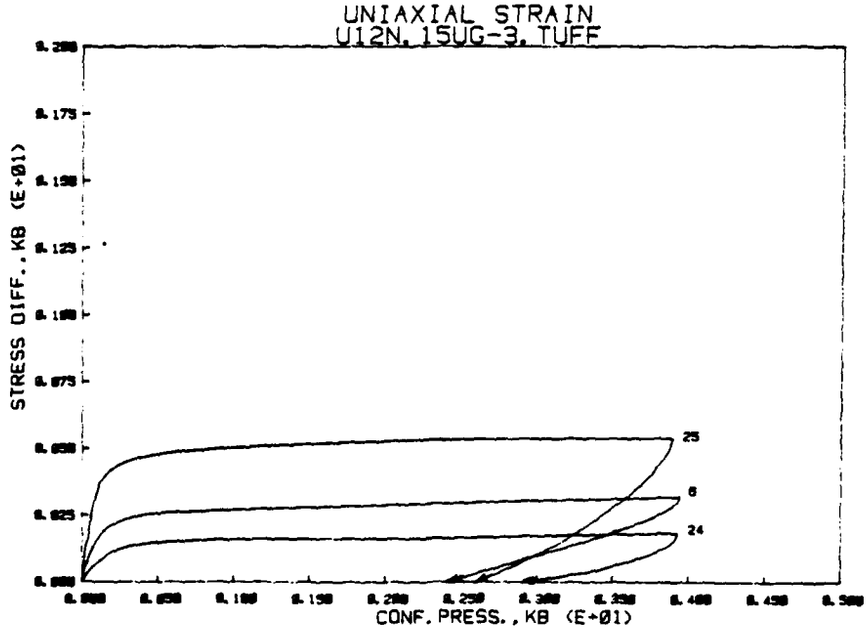

Figure C3b

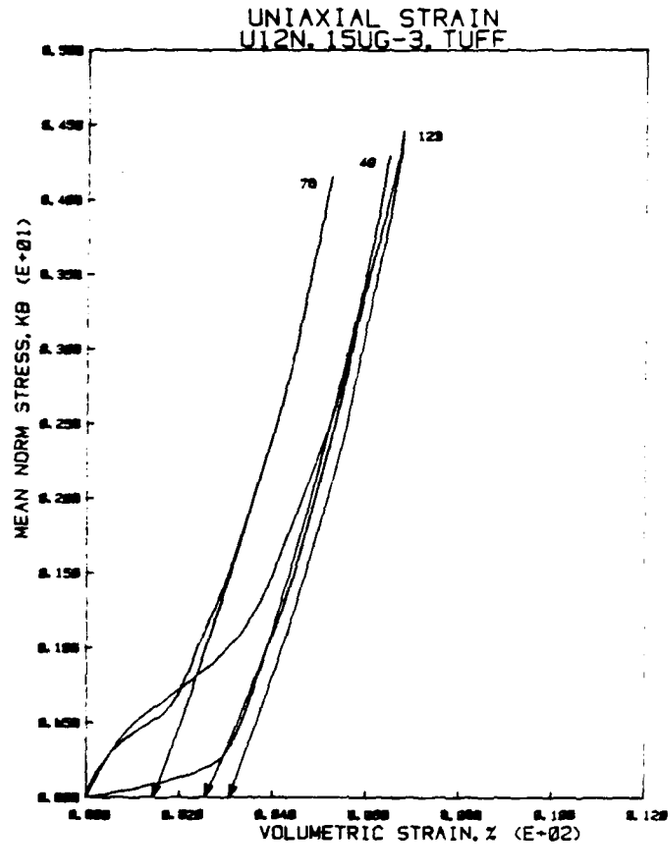

Figure C9a

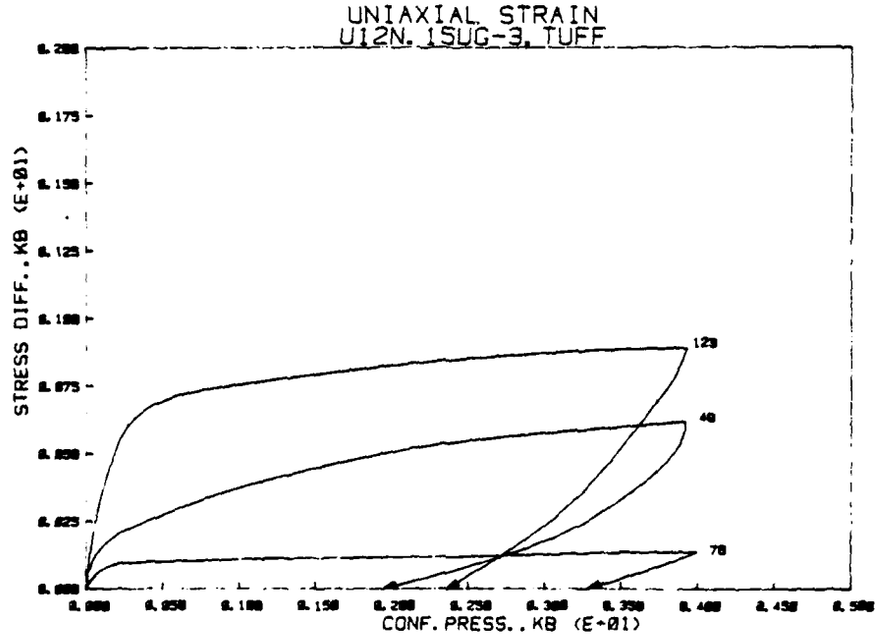

Figure C9b

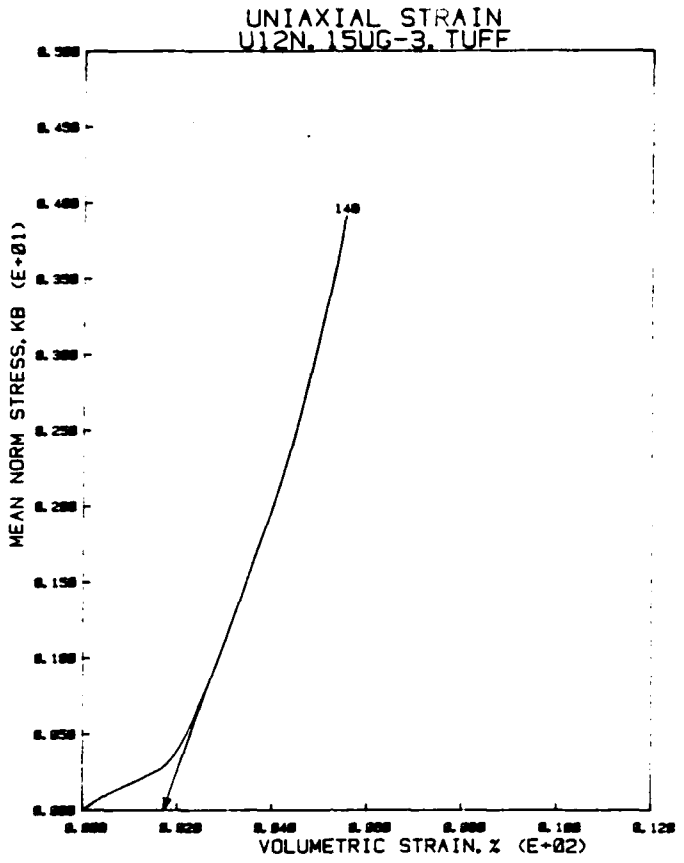

Figure C10a

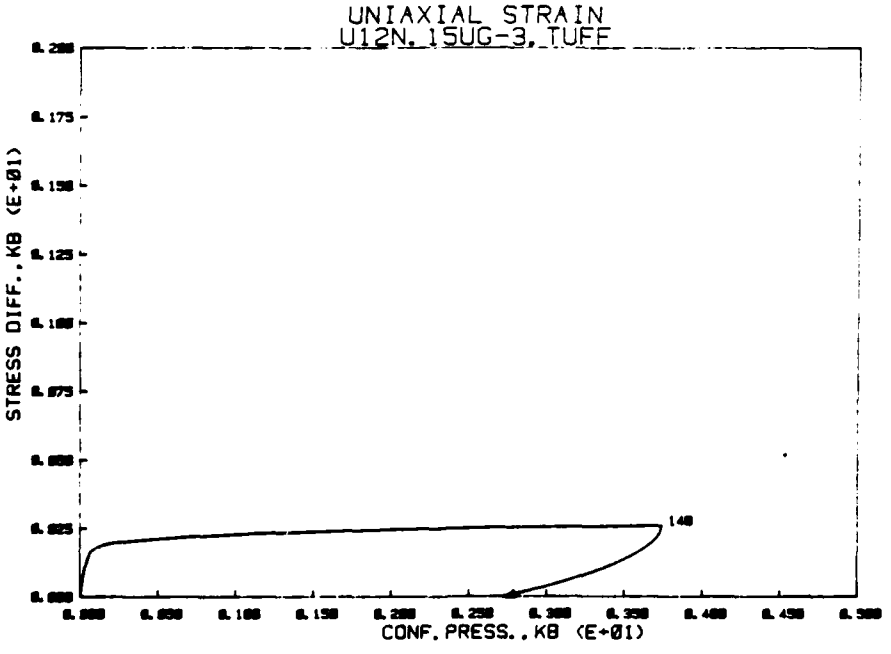

Figure C10b

III. 2C4 GROUT

MATERIAL PROPERTIES OF 2C-4 GROUT IN SUPPORT OF THE NEVADA TEST SITE NUCLEAR TEST PROGRAM

by

C. H. Cooley
C. Sakellariou
S. W. Butters
J. F. Schatz
J. W. LaComb

Submitted to:

Defense Nuclear Agency
Nevada Test Site
Mercury, Nevada

Attn: Mr. J. W. LaComb

Submitted by:

Terra Tek, Inc.
University Research Park
420 Wakara Way
Salt Lake City, Utah 84108

TR 81-56
May, 1981

TABLE OF CONTENTS

LIST OF FIGURES

List of Figures (continued)

LIST OF TABLES

NOMENCLATURE

P_c	The pressure of the confining fluid in a hydrostatic or triaxial test cell, bars
P_p	Pore fluid pressure, bars
S_r	degree of saturation (percent by void volume)
V_{av}	air void content (percent by total volume)
w	moisture content (percent by total weight)
$\Delta V/V$	Volume strain, % strain
ε	Strain rate, in/in/sec
$\varepsilon_{1,2,3}$	Principle strain
η_t	total porosity (percent by total volume)
ρ_d	dry bulk density after oven drying (gm/cm^3)
ρ_g	Grain density (density of solids)(gm/cm^3)
ρ_{H_2O}	Density of water (gm/cm^3)
ρ_w	In-situ bulk density (wet or "as-received" density)(gm/cm^3)
$\sigma_{1,2,3}$	Principle stresses, bars

1. INTRODUCTION

The Defense Nuclear Agency (DNA) requires a knowledge of the mechanical and physical properties of materials (both natural and man-made) which are used in conjunction with its underground testing program at the Nevada Test Site. This report describes the materials testing program conducted by Terra Tek on 2C-4 grout from August 1980 through April 1981. The contract number under which this work was done was DNA-001-81-C-0037.

The program goal was to conduct various mechanical tests on a grout that was formulated and treated to have extremely consistent mechanical and physical properties. The test program addressed curing, strain rate effects, physical and mechanical properties and permeability. The results are being used to assist in further general development and verification of computer codes that are used in nuclear blast effects analysis, and specifically to assist in the analysis of the grout sphere explosive tests being conducted by the Stanford Research Institute.

Many people in addition to Terra Tek and DNA Test Directorate Staffs have contributed to the planning and execution of this work. Included are Russ Duff at Systems Science and Software, Alex Florence at Stanford Research Institute, Carl Keller at DNA Field Command Headquarters, Albuquerque, New Mexico and Dan Patch at Pacifica Technology. We thank them all.

Ninety-seven successful tests were run on the grout (aside from physical property measurements). They can be grouped into the general categories of uniaxial strain tests, strain rate tests, hydrostatic compression tests, triaxial compression tests, permeability measurements, special drainage test, and physical property measurements.

The overall test matrix is shown in Table 1. In each category, we indicate the number of tests conducted of each test type or the number of tests conducted at each condition. Where tests followed one another on the same samples, it is indicated by arrows.

Table 1

2C4 Grout Test Matrix

Showing the Number of Tests Conducted of Each Test Type or the Number of Tests Conducted at Each Condition, Whichever Applies

UNIAXIAL STRAIN TESTS CURING TIME EFFECTS STUDY

Test Type	Time After Cast 7	14	16	18	21	28	56
Uniaxial Strain (Undrained and Cycled)							
Cast • Room Temperature	2	2			2	2	2
Cast • Refrigerated			3	3	3	3	3

STRAIN RATE STUDY

Test Type	Strain Rate (in/in/sec) 10^{-6}	10^{-4}	10^{-3}	10^{-2}	10^{-1}
Unconfined Compression	2	2	2	2	2
Uniaxial Strain (Undrained)	3	*	3		
Triaxial Compression (Undrained; σ_3 = 0.5 kb)	1	*	1		

HYDROSTATIC COMPRESSION TESTS TO σ_3 = 4 KBARS

Test Conditions

- o Pore Pressure Controlled
  - Pp 10 bars — ② **
  - Pp 500 bars — ②
- o Unjacketed Cp = Pp — ②
- o Undrained — ②

TRIAXIAL COMPRESSION TESTS

Test Conditions	Conf. Pressure, kb 0	0.069	¼	½	1	2	4
o Pp = 10 bars		1	1	1	1		②
o Pp = 500 bars				1	1		②
o Undrained	1		1	1	1	1	1
o Undrained but previously stressed to σ_3 = 4 kb					1		①
o Unjacketed Cp = Pp							②
o After uniaxial strain tests							
Undrained			2	2	2	2	2
Drained			1	1	1	1	1

PERMEABILITY MEASUREMENTS, CONFINING PRESSURE EFFECT AND STRESS CYCLING EFFECT

Test Conditions	
Untested	2
Stress Cycled	2

SPECIAL DRAINAGE TEST	1
PHYSICAL PROPERTIES SAMPLES TESTED	18

*Conducted in other studies
**Arrows indicate the sequence of testing.

Table 1

2C4 Grout Test Matrix

Showing the Number of Tests Conducted of Each Test Type or the Number of Tests Conducted at Each Condition, Whichever Applies

UNIAXIAL STRAIN TESTS CURING TIME EFFECTS STUDY

Test Type	Time After Cast: 7	14	16	18	21	28	56
Uniaxial Strain (Undrained and Cycled)							
Cast + Room Temperature	2	2			2	2	2
Cast + Refrigerated			3	3	3	3	3

STRAIN RATE STUDY

Test Type	Strain Rate (in/in/sec): 10^{-5}	10^{-4}	10^{-3}	10^{-2}	10^{-1}
Unconfined Compression	2	2	2	2	2
Uniaxial Strain (Undrained)	3	*	3		
Triaxial Compression (Undrained; σ_3 = 0.5 kb)	1	*	1		

HYDROSTATIC COMPRESSION TESTS TO σ_3 = 4 KBARS

Test Conditions

- o Pore Pressure Controlled
  - Pp 10 bars
  - Pp 500 bars
- o Unjacketed Cp = Pp
- o Undrained

TRIAXIAL COMPRESSION TESTS

Test Conditions	Conf. Pressure, kb: 0	0.069	½	¼	1	2	4
o Pp = 10 bars		1	1	1	1		
o Pp = 500 bars				1	1		
o Undrained	1		1	1	1	1	1
o Undrained but previously stressed to σ_3 = 4 kb					1		
o Unjacketed Cp = Pp							
o After uniaxial strain tests							
Undrained			2	2	2	2	2
Drained			1	1	1	1	1

PERMEABILITY MEASUREMENTS, CONFINING PRESSURE EFFECT AND STRESS CYCLING EFFECT

Test Conditions	
Untested	2
Stress Cycled	2
SPECIAL DRAINAGE TEST	1
PHYSICAL PROPERTIES SAMPLES TESTED	18

*Conducted in other studies

**Arrows indicate the sequence of testing.

2. EXPERIMENTAL PROCEDURES

This section describes procedures ranging from sample preparation to testing. A general outline is given which is then followed by more detailed descriptions of each test type. In order to assure uniform 2C-4 grout properties during the extended time required to complete the test program, it was necessary to establish a procedure to equalize the state of cure in all samples. The grout samples were poured and initially cured at the Stanford Research Institute (SRI). On the seventh day of cure, the samples, submerged in water, were shipped to Terra Tek; where on the 14th day of cure they were refrigerated at 5°C until they were tested. Verification tests were performed, and it was determined that the refrigeration process had indeed retarded any further aging. All samples were thereafter considered to be at identical states of cure.

The following tests were successfully conducted (see Table 1):

a. Physical Properties (18 tests)

b. Uniaxial Strain (25 tests)

c. Hydrostatic Compression (7 tests)

d. Triaxial Compression (38 tests)

e. Permeability Measurements (4 tests)

f. Uniaxial and Triaxial Strain Rate (22 tests)

g. Special Drainage Test (1 Test)

All of these procedures have been described in previous papers and reports [Refs. 1-4]; however, condensed descriptions are included here for clarity and completeness.

Mechanical compression tests, i.e., b, c, d, f and g of the above, were conducted on right circular cylinders of 2C-4 grout 2 inches in diameter by

2.5 inches long. The sample ends were cut and ground to be flat and parallel within 0.001 inches. Samples were isolated from the pressure vessel fluid environment by jacketing with a polyurethane sheet 0.010 inches thick. The jacket was sealed at the sample ends by lock wire which was securely tightened against hardened steel end caps.

A triaxial servo-controlled testing machine was used to subject the samples to the desired stress states at controlled strain rates. Axial and lateral strains were measured using strain-gaged cantilever beam transducers with an estimated accuracy of 0.025% strain. Stress difference was determined with a strain-gaged load cell to an accuracy of ±20 bars and confining stress and pore fluid pressures were measured using pressure transducers with accuracies of ±40 bars and ±5 bars, respectively.

2.1 Physical Properties Measurements

To check the consistency and adequacy of the grout preparation and handling, physical property measurements were made. Wet density, grain density, and water content were measured. From these measurements dry density, porosity, saturation and air voids were calculated. Formulas used for calculation are given in Appendix A.

Wet bulk density was measured using a water immersion technique. The sample was weighed, then sealed with bees wax of known density. The sample was then weighed while submerged in distilled water. The sample weight in air, the sample bouyant weight, and the density of the water and bees wax were used to calculate the sample volume. The weight and the sample volume were then used to calculate density.

Water content was determined by drying and weighing the dried sample. The difference between the as-received weight and the dry weight divided by the as-received weight yields water content by wet weigh

Grain density was measured by a water pycnometer technique. Finely crushed grout samples were placed into a volume-calibrated flask. The flask was filled with water to a precise level, the air evacuated, and the flask weighed. Knowing the tare weight of the flask, density of water, the precise volume of the grain-water mixture, and the total weight, the grain density was calculated.

2.2 Uniaxial Strain Tests

Uniaxial strain tests were conducted to determine permanent compaction, following a strain path corresponding to the initial phase of explosive loading. These tests were also used to verify that the 2C-4 grout properties were consistent, and therefore confirm that the refrigeration technique did sufficiently slow the curing process. To do this, these experiments were conducted on samples of different cure ages.

Also, to ascertain the damage done to the grout by cyclic loading, two cycles of uniaxial strain were conducted on each sample.

In the uniaxial strain tests the samples were stressed axially at a constant axial strain rate of approximately 10^{-4} sec^{-1} while the confining pressure was controlled such that the lateral strain was kept as near to zero as possible. These tests were conducted until the confining pressure reached 4 kbars. Data recorded were axial load, confining pressure, axial strain and lateral strain.

2.3 Hydrostatic Compression Tests

Hydrostatic compression tests were conducted to provide the pressure versus volume strain compression data for 2C-4 grout up to a confining pressure of 4 kbars. Three types of hydrostatic compression tests were conducted. They were:

Semi-Drained* (pore pressure controlled) - Drained experiments provide a measure of the pore-volume response of the material. For these tests confining pressure and pore pressure were initially increased together at an approximately equal rate until the desired test pore pressure was reached. From this point, confining pressure was increased while pore pressure was held constant. End caps for the drained experiments were fitted with drain ports that connected directly to a pore fluid volume measurement system that was located outside the triaxial cell. With this system the pore pressure was maintained and the fluid volume exuded from the rock was measured. Estimated accuracy of the fluid volume measurement is ±0.05 ml. The volume of exuded pore fluid was measured for comparison with strain transducer data. Confining pressure was cycled back to approximately zero effective stress after attaining 1.3 kbars and 2.7 kbars confining pressure, to obtain unloading data. However, before reducing confining pressure, the pore fluid was allowed to drain at constant confining pressure in hopes of achieving stable conditions. (Pore fluid drainage is time-dependent due to the characteristics of fluid flow through a porous medium. Porous flow, and the small permeability of these specimens, caused rather large characteristic times for drainage.) Attempts at stabilization were stopped when exuded pore fluid amounts were small, usually after about 5 minutes, however, this time was probably not sufficient to achieve full drainage.

Unjacketed - Unjacketed tests are a measure of grain compression. For these experiments the polyurethane jacket was perforated to allow the pore fluid pressure to equilibrate with the confining fluid pressure. Confining pressure was increased to 4 kbars at a rate of approximately 7 bars/sec.

*The term semi-drained is used because full drainage was not achieved for the tests described here. See Sections 3.3, 3.5 and 3.7 for a full explanation.

Undrained - Undrained tests are a simulant of material-pore-fluid response under extremely rapid-loading conditions. These tests were conducted to 4 kbars confining pressure. Loading rate was approximately 7 bars/sec. Confining pressure was cycled back to zero when it reached approximately 1.3 kbars and 2.7 kbars.

2.4 Triaxial Compression Tests

Triaxial compression tests were conducted to determine the failure strength of 2C-4 grout under both drained and undrained conditions and also in some cases, to determine the sample alterations introduced by previous load cycling.

Samples were tested in a triaxial cell at constant confining pressure. Axial stress was applied via the machine loading piston at a load rate resulting in a strain rate of approximately 10^{-4} sec^{-1}. Axial and lateral strains, load and confining pressure were measured. All tests were conducted to approximately 10% axial strain.

All drained tests were conducted using the pore fluid system explained in the Section 2.3. Pore pressure was held constant and exuded pore fluid volume was measured. The same comment regarding full drainage as mentioned in the previous section applies here.

For undrained tests, in some instances, the shear stress was cycled to zero before failure to obtain unloading stiffness.

Unjacketed triaxial compression tests were conducted with a perforated jacket and loaded to failure.

For some of the triaxial compression tests, samples were pre-tested. Two types of pre-tests were done: 1) hydrostatic compression to 4 kb followed by decompression to confining pressure at which the triaxial test was conducted, and 2) two uniaxial strain tests to 4 kbars (the samples used for these tests

were the same samples used to verify the refrigeration technique described above).

2.5 Permeability Measurements

The mechanical properties determined by the tests described above, in cases where some drainage was allowed to occur, depend on the fluid movement in the sample and therefore on the permeability of the sample. To determine the pertinent permeability values, several permeability tests were done, both on untested material and on pre-tested material.

On previously untested material, permeability measurements were made on saturated samples that were 2 inches in diameter by 0.5 inches long. Then, a sample cut contiguously to the above sample, but 2 inches in diameter by 2.5 inches long, was tested to 4 kb in uniaxial strain. Finally, a wafer 0.5 inches long was cut from the uniaxially tested sample. This wafer was used for the final permeability measurement.

Permeability was measured by a transient technique using distilled water. The jacketed sample was connected to two known volumes. A pressure step, ΔP, was introduced into one of the volumes. It diminished as fluid flowed into the sample, and from the time-pressure decay curve, and knowledge of fluid compressibility, system volumes and sample geometry, permeability was calculated. The method of calculation used is given in Ref. 2. Permeability measurement resolution is approximately 0.1 microdarcy.

2.6 Strain Rate Tests

Since drainage-dependent mechanical properties depend on time-dependent fluid movement within the sample, variation in those properties might be expected with varying strain rates. Also, some true material-caused strain rate dependence has been observed for strain rates between 10^{-5} and 10^{-1} sec^{-1} in

rocks [Ref. 5]. To determine the magnitude of strain rate effects on strength, unconfined compression, uniaxial strain and confined triaxial compression, tests were conducted at various strain rates in the 10^{-5} to 10^{-1} sec^{-1} regime. These tests were generally conducted as described in the foregoing sections except for the variation in strain rate. Strain rates reported are accurate within ±10% at 10^{-1} sec^{-1} and within ±1% at all other rates.

2.7 Special Drainage Test

To aid in determining the true drained response of 2C-4 grout, a special drainage test was performed. This test was similar to the "semi-drained" hydrostatic compression tests to 4 kbars as described in Section 2.3, however, it differed from the previous tests in that longer pore pressure equilibration times were allowed (30 minutes as compared to approximately 5-6 minutes for the semi-drained tests) after each confining pressure increase and in that the pore fluid volume exuded as a function of time for each equilibration period was recorded. Also, no triaxial compression test was conducted after the first hydrostatic compression. Instead, the confining pressure was reduced to 0.3 kbars and pore fluid drainage was allowed for approximately 48 hours. Then subsequent hydrostatic compression cycles to a maximum of 4 kbars were conducted again using the same procedure.

3. RESULTS

Three batches of 2C-4 grout, sealed to maintain wetness, were sent to Terra Tek. Each batch, labeled 1, 2, 3 throughout this report, consisted of 26 tubes of grout that were 2 inches in diameter by 12 inches long. Each tube was numbered 1 through 26. (In the mixing procedure at SRI, tube 1 was vibrated first, immediately after casting, and tube 26 was vibrated last, approximately 45 minutes after casting.) The labeling system includes batch and tube numbers. For example, 2-15 is a sample taken from batch 2, tube 15. If two samples were taken from the same tube, they were labeled "a" and "b".

3.1 Physical Properties

Physical properties measurements were made on three tubes from each batch: one that was vibrated immediately (i.e. low tube number), one that was vibrated after approximately 20 minutes, and one that was vibrated after 40 minutes. Two full suites (labeled "a" and "b") of physical property tests were conducted on each tube. The results are shown in Table 1.

Consistency of the physical properties was excellent among all three batches. The casting and handling of the grout were concluded to be adequate for the testing program.

3.2 Uniaxial Strain Tests

Samples were tested in uniaxial strain at ages of 7, 14, 21, 28 and 56 days (2 tests each age). Upon the 14th day of cure, however, a group of samples for uniaxial strain were refrigerated (while submerged in water) at 5°C (40°F). These refrigerated samples were then tested in uniaxial strain at refrigerated ages of 16, 18, 21, 28 and 56 days (3 tests at each age) for comparison with unrefrigerated samples. All tests in this part of the test

Table 2

2C4 Grout

Physical Properties

Sample Designation	Density (gm/cc)			Water by Wet Weight (%)	Porosity (%)	Saturation (%)	Calculated Air Voids (%)
	As-Received	Dry	Grain				
1-3a	2.20	1.81	2.97	17.6	39.0	99.1	0.3
1-3b	2.20	1.81	2.97	17.6	39.2	98.8	0.5
1-12a	2.19	1.80	2.99	17.7	39.7	97.7	0.9
1-12b	2.18	1.80	2.98	17.7	39.8	97.5	1.0
1-23a	2.19	1.80	2.95	17.7	38.8	99.8	0.1
1-23b	2.20	1.84	2.94	16.4	37.5	96.4	1.3
2-3a	2.19	1.80	2.99	17.7	39.7	97.9	0.8
2-3b	2.19	1.80	3.00	17.8	39.9	97.5	1.0
2-12a	2.21	1.83	2.98	17.2	38.6	98.3	0.6
2-12b	2.24	1.87	2.98	16.5	37.2	99.1	0.3
2-25a	2.20	1.83	2.96	16.9	38.3	97.0	1.1
2-25b	2.20	1.81	2.98	17.5	39.2	98.1	0.7
3-2a	2.21	1.82	2.99	17.4	39.1	98.4	0.6
3-2b	2.22	1.85	3.00	16.8	38.4	97.0	1.1
3-12a	2.18	1.79	2.98	17.8	39.7	97.8	0.9
3-12b	2.18	1.79	2.97	17.8	39.7	97.6	0.9
3-24a	2.20	1.82	2.98	17.4	39.0	98.5	0.6
3-24b	2.19	1.80	2.97	17.7	39.3	98.6	0.6

program were undrained and cycled. The number of tests of each type are given in Table 2. Results are summarized in Figures 1 through 7. Detailed results are given in Appendix B. The prime test result used for comparison is permanent compaction, given as percent volume strain remaining following one uniaxial strain load-unload cycle.

Table 3

Uniaxial Strain Tests - Curing Time Effects
Showing Number of Tests

Test Type	Time After Cast (Days)						
	7	14	16	18	21	28	56
Room Temperature	2	2			2	2	2
Refrigerated			3	3	3	3	3

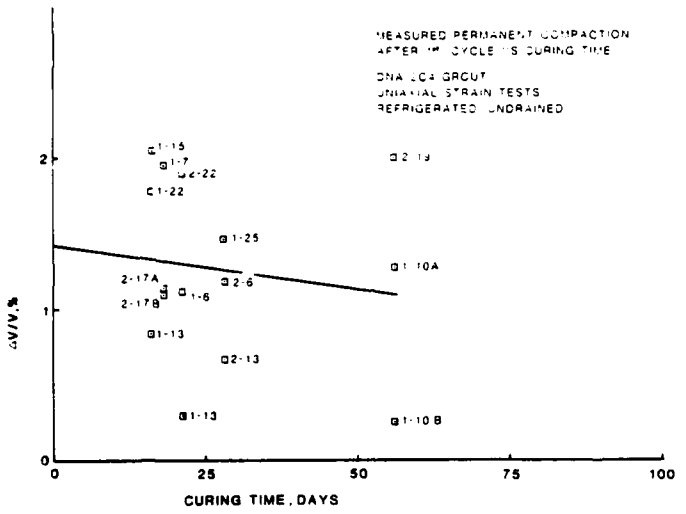

Figure 1. Measured Permanent Compaction After 1st 1-D Cycle versus Curing Time - Refrigerated.

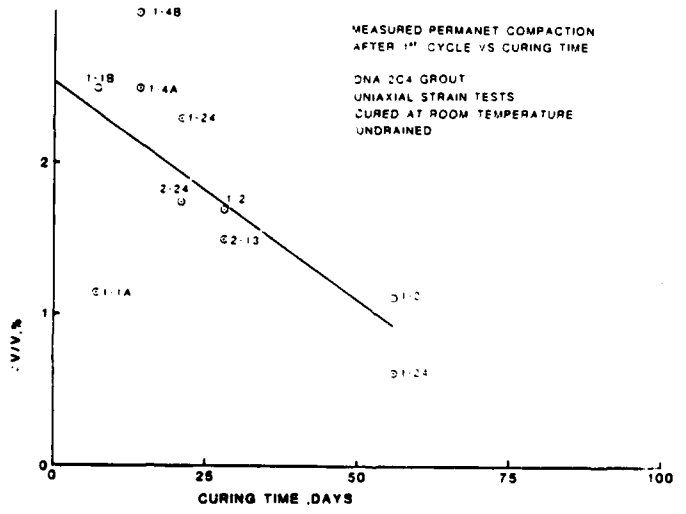

Figure 2. Measured Permanent Compaction After 1st 1-D Cycle versus Curing Time - Cured at Room Temperature.

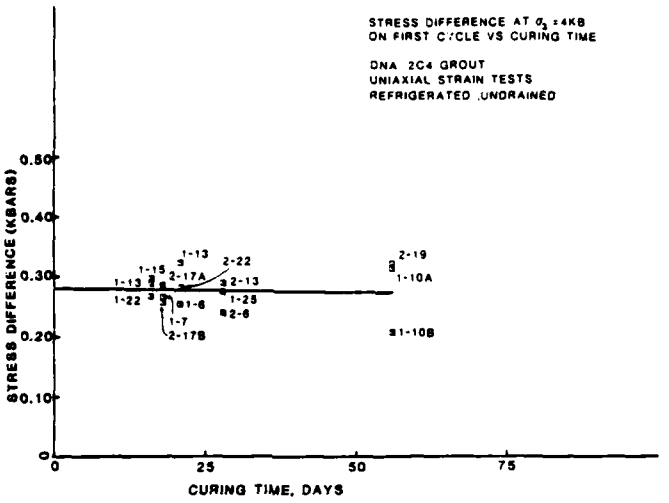

Figure 3. Stress Difference at σ_3 = 4 kb on First 1-D Cycle versus Curing Time - Refrigerated.

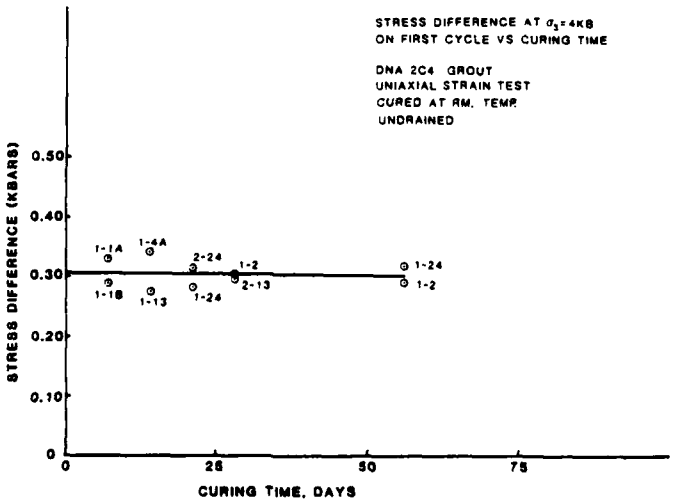

Figure 4. Stress Difference at σ_3 = 4 kb on First 1-D Cycle versus Curing Time - Cured at Room Temperature.

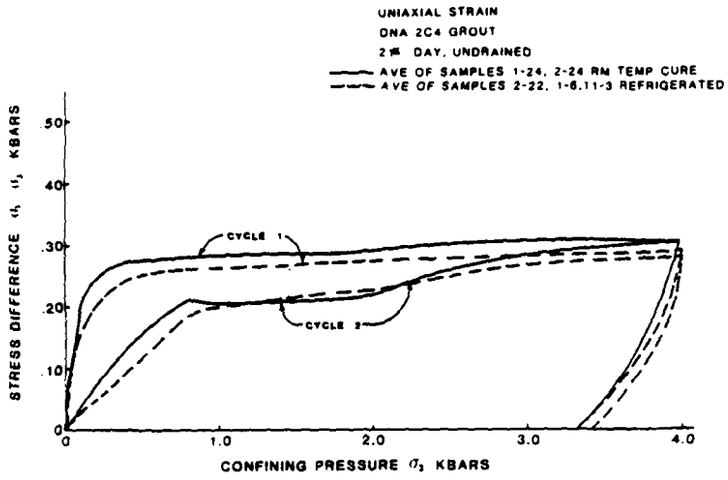

Figure 5. Uniaxial Strain - 21st Day

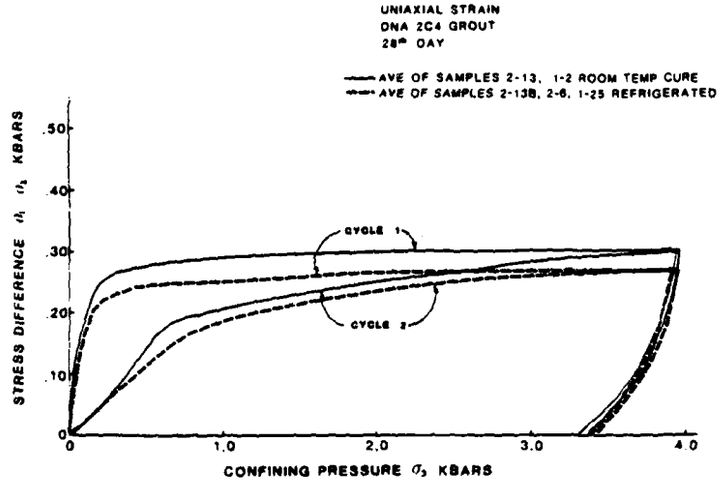

Figure 6. Uniaxial Strain - 28th Day.

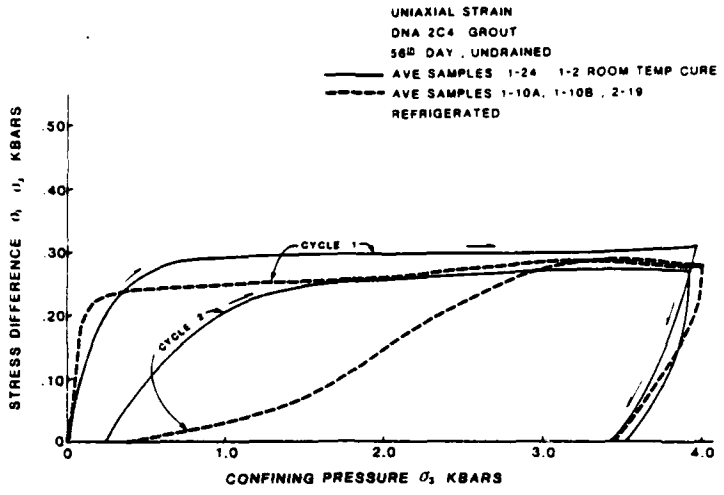

Figure 7. Uniaxial Strain - 56th Day.

Room-temperature cured samples show a definite curing-time effect. This is shown in Figure 2. A decrease in permanent compaction is seen as a function of curing time. A least-squares line with a slope of -0.03% volume strain/day fits the data. The decrease in permanent compaction with curing time indicates a strengthening caused by curing. In comparison, results for samples refrigerated on the 14th day, shown in Figure 1, indicate little effect.

For the same tests, no significant change is seen in maximum stress difference (Figures 3 and 4) sustained during the first cycle at ultimate confining pressures by the refrigerated and room temperature samples as the cure proceeds. However, if the averaged shear stress versus confining pressure plots, Figures 5 through 7, from samples tested at 56, 28, and 21 days are compared, one finds that the room temperature cured samples sustain higher stress differences than the refrigerated samples on the 1st and 2nd cycles at confining pressures below 1 kbar. This further confirms that the refrigerated samples do not gain strength with age as compared to the room temperature-cured samples.

Results of the uniaxial strain tests indicate, therefore, that refrigerating the samples did sufficiently slow the curing process such that the changes in material properties associated with curing were small as compared to the normal data variation. Thus, a set of material samples with uniform properties was available for the entire extended test program.

3.3 Hydrostatic Compression Tests

Semi-drained (with pore pressure, P_p, equal to 10 bars and 500 bars and with measurement of fluid loss), undrained, and unjacketed hydrostatic compression tests were conducted to 4 kbar confining pressure. Table 3 gives the number of tests conducted in each category.

Table 4

Hydrostatic Compression Tests
Showing Number of Tests

Test Type	No. of Tests
Pore Pressure-Controlled	
i) P_p = 10 bars*	2
ii) P_p = 500 bars*	1
Unjacketed $P_c = P_p$	2
Undrained	2

*Measured exuded fluid

Results from the hydrostatic compression tests are summarized in Figure 8. Also presented, for reference now, and to be discussed later, are the compressibility of water [Ref. 6], the compressibility of a sand (Lapis Lustre [Ref. 3]), and an estimate of the grain compressibility of 2C-4 grout based on the compressibility of an equivalent mixture of hydrating gypsum and sand.

Individual semi-drained, undrained, and unjacketed hydrostatic compression results are given in Figures 9 through 15 respectively.

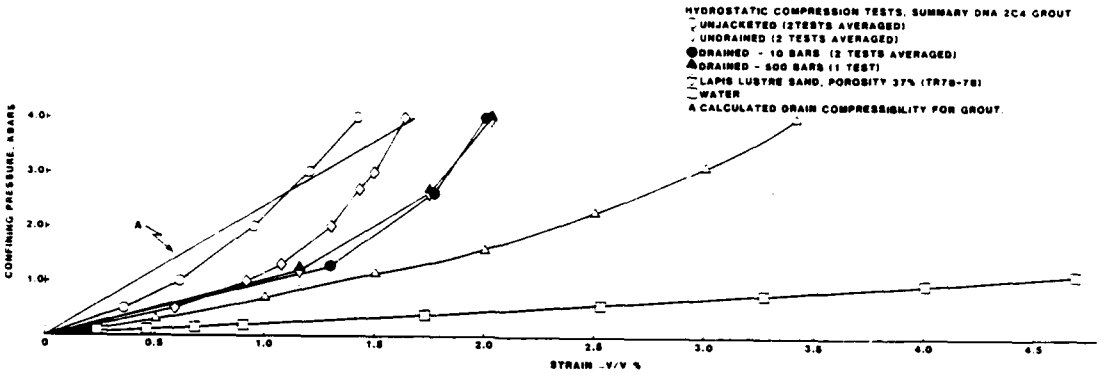

Figure 8. Hydrostatic Compression Test Summary.

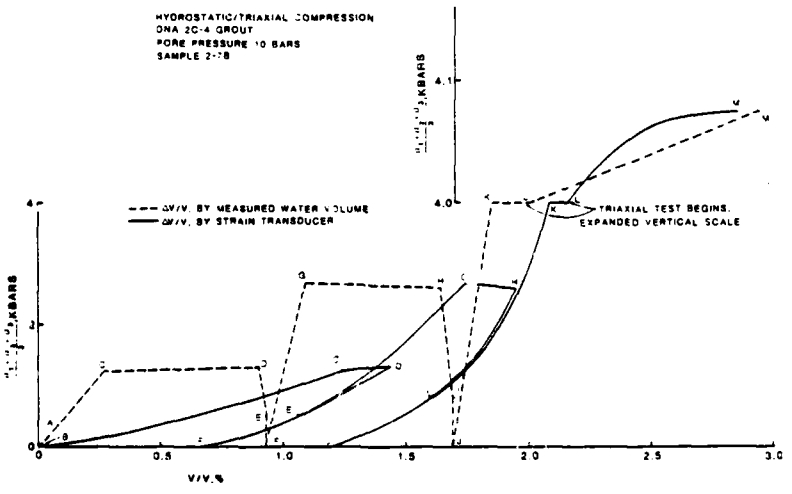

Figure 9. Hydrostatic/Triaxial Compression, Pore Pressure 10 Bars.

AD-A128 368 PROPERTIES OF TUFFS GROUT AND OTHER MATERIALS(U) TERRA TEK INC SALT LAKE CITY UT C H COOLEY ET AL. 01 JAN 82 TTI-TR-82-05 DNA-5986F DNA001-78-C-0395 2/3

UNCLASSIFIED F/G 8/7 NL

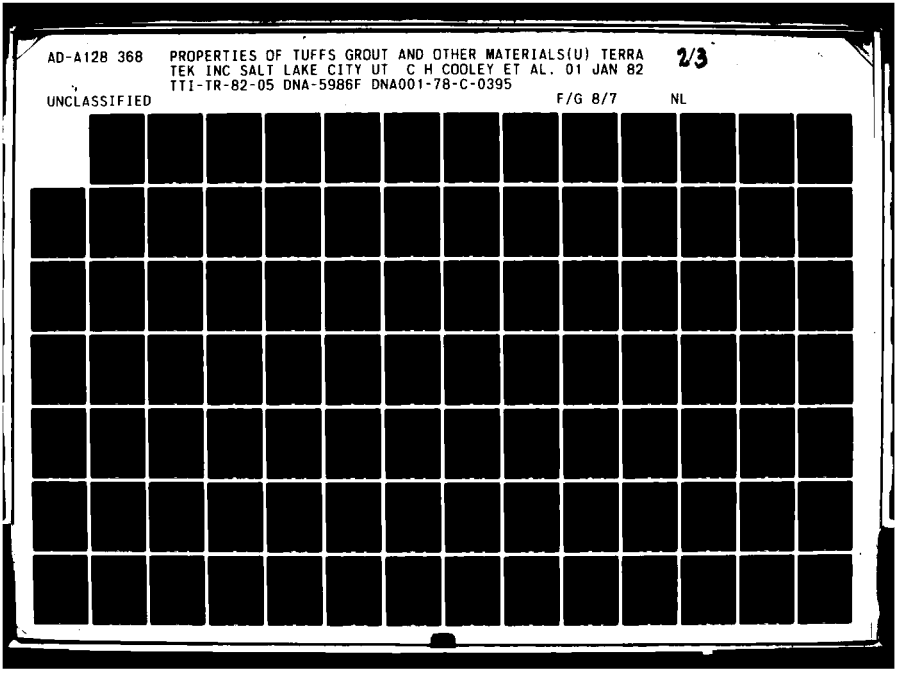

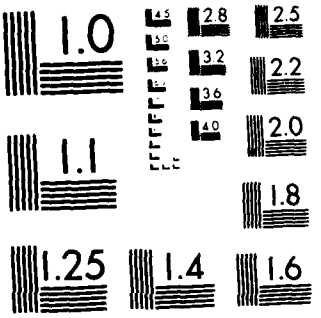

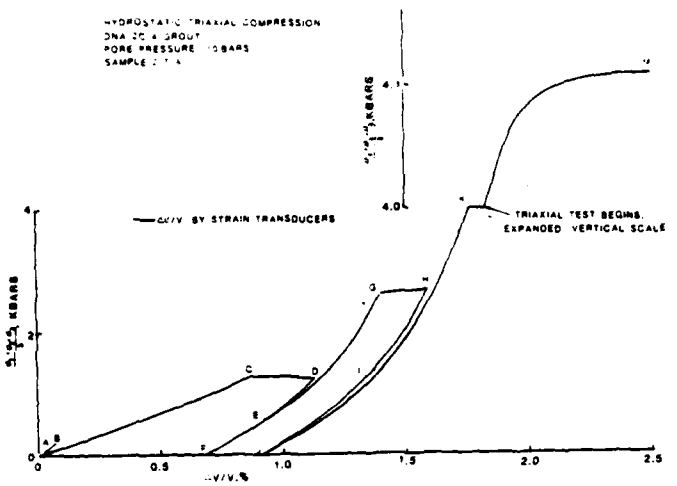

Figure 10. Hydrostatic/Triaxial Compression, Pore Pressure 10 Bars.

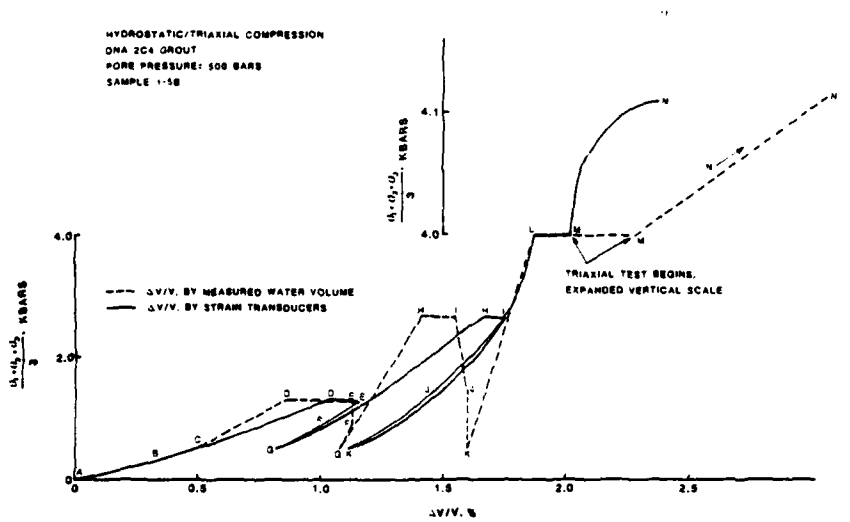

Figure 11. Hydrostatic/Triaxial Compression, Pore Pressure 500 Bars.

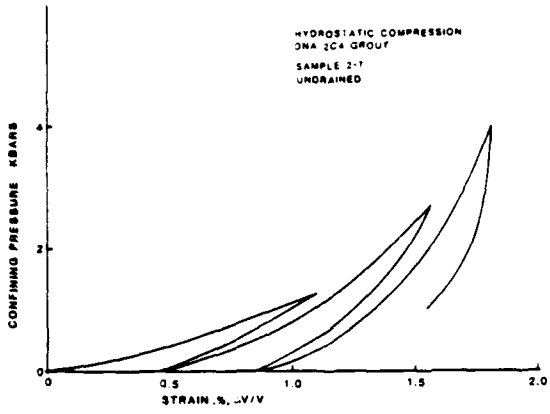

Figure 12. Hydrostatic Compression, Undrained.

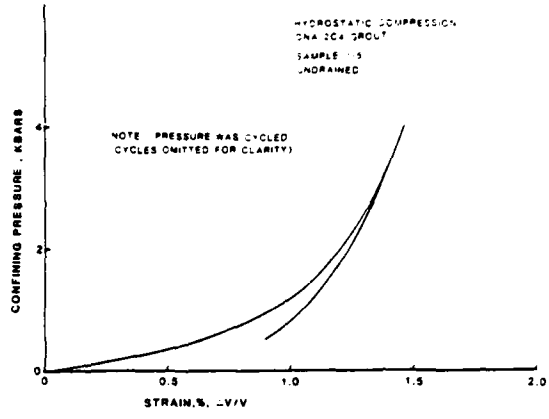

Figure 13. Hydrostatic Compression, Undrained.

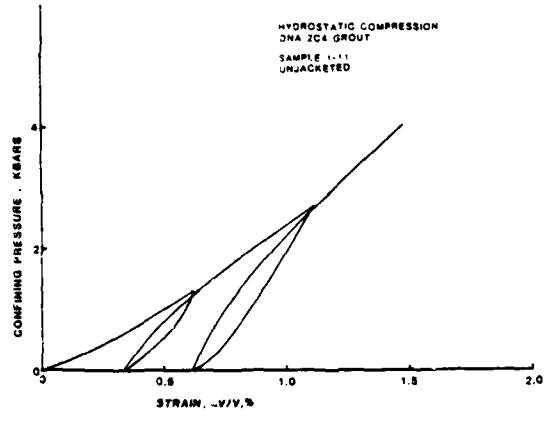

Figure 14. Hydrostatic Compression, Unjacketed.

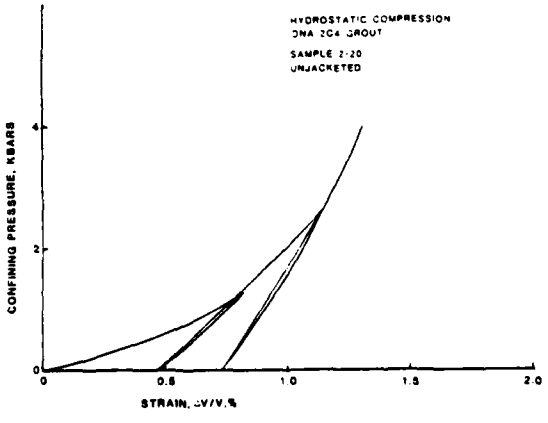

Figure 15. Hydrostatic Compression, Unjacketed.

Tables 4 and 5 give a comparison of the volume strains calculated from the strain transducer data and the volume strains calculated from the exuded pore fluid data during semi-drained tests. The test with pore pressures of 10 bars (Figure 9) and 500 bars (Figure 11) differ somewhat in how the pore fluid volume change is measured and presented. For the 10 bar test, pore fluid volume data starts at low pressure while for the 500 bar test data starts at ~500 bars. This is done because the confining pressure must be maintained slightly larger than pore pressure at all times to prevent jacket rupture. For the 500 bar test, pore pressure was continuously increased until somewhat greater than 500 bars confining pressure was reached. Therefore, constant pore pressure drainage information is not available until the pore pressure equaled approximately 500 bars.

For help in comparing these data, the following comments are offered: the unjacketed sample (see Figure 8) exhibited the stiffest response during the hydrostatic compression test. The undrained hydrostatic test results are bounded by the unjacketed test results and undrained tests on Lapis Lustre sand (which was unconsolidated and had a porosity of approximately 40%). One would expect the undrained behavior of the cemented 2C-4 grout to lie between these two bounds, as it does. The stiffest possible response would correspond approximately to one minus porosity times stiffness of the grains (unjacketed test) and the most compliant undrained response would correspond to that of an unconsolidated, uncemented material composed of the same material and having the same porosity (sand test).

Exuded Pore Fluid Results - For the 10 bar test, as seen in Table 4 and Figure 9, the final total strain as measured by exuded pore fluid agrees relatively well with the strain transducer results. Note, however, that during the test, the fluid volume lags the transducer volume, as would be expected for time-dependent drainage.

TABLE 5

HYDROSTATIC/TRIAXIAL COMPRESSION

DNA 2C-4 GROUT: 8/6/80 POUR

PORE PRESSURE = 10 BARS

SAMPLE 2-7B

Interval	Mean Stress kb	Incremental* Volume Strain, % (by water volume)	Accumulated Total Strain from pt. D	Incremental* Volume Strain, % (by strain transducers)	Accumulated Total Strain from pt. D
A-B	0			+ .01	
B-C**	1.2	+.27		+1.24	
C-D	1.3	+.63	0.90	+ .19	1.43
D-E	0.5	+.03	0.93	- .39	1.04
E-F	0	0	0.93	- .38	0.66
F-G	2.6	+.16	1.09	+1.07	1.73
G-H	2.6	+.55	1.64	+ .20	1.93
H-I	0.8	+.05	1.69	- .35	1.58
I-J	0	0	1.69	- .39	1.19
J-K	4.0	+.16	1.85	+ .88	2.07
K-L	4.0	+.16	2.01	+ .08	2.15
L-M	4.1	+.93	2.94	+ .69	2.84

*Positive means volume compaction.
**Point from which the pore pressure was held constant and from which fluid volume measurements were made.

TABLE 6

HYDROSTATIC/TRIAXIAL COMPRESSION

DNA 2C-4 GROUT: 8/6/80 POUR

PORE PRESSURE = 500 BARS

SAMPLE 1-5B

Interval	Mean Stress kb	Incremental* Volume Strain, % (by water volume)	Accumulated Total Strain from pt. D	Incremental* Volume Strain, % (by strain transducers)	Accumulated Total Strain from pt. D	Accumulated Total Strain from pt. A
A-B	0.3			+.33		
B	0.3			0		0.33
B-C	0.5			+.15		0.48
C	0.5			0		0.48
C-D**	1.3	+.38		+.56		1.04
D-E	1.3	+.27	0.65	+.11	0.67	1.15
E-F	0.9	0	0.65	-.15	0.52	1.00
F-G	0.5	-.05	0.60	-.18	0.34	0.82
G-H	2.7	+.33	0.93	+.85	1.19	1.67
H-I	2.7	+.14	1.07	+.07	1.26	1.74
I-J	1.4	+.05	1.12	-.29	0.97	1.45
J-K	0.5	0	1.12	-.33	0.64	1.12
K-L	4.0	+.27	1.39	+.75	1.39	1.87
L-M	4.0	+.41	1.80	+.15	1.54	2.02
M-N	4.1	+.88	2.68	+.36	1.90	2.38

*Positive means volume compaction.
**Point from which the pore pressure was held constant and from which fluid volume measurements were made.

For the 500 bar test, as seen from Table 5 and Figure 11, the volume strain interpreted from measurements of the exuded pore fluid taken from point D is larger than the volume strain measured by strain transducers taken from point D. During hydrostatic compression loading to 500 bars, water was compressed in the pore pressure generator to establish 500 bars pore pressure. As will be shown later, 2C-4 grout is very impermeable and therefore required considerable equilibration time. It is therefore possible that during the hydrostatic compression to 500 bars confining pressure less water came out of the sample than should have for complete drainage. This would have resulted in more volume change of the pressure generator than necessary to establish 500 bars external pore pressure had equilibrium been maintained. In turn, generator volume would later be increased even more as further drainage occurred. This possibility is supported if one totals the transducer strain from point A, the onset of testing, instead of from point D. The result is 2.38%, which agrees better with the 2.68% strain as measured by the exuded pore fluid for the total test than it does with the value from point D.

All of the above information indicates that drainage time is a very important parameter in these tests. The measured permeabilities (given later in Section 3.5) were often less than 1 μdarcy. Such low permeabilities would cause equilibration times for samples of these dimensions to be greater than 1 hour. For these, tests times of only 5 minutes were allowed. Therefore, it is likely that the tests described in this section were not fully drained, but instead "semi-drained". A special drainage test is described in Section 3.7.

3.4 Triaxial Compression Tests

Ten semi-drained tests were conducted at confining pressures from 0.069 kb to 4 kbar and at pore pressures equal to either 10 or 500 bars. Seven undrained tests were conducted at confining pressures between 0 and 4 kbars

confining stress and thirteen undrained and semi-drained triaxial compression experiments were conducted on samples that had been pre-tested. Two unjacketed experiments were conducted at a confining pressure of 4 kbars. Table 6 shows in detail the number of tests conducted of each experiment type.

Strength results for the foregoing tests are summarized in Figures 16 through 20. Figure 21 compares uniaxial strain test data on un-tested and cycled samples with triaxial compression data on untested and cycled samples. Figure 22 compares stress-strain data for the different types of triaxial tests at 1/2 kbar and Figure 23 compares undrained triaxial compression data at different confining pressures. The individual test data for all tests conducted in this section are given in Appendix C.

Table 7

Triaxial Compression Tests Showing Number of Tests

Test Type	Confining Pressure, kb						
	0	0.069	1/4	1/2	1	2	4
Drained							
i) P_p = 10 bars		1	1	1	1		2
ii) P_p = 500 bars				1	1		2
Undrained	1	1	1	1	1	1	1
Pre-Tested							
i) Undrained hydrostatic compression				1	1		
ii) Undrained uniaxial strain		2	2	2	2		2
iii) Drained uniaxial strain		1	1	1	1		1

Grout strength below 2 kbars confining stress is significantly reduced by pre-testing the samples. As seen from Figures 19, 20 and 21 this is true regardless if the test is drained or undrained or how the pre-testing was done, whether in a hydrostatic compression test or a uniaxial strain test. Furthermore, pre-testing reduced the stress difference sustained in uniaxial strain as shown in Figure 21. At the onset of testing the undrained uniaxial

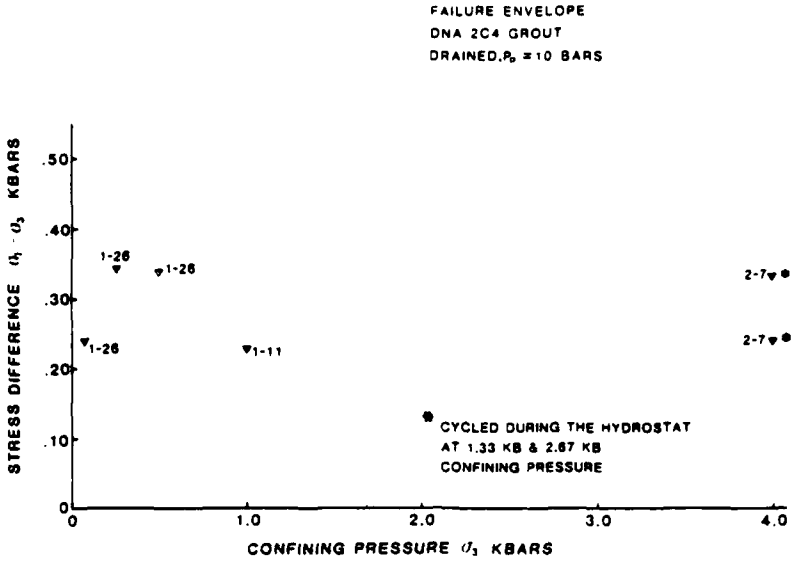

Figure 16. Failure Envelope, Drained, P_p = 10 Bars.

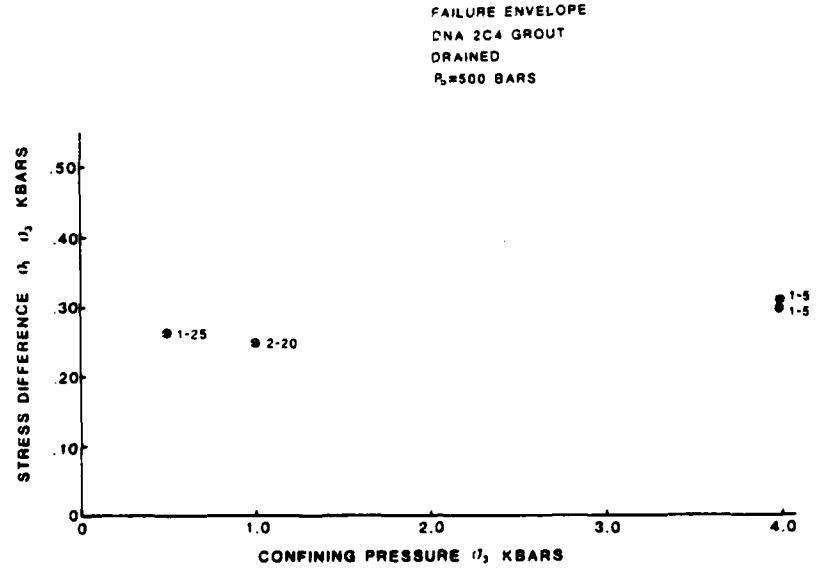

Figure 17. Failure Envelope, Drained, P_p = 500 Bars.

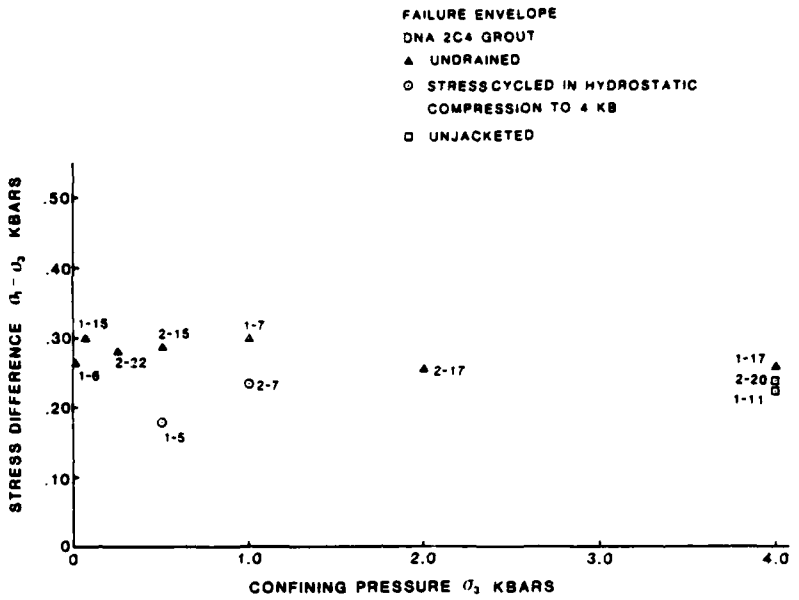

Figure 18. Failure Envelope, Undrained, Stress Cycled in Hydrostatic Compression to 4 kb, Unjacketed.

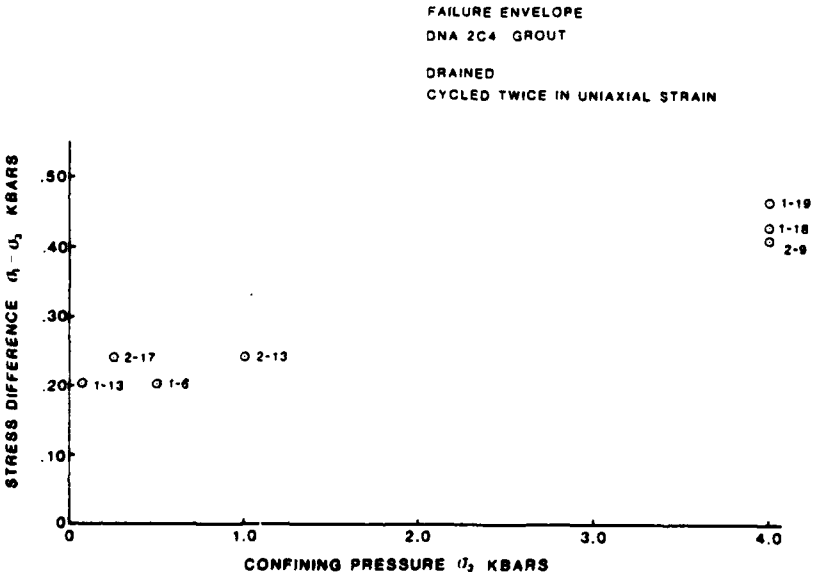

Figure 19. Failure Envelope, Drained, Cycled Twice in Uniaxial Strain.

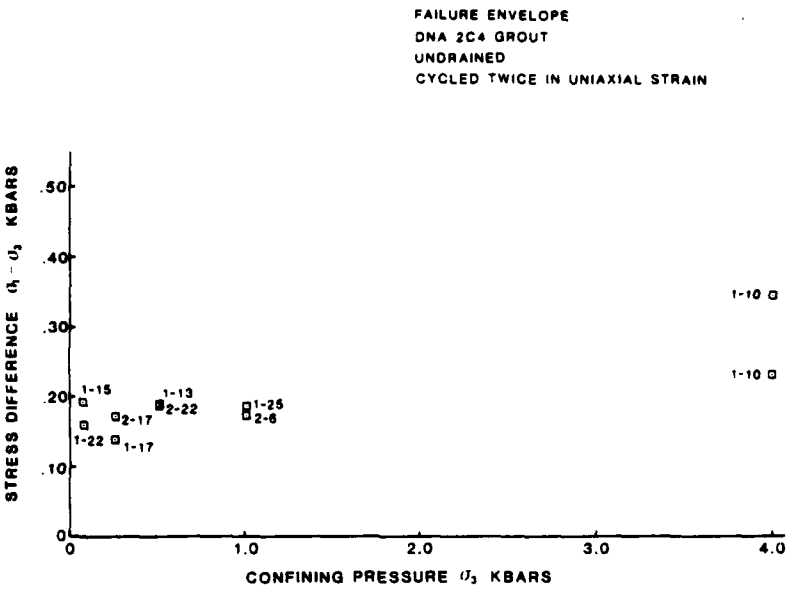

Figure 20. Failure Envelope, Undrained, Cycled Twice in Uniaxial Strain.

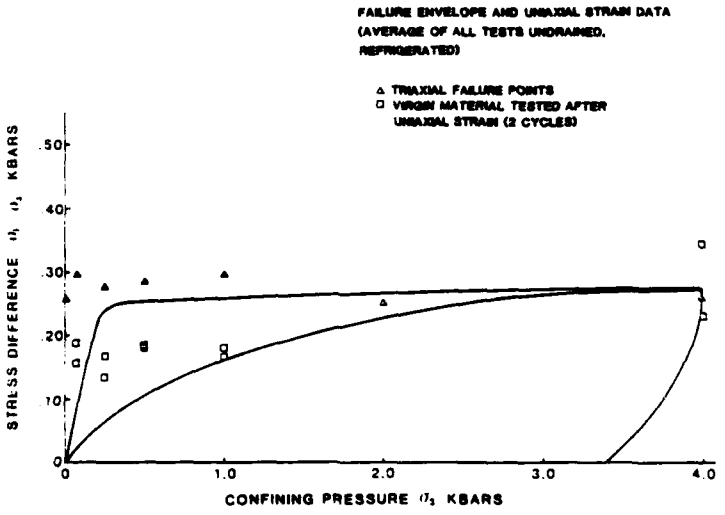

Figure 21. Failure Envelope and Uniaxial Strain Data (Average of all Undrained, Refrigerated Tests).

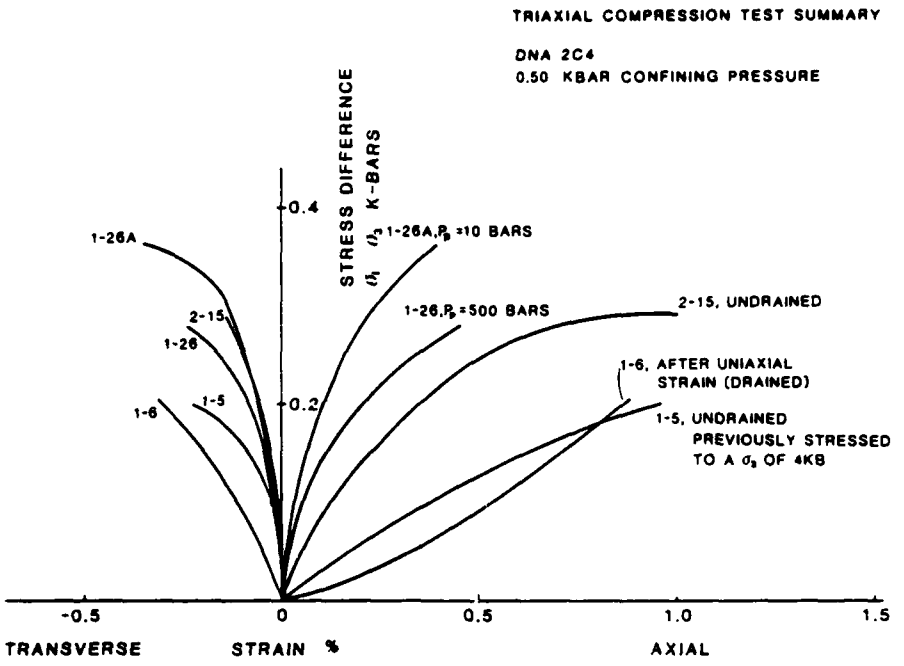

Figure 22. Triaxial Compression Test Summary, 0.50 kbar Confining Pressure.

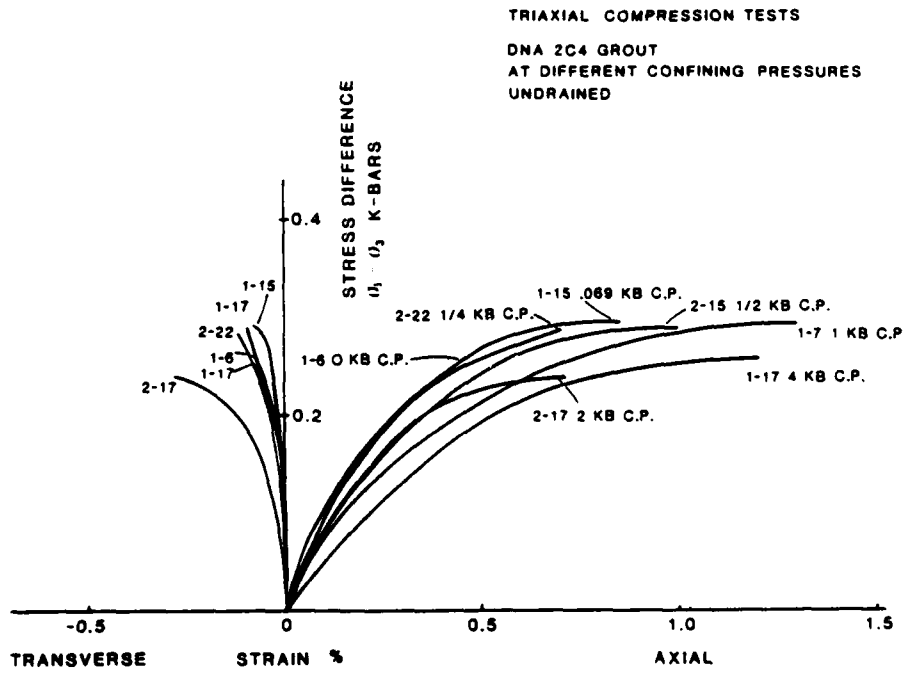

Figure 23. Triaxial Compression Tests, At Different Confining Pressures, Undrained.

strain data from untested samples lies slightly below the triaxial data for untested samples, as expected. During the 2nd cycle the 1-D strain test data suggests weakening of the material. When compared to the triaxial compression results on pre-tested samples the stress sustained during the uniaxial strain test is found, as before and as expected, to be slightly less for confining pressures less than 2 kbars. Above 2 kbars all the data coincide (i.e., average stress difference equals approximately 0.25 kbars).

Grout strengths for the previously untested samples are not strongly dependent on the test type, i.e. semi-drained, undrained or unjacketed. The unjacketed tests are perhaps slightly weaker at 4 kbars (Figure 18).

Perhaps an estimate of true drained strength at 4 kb confining stress is found from the data in Figure 19, presenting drained triaxial compression results on samples that have been pre-tested. Because these samples are damaged and have greater permeability (see the section on permeability results), one would expect them to drain more completely. These are by far the strongest samples at 4 kb confining stress. It might be reasonable to assume that a previously untested sample that was allowed to drain completely might be as strong as these cycled samples, although a complicating factor is that pre-compaction, as caused by pre-testing, could by itself be expected to increase strength.

It is interesting to note that by the end of the triaxial portion of these tests the exuded pore fluid volume begins to better agree with the strain transducer measurements (Figures 9 and 11). At some point during triaxial testing, samples apparently approached complete drainage. This is further supported by the data in Figure 22 which show that the drained samples were significantly stiffer during the triaxial portion of the experiment than the undrained samples. Whether this drainage occurred completely enough and

soon enough to provide a true fully-drained strength measurement is, however, still somewhat uncertain.

3.5 Permeability Measurements

Permeability measurements were made on two untested and two cycled samples at confining pressures between 13.8 bars and 483 bars (see Table 7). Pore pressure was maintained at 6.9 bars throughout. Figures 24 and 25 compare the previously untested sample permeability with the cycled sample permeability as functions of confining stress.

Table 8

Permeability Determinations Showing Number of Tests

Test Type	No. of Tests
Untested Samples	2
Cycled Samples	2

In both cases, permeability of the previously untested sample was about one microdarcy. Samples from tube 2-25 show an approximate doubling of permeability after being uniaxially strained, whereas samples from tube 1-18 show an order of magnitude increase. A large amount of permeability increase is therefore associated with test-caused damage. With increasing effective confining stress, the permeability decreased for both previously untested and stress cycled samples. At approximately ½ kbar effective stress, the measured permeability for both is equal and less than 0.2 μdarcies.

3.6 Strain Rate Tests

This section of the testing program was conducted in three parts. First, a series of unconfined tests were run. Strain rates were varied from 10^{-5} sec^{-1} to 10^{-1} sec^{-1}. Two tests were run at each strain rate for a total of 10 tests.

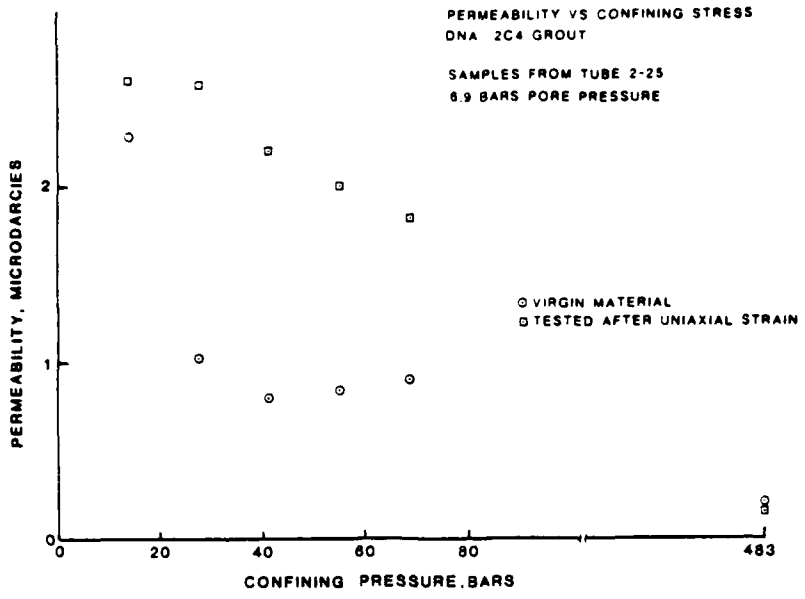

Figure 24. Permeability versus Confining Stress.

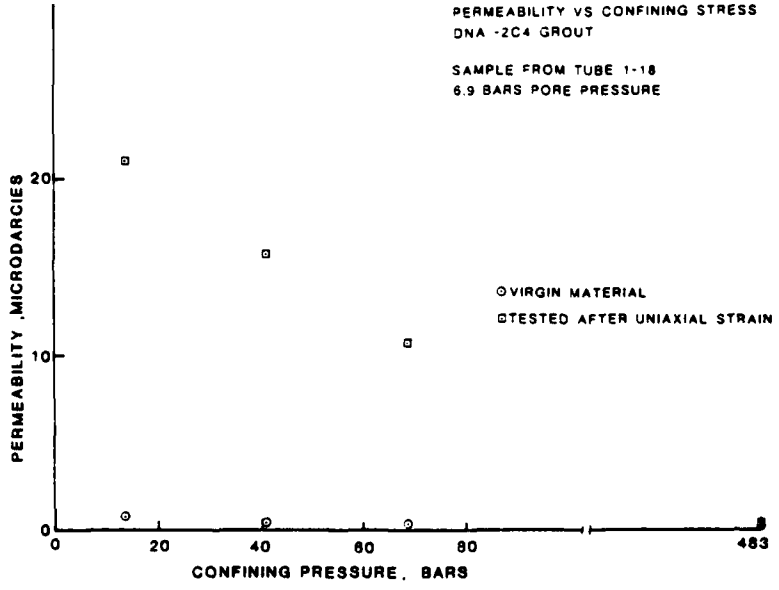

Figure 25. Permeability versus Confining Stress.

Second, a series of uniaxial strain tests were run at rates of 10^{-5} sec^{-1} to 10^{-3} sec^{-1}. Three tests were conducted at each strain rate for a total of 9 tests.

Third, a series of triaxial compression tests were run at a confining pressure of 0.5 kbars. The strain rates varied from 10^{-5} sec^{-1} to 10^{-3} sec^{-1}, with one test at each strain rate.

The entire test matrix is summarized in Table 8.

Table 9

Strain Rate Tests Showing Number of Tests

Test Type	10^{-5}	10^{-4}	10^{-3}	10^{-2}	10^{-1}
Unconfined Compression	2	2	2	2	2
Uniaxial Strain Undrained	3	3	3		
Triaxial Compression Undrained	1	1	1		

Reviewing all the strength data shown in Figure 26 and the stress-strain data shown in Figures 27, 28 and 29, no evident trends with changing strain-rate are observed. Individual test data are found in Appendix D.

3.7 Special Drainage Test

This test was designed to allow significantly more drainage time (30 minutes up to 48 hours) than for the semi-drained tests (5 minutes). Data from this test are presented in Figure 30 in which volume strains as measured by the strain transducers and as measured by the exuded pore fluid are compared. Also, in Figures 31 and 32 the volume produced from the sample as a function of time is presented for each equilibration period. Table 9 presents the incremental and accumulated volume strains and the approximate time duration for each interval of the experiment.

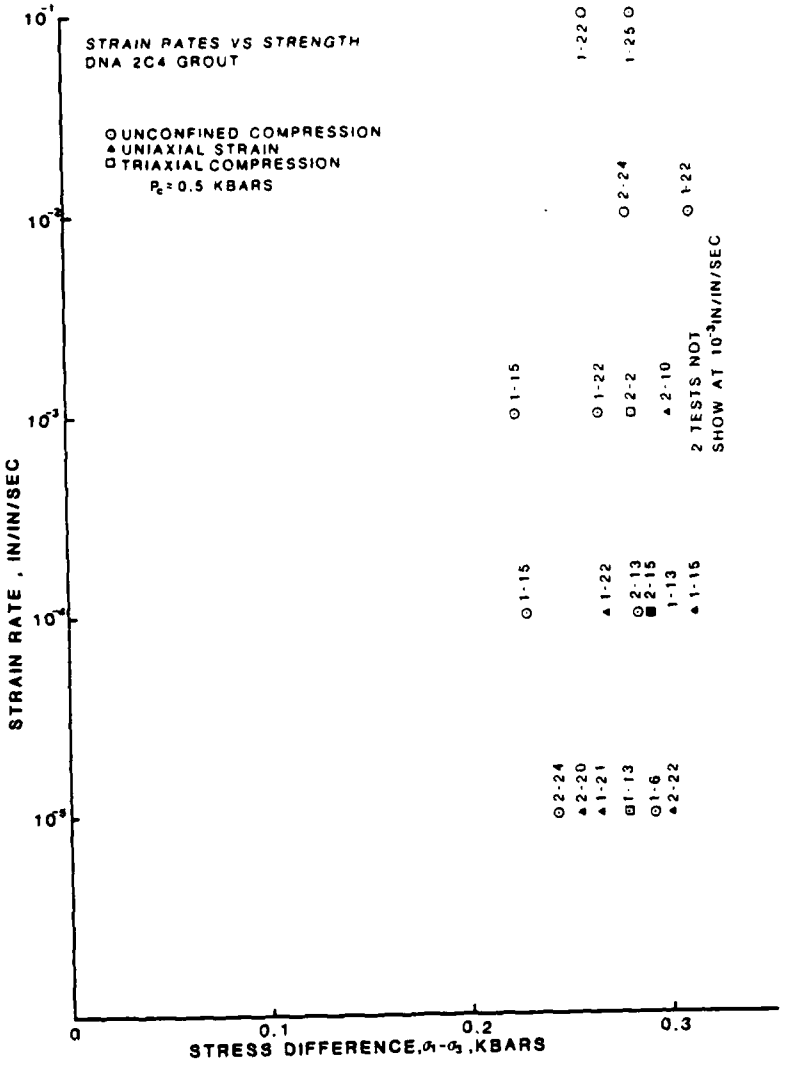

Figure 26. Strain Rates versus Strength.

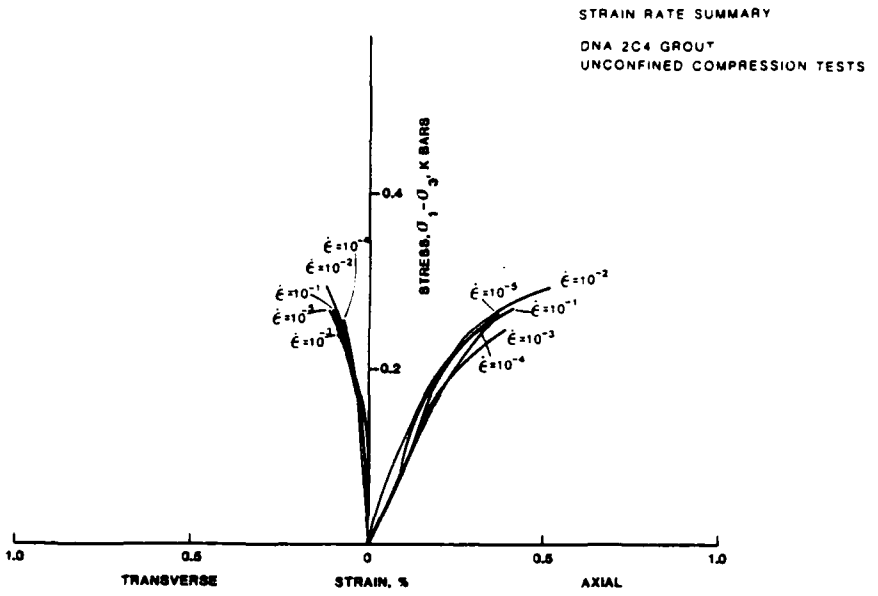

Figure 27. Strain Rate Summary for Unconfined Compression Tests.

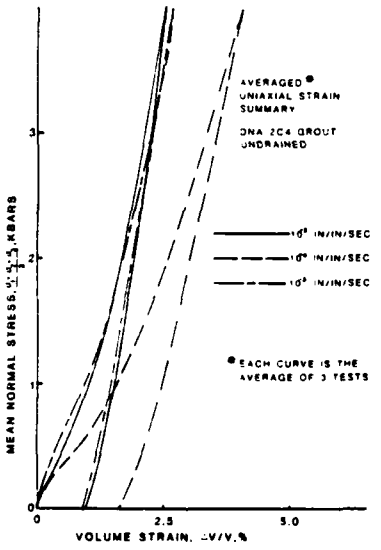

Figure 28. Averaged Uniaxial Strain Summary.

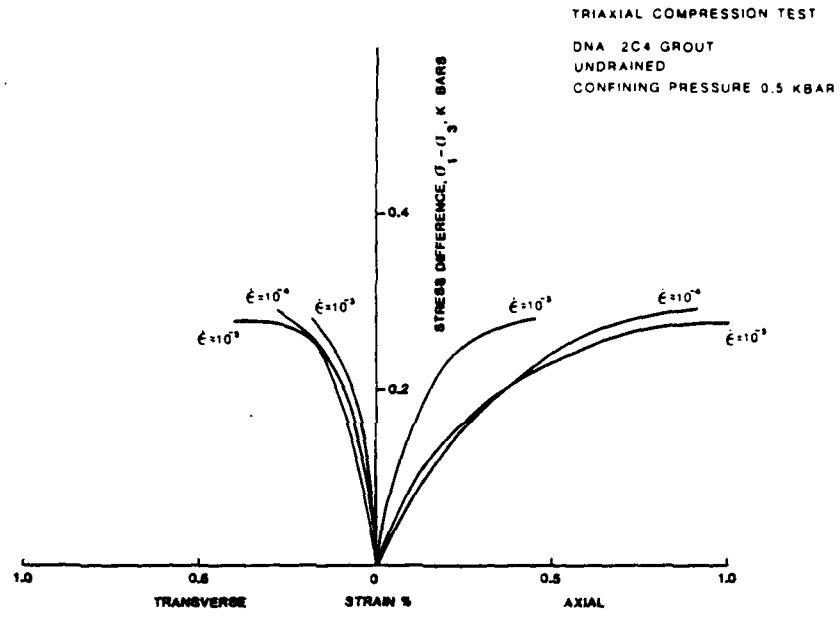

Figure 29. Triaxial Compression Test Summary, Confining Pressure 0.5 kbar.

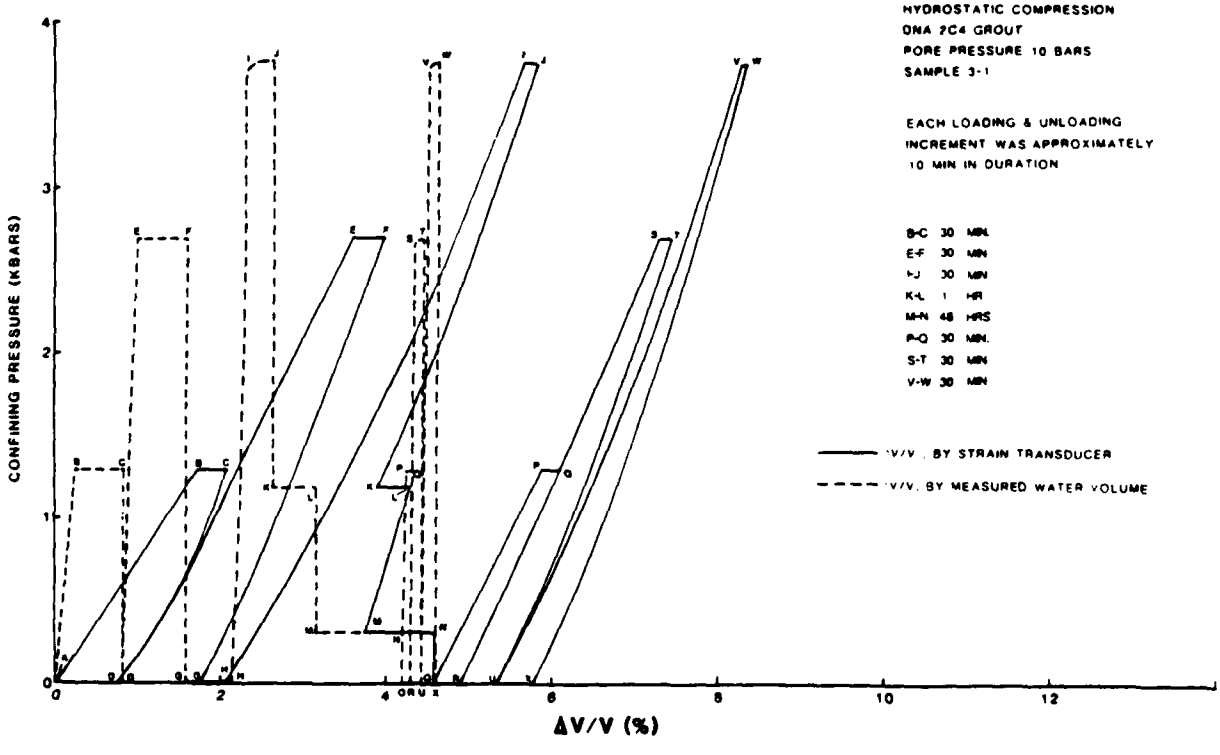

Figure 30. Special Drainage Test, Pore Pressure 10 Bars.

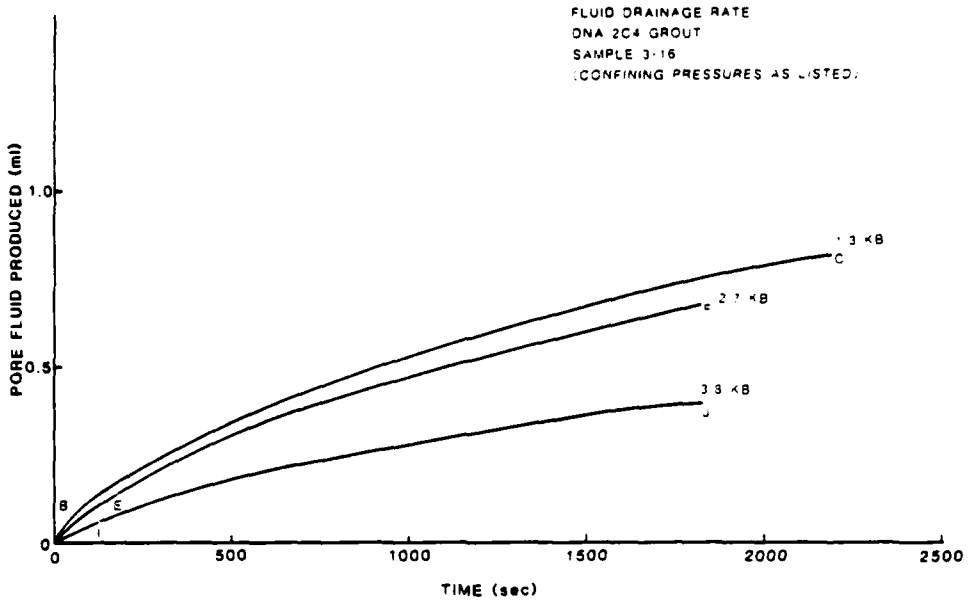

Figure 31. Fluid Drainage Rate.

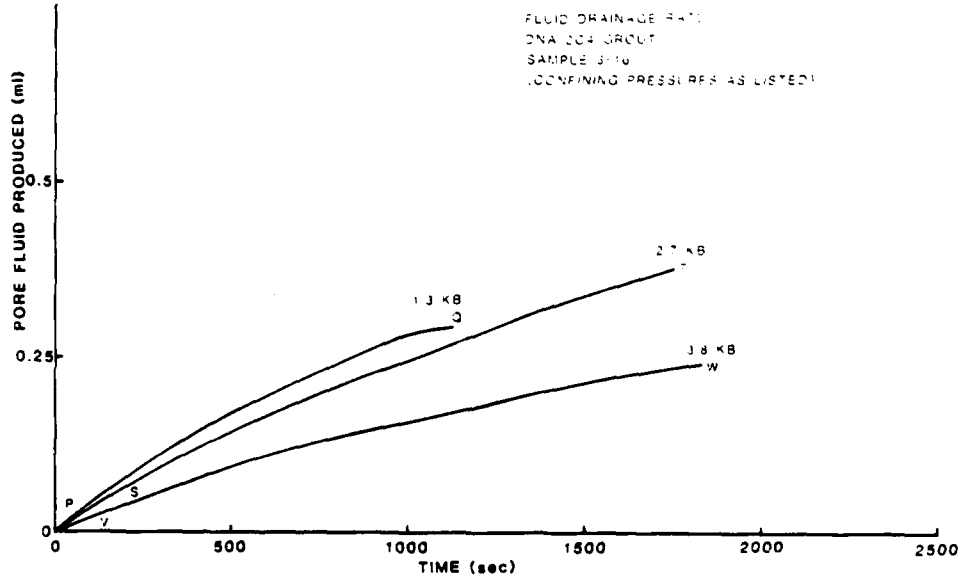

Figure 32. Fluid Drainage Rate.

TABLE 10

HYDROSTATIC COMPRESSION TEST

DNA 2C-4 GROUT

PORE PRESSURE = 10 BARS

Interval	Mean Stress (kb)	Incremental Volume Strain, % (by water volume)	Accumulated Total Strain	Incremental Volume Strain, % (by strain transducers)	Accumulated Total Strain	Interval Duration (approx.)
A-B	1.3	0.26	0.26	+1.72	1.72	*
B-C	1.3	0.58	0.84	+0.36	2.08	30 min
C-D	0	0.0	0.84	-1.32	0.76	*
D-E	2.7	0.16	1.00	+2.84	3.60	*
E-F	2.7	0.60	1.60	+0.38	3.98	30 min
F-G	0	0.0	1.60	-2.22	1.76	*
G-H	0	0.54	2.14	+0.30	2.06	20 min
H-I	3.8	0.16	2.30	+3.60	5.66	*
I-J	3.8	0.34	2.64	+0.16	5.82	30 min
J-K	1.2	0.02	2.66	-1.88	3.94	*
K-L	1.2	0.50	3.16	+0.38	4.33	1 hour
L-M	0.3	0.02	3.18	-0.56	3.76	*
M-N	0.3	1.02	4.20	+0.84	4.60	48 hours
N-O	0	0	4.20	0	4.60	*
O-P	1.3	0.04	4.24	+1.28	5.88	*
P-Q	1.3	0.08	4.32	+0.20	6.08	30 min
Q-R	0	-0.02	4.30	-1.18	4.90	*
R-S	2.7	+0.02	4.32	+2.38	7.28	*
S-T	2.7	0.12	4.44	+0.16	7.44	30 min
T-U	0	0	4.44	-2.08	5.36	*
U-V	3.8	0.08	4.52	+2.92	8.28	*
V-W	3.8	0.10	4.62	+0.06	8.34	30 min
W-X	0	0	4.62	-2.56	5.78	*

*Loading and unloading increments were approximately 10 minutes in duration.

From Figure 30 it is evident that despite the significantly longer equilibration times, complete drainage is still not always reached during intermediate cycles. For example, had there been complete drainage at 4 kbars, the two strain measurement methods would have agreed and both would be located to the right of point "I" as measured by the strain transducers. That this is true is demonstrated by point "N" which was measured after 48 hours of equilibration time. Here both strain measurements agree within experimental error, and it appears that full drainage had occurred.

It appears that given enough time, complete drainage does occur and the two strain measurement methods agree. Thus, it should be possible to estimate the final strain at each pressure increment using the volume produced versus time data and an appropriate mathematical analysis. Such an analysis using a diffusion model and certain simplifying assumptions has identified complexi-

ties that must be included in the final analysis: First, the permeability is strongly dependent on effective stress. This must be accounted for because effective stress changes dramatically with drainage time, especially at the lower confining pressures, as can be inferred from Figures 31 and 32. Second are the effective stress increases, step-wise and incremental. This causes superimposed decays, each with a different time constant, which also must be accounted for.

4. SUMMARY AND CONCLUSIONS

- The casting and curing process adopted produces 2C-4 grout with consistent properties.
- Refrigerating the samples at 14 days of cure slows the curing process sufficiently to allow testing to continue on refrigerated samples after 14 days and yet maintain 14 day properties.
- Permeability to water is approximately 1 μdarcy at an effective confining stress of 6.9 bars. With increased effective confining stress to ½ kbar permeability diminishes to less than 0.2 μdarcies. Subjecting samples to a uniaxial strain test to 4 kbars dramatically increases permeability at 6.9 bars effective confining stress. As effective confining stress increases to ½ kbar, however, permeability again decreases to its originally low value of less than 0.2 μdarcies.
- "Drained" hydrostatic compression tests were only "semi-drained" because of the long drainage times required for the low-permeability material.
- The special drained test showed that complete drainage will occur in less than 48 hours at 0.3 kbars confining pressure. Further, it should be possible to estimate the drained behavior. These estimates are pending the application of the appropriate analytical technique.
- At confining pressures below 2 kbars cycled samples are significantly weaker than previously untested samples.
- Unjacketed samples are weaker than undrained samples at 4 kbars confining stress. The true drained strength of 2C-4 grout at 4 kbars confining stress has an approximate lower bound of 0.30 kbars which is the measured strength of the drained uncycled samples, and an approximate upper bound of 0.42 kbars which is the measured strength of the drained cycled samples.

- Within the resolution of these experiments, there are no perceptible strain rate effects for uniaxial strain tests and triaxial compression tests conducted at strain rates between 10^{-5} sec^{-1} and 10^{-3} sec^{-1} and for unconfined compression tests conducted at strain rates between 10^{-5} sec^{-1} and 10^{-1} sec^{-1}.

5. REFERENCES

1. Dropek, R.K., S.W. Butters and A.H. Jones, "Methods for Determination of Physical Properties of Rock Materials," TR 75-13, October 1975.

2. Brace, W.F., J.B. Walsh and W.T. Frangos, "Permeability of Granite Under High Pressure", JGR, Vol. 73, No. 6, March 1968.

3. Gardner, D.S., S.W. Butters and A.H. Jones, "Material Properties of Nevada Test Site Tuff," TR 78-78, November 1978.

4. Pratt, H.R., S.J. Green, A.H. Jones and W.F. Brace, "Physical and Mechanical Properties of Selected Geologic Materials, A Compendium," TR 75-3, January 1975.

5. Isenberg, J. (editor), "Nuclear Geoplosics, Part Two: Mechanical Properties of Earth Materials," DNA 1285 H 2, November 1972.

6. Keenan and Keys "Steam Tables" John Wiley and Sons, 1978.

6. APPENDICES

APPENDIX A

PHYSICAL PROPERTIES FORMULAE

The symbols and equations used for the measured and calculated physical properties are as follows:

Symbols

*ρ_w = in-situ bulk density (wet or "as-received" density)(gm/cm^3)

*ρ_g = grain density (density of solids)(gm/cm^3)

ρ_{H_2O} = density of water (gm/cm^3)

*w = moisture content (percent by wet weight)

ρ_d = dry bulk density after oven drying (gm/cm^3)

η_t = total porosity (percent of total rock volume)

S_r = degree of saturation (percent of void volume)

V_{av} = air void content (percent of total rock volume)

Equations

$$\rho_d = \rho_w \left(1 - \frac{w}{100}\right)$$

$$\eta_t = 100 \times \left(1 - \frac{\rho_d}{\rho_g}\right)$$

$$S_r = 100 \times \frac{(w \times \rho_w)}{(\eta_t \times \rho_{H_2O})}$$

$$V_{av} \approx 100 \times [1 + \rho_d (1 - 1/\rho_g) - \rho_w]$$

*Measured parameters.

APPENDIX B

CURING TIME EFFECTS

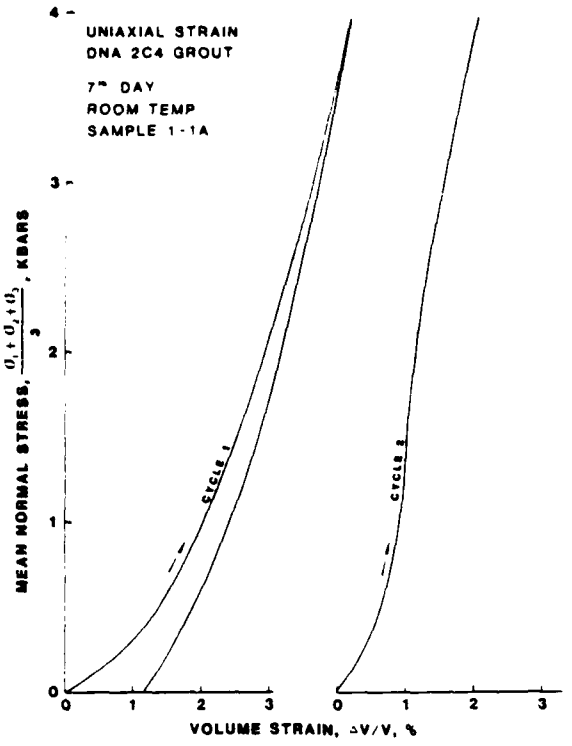

Figure B1a

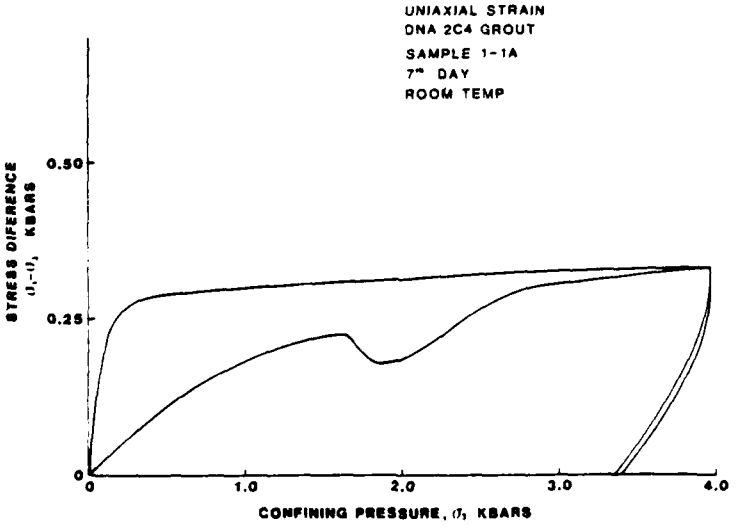

Figure B1b

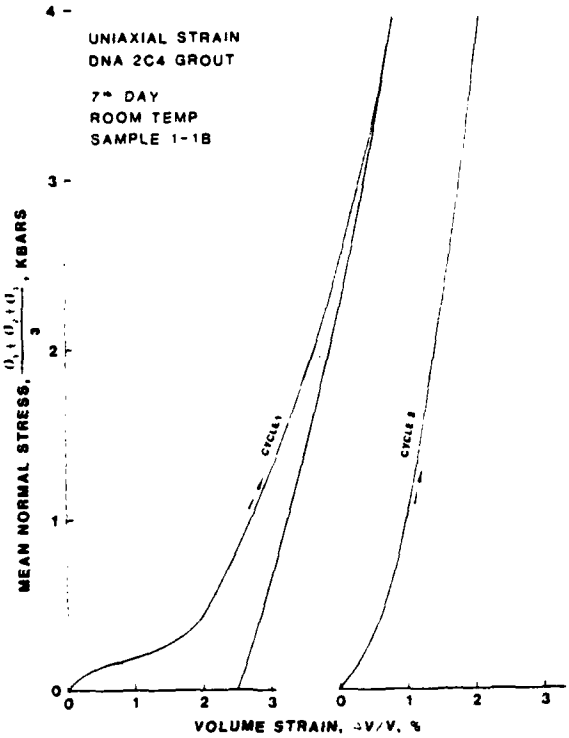

Figure B2a

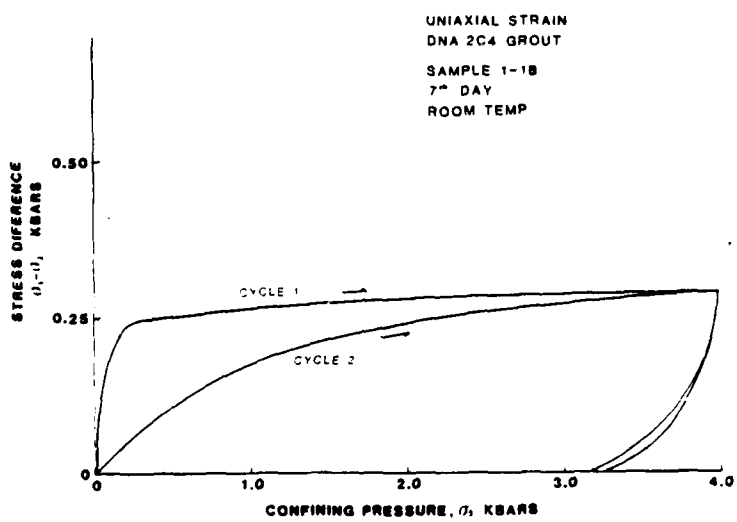

Figure B2b

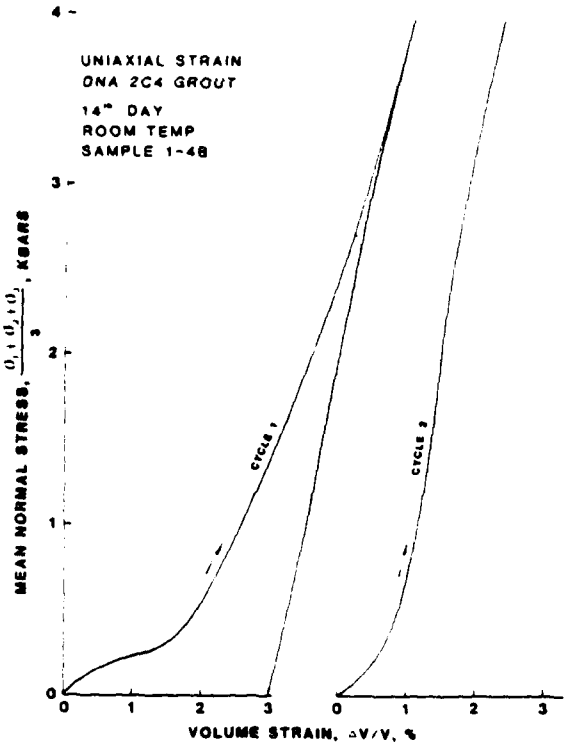

Figure B3a

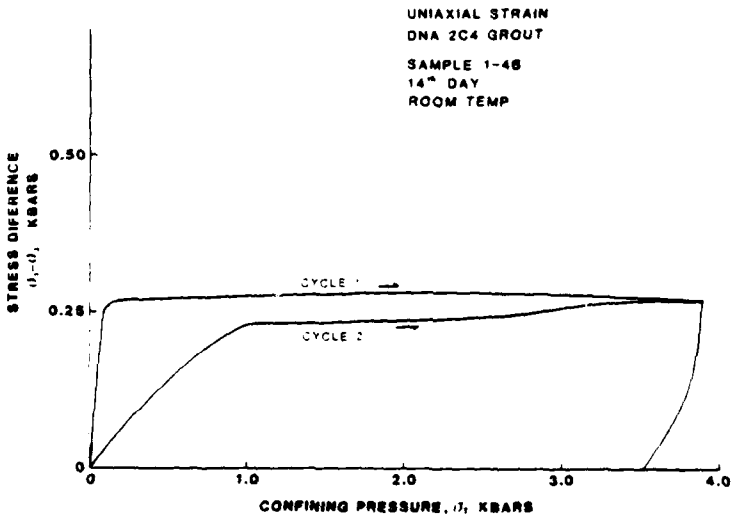

Figure B3b

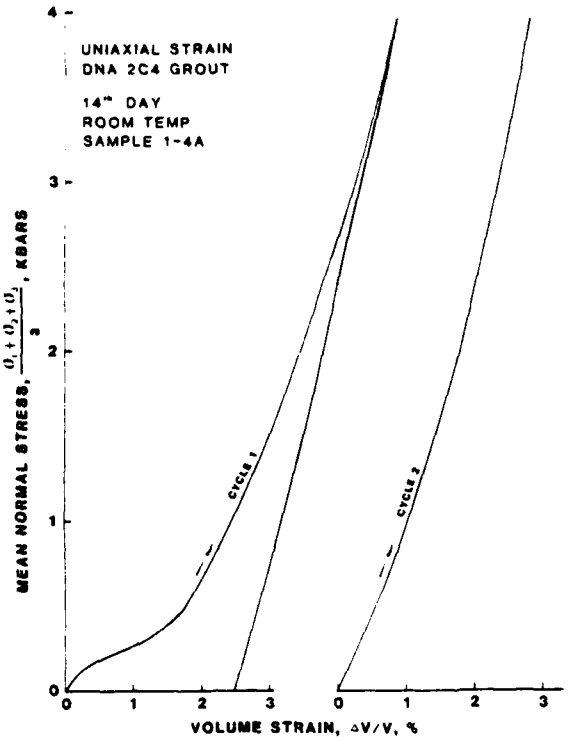

Figure B4a

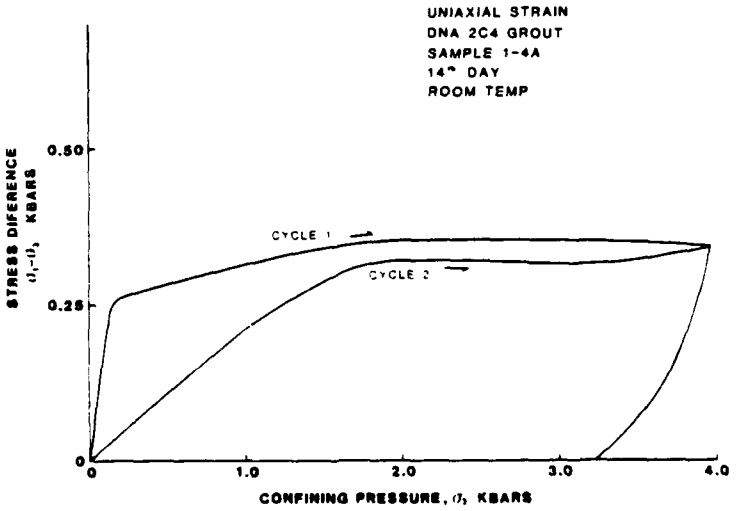

Figure B4b

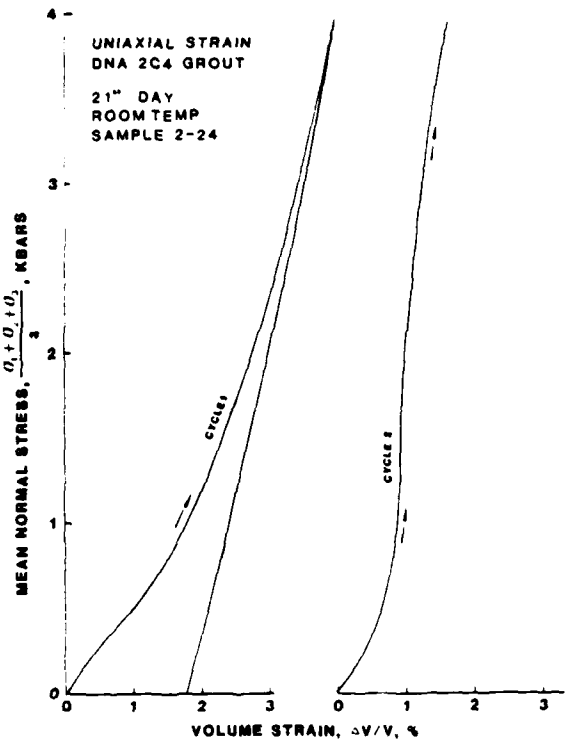

Figure B5a

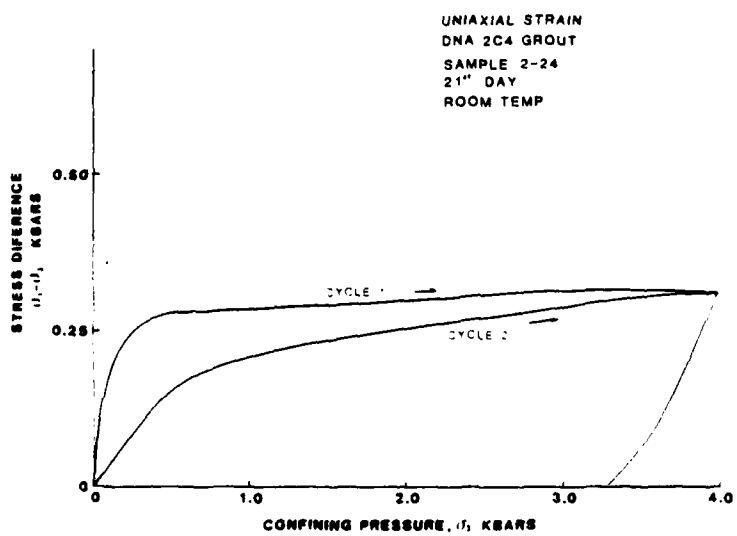

Figure B5b

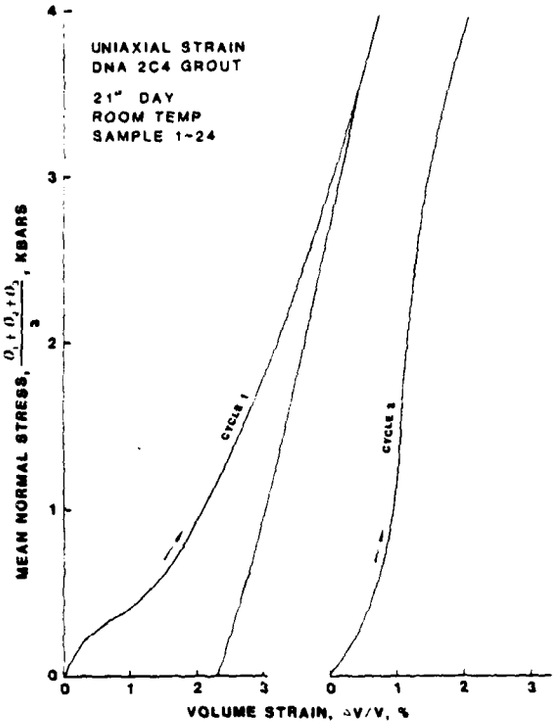

Figure B6a

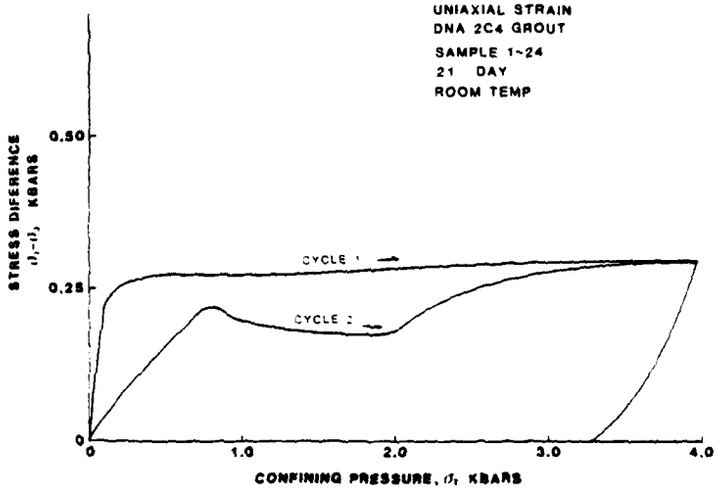

Figure B6b

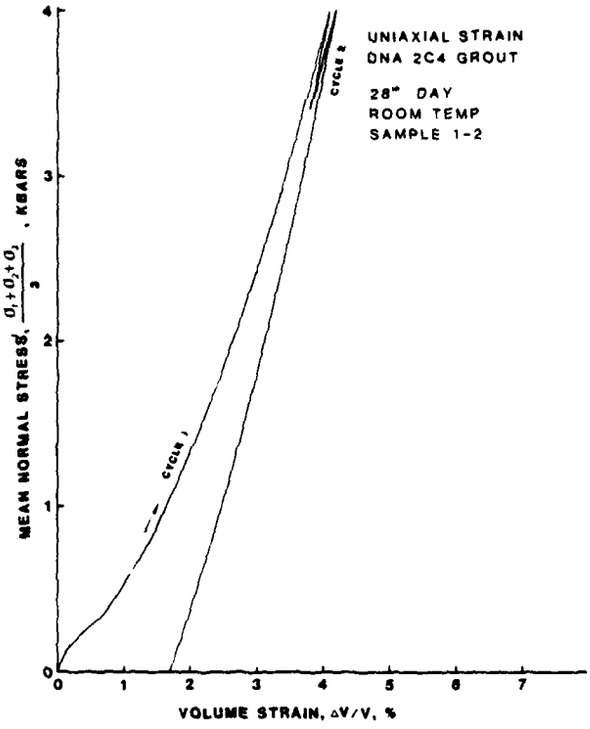

Figure B7a

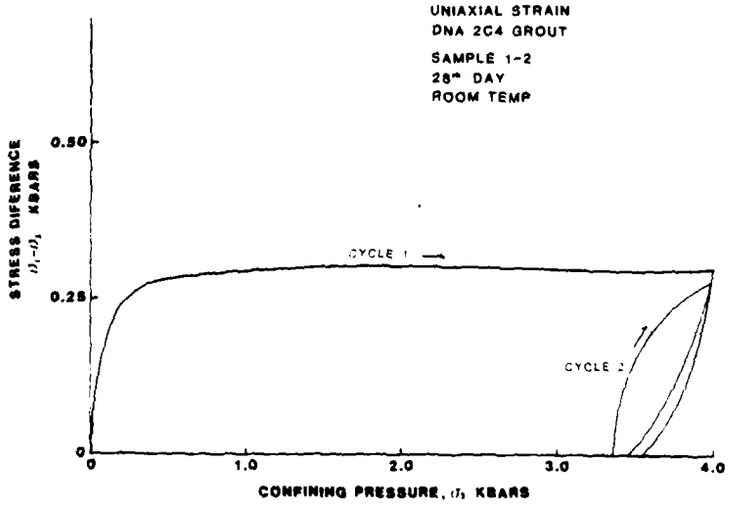

Figure B7b

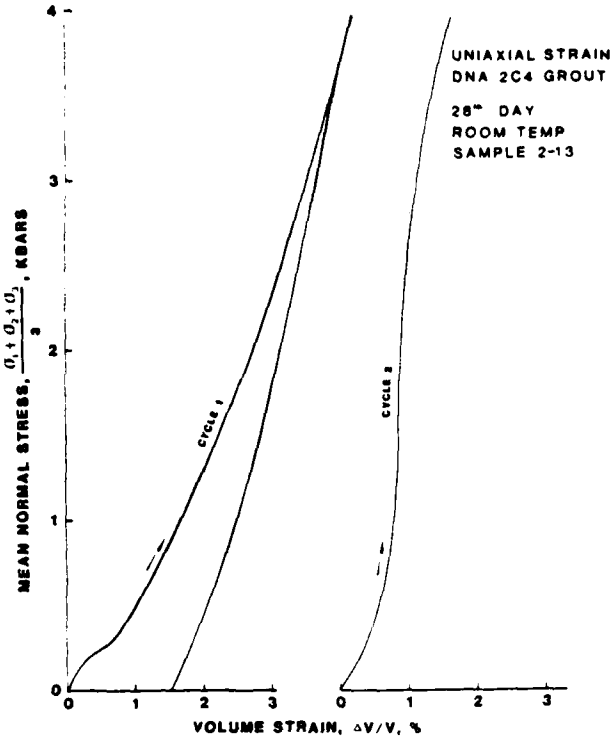

Figure B8a

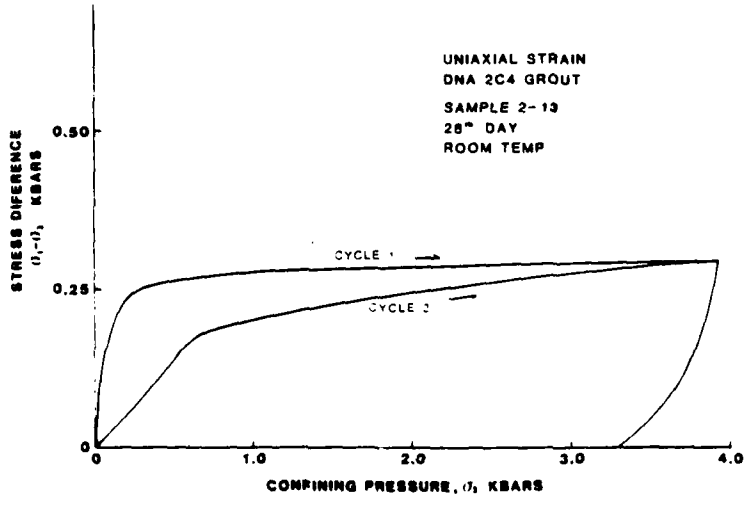

Figure B8b

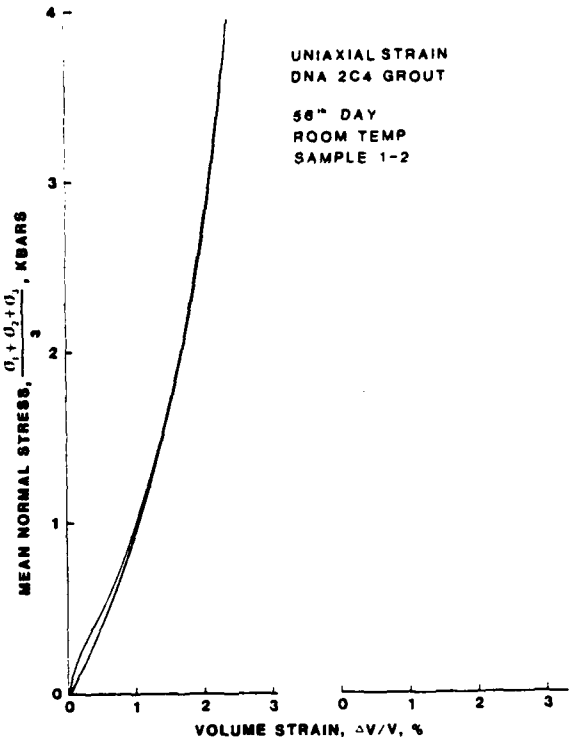

Figure B9a

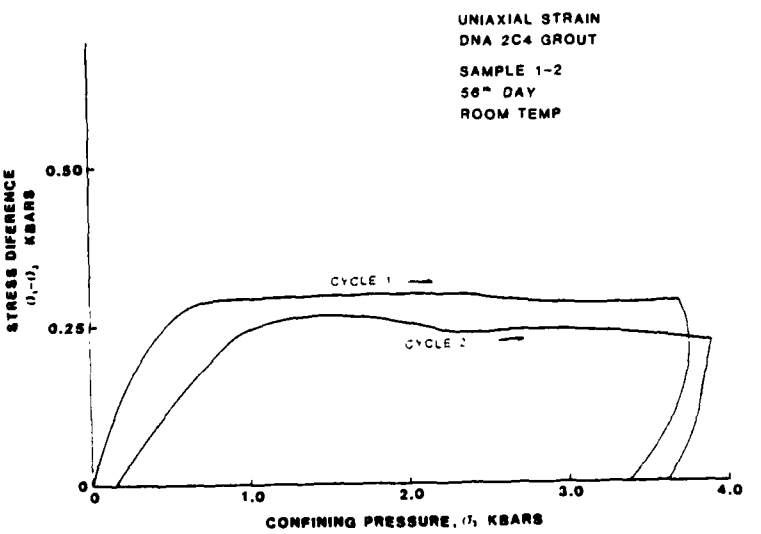

Figure B9b

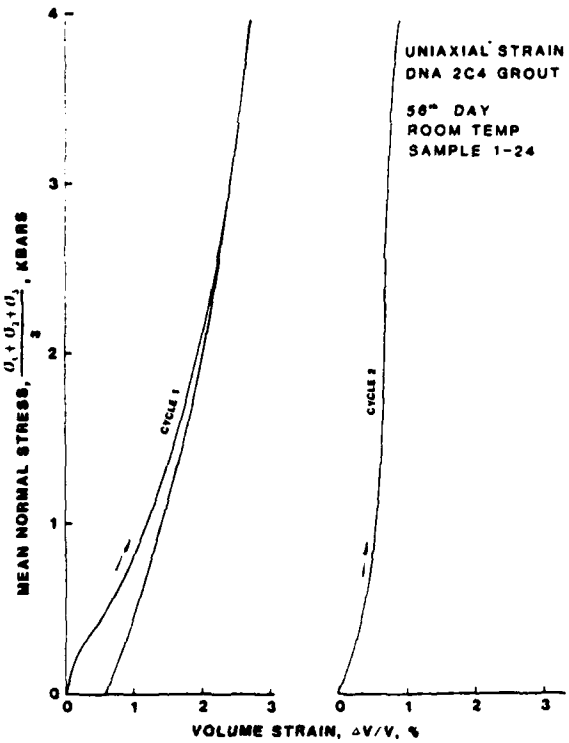

Figure B10a

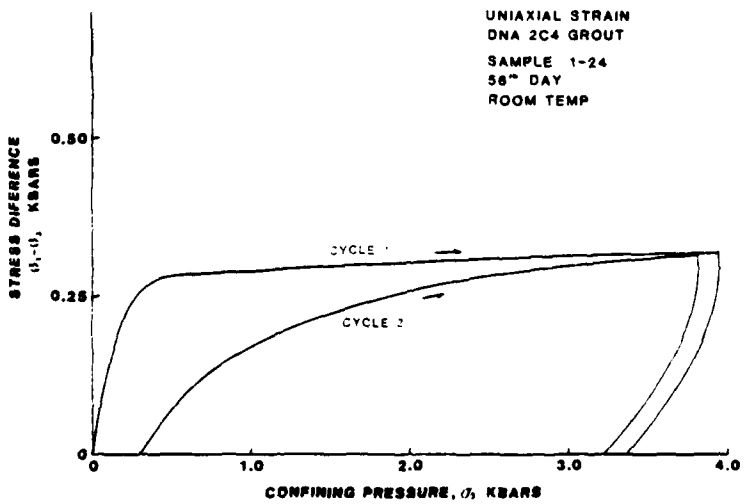

Figure B10b

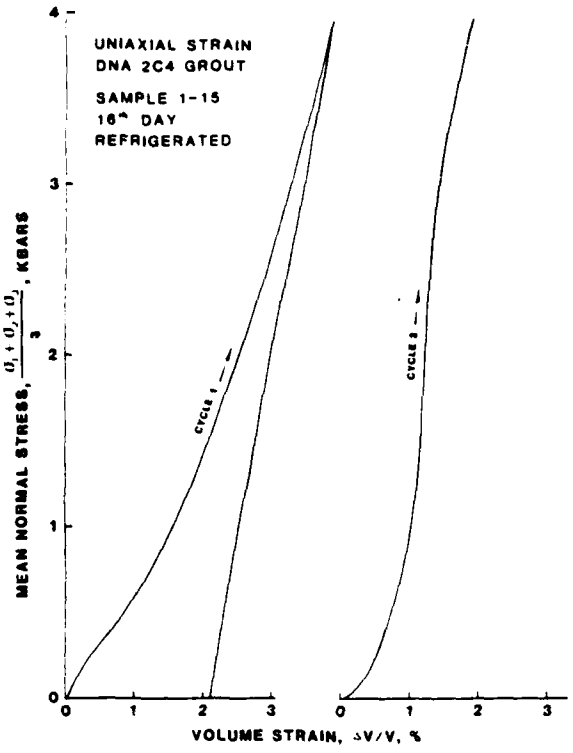

Figure B11a

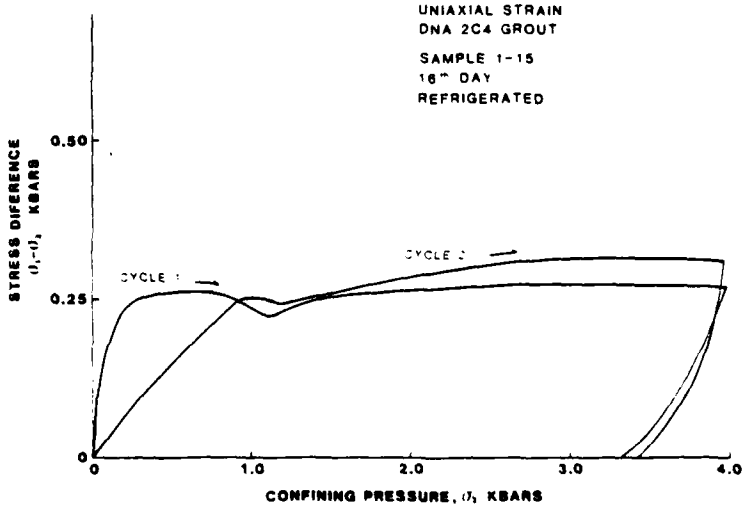

Figure B11b

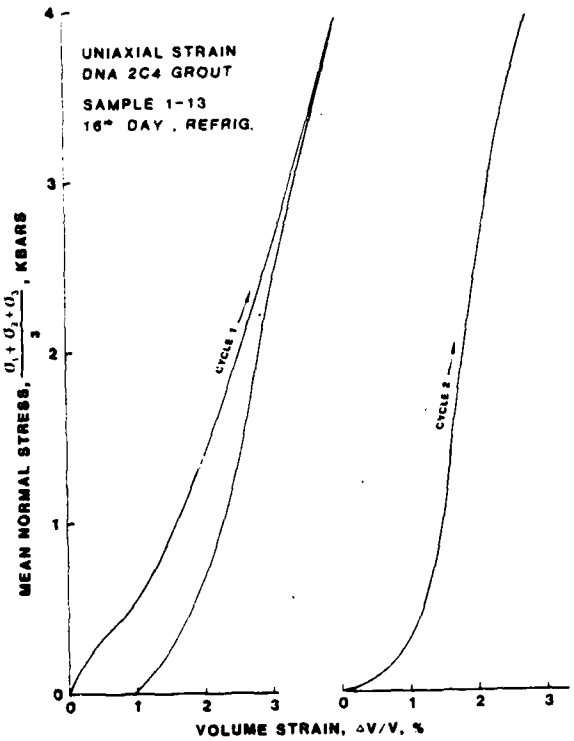

Figure B12a

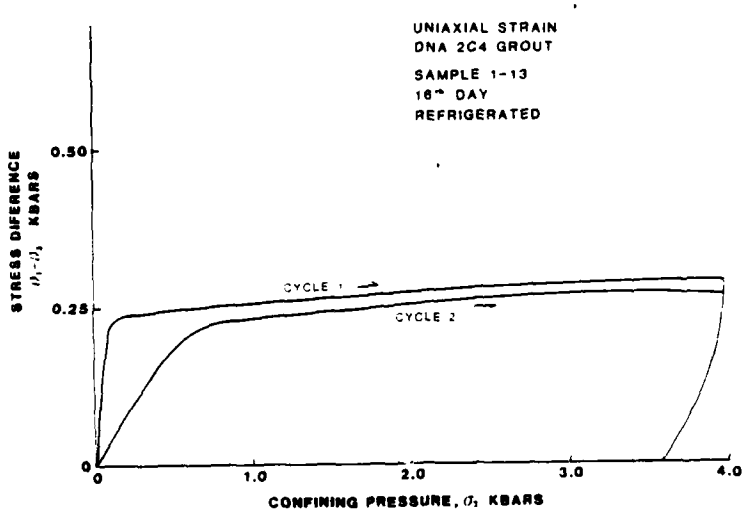

Figure B12b

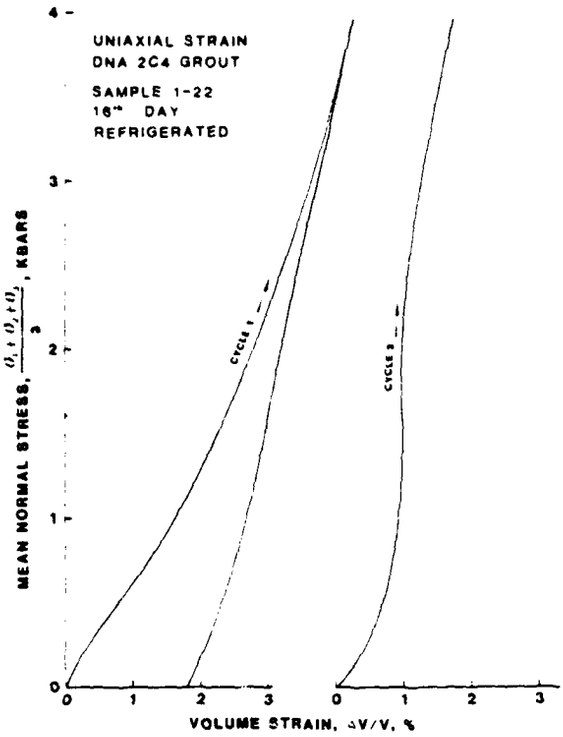

Figure B13a

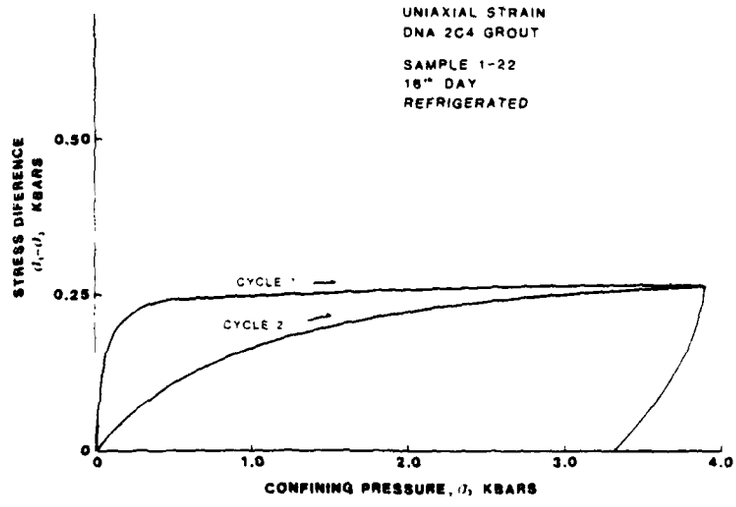

Figure B13b

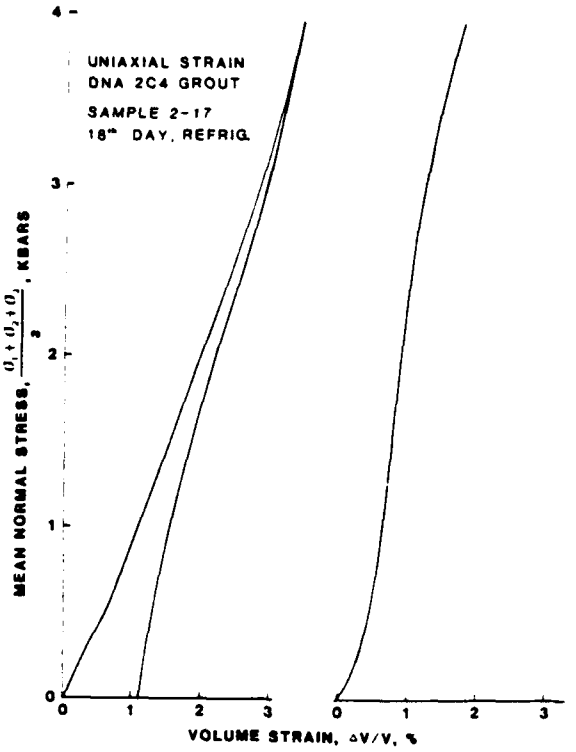

Figure 514a

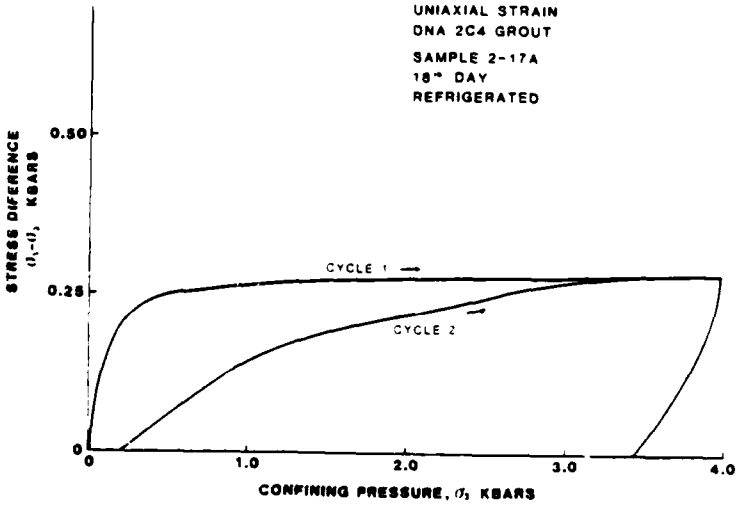

Figure B14b

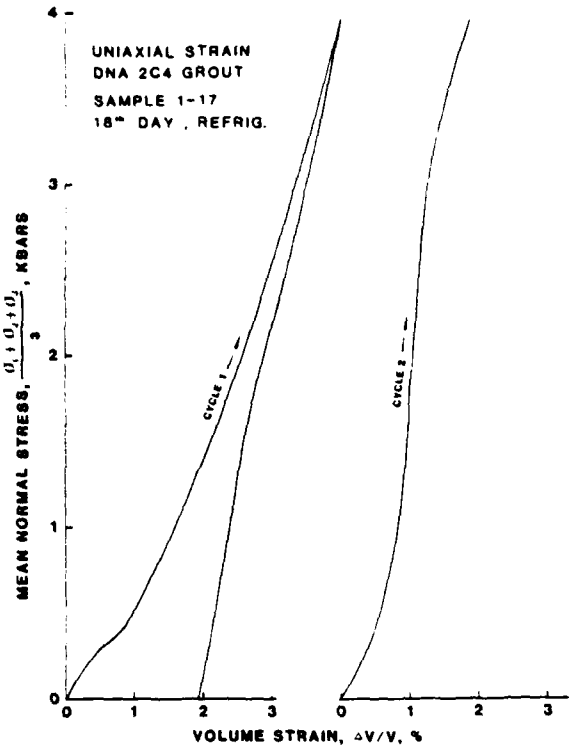

Figure B15a

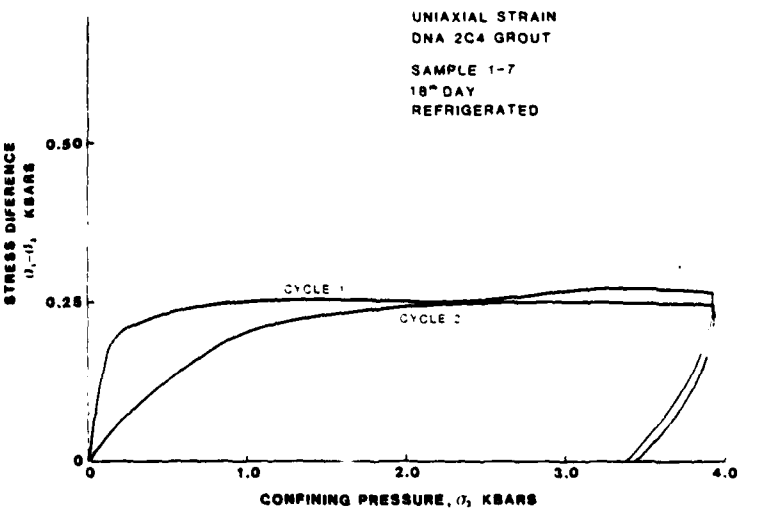

Figure B15b

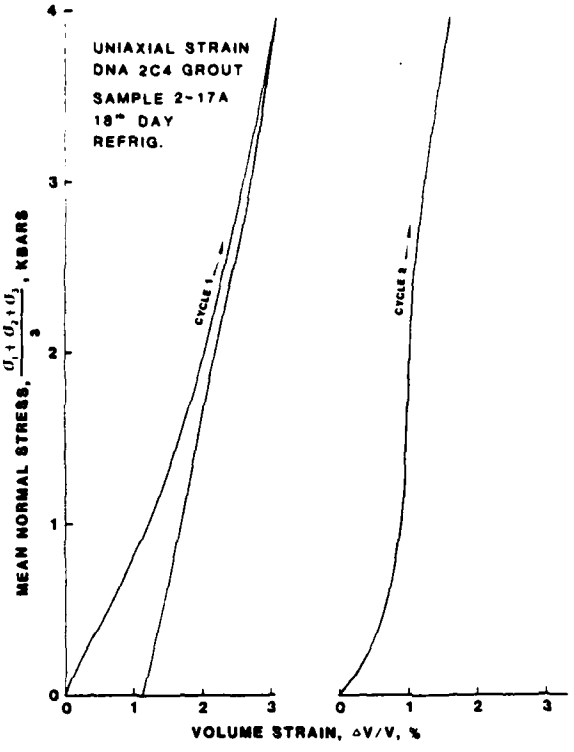

Figure B16a

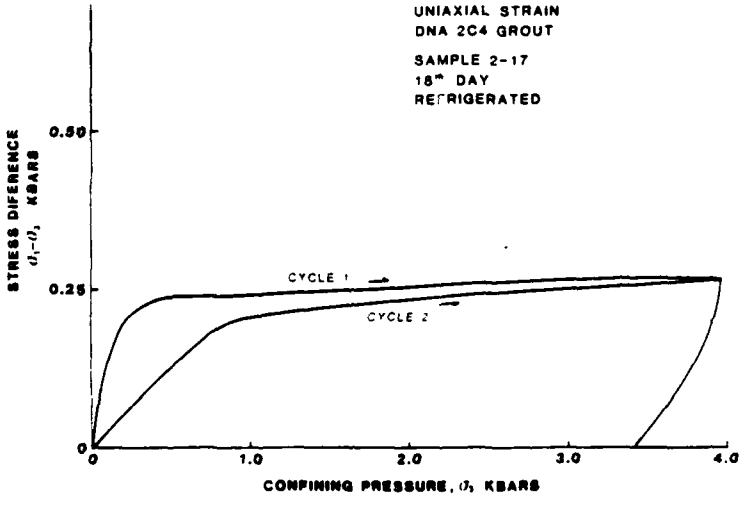

Figure B16b

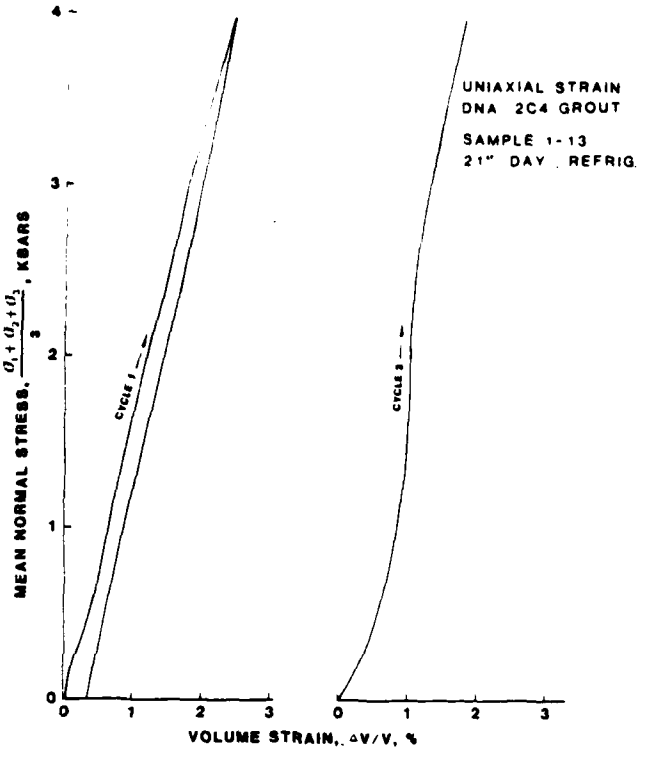

Figure B17a

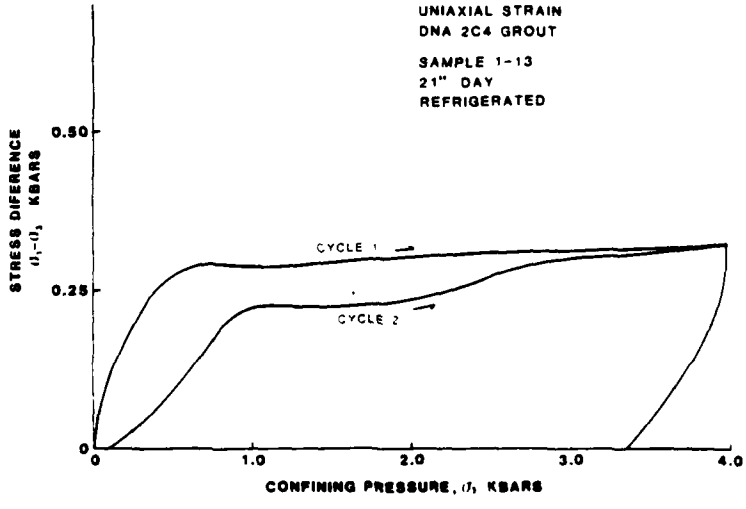

Figure B17b

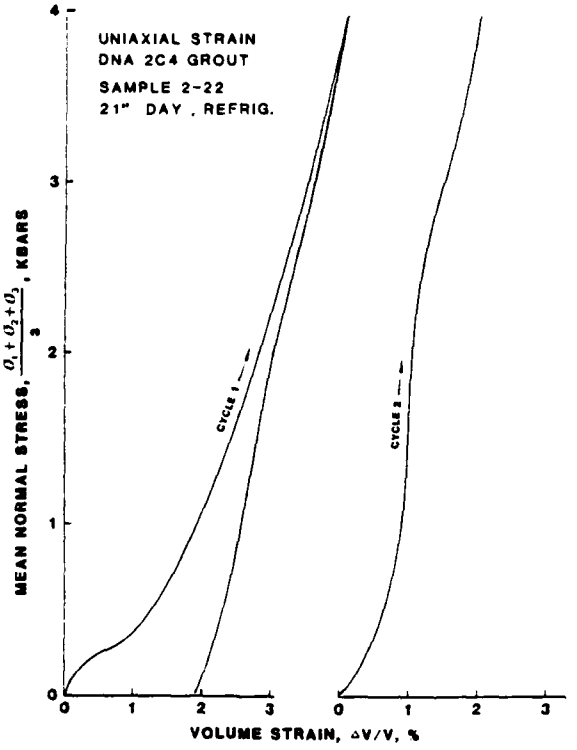

Figure B18a

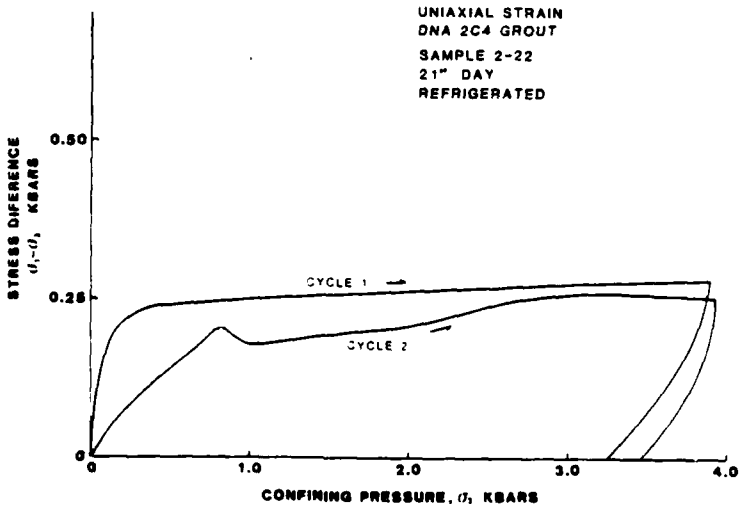

Figure B18b

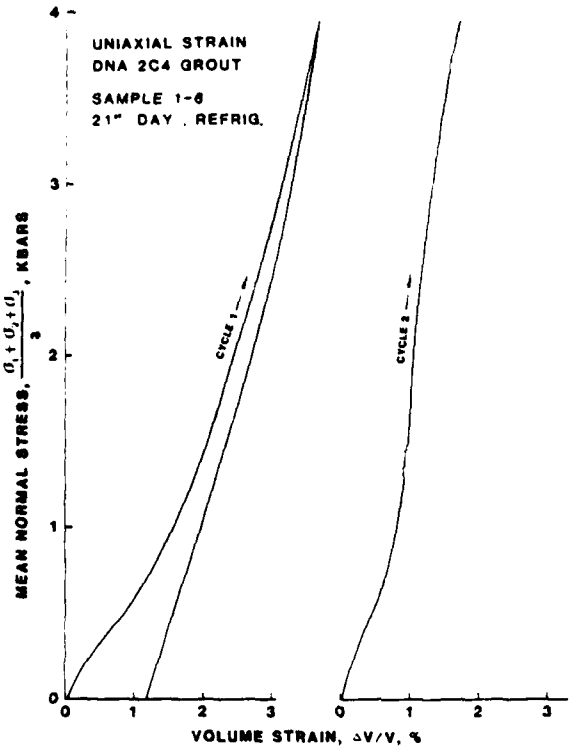

Figure B19a

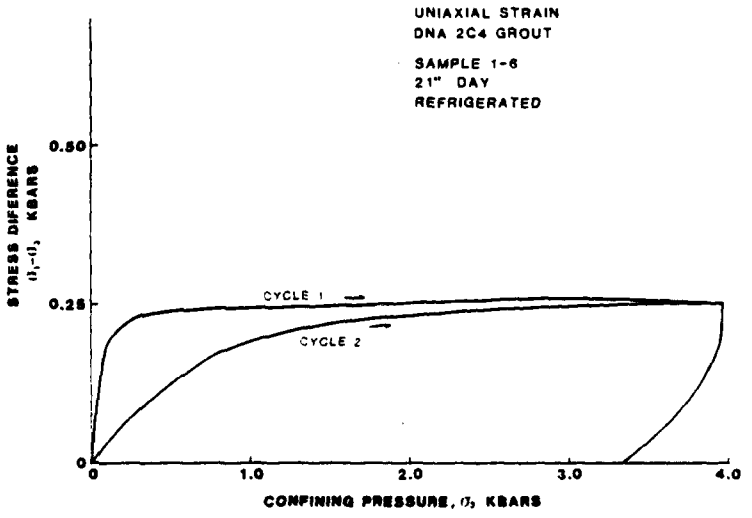

Figure B19b

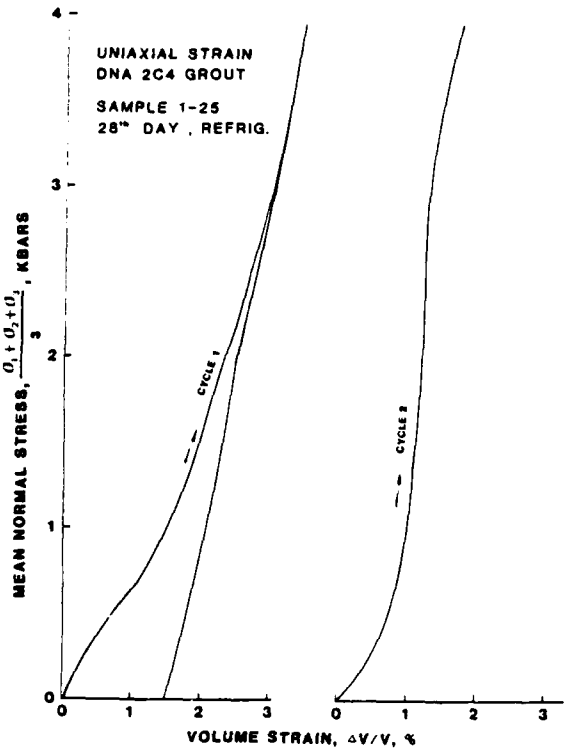

Figure B20a

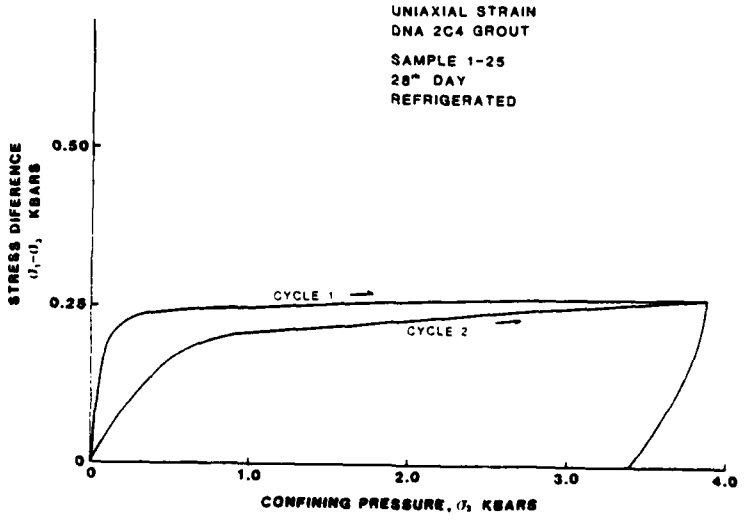

Figure B20b

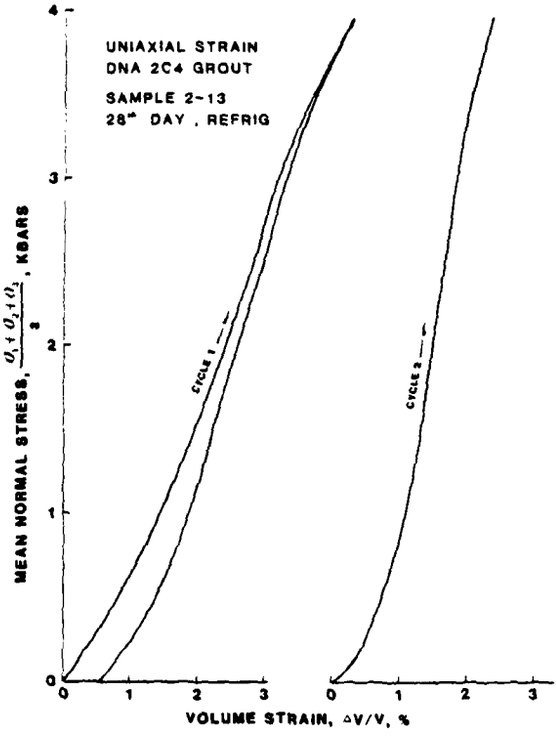

Figure B21a

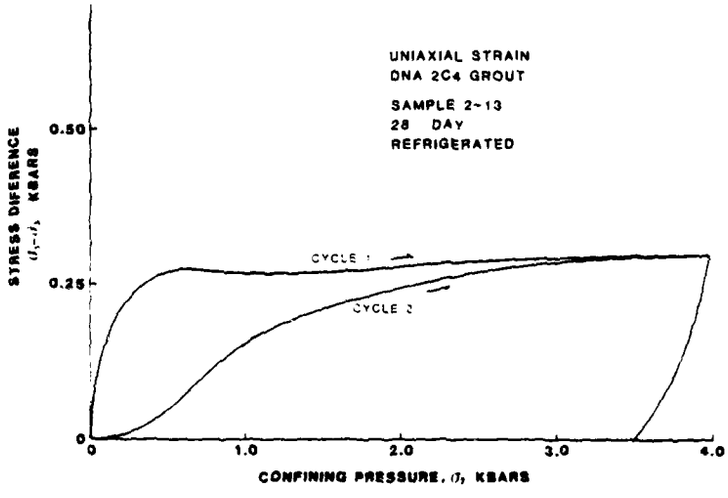

Figure B21b

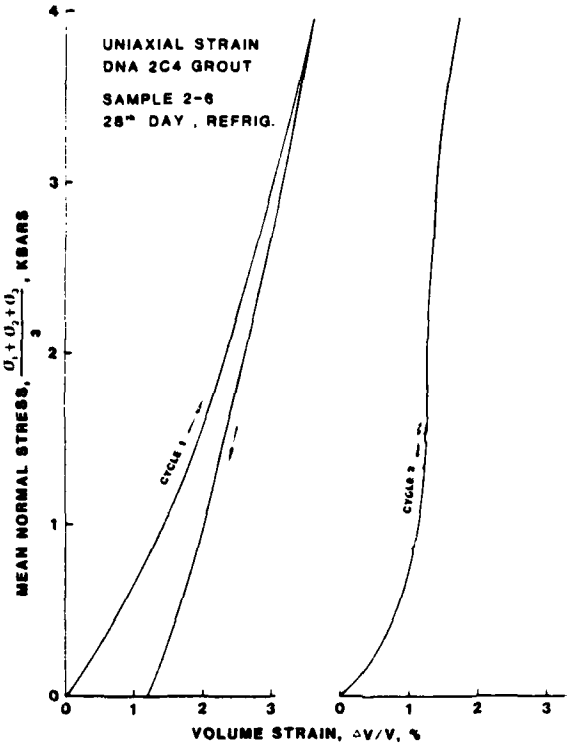

Figure B22a

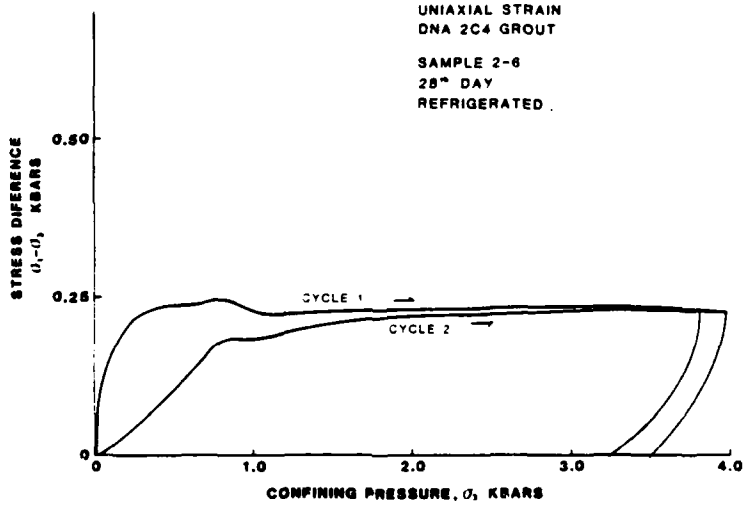

Figure B22b

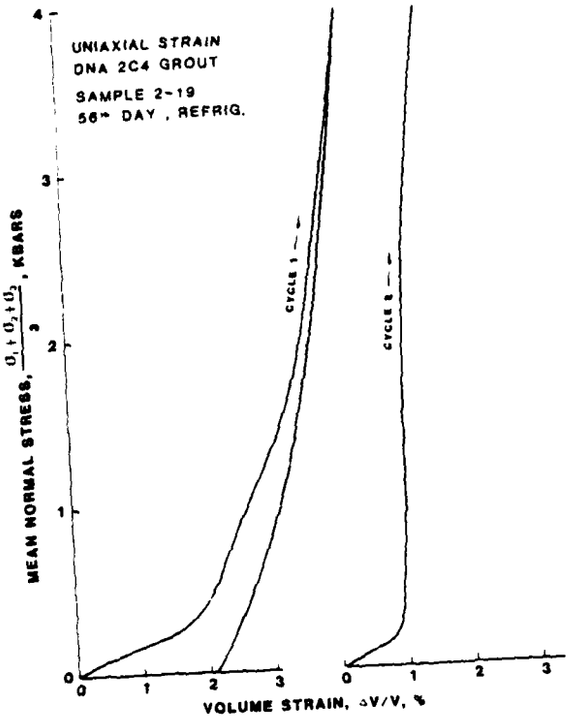

Figure B23a

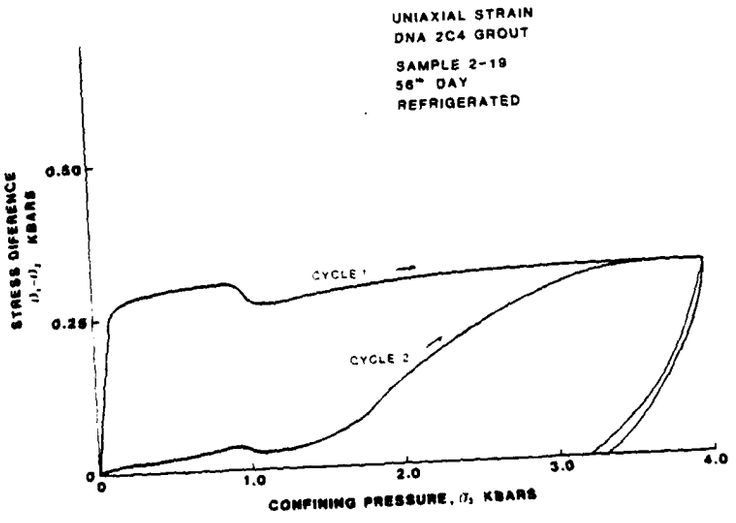

Figure B23b

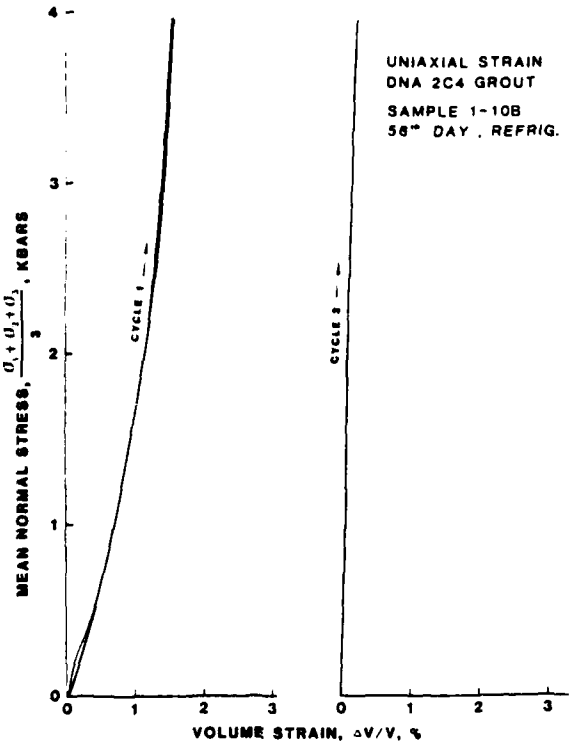

Figure B24a

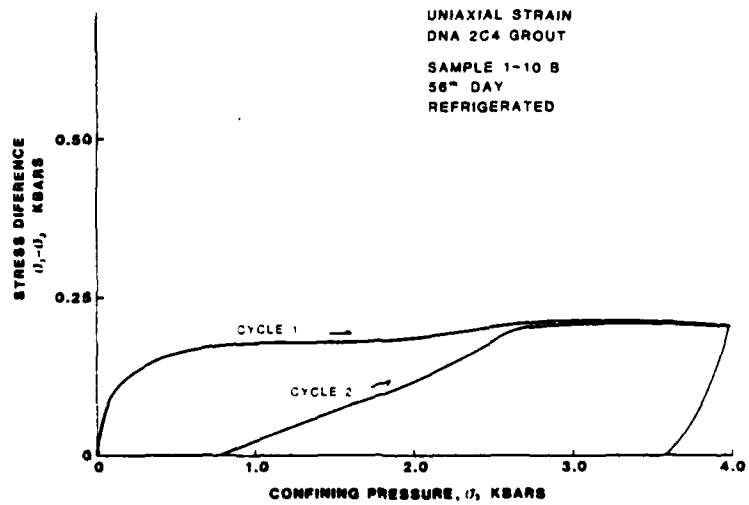

Figure B24b

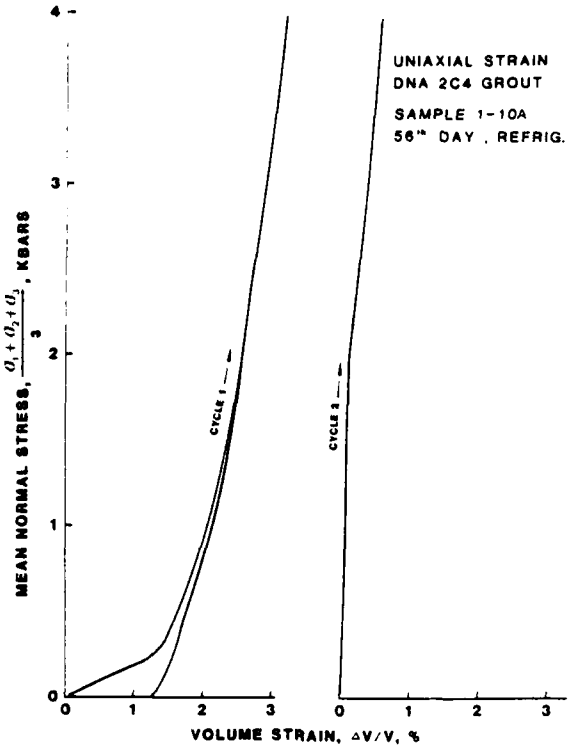

Figure B25a

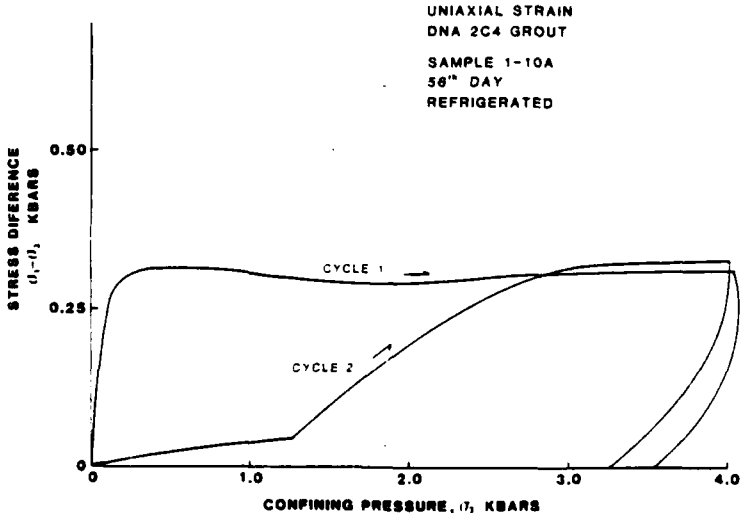

Figure B25b

APPENDIX C

FAILURE ENVELOPES

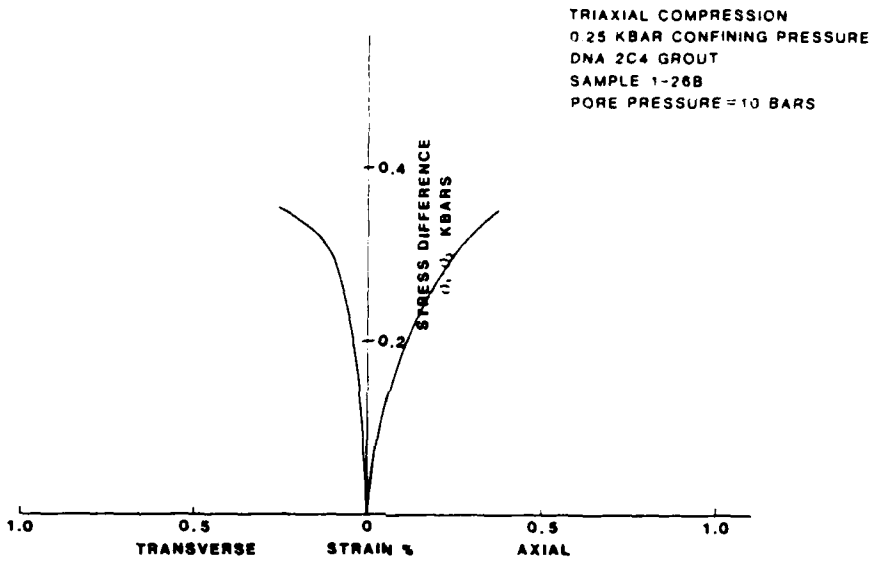

Figure C1

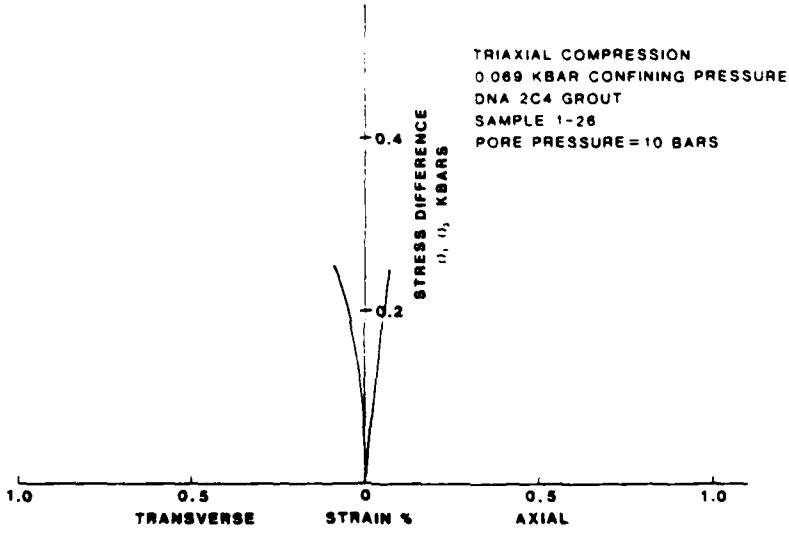

Figure C2

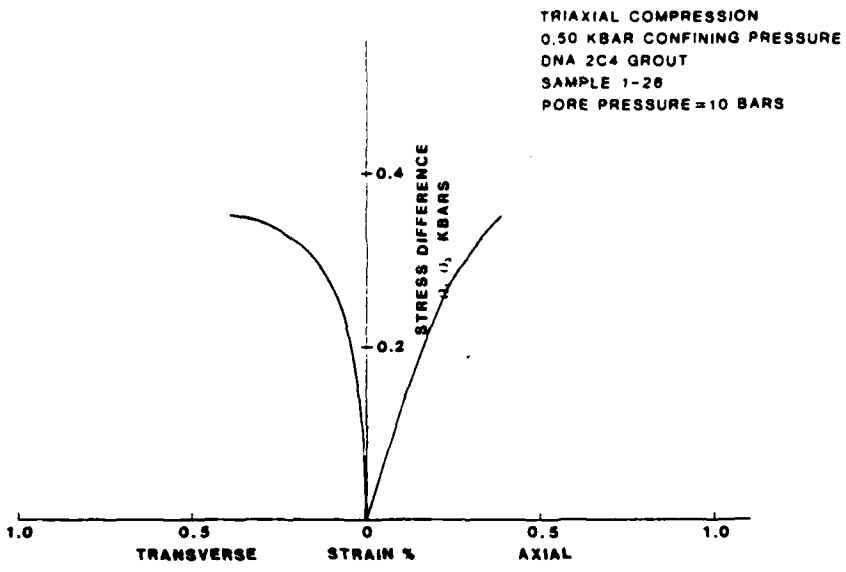

Figure C3

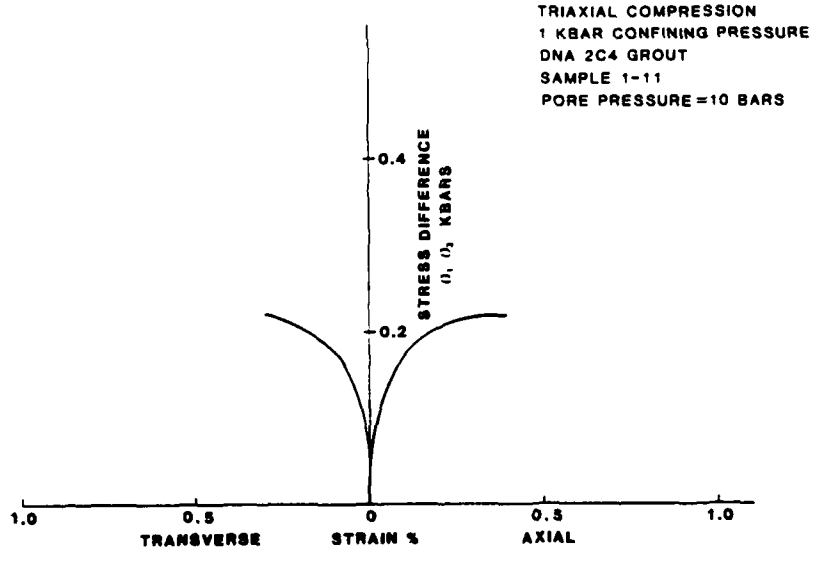

Figure C4

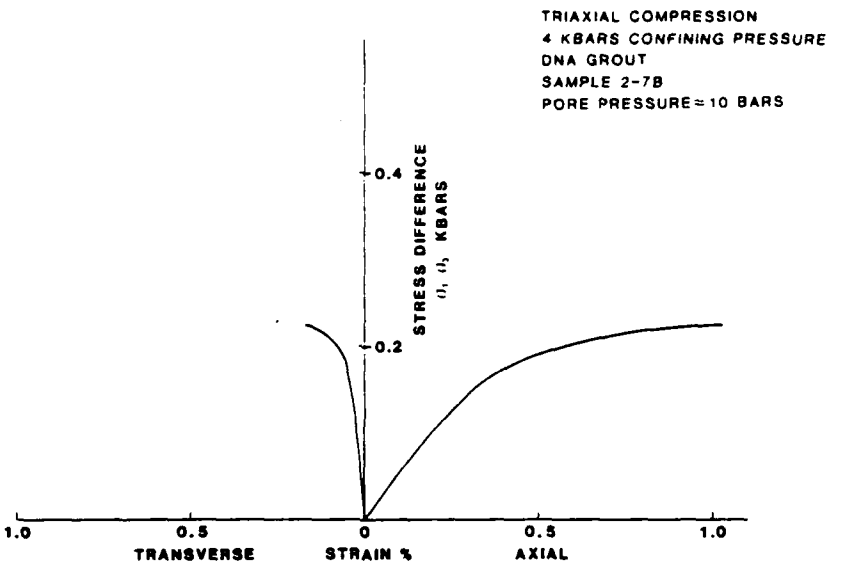

Figure C5

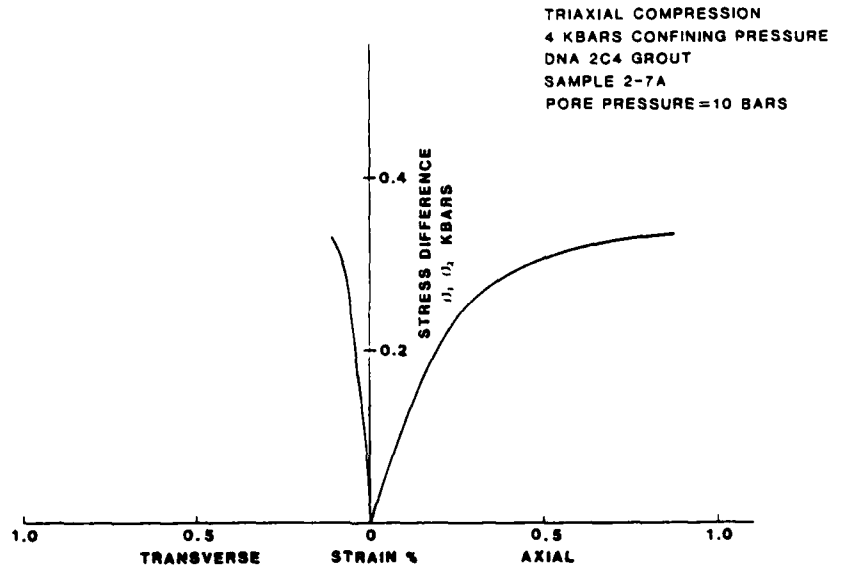

Figure C6

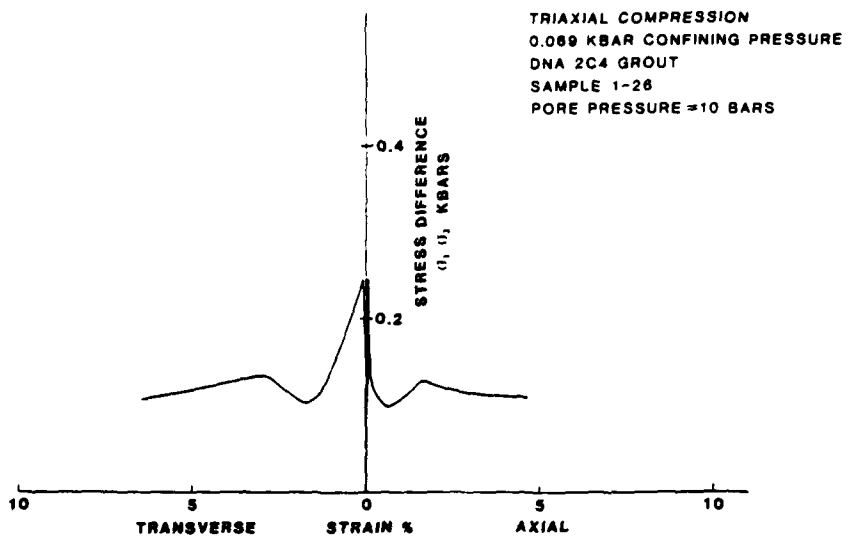

Figure C7

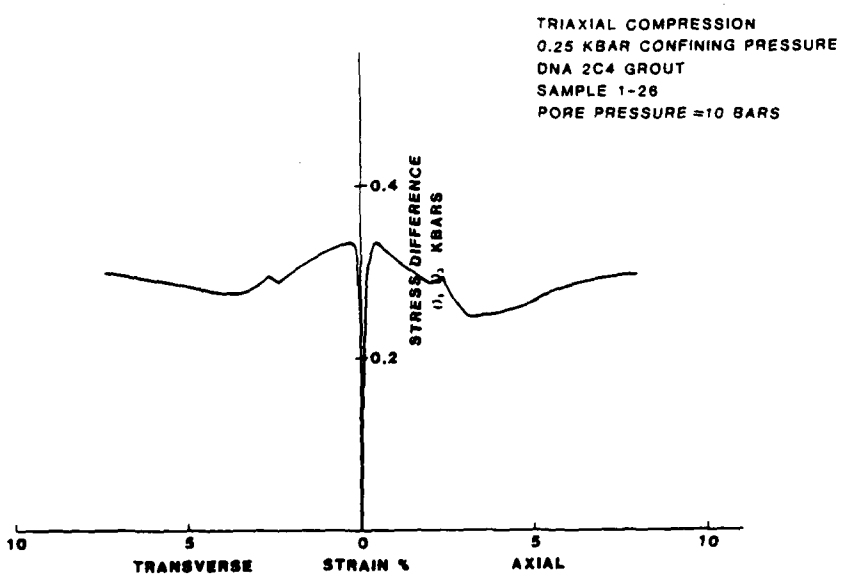

Figure C8

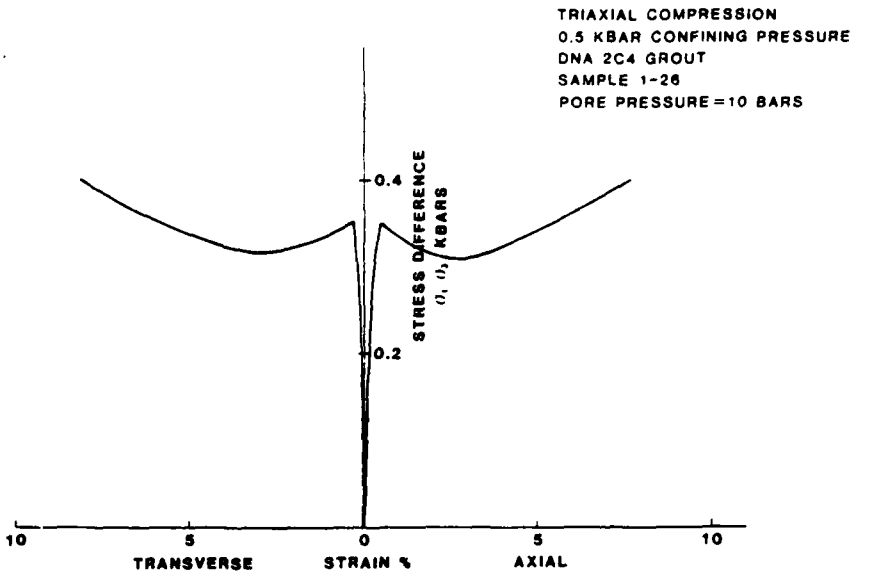

Figure C9

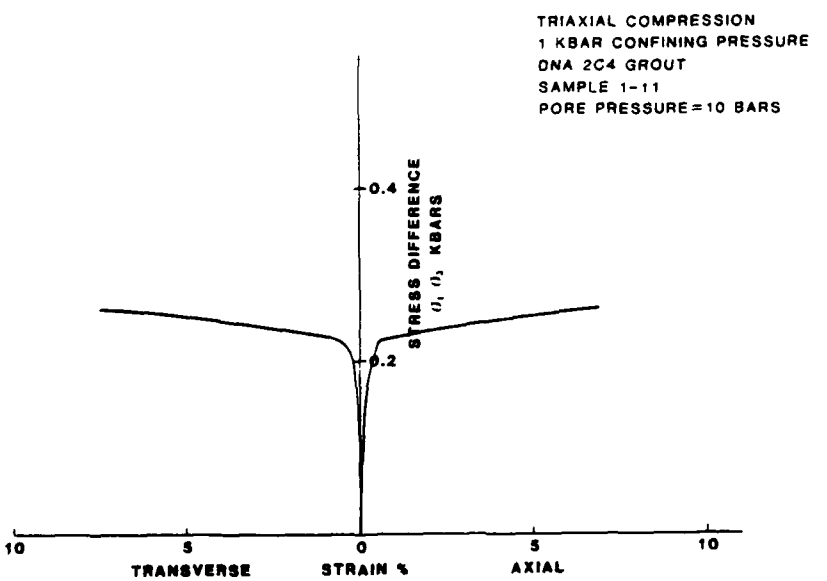

Figure C10

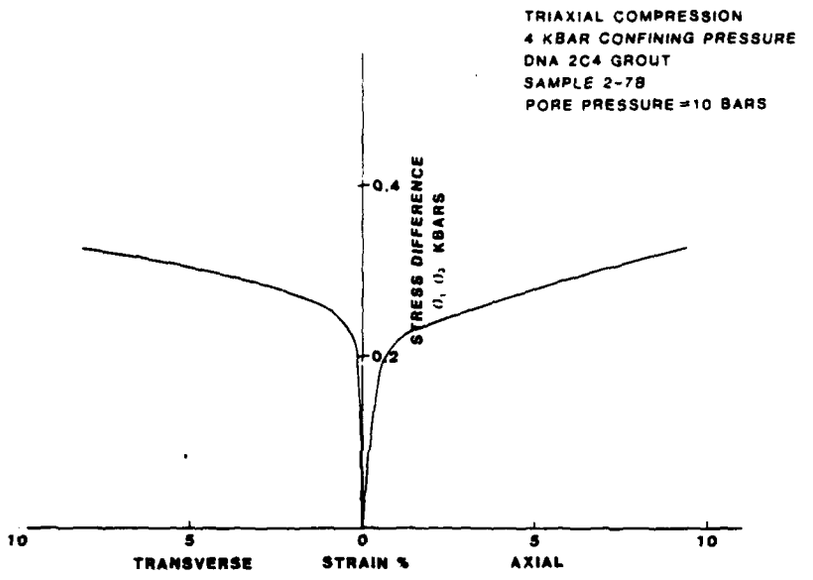

Figure C11

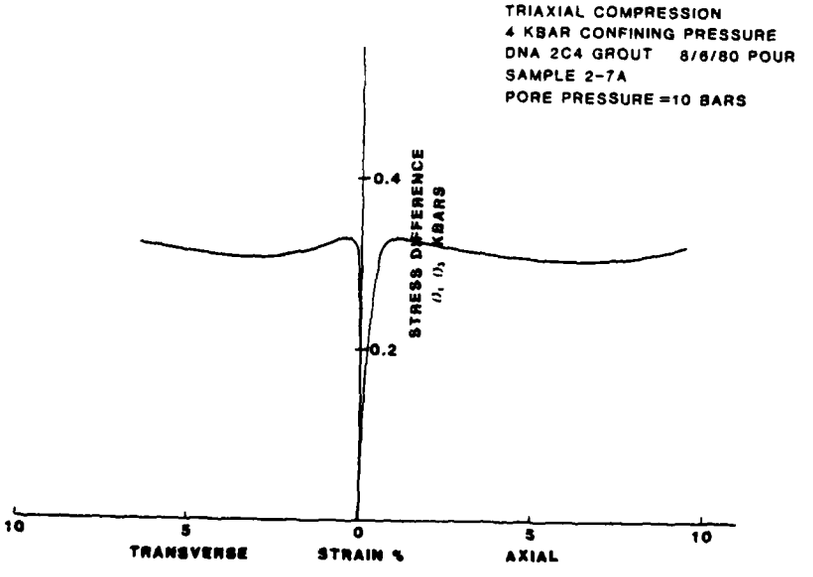

Figure C12

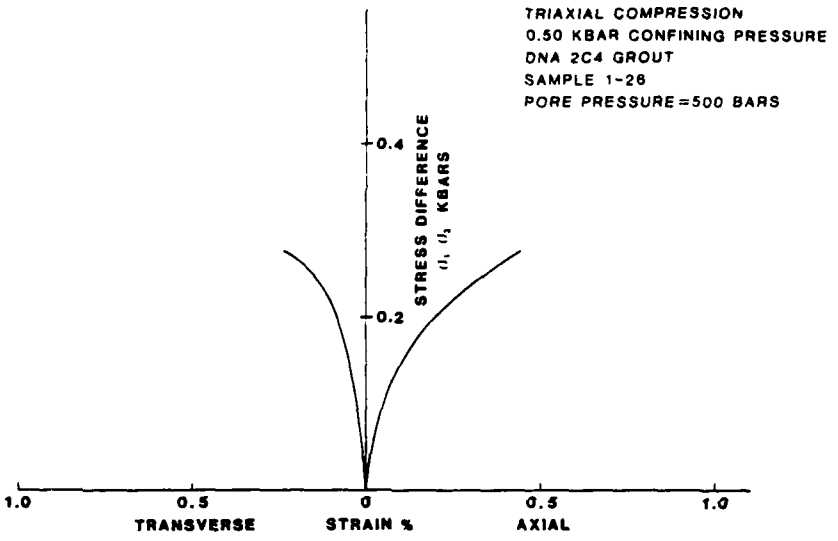

Figure C13

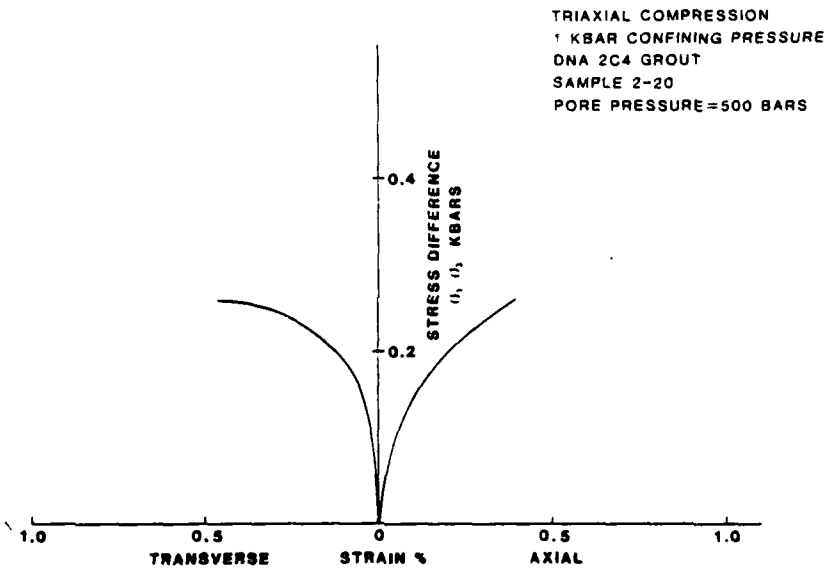

Figure C14

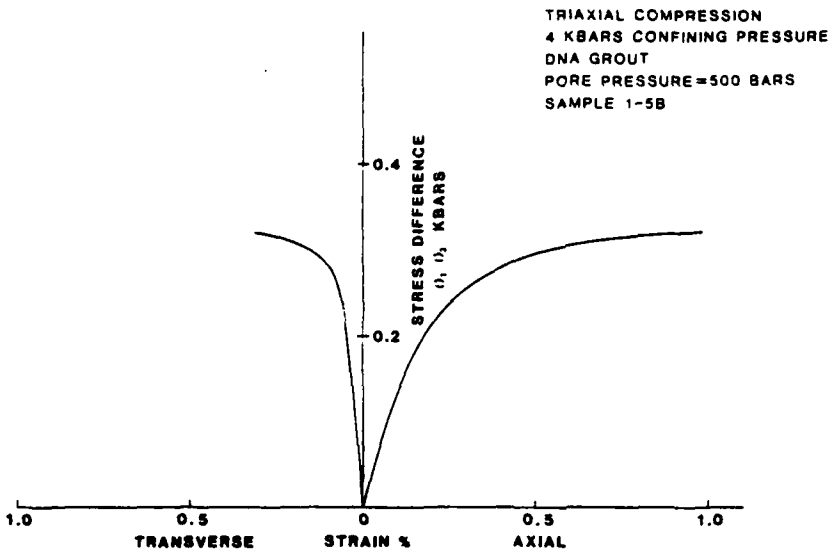

Figure C15

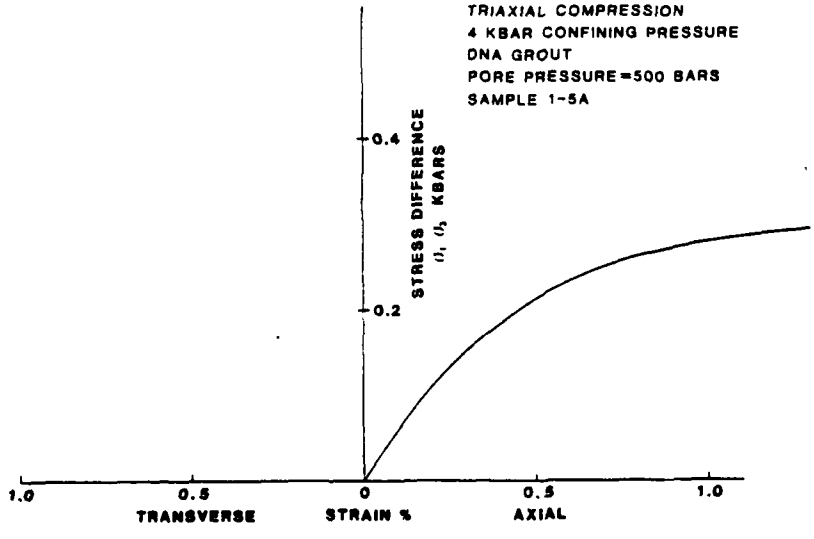

Figure C16

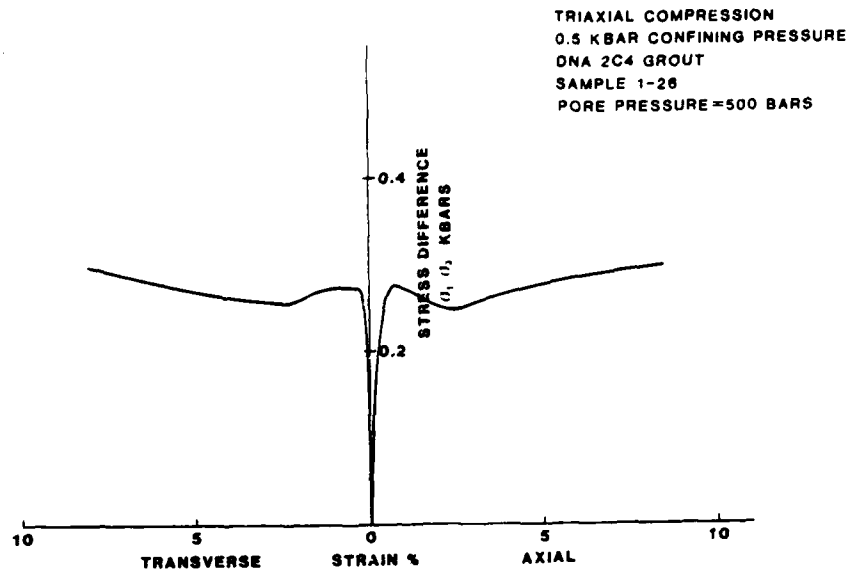

Figure C17

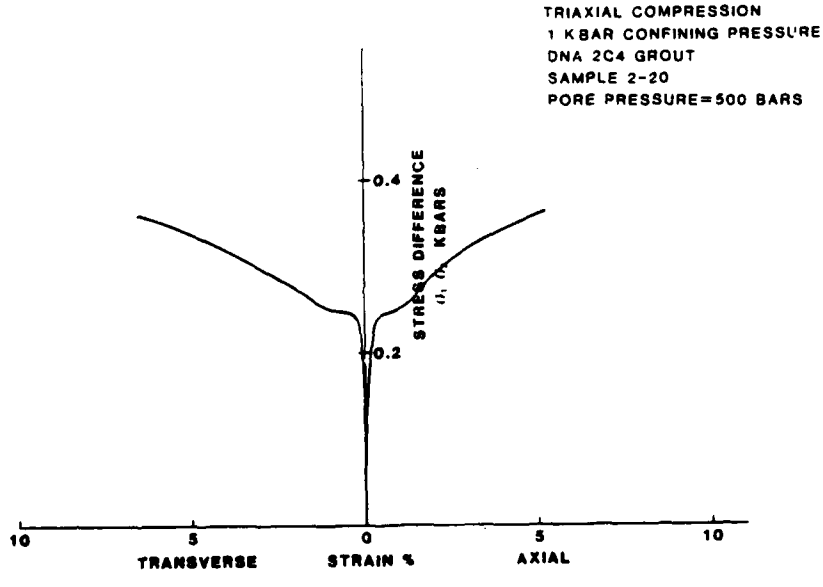

Figure C18

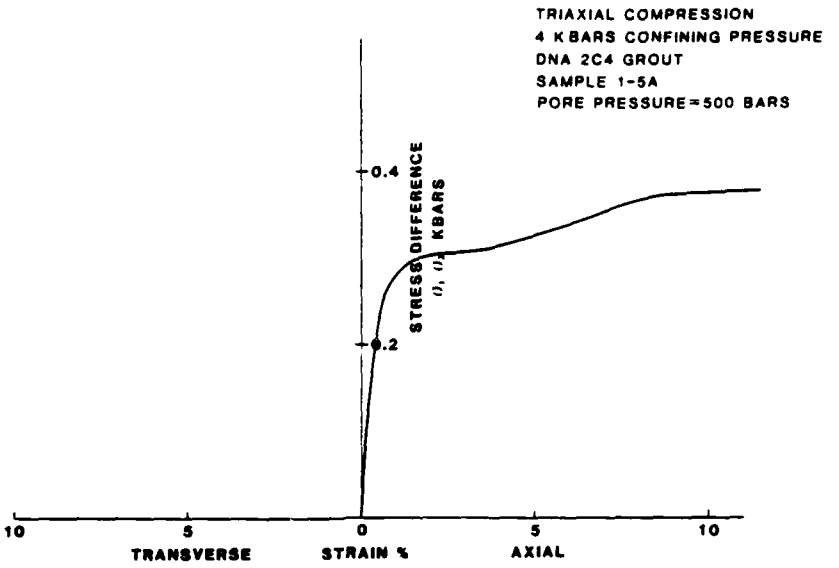

Figure C19

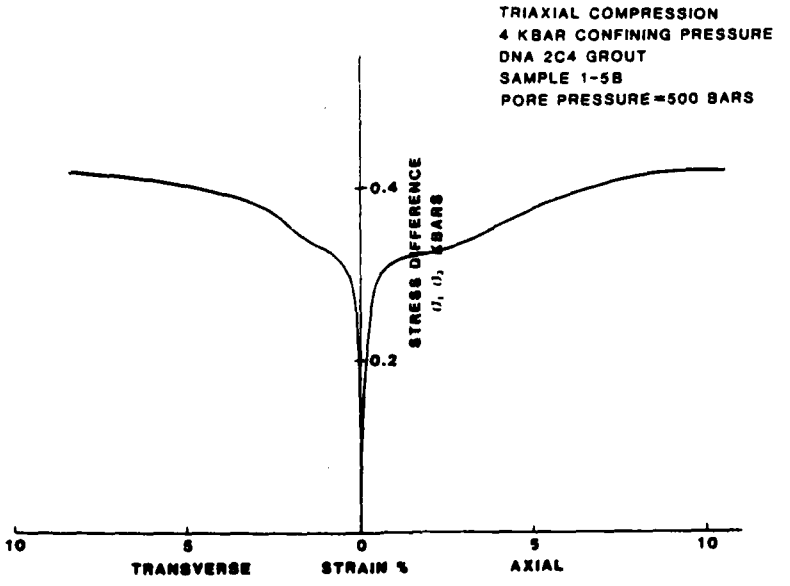

Figure C20

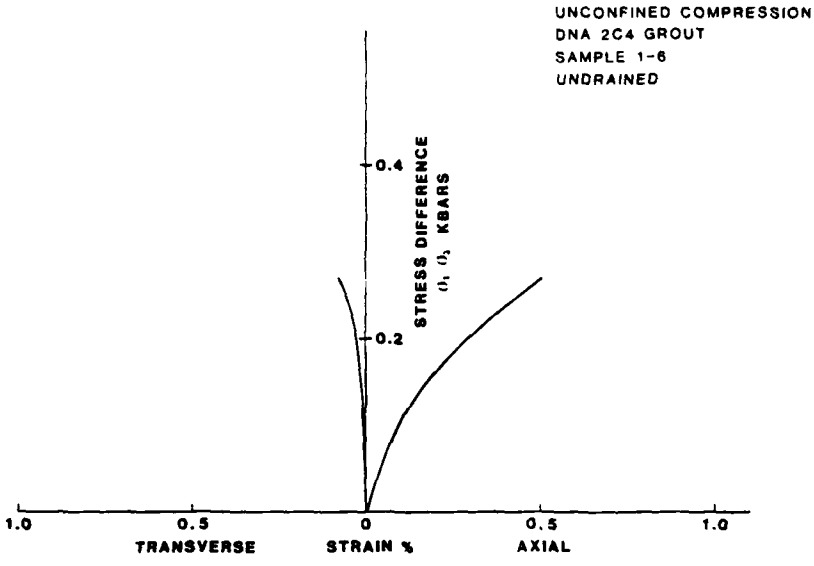

Figure C21

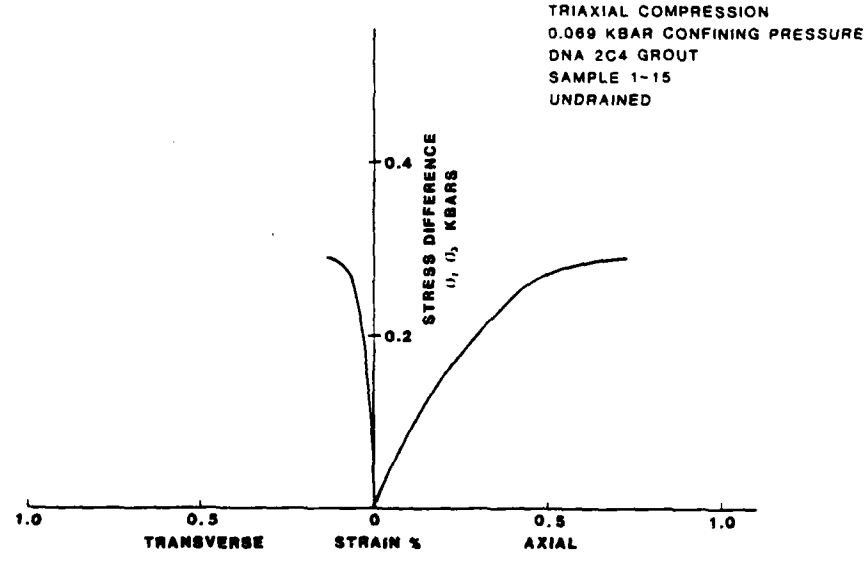

Figure C22

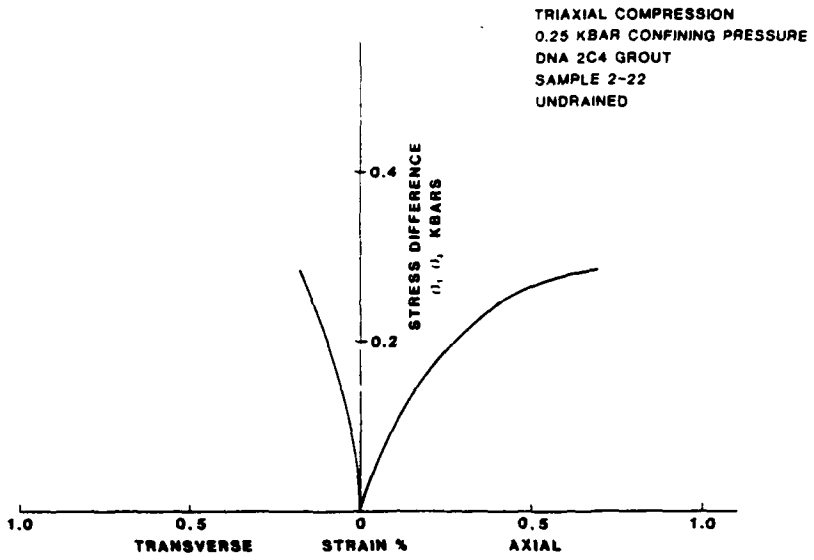

Figure C23

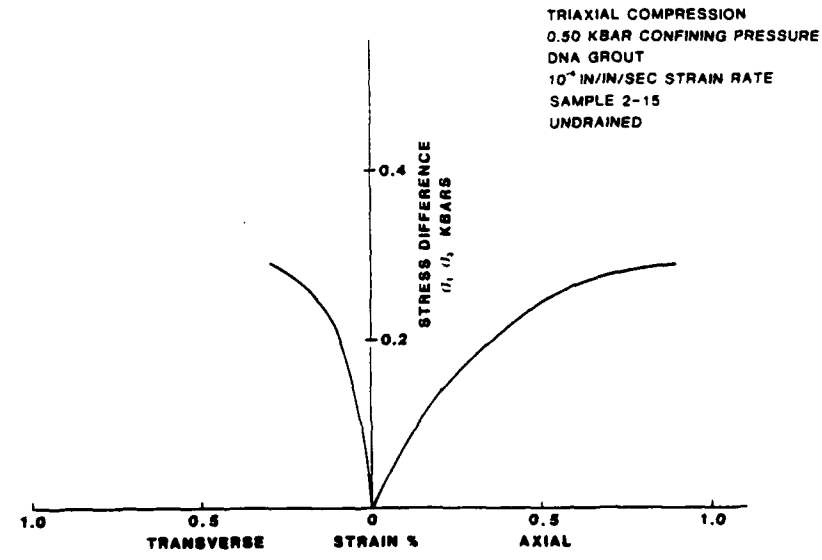

Figure C24

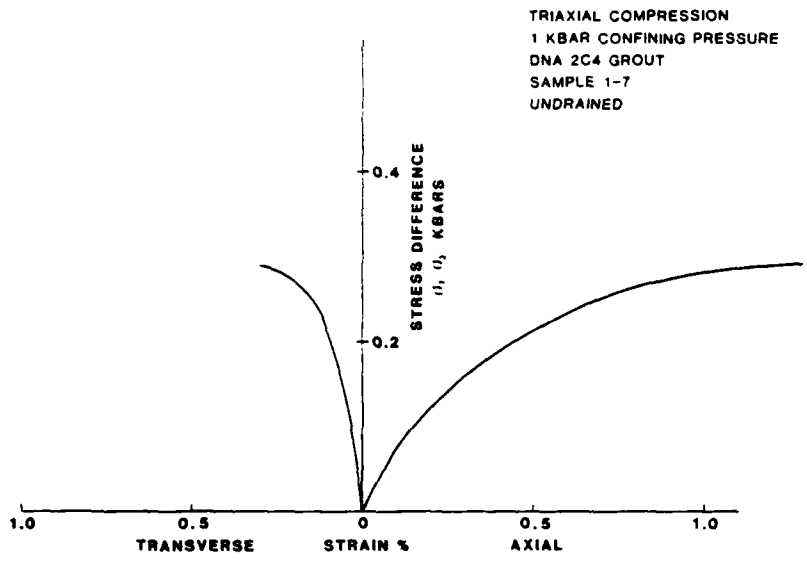

Figure C25

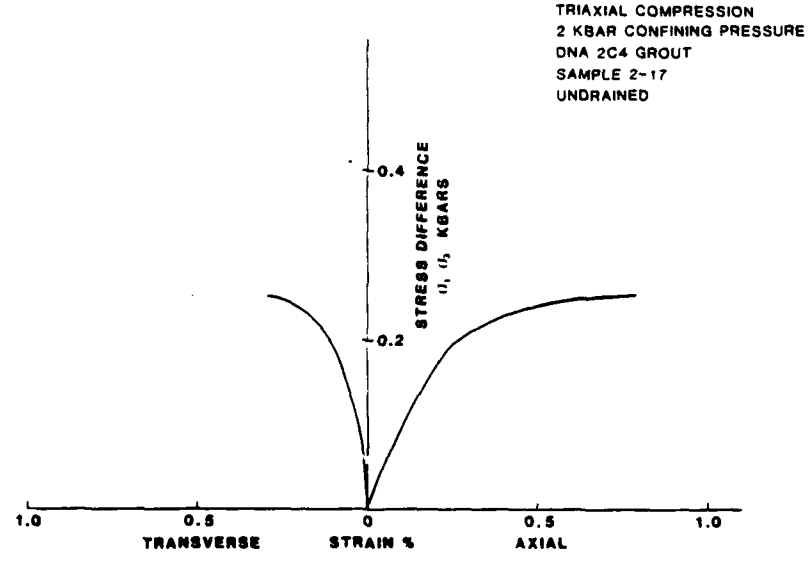

Figure C26

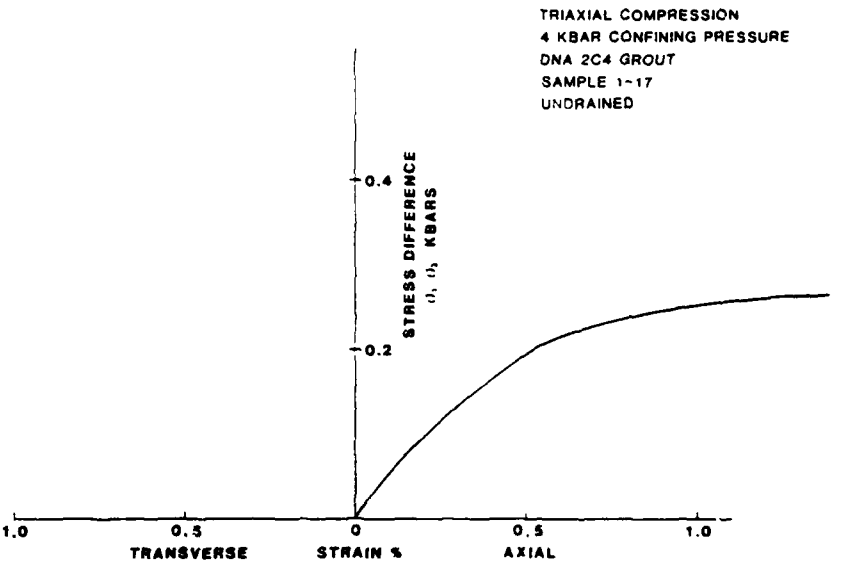
TRIAXIAL COMPRESSION
4 KBAR CONFINING PRESSURE
DNA 2C4 GROUT
SAMPLE 1-17
UNDRAINED
STRESS DIFFERENCE
$\sigma_1 - \sigma_3$, KBARS
0.4
0.2
1.0
0.5
0
0.5
1.0
TRANSVERSE
STRAIN %
AXIAL

Figure C27

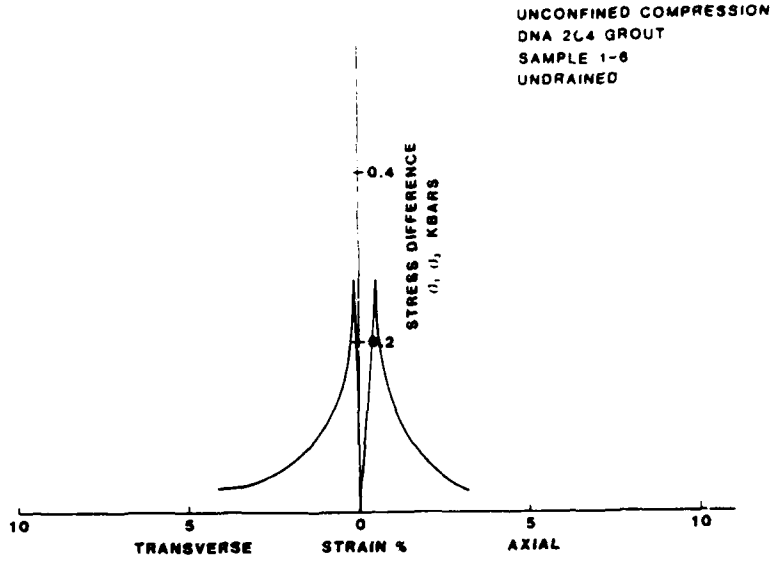

Figure C28

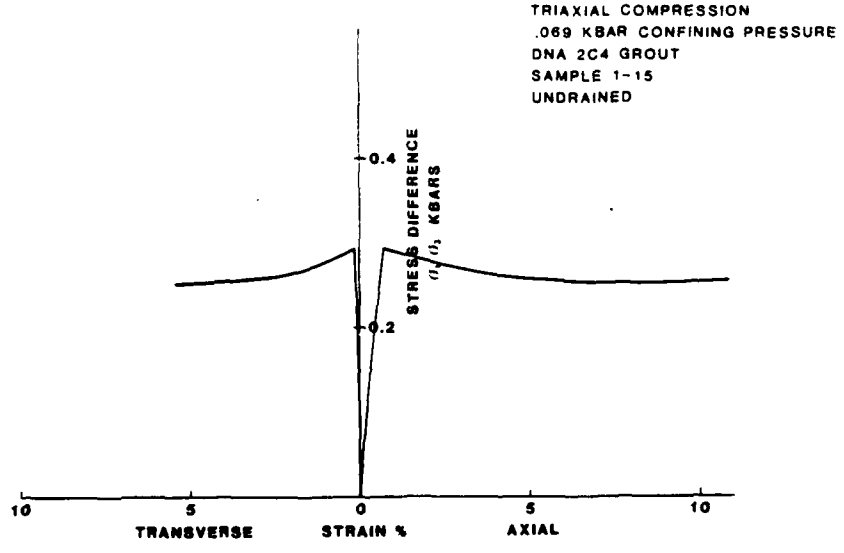

Figure C29

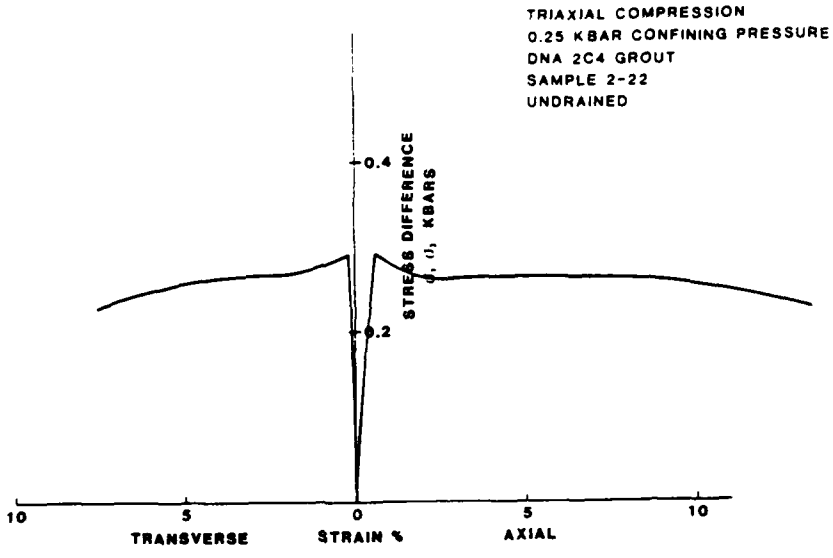

Figure C30

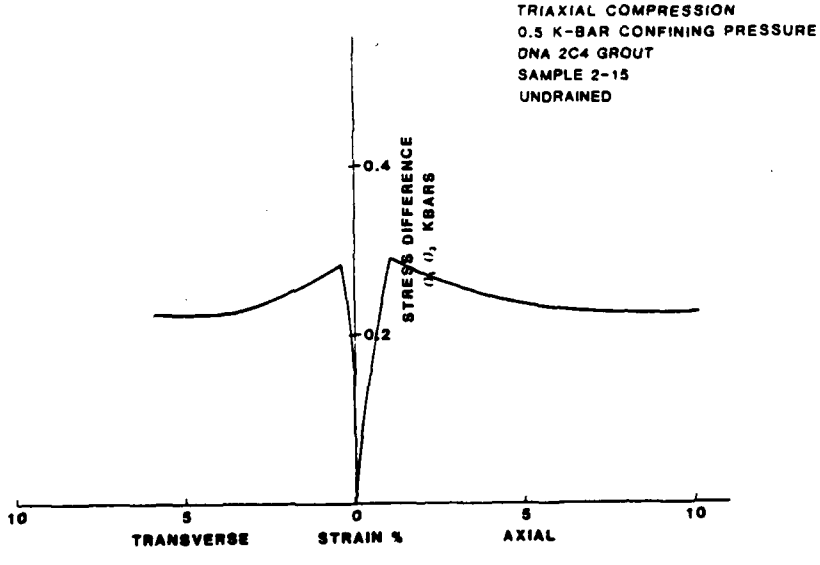

Figure C31

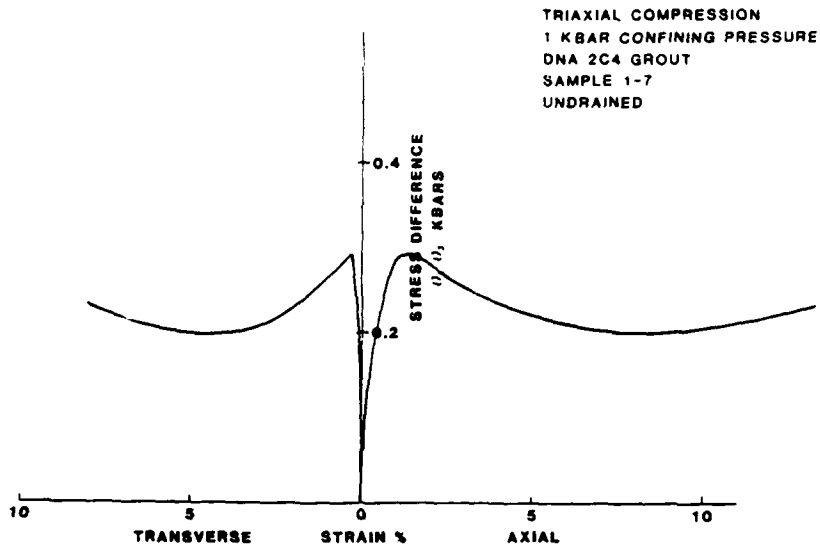

Figure C32

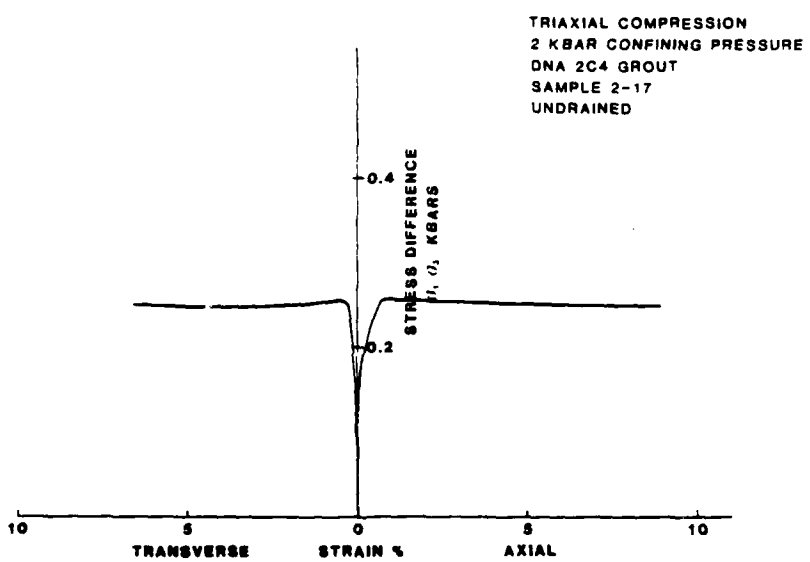

Figure C33

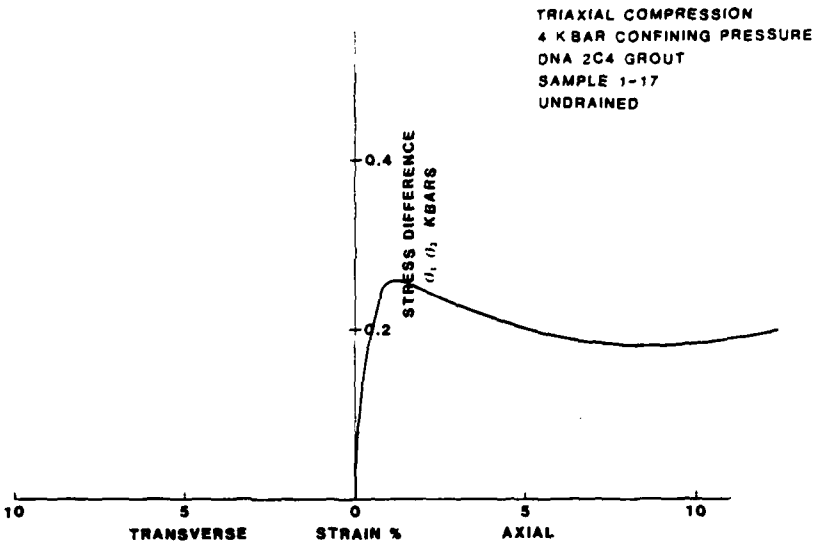
TRIAXIAL COMPRESSION
4 K BAR CONFINING PRESSURE
DNA 2C4 GROUT
SAMPLE 1-17
UNDRAINED
0.4
0.2
STRESS DIFFERENCE
$(\sigma_1 - \sigma_3)$, KBARS
10
5
0
5
10
TRANSVERSE
STRAIN %
AXIAL

Figure C34

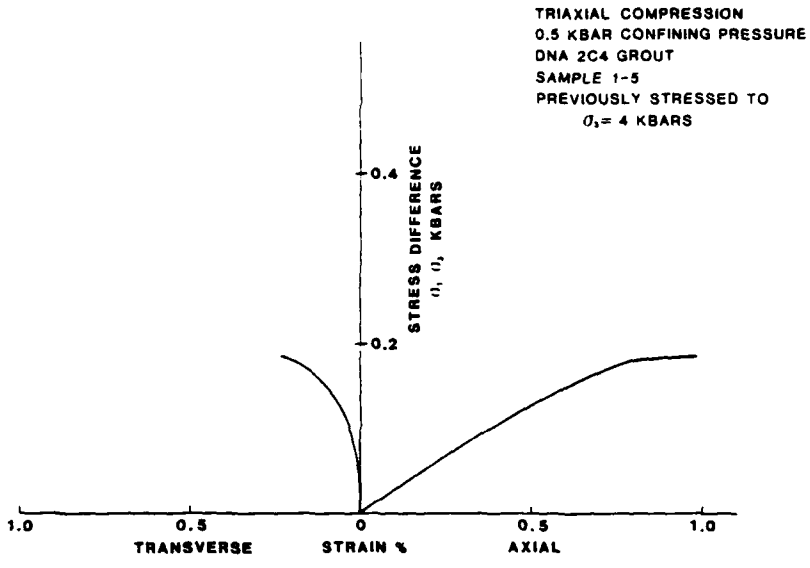

Figure C35

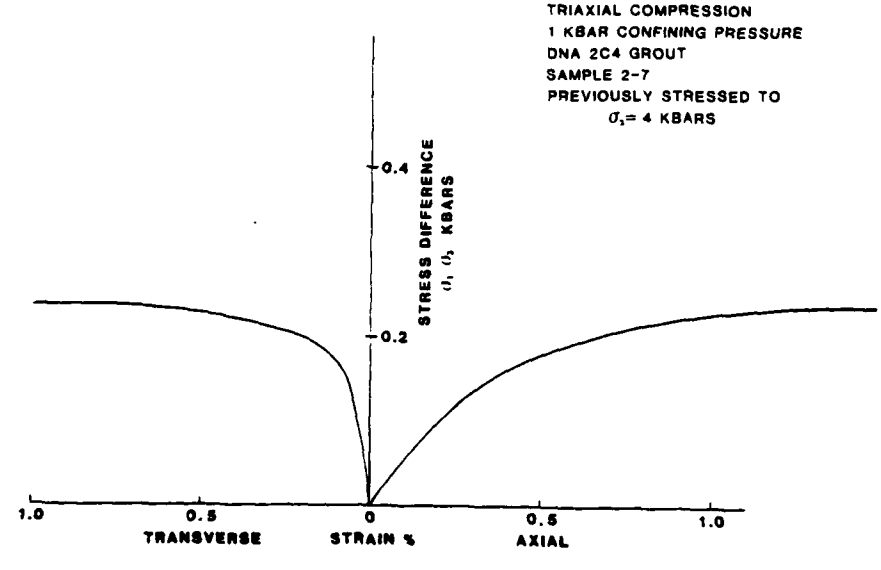

Figure C36

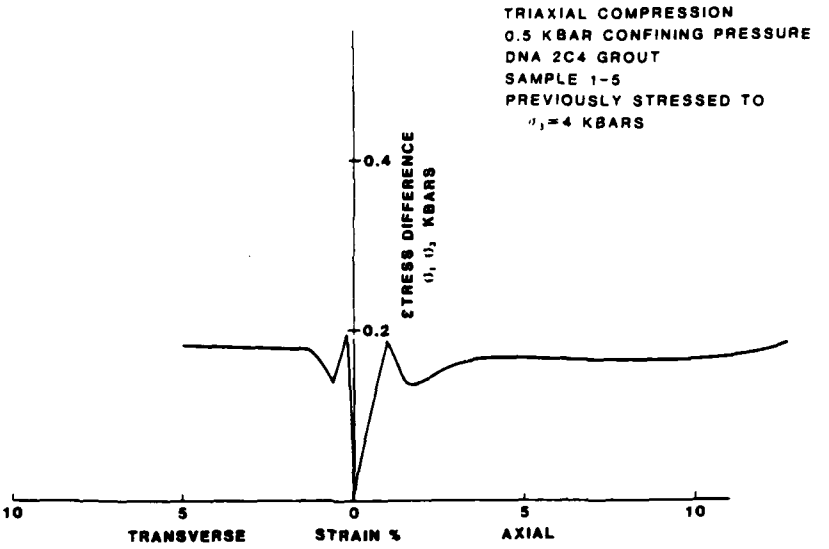

Figure C37

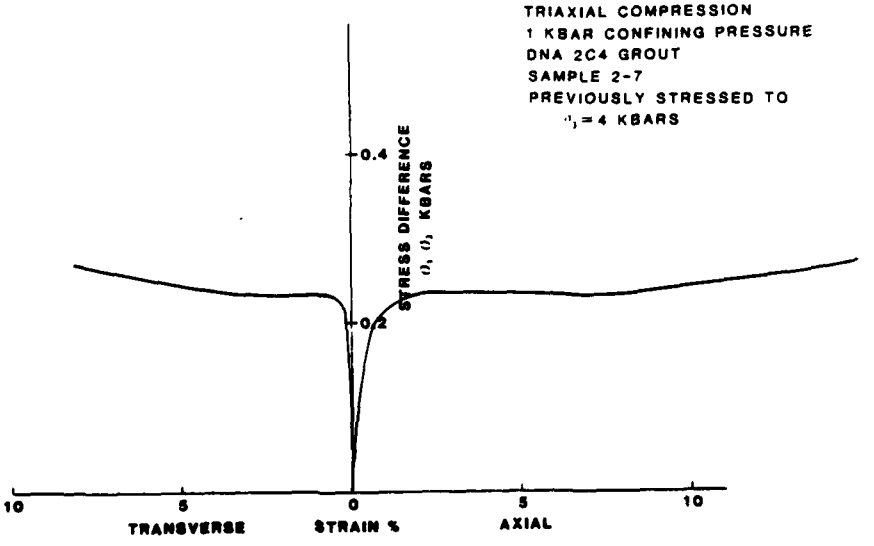

Figure C38

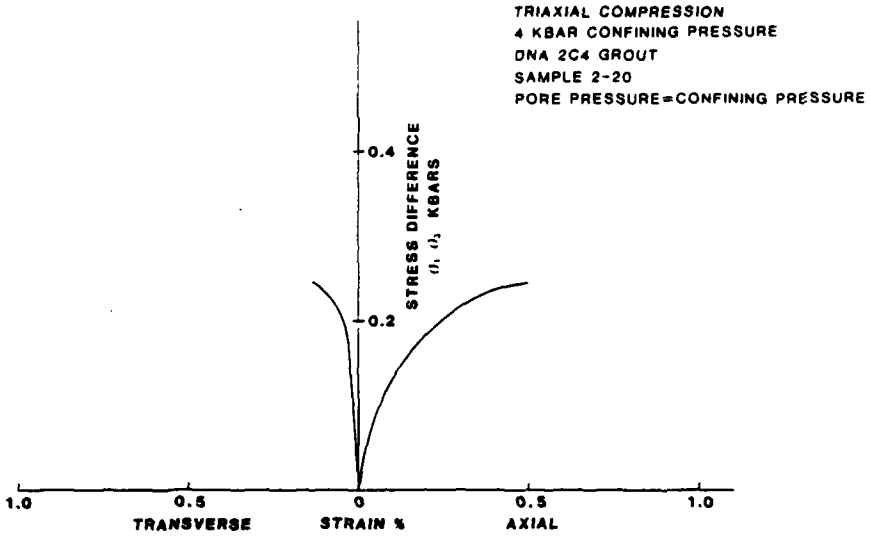

Figure C39

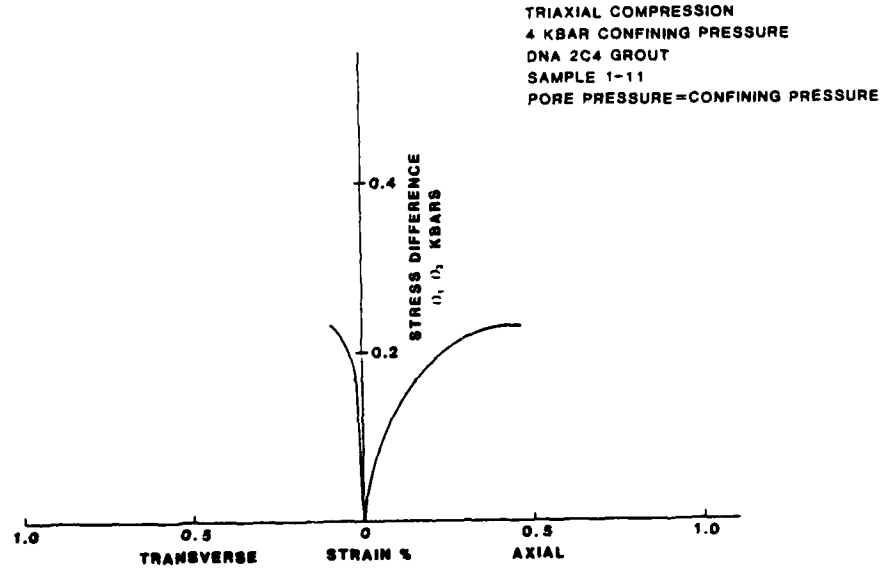

Figure C40

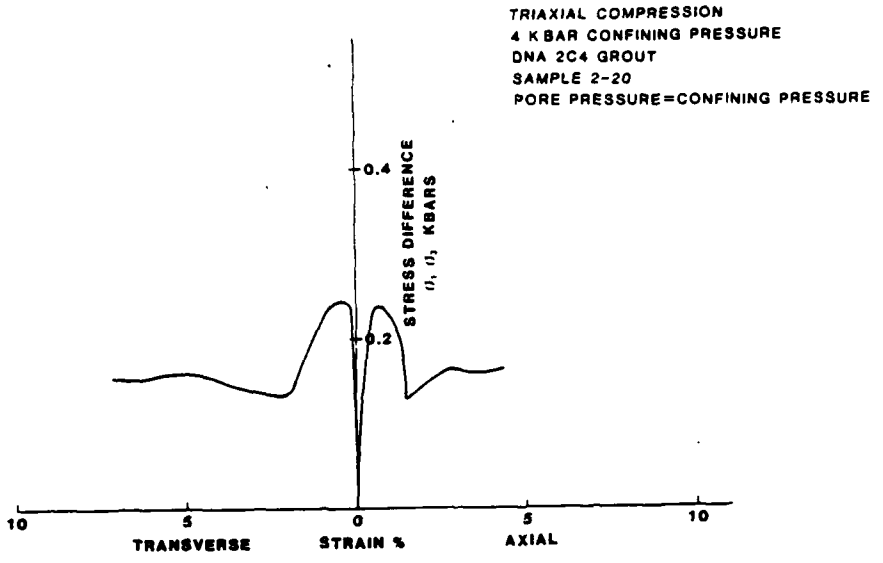

Figure C41

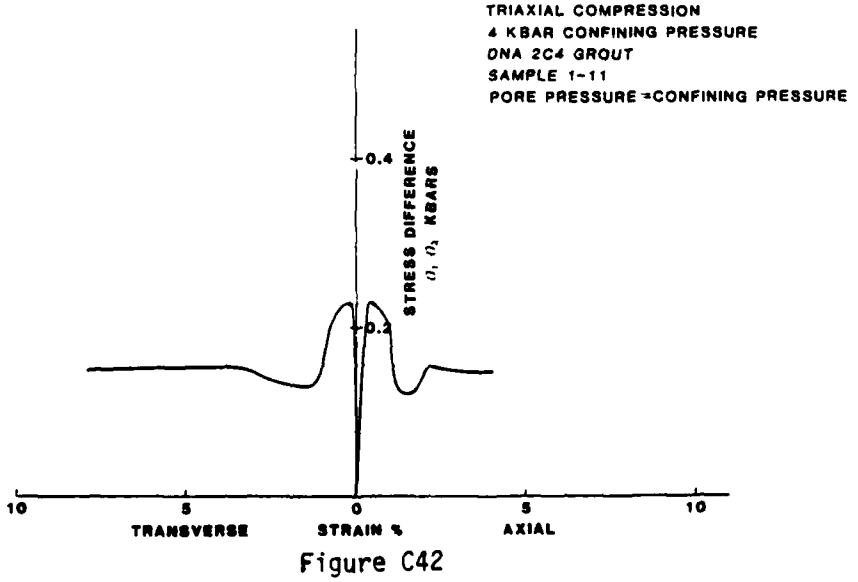

Figure C42

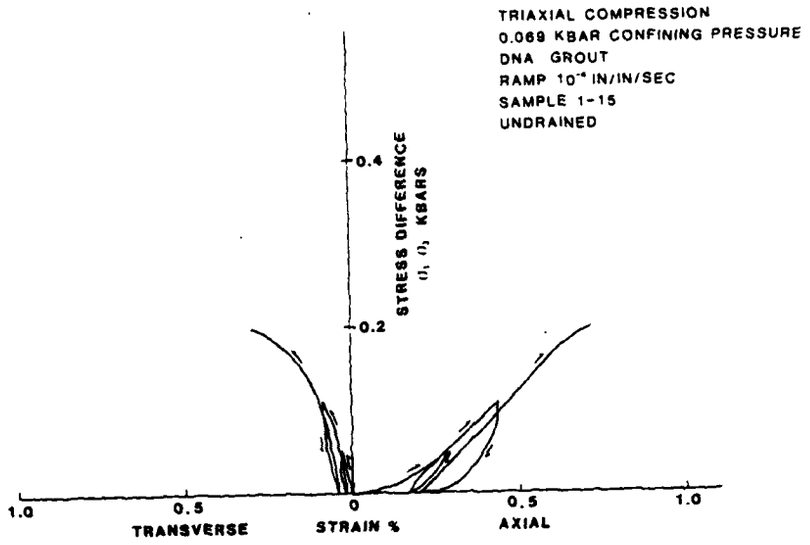

Figure C43

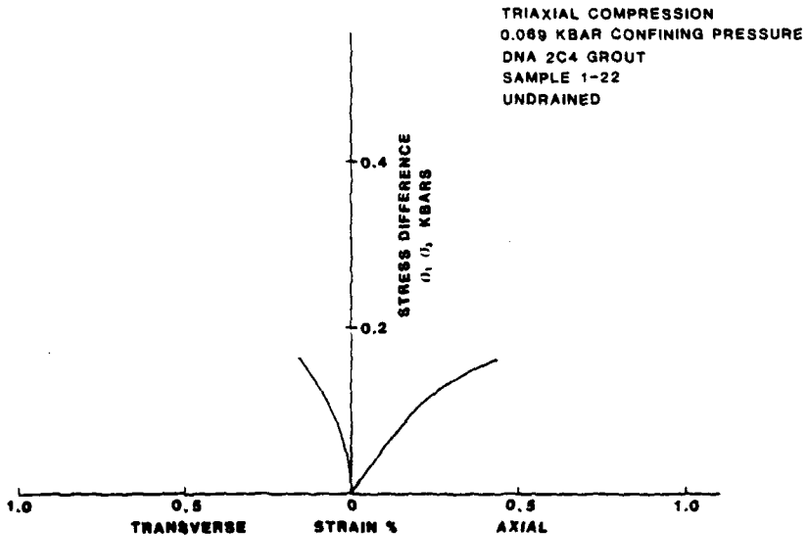

Figure C44

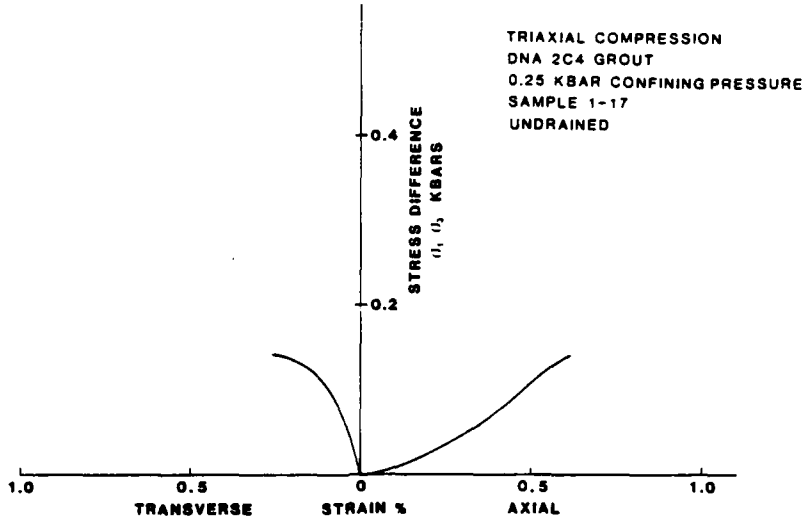

Figure C45

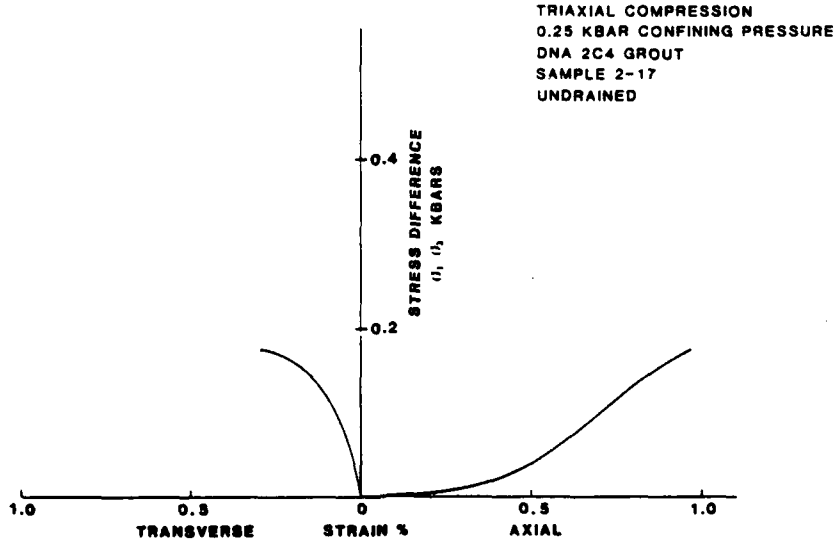

Figure C46

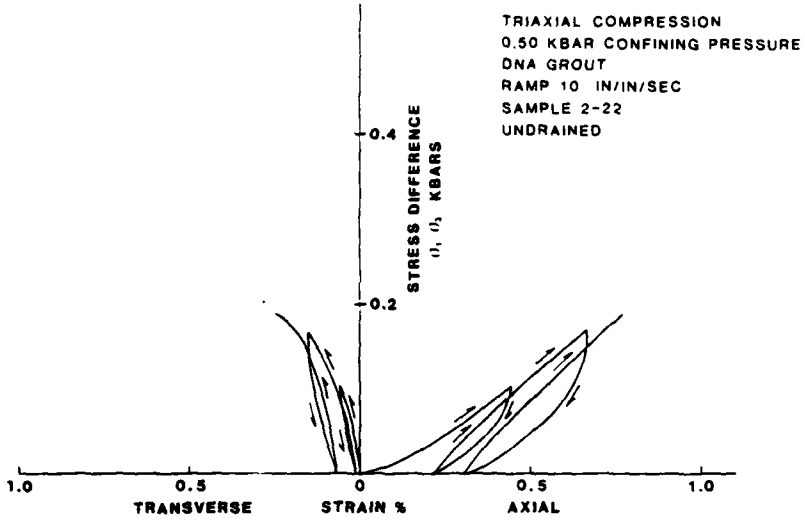

Figure C47

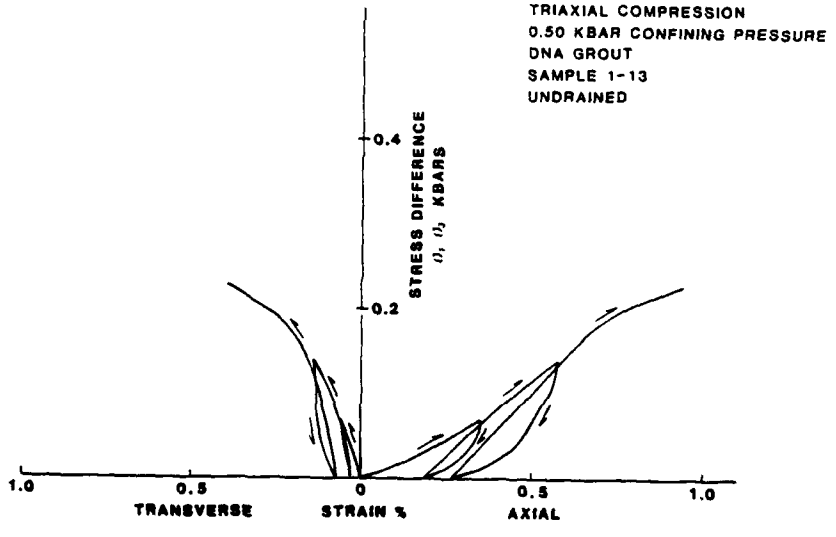

Figure C48

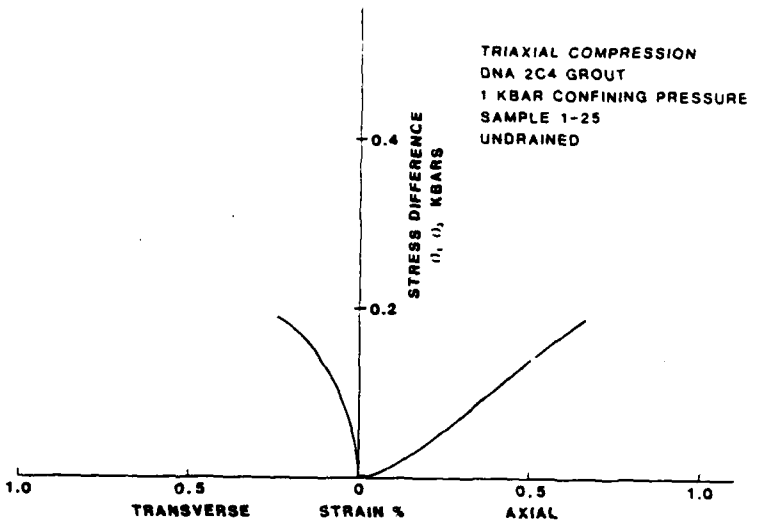

Figure C49

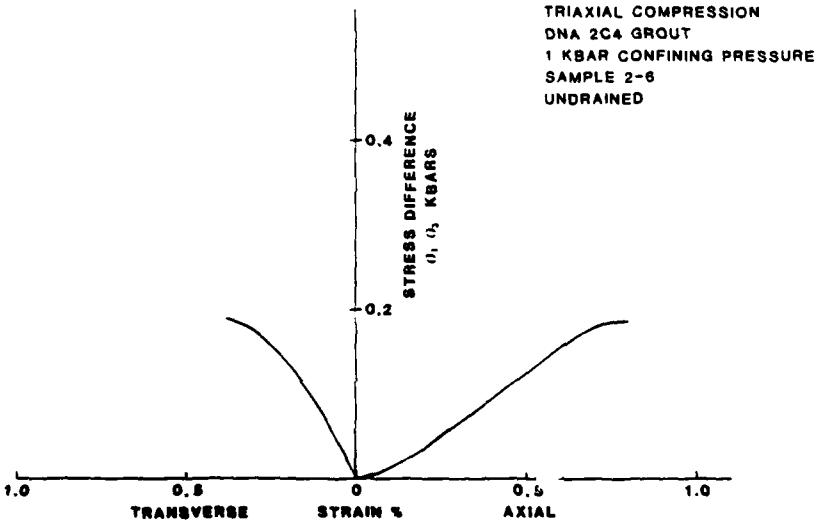

Figure C50

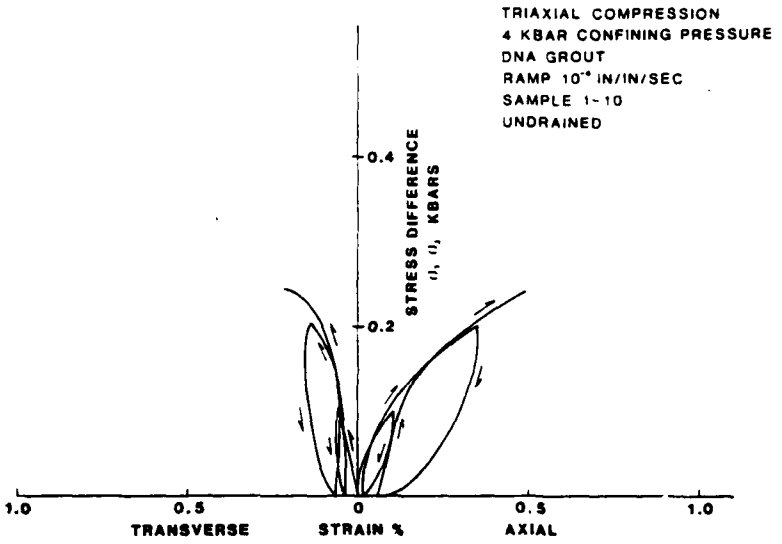

Figure C51

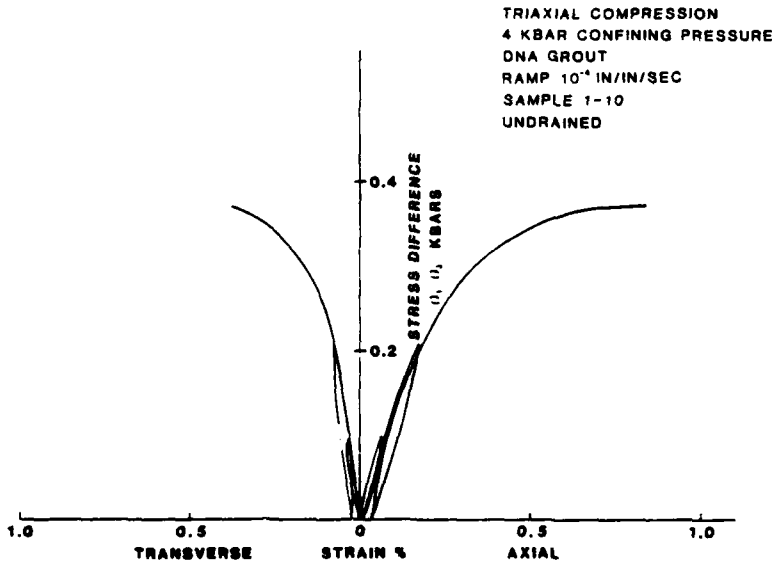

Figure C52

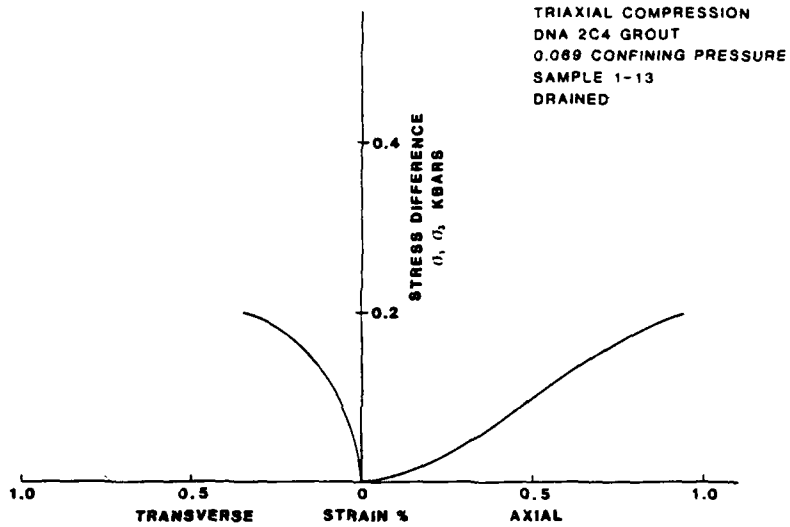

Figure C53

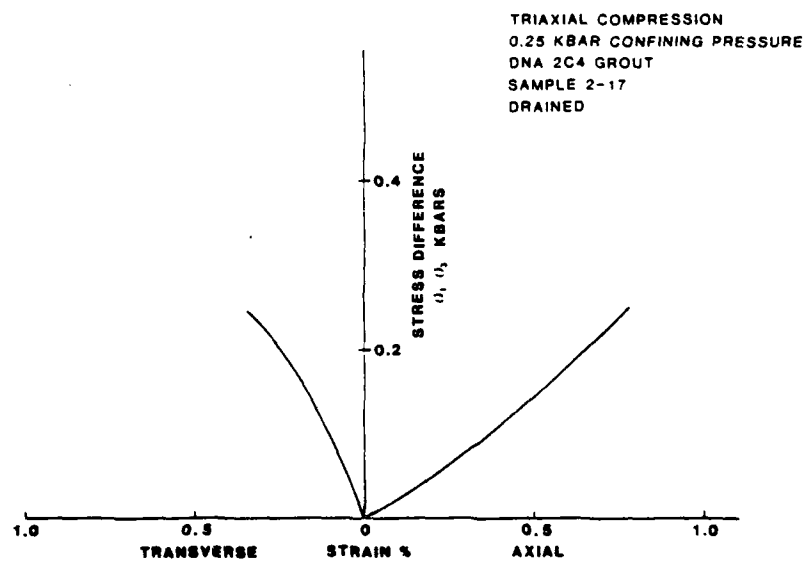

Figure C54

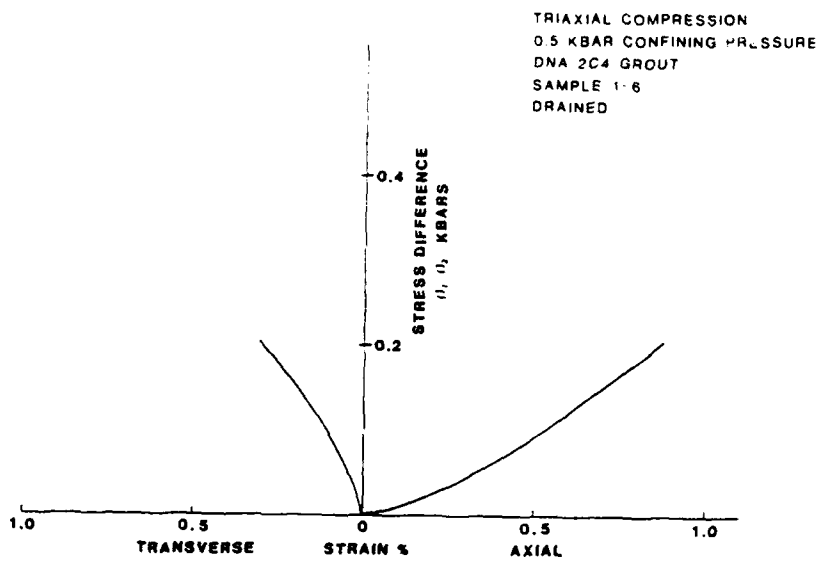

Figure C55

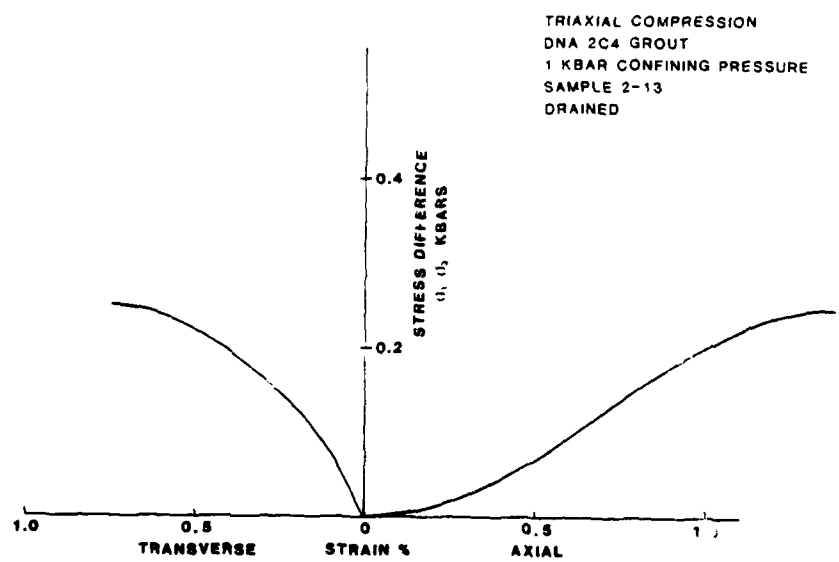

Figure C56

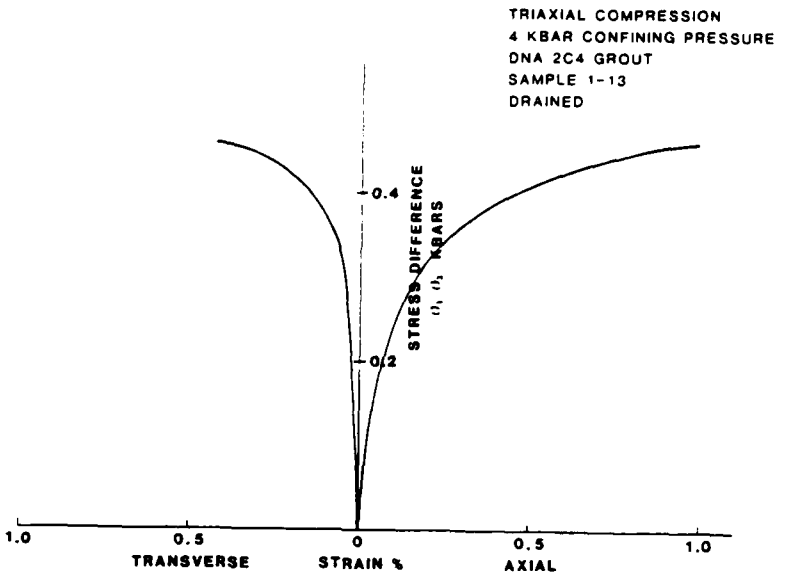
TRIAXIAL COMPRESSION
4 KBAR CONFINING PRESSURE
DNA 2C4 GROUT
SAMPLE 1-13
DRAINED
0.4
0.2
1.0
0.5
0
0.5
1.0
TRANSVERSE
STRAIN %
AXIAL

Figure C57

APPENDIX D

STRAIN RATE EFFECTS

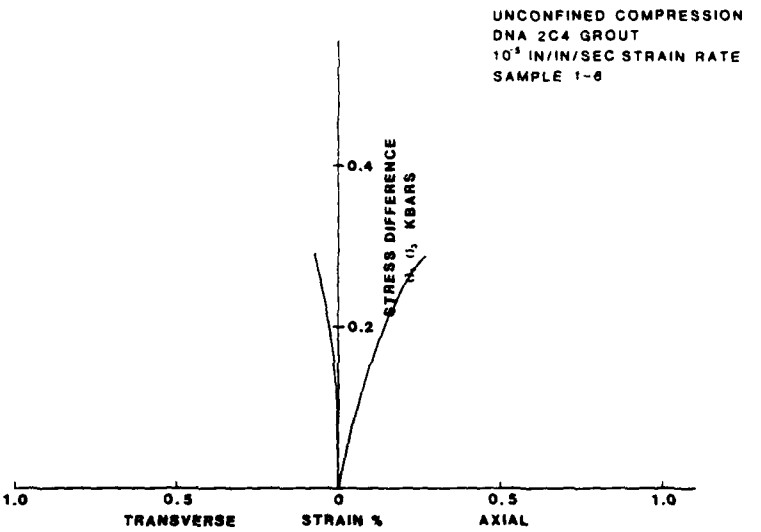

Figure D1

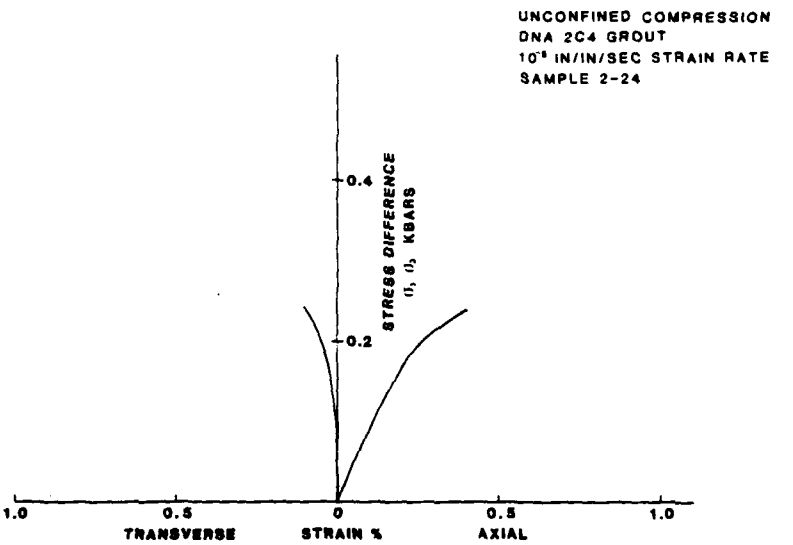

Figure D2

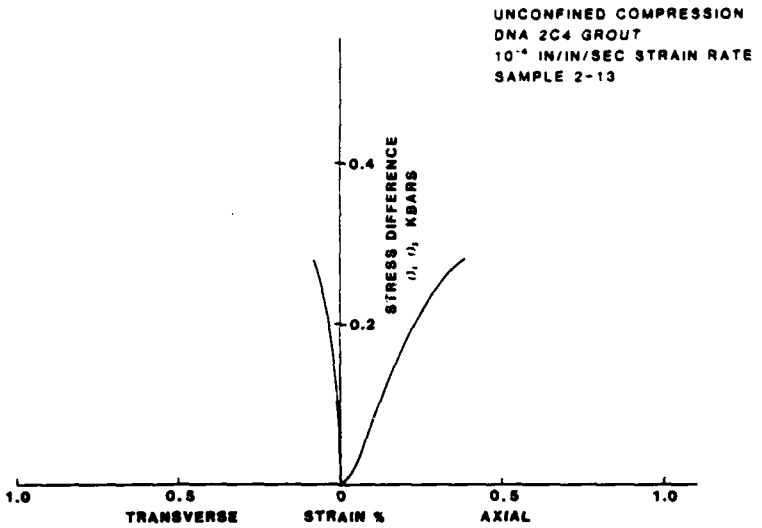

Figure D3

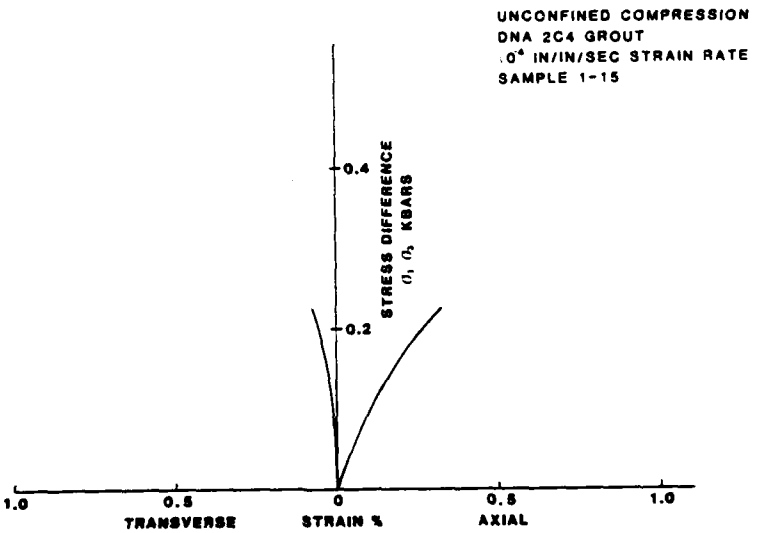

Figure D4

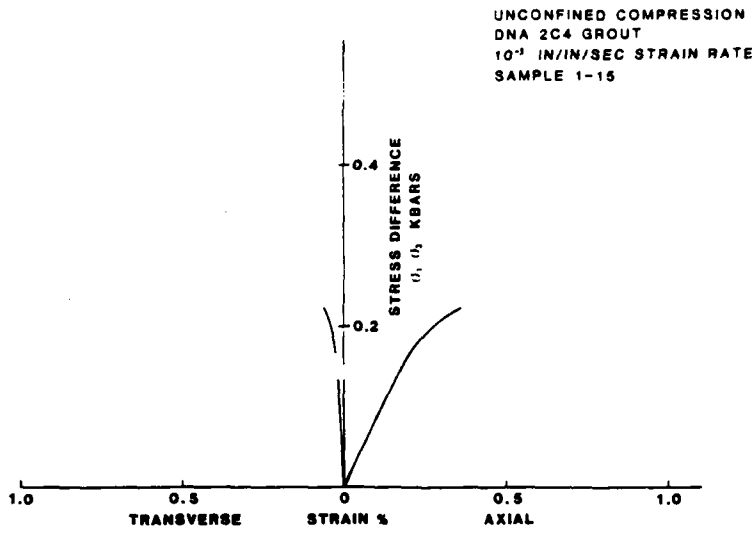

Figure D5

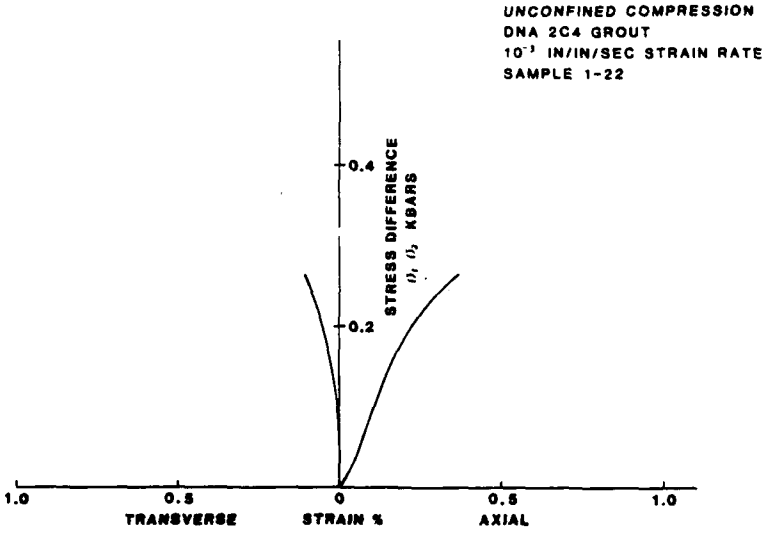

Figure D6

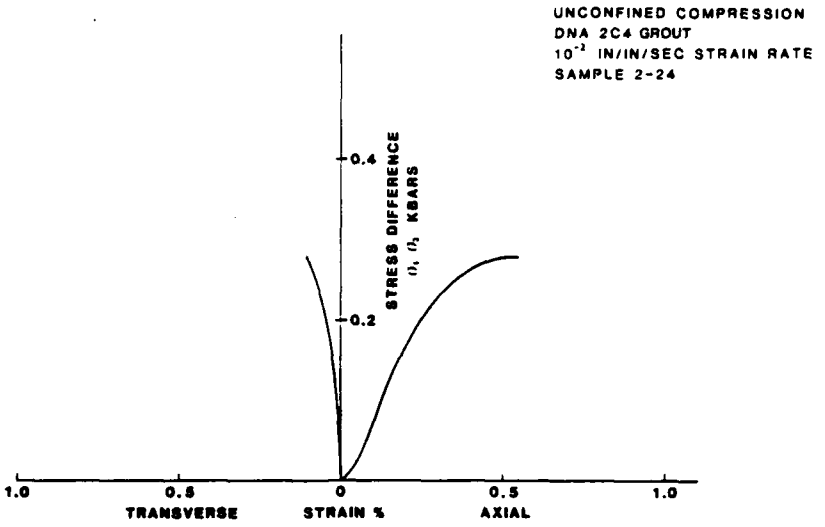

Figure D7

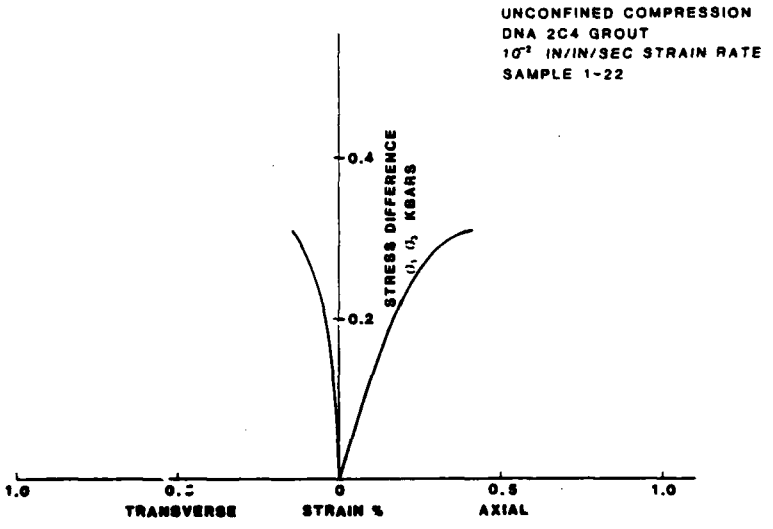

Figure D8

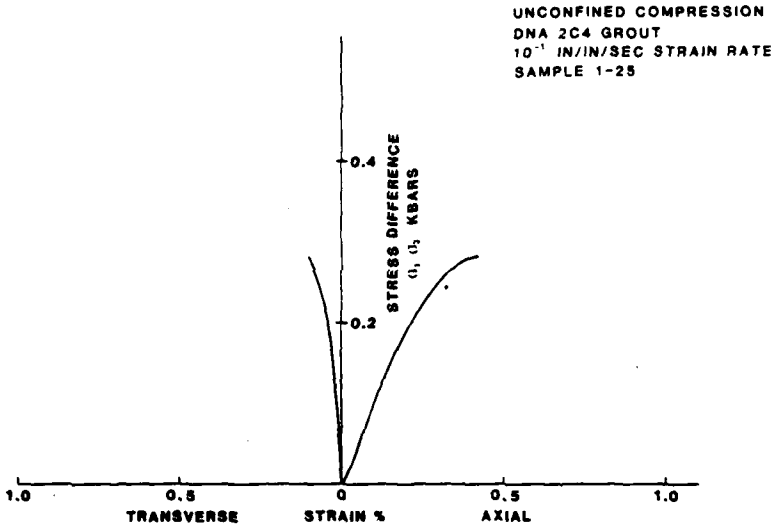

Figure D9

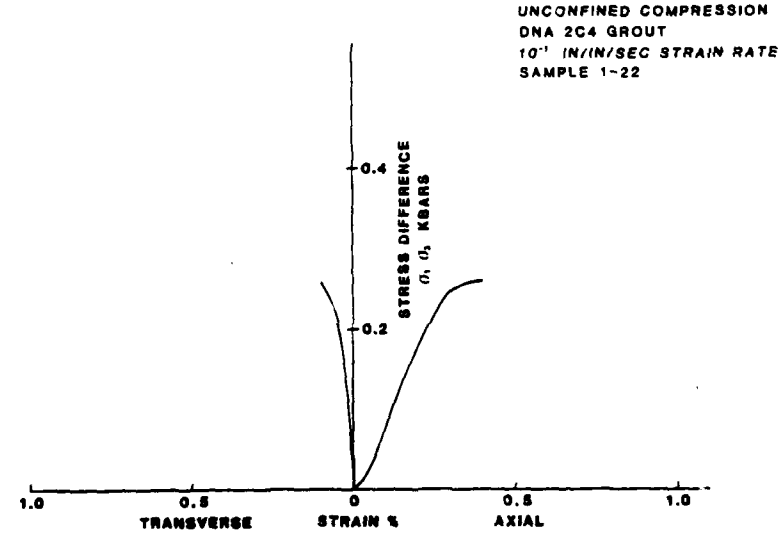

Figure D10

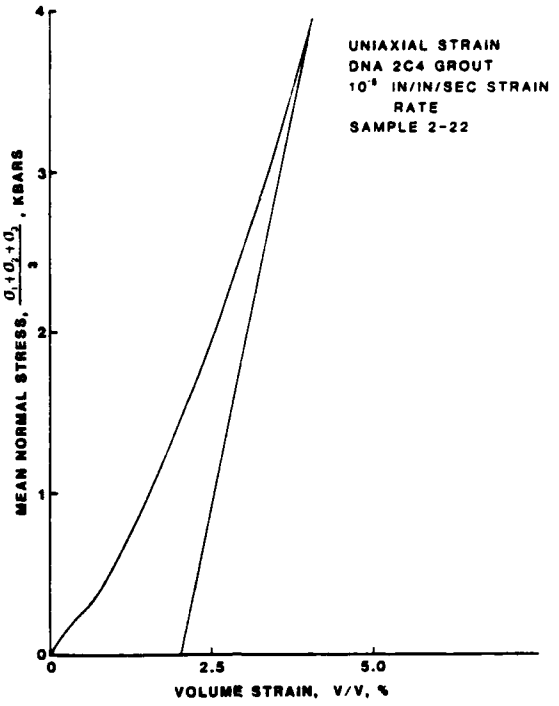

Figure D11a

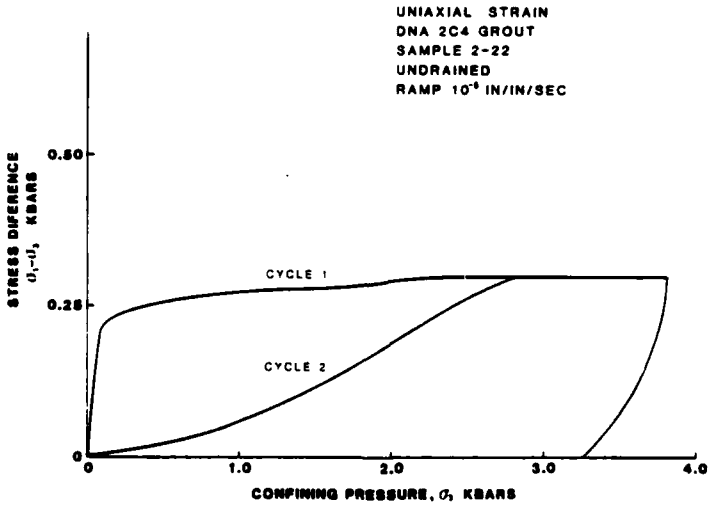

Figure D11b

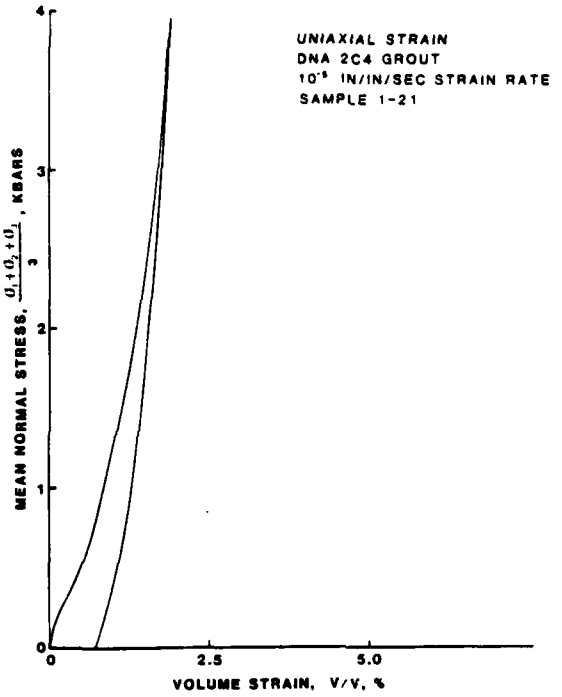

Figure D12a

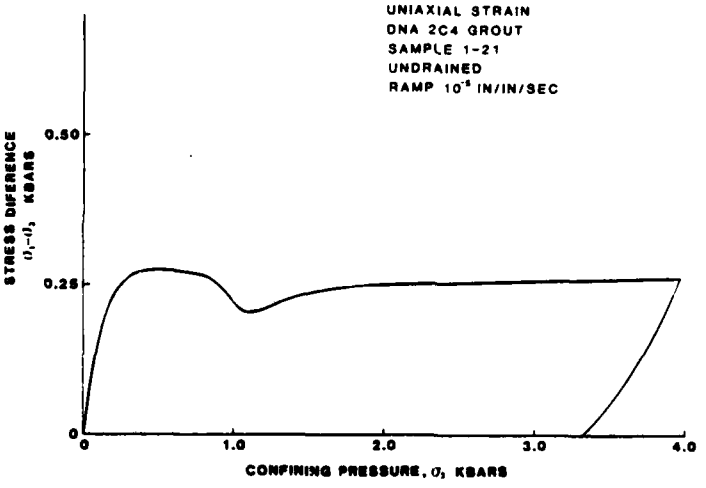

Figure D12b

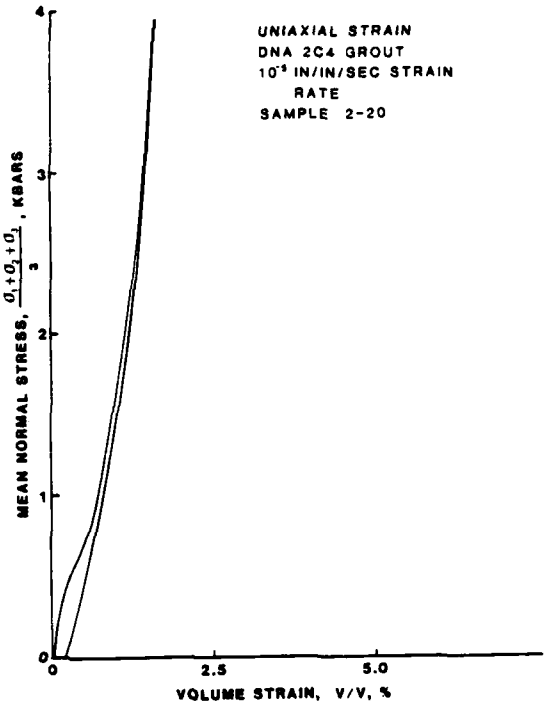

Figure D13a

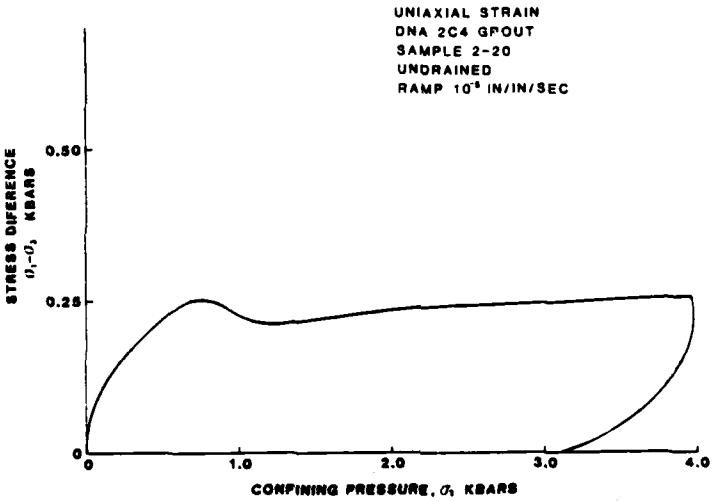

Figure D13b

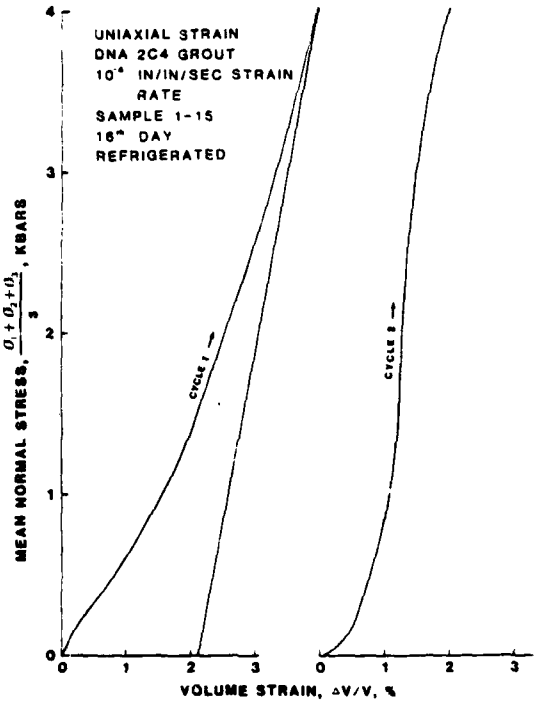

Figure D14a

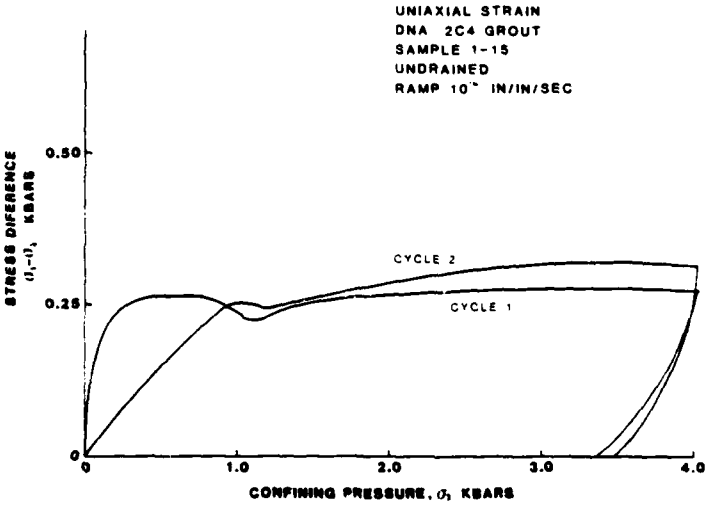

Figure D14b

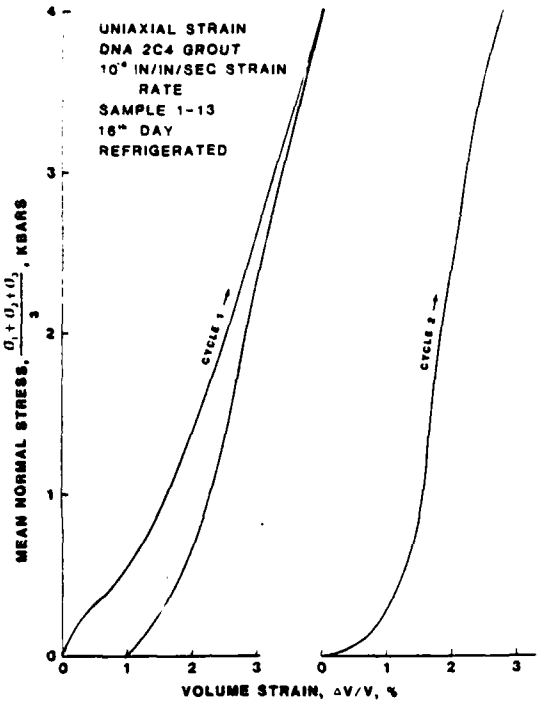

Figure D15a

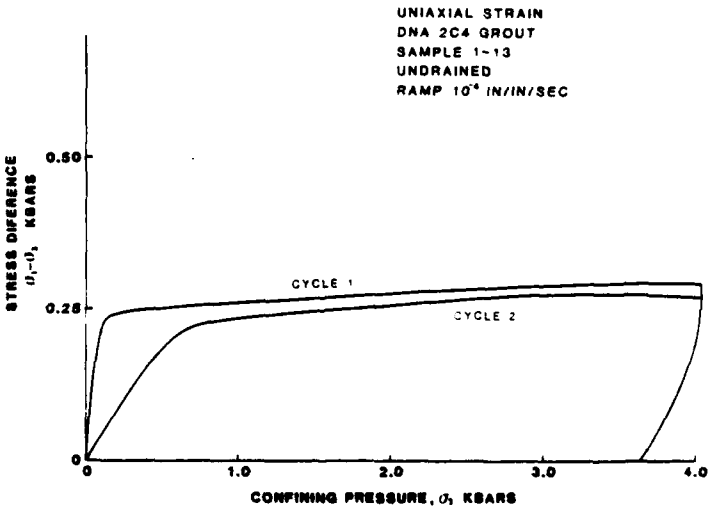

Figure D15b

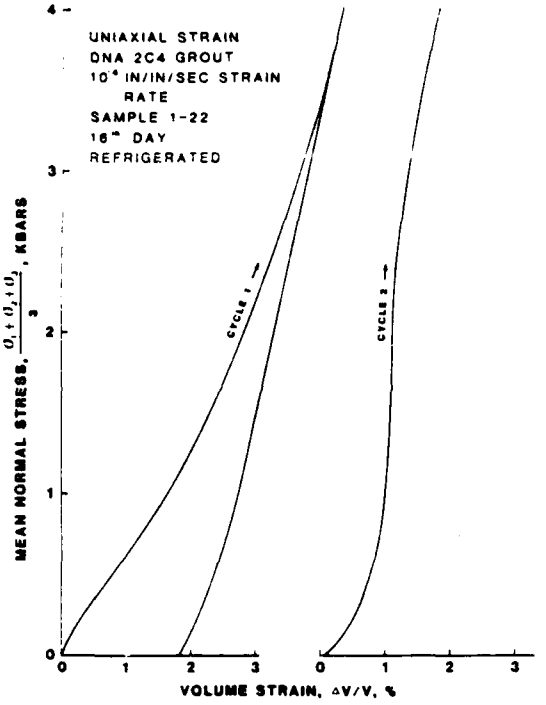

Figure D16a

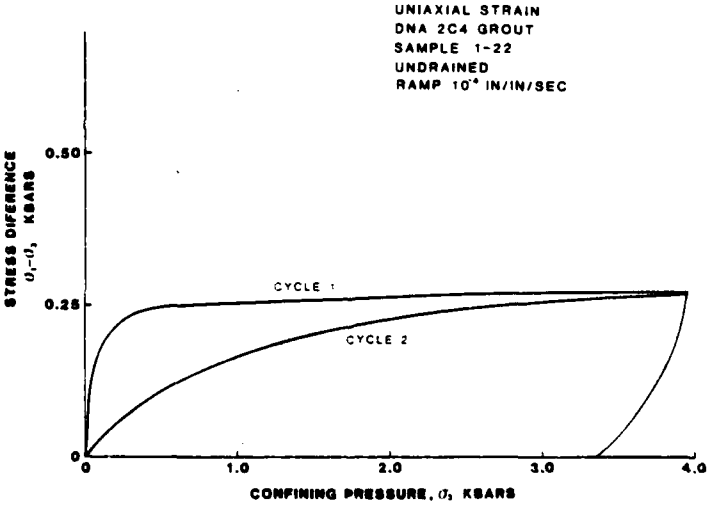

Figure D16b

AD-A128 368 PROPERTIES OF TUFFS GROUT AND OTHER MATERIALS(U) TERRA TEK INC SALT LAKE CITY UT C H COOLEY ET AL. 01 JAN 82 TTI-TR-82-05 DNA-5986F DNA001-78-C-0395 3/3

UNCLASSIFIED F/G 8/7 NL

END
DATE FILMED
6 83
DTIC

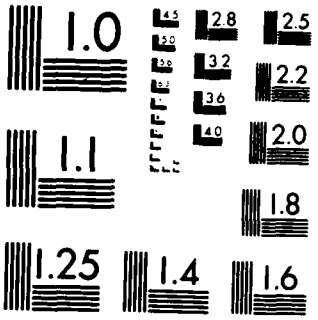

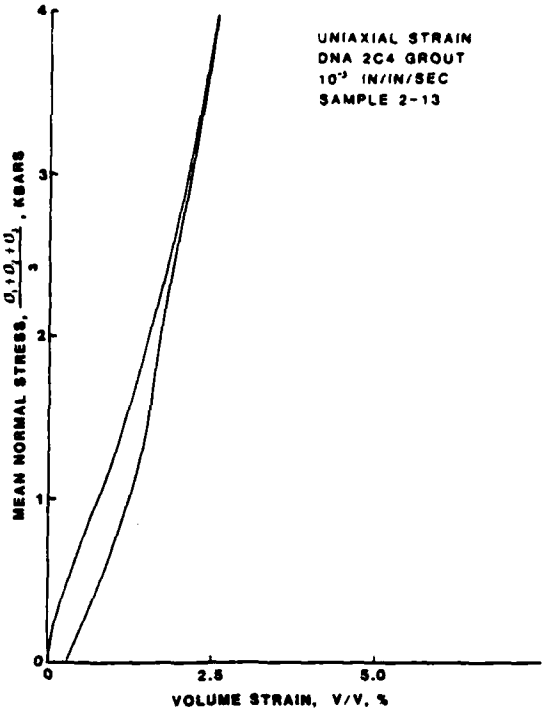

Figure D17a

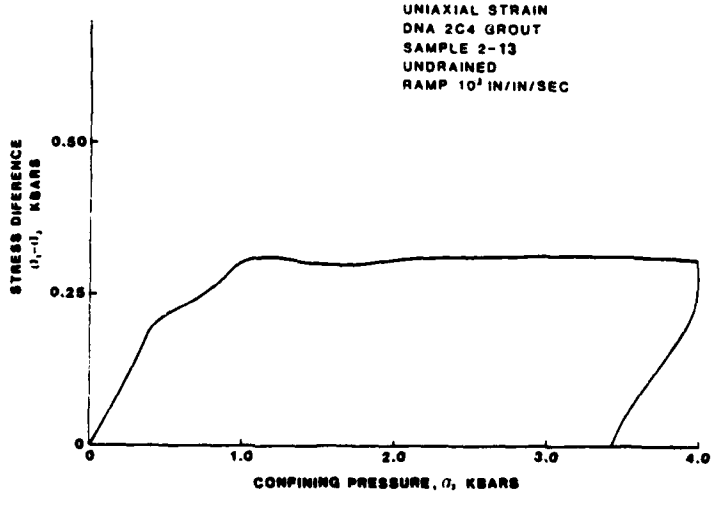

Figure D17b

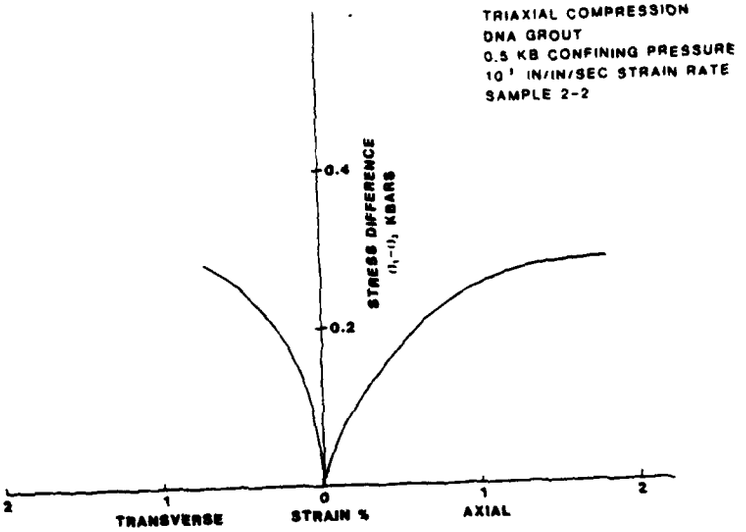

Figure D18

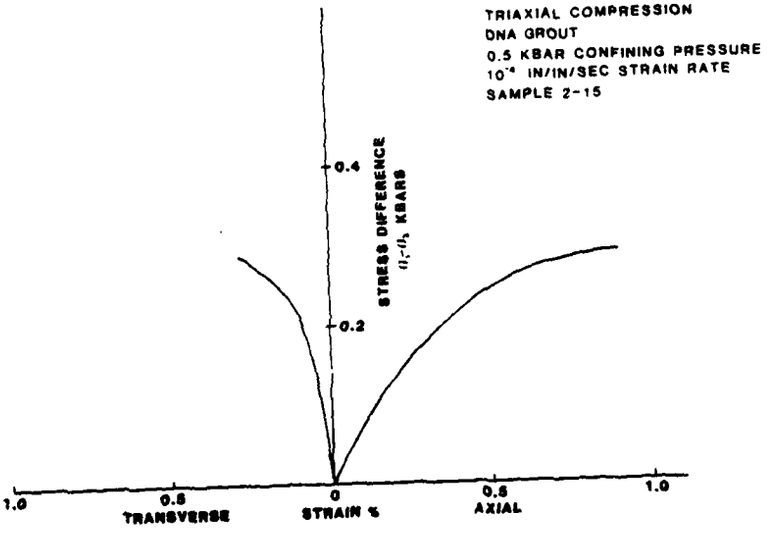

Figure D19

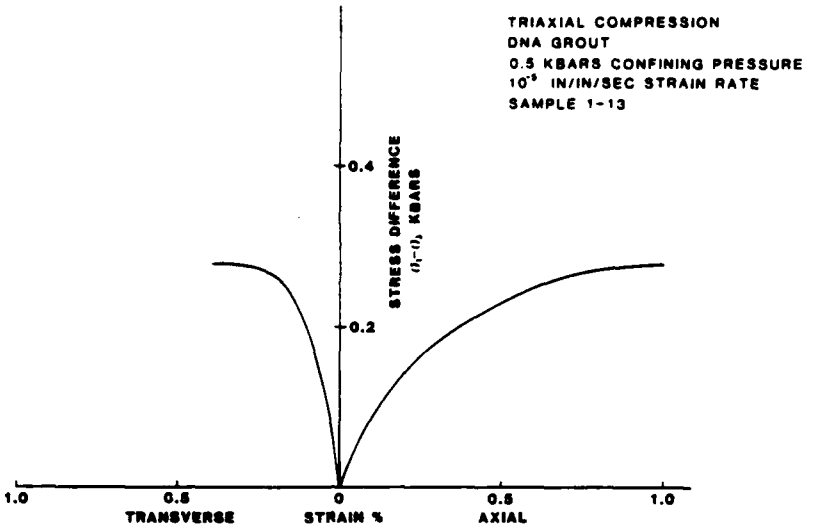
TRIAXIAL COMPRESSION
DNA GROUT
0.5 KBARS CONFINING PRESSURE
10^{-5} IN/IN/SEC STRAIN RATE
SAMPLE 1-13
STRESS DIFFERENCE
$(\sigma_1-\sigma)$, KBARS
0.4
0.2
1.0
0.5
TRANSVERSE
0
STRAIN %
0.5
AXIAL
1.0

Figure D20

IV. COAL TAR EPOXY

Introduction

Three series of tests were run on samples of coal tar epoxy (CTE)-pea gravel mistures, in order to determine their behavior when subjected to elevated stress at room temperature and elevated temperatures and in a steam atmosphere.

Results of the first test series consist of previously unreported data on CTE. These include results of room temperature triaxial compression tests conducted at 0, 1, 2 and 4 kbar confining pressure, and uniaxial strain tests conducted to 4 kbar confining pressure.

The second and third test series have been reported previously in the form of letter reports. Results of unconfined compression tests conducted at room temperature and a sample treated at 100°C were included in a letter to J. LaComb dated March 30, 1981. Results of CTE creep experiments were submitted in the letter to J. LaComb dated October 1, 1981. For completeness, results of these two test series are included in this section.

Triaxial Compression and Uniaxial Strain Tests at Room Temperature

In order to develop a better understanding of the mechanical behavior of coal tar epoxy (CTE)-pea gravel mixtures, a series of triaxial and uniaxial strain tests were performed. Triaxial compression tests at 0, 2 and 4 kbars confining pressure were conducted, as well as uniaxial compression tests to 4 kbars. These tests were all at room temperature.

Figures 1 to 7b are plots of strain as a function of stress difference, and strain as a function of confining pressure for the triaxial compression tests. Figures 8a to 9b show volume strain versus the mean normal stress, and stress difference versus confining pressure for the uniaxial compression tests.

The CTE material showed permanent compactions of approximately 0.5% and 1.0% by volume after the uniaxial tests.

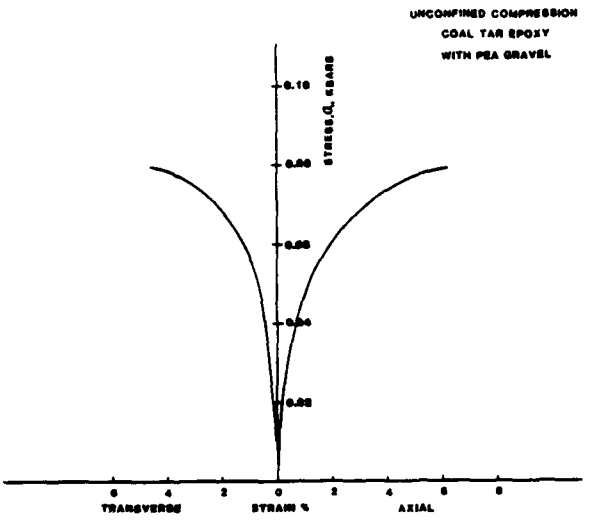

Figure 1

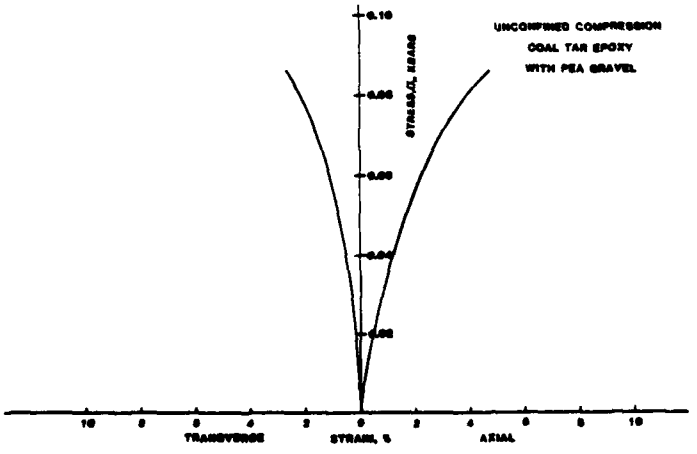

Figure 2

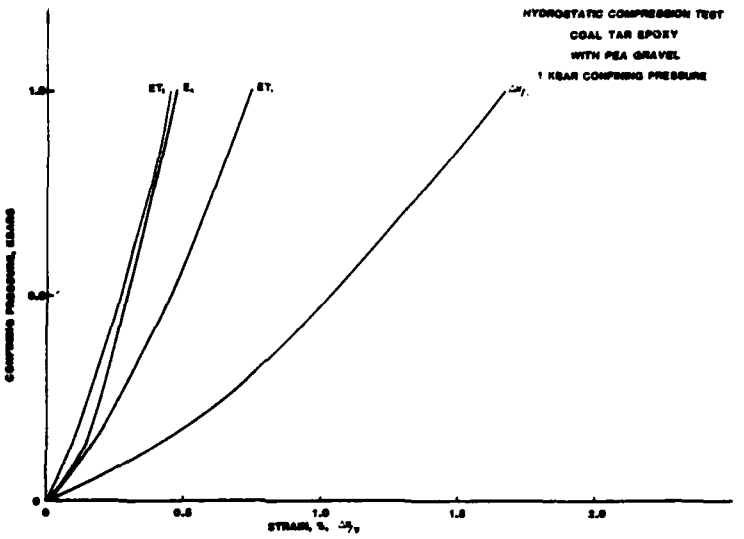

Figure 3A

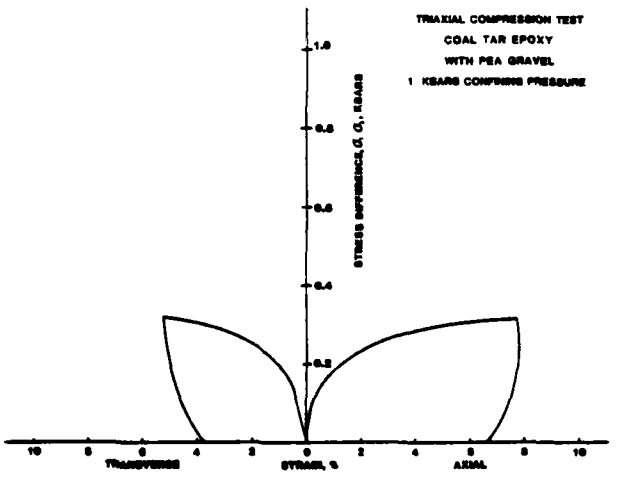

Figure 3B

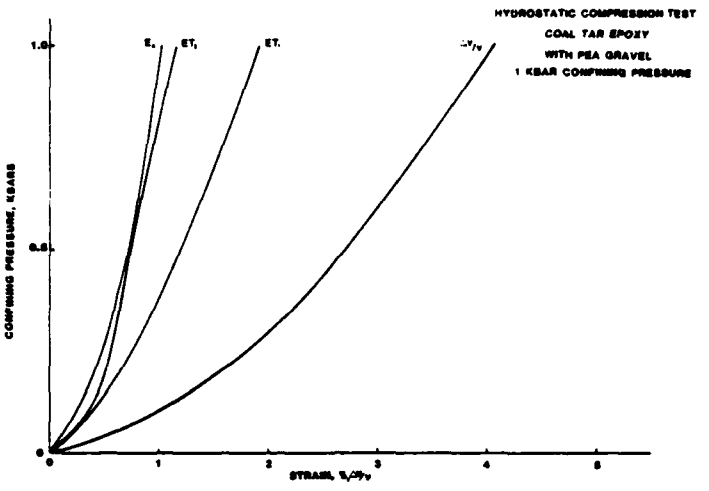

Figure 4A

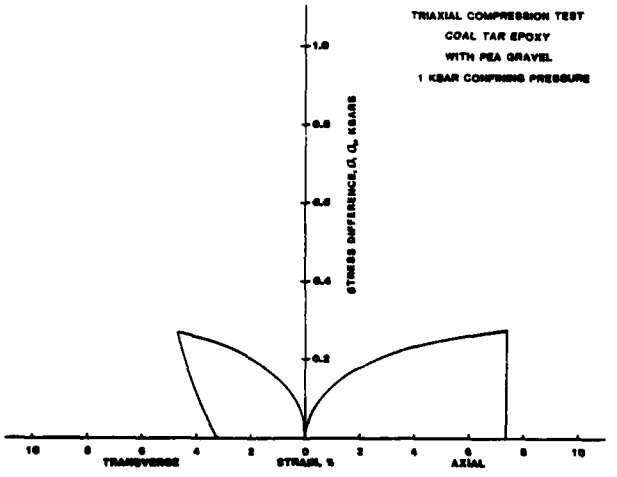

Figure 4B

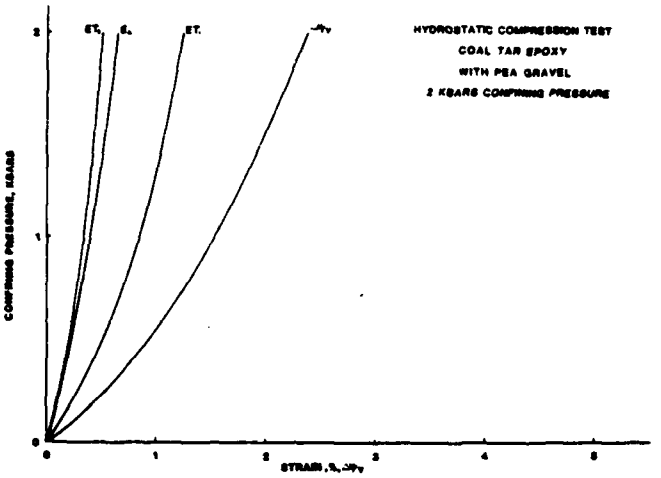

Figure 5A

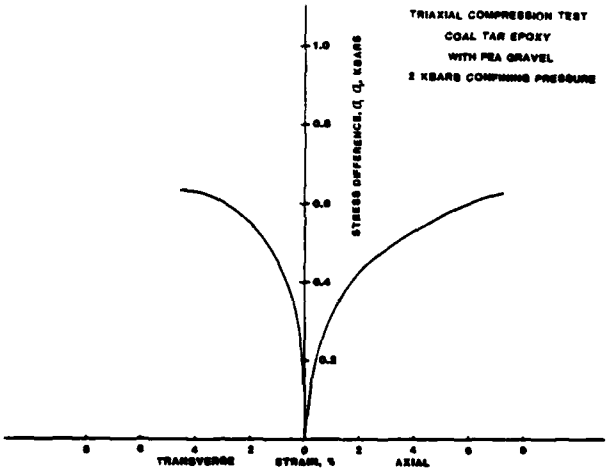

Figure 5B

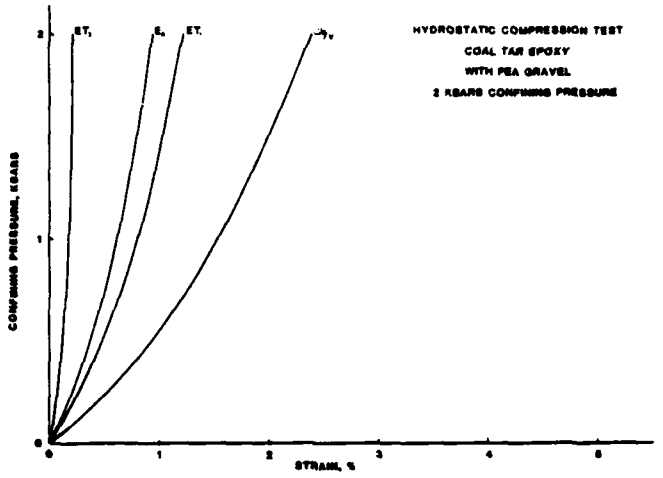

Figure 6A

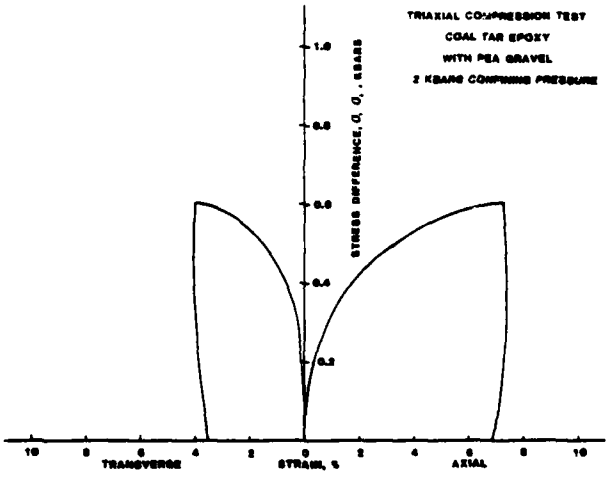

Figure 6B

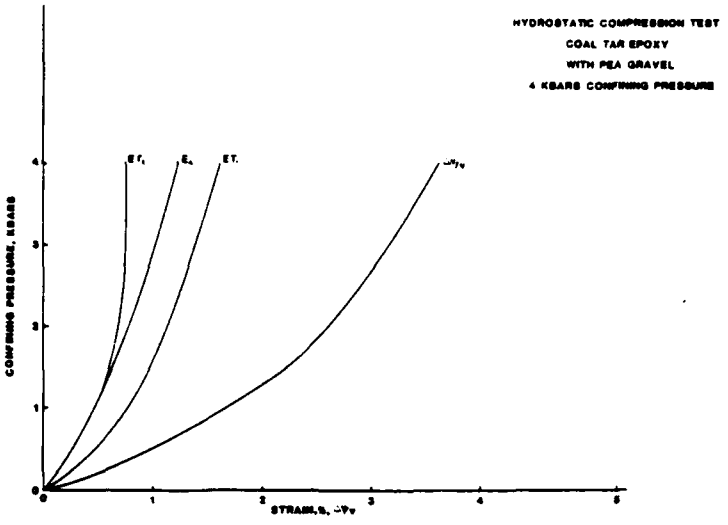

Figure 7A

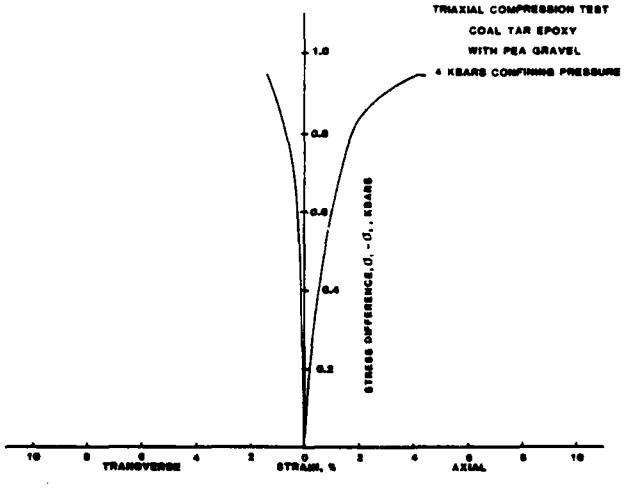

Figure 7B

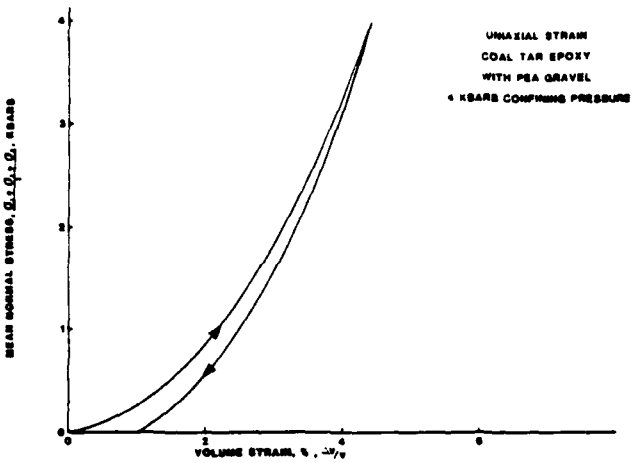

Figure 8A

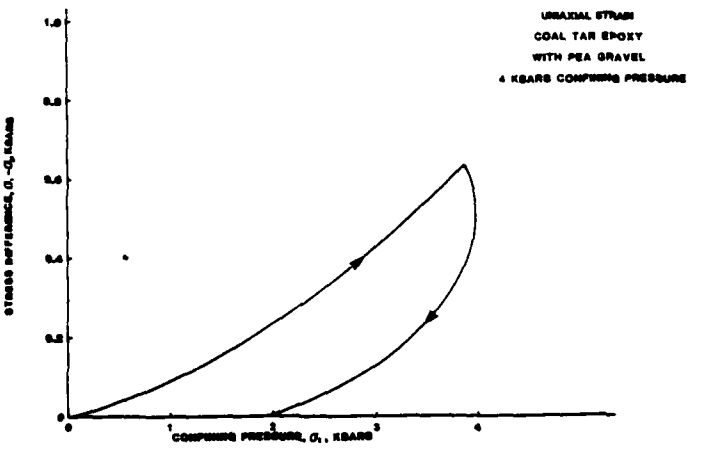

Figure 8B

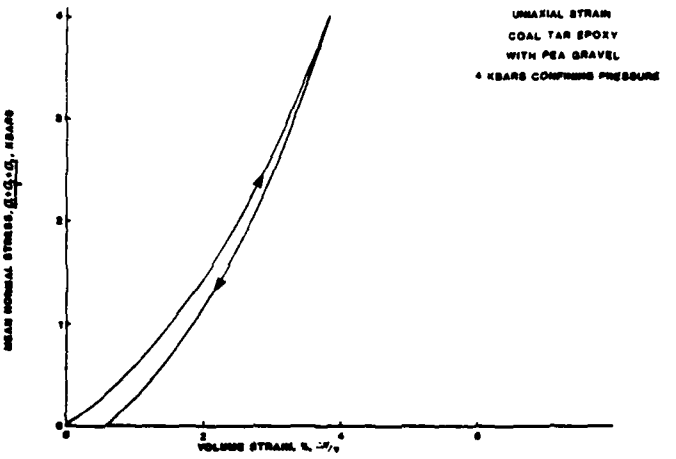

Figure 9A

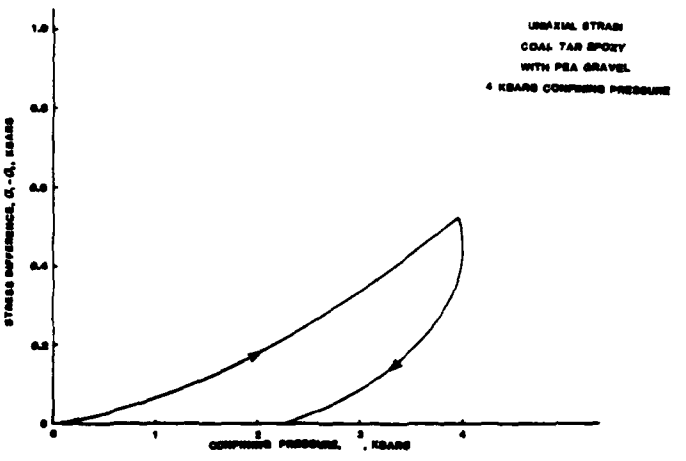

Figure 9B

Unconfined Compression Test at Room Temperature and 100°C

Figure 10 is a plot comparing the unconfined compressive strengths at room temperature and ~100°C. In the elevated temperature test the prepared CTE sample was immersed in boiling water (96°C in Salt Lake City) for approximately 24 hours and was then quickly instrumented and tested to failure in compression. As can be seen, the relative unconfined compressive strengths of the samples tested at room and elevated temperatures differ by more than an order of magnitude.

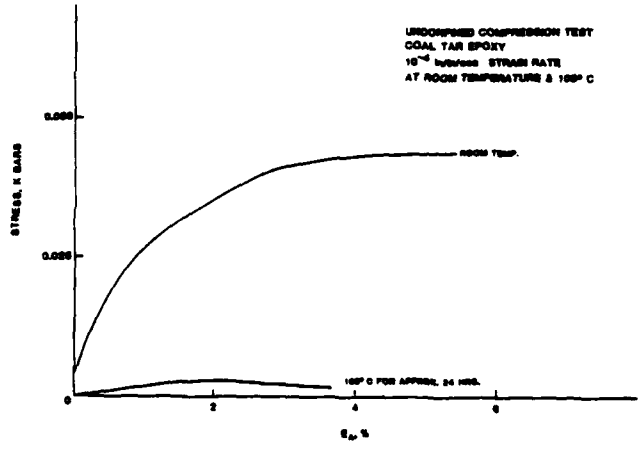

Figure 10. Unconfined Compression of CTE with Pea Gravel at Room Temperature and 100°C.

Creep Experiments at ~100°C

The creep response of CTE-pea gravel mixtures at elevated temperatures was also investigated. In these series of tests, 2 and 4 inch long samples of 2 inch diameter CTE material were mounted in the apparatus shown diagramatically in Figure 11. This apparatus consisted of a free hanging vertical rod fastened at its upper end to a support structure. Dead weights, a platten and the sample were all subsequently placed coaxially on the rod. A 0.57 in^2 washer and nut supported the components. An open ended cylinder mounted on the underside of the platten encased the CTE sample material. This cylinder had vent holes drilled near the upper end to allow vertical steam circulation. The washer area and the dead weights combined to produce a compressive stress of 6.9 bars on the sample.

Saturated steam (~96°C) was allowed to contact the side and end surfaces of the CTE sample. The creep displacement of the sample was measured by a dial gage (having a resolution of 0.001 inches) indicating the platen position. The time displacement data were collected for periods of up to 56 hours. The displacement as a function of time (displacement being plotted instead of strain due to stress field inhomogeneities) for the four samples tested are shown in Figure 12. The general characteristics of primary and secondary creep are evident in the samples. There are, however, significant variances in the curves. The most probable cause of these variances is the effect of the full-sized pea gravel filler on a small sample. A larger sample would tend to minimize the inhomogeneous effects of the filler. And in fact the two 4 inch long samples did exhibit the most consistent response.

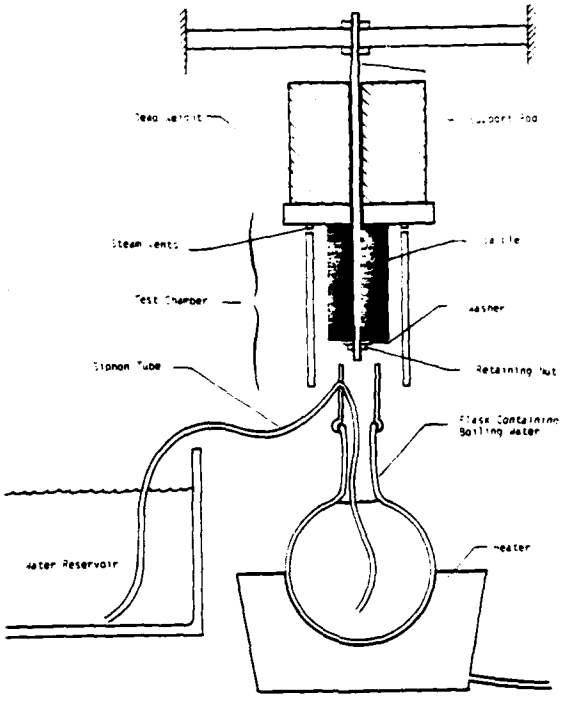

Figure 11
Elevated temperature creep apparatus used in CTE tests.

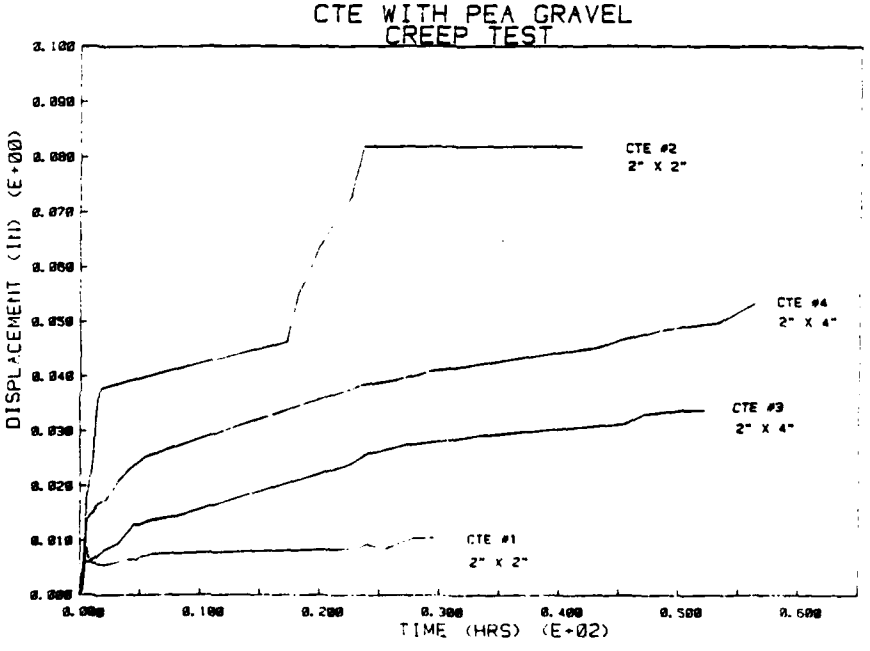

Figure 12
Creep response of CTE with pea gravel at 100°C.

DISTRIBUTION LIST

DEPARTMENT OF DEFENSE

Defense Nuclear Agency
ATTN: SPSS, D. Linger
ATTN: SPSS, G. Ullrich
ATTN: SPTD, T. Kennedy
ATTN: STSP
4 cy ATTN: TITL

Defense Technical Information Center
12 cy ATTN: DD

Field Command
Defense Nuclear Agency
ATTN: FCT
ATTN: FCTO
ATTN: FCTE
ATTN: FCTK, B. Ristvet
10 cy ATTN: FCTK, C. Keller
10 cy ATTN: FCTC, J. LaComb

Field Command
DNA Det 1
Lawrence Livermore National Lab
ATTN: FC-1
ATTN: Document Control

DEPARTMENT OF THE ARMY

Dep Chief of Staff for Rsch, Dev & Acq
ATTN: NBC Division

Explosive Excavation Rsch Laboratory
ATTN: Document Control

Harry Diamond Labs
ATTN: DRXDO-N-P

US Army Engineer Center
ATTN: ATSEN-SV-L

US Army Engr Waterways Exper Station
ATTN: D. Day
ATTN: J. Boa
ATTN: J. Zelasko
ATTN: W. Flathau
ATTN: Rsch Center Lib
ATTN: L. Ingram
ATTN: P. Hadala
ATTN: J. Jackson
ATTN: J. Ehrgot

DEPARTMENT OF THE NAVY

Chief of Naval Research
ATTN: Document Control

Naval Ordnance Station
ATTN: Code 121

Naval Construction Battalion Center
ATTN: J. Allgood

Naval Research Laboratory
ATTN: Code 1065
ATTN: Code Cont Branch

DEPARTMENT OF THE AIR FORCE

AF Cambridge Research Labs
ATTN: LWW, K. Thompson

Air Force Weapons Lab
ATTN: DE-I
ATTN: DEV-G, J. Bratton
ATTN: NTE, M. Plamondon
ATTN: SES, R. Henning
ATTN: Technical Library
ATTN: DEX

DEPARTMENT OF ENERGY

Department of Energy
ATTN: R. Newman
ATTN: Technical Library

OTHER GOVERNMENT AGENCIES

Bureau of Mines
ATTN: T. Ricketts
ATTN: T. Atchison

Department of the Interior
Bureau of Mines
ATTN: L. Obert

Department of the Interior
US Geological Survey
ATTN: R. Carroll
ATTN: W. Twenhofel
ATTN: T. Fernald
ATTN: P. Orkild

US Environmental Protection Agency
ATTN: R. Stanley

DEPARTMENT OF ENERGY CONTRACTORS

Holmes & Narver, Inc
ATTN: J. Calovini A-6

University of California
Lawrence Livermore National Lab
ATTN: J. Hearst
ATTN: V. Wheeler
ATTN: Dr McKauge
ATTN: H. Rodean
ATTN: R. Terhune
ATTN: J. Shearer
ATTN: B. Hudson
ATTN: J. Carothers
ATTN: A. Morrison
ATTN: C. Olsen
ATTN: G. Higgins

Los Alamos National Lab
ATTN: T. Kunkle
ATTN: T. Scolman
ATTN: Reports Library
ATTN: F. App
ATTN: R. Brownlee
ATTN: B. Killian
ATTN: J. House

DEPARTMENT OF ENERGY CONTRACTORS (Continued)

Reynolds Electrical & Engr Co, Inc
ATTN: FOD/DOD, H. Edwards

Sandia National Laboratories
ATTN: C. Gulick
ATTN: C. Smith
ATTN: C. Broyles
ATTN: C. Mehl

DEPARTMENT OF DEFENSE CONTRACTORS

Agbabian Associates
ATTN: Document Control
ATTN: C. Bagge

Boeing Aerospace Co
ATTN: K. Fridell

Fenix & Scission
ATTN: F. Waltman
ATTN: D. Townsend

Geotechnical Instrumentation & Grouting, Inc
ATTN: Tech Library

H Tech
ATTN: B. Hartenbaum

Ken O'Brien & Associates, Inc
ATTN: D. Donegan

Massachusetts Inst of Technology
ATTN: W. Brace

Merritt Cases, Inc
ATTN: J. Merritt

University of Nevada
ATTN: P. Penske
ATTN: C. Case

DEPARTMENT OF DEFENSE CONTRACTORS (Continued)

Kaman Tempo
ATTN: DASIAC

Pacific-Sierra Research Corp
ATTN: H. Brode, Chairman SAGE

Pacifica Technology
ATTN: D. Patch
ATTN: J. Kent

R&D Associates
ATTN: R. Schaefer
ATTN: J. Lewis

S-Cubed
ATTN: R. Duff
ATTN: Document Control
ATTN: E. Peterson

Shock Hydrodynamics, Inc
ATTN: K. Kreyenhagen

SRI International
ATTN: A. Florence
ATTN: H. Lindberg

Structural Mechanics Associates
ATTN: R. Kennedy

Terra Tek, Inc
ATTN: S. Green
4 cy ATTN: C. Cooley
4 cy ATTN: R. Smith
4 cy ATTN: J. Schatz

TRW Electronics & Defense Sector
ATTN: RI/2162, M. Schrader

Weidlinger Assoc Consulting Engineers
ATTN: M. Baron


MEI
8